A RECURSIVE PSEUDO FATIGUE CRACKING DAMAGE MODEL FOR ASPHALT PAVEMENTS

by

Kenneth Adomako Tutu

A dissertation submitted to the Graduate Faculty of
Auburn University
in partial fulfillment of the
requirements for the Degree of
Doctor of Philosophy

Auburn, Alabama
August 4, 2018

Approved by

David H. Timm, Chair, Brasfield and Gorrie Professor, Civil Engineering
J. Brian Anderson, Associate Professor, Civil Engineering
Carolina M. Rodezno, Assistant Research Professor, National Center for Asphalt Technology
Fabricio Leiva-Villacorta, Assistant Research Professor, National Center for Asphalt Technology
April E. Simons, Assistant Professor, Building Science

ABSTRACT

Bottom-up fatigue cracking in asphalt pavements is a complex distress mechanism influenced by traffic, structural and environmental conditions. Fatigue damage itself changes the properties of the asphalt concrete (AC), which affects a pavement's structural capacity. Most fatigue cracking damage models neglect damage induced-changes in the AC. Also, the complexity of the distress mechanism has culminated in intricate models unsuitable for routine application. This study developed a simple recursive model that simulates fatigue cracking damage more realistically by accounting for damage-induced changes in AC. The proposed pseudo fatigue cracking damage model, premised on layered elastic theory, is a strain-based phenomenological model that implements incremental-recursive damage accumulation without the need for transfer functions, a key limitation of conventional mechanistic-empirical fatigue models. The model has two key assumptions: fatigue damage causes deterioration of AC modulus, and critical tensile strain at the bottom of the AC layer is a fatigue damage determinant. Bending beam fatigue testing, an established laboratory method for simulating bottom-up fatigue cracking, was the foundation for the pseudo fatigue damage model's development. The data comprised of 151 beam fatigue test results from 20 different AC mixtures constructed at the National Center for Asphalt Technology Pavement Test Track. A functional form was identified for the pseudo fatigue cracking damage model which, after calibration and validation, demonstrated good predictive capability for measured beam fatigue curves. The model inputs are the initial AC modulus, fatigue endurance limit, initial critical strain at the AC layer bottom and a failure criterion (reduction in initial AC modulus). The model simulates a pavement system in WESLEA, a multilayered analysis program, to generate a fatigue damage curve. Upon field validation, the pseudo fatigue damage model can be incorporated in mechanistic pavement design procedures. The pseudo fatigue damage model, by eliminating transfer functions and considering damage-induced changes in AC, represents considerable progress toward full-mechanistic fatigue analysis, a major goal of asphalt pavement research.

ACKNOWLEGEMENTS

I would like to thank Dr. David Timm, my major advisor, for his extraordinary support and direction in the preparation of this dissertation. He demonstrated an exceptional commitment to my mentorship and provided the much-needed guidance for improving my research skills and professional development. I acknowledge my other committee members – Dr. Brian Anderson, Dr. Carolina Rodezno and Dr. Fabricio Leiva-Villacorta – for providing valuable feedback and a supportive environment. This research would have been impossible without the availability of high-quality research data at the National Center for Asphalt Technology (NCAT). I thank the Test Track sponsors and the NCAT team, particularly Adam Taylor for his assistance with the beam fatigue test data, as well as Dr. Brian Prowell of Advanced Materials Services. My colleague NCAT graduate students offered friendship and encouragement, for which I am thankful. Finally, I am grateful to my family for their unwavering patience, encouragement and spiritual support.

TABLE OF CONTENTS

ABSTRACT ..... **ii**

ACKNOWLEGEMENTS ..... **iii**

LIST OF TABLES ..... **vii**

LIST OF FIGURES ..... **viii**

CHAPTER 1: INTRODUCTION **1**

1.1 Background 1

1.2 Problem Statement 4

1.3 Objective 5

1.4 Scope of Work 5

CHAPTER 2: LITERATURE REVIEW **6**

2.1 Fatigue Modeling Methods 6

2.1.1 Empirical Models 6

2.1.2 Phenomenological Models 6

2.1.3 Dissipated Energy-Based Models 9

2.1.4 Fracture Mechanics-Based Models 14

2.1.5 Continuum Damage Mechanics-Based Models 18

2.2 Laboratory Fatigue Characterization 20

2.3 Summary of Literature Review 25

CHAPTER 3: DEVELOPMENT OF PSEUDO FATIGUE CRACKING DAMAGE MODEL **27**

3.1 Data Acquisition 27

3.1.1 Beam Fatigue Testing 30

3.1.2 Prediction of Fatigue Endurance Limits 36

3.2 Description of Pseudo Fatigue Cracking Damage Model 40
3.3 Formulation of Pseudo Fatigue Cracking Damage Model 41
3.3.1 Preliminary Specifications of Pseudo Fatigue Cracking Damage Model 41
3.3.2 Performance of Preliminary Pseudo Fatigue Cracking Damage Models 48
3.3.3 Selected Pseudo Fatigue Cracking Damage Model 49
3.4 Calibration of Pseudo Fatigue Cracking Damage Model 51
3.4.1 Determination of β-Parameters 52
3.4.2 Formulation of β-Parameter Regression Model 57
3.4.3 Preliminary β-Parameter Regression Models 64
3.4.4 New Generation of β-Parameter Regression Models 70
3.5 Summary of Pseudo Fatigue Cracking Damage Model Development 79
CHAPTER 4: VALIDATION OF PSEUDO FATIGUE CRACKING DAMAGE MODEL 81
4.1 Validation of β-Parameter Regression Models 82
4.2 Validation of Pseudo Fatigue Cracking Damage Model 90
4.3 Results of Pseudo Fatigue Cracking Damage Model Validation 90
4.4 Summary of Pseudo Fatigue Cracking Damage Model Validation 99
CHAPTER 5: INCORPORATION OF PSEUDO FATIGUE CRACKING DAMAGE MODEL IN MECHANISTIC PAVEMENT DESIGN 101
5.1 Design Based on Equivalent Axle Load and Equivalent Temperature Concepts 102
5.2 Design Based on Axle Load Spectra and Equivalent Temperature Concepts 103
CHAPTER 6: SUMMARY, CONCLUSIONS AND RECOMMENDATIONS 105
6.1 Summary and Conclusions 105
6.2 Recommendations 107
REFERENCES 110
APPENDICES 122

Appendix A - AC Mixture Properties and Fatigue Performance Characteristics

Appendix B - Fatigue Endurance Limits Determined Using NCHRP 9-44A and NCHRP 09-38 Procedures

Appendix C - Pavement Cross-Sections Simulated for Model Calibration

Appendix D - Pavement Cross-Sections Simulated for Model Validation

Appendix E - Pearson Correlation Matrix for Regression Variables

Appendix F - Plots of Predicted Versus Expected β-Parameters

LIST OF TABLES

Table 3.1 Summary of Beam Fatigue Test Data Used for Model Calibration…….29

Table 3.2 Summary of Beam Fatigue Test Data Used for Model Validation……..29

Table 3.3 Summary Information on Mixtures Used for Model Calibration…….29

Table 3.4 Summary Information on Mixtures Used for Model Validation……..30

Table 3.5 Pavement Simulated with Pseudo Fatigue Cracking Damage Models…..…..43

Table 3.6 Performance of Trial Pseudo Fatigue Cracking Damage Models……45

Table 3.7 Pavement Cross-Sections Simulated for Determination of β-Parameters……52

Table 3.8 Potentially Relevant Variables for β-Parameter Regression Model…….59

Table 3.9 Preliminary β-Parameter Regression Models……...65

Table 3.10 New Generation of β-Parameter Regression Models……...70

Table 3.11 Regression Coefficients for β-Parameter Model 1……...77

Table 3.12 Regression Coefficients for β-Parameter Model 2……...78

Table 3.13 Regression Coefficients for β-Parameter Model 3……...78

Table 3.14 Regression Coefficients for β-Parameter Model 4……...78

Table 3.15 Regression Coefficients for β-Parameter Model 5……...79

Table 4.1 Summary Information on Cross-Sections Simulated for Model Validation…..82

Table 4.2 Reduction in Initial AC Modulus in Pseudo Fatigue Damage Model Validation…….95

LIST OF FIGURES

Figure 1.1 Bottom-up Fatigue Cracking……..1

Figure 2.1 Crack Loading Modes in Fracture Mechanics…….14

Figure 2.2 Illustration of the Cohesive Zone Model……..16

Figure 2.3 Bending Beam Fatigue Test Device…….20

Figure 2.4 Dimensions of Bending Beam Fatigue Test Specimen……21

Figure 2.5 AC Stiffness Deterioration Curve (Deacon, 1965)……..24

Figure 2.6 AC Stiffness Deterioration Curve (Freeme and Marais, 1973)……24

Figure 3.1 NCAT Pavement Test Track……28

Figure 3.2 Coefficient of Variation of Initial AC Stiffness in Beam Fatigue Testing…...32

Figure 3.3 Coefficient of Variation of Load Cycles to Failure in Beam Fatigue Testing.33

Figure 3.4 Fatigue Curves of Three Replicate Beams Tested at 200με……....34

Figure 3.5 Fatigue Curves of Three Replicate Beams Tested at 400με……35

Figure 3.6 Fatigue Curves of Three Replicate Beams Tested at 800με……35

Figure 3.7 Fatigue Endurance Limits from NCHRP 9-44A and NCHRP 09-38 Models..39

Figure 3.8 Flowchart for Executing Preliminary Pseudo Fatigue Damage Models……..42

Figure 3.9 Measured Beam Fatigue Curve versus Predicted Fatigue Curves……...49

Figure 3.10 Flowchart for Executing Pseudo Fatigue Cracking Damage Model……53

Figure 3.11 Cumulative Distribution of Coefficient of Determination Values…….....55

Figure 3.12 Sample Plots of Beam Fatigue Versus Predicted Damage Curves……..56

Figure 3.13 Regression Process for Formulating β-Parameter Model……58

Figure 3.14 Pairwise Scatter Plots of Selected β-Parameter Predictor Variables……61

Figure 3.15 Diagnostic Plots for β-Parameter Regression Model A…….66

Figure 3.16 Diagnostic Plots for β-Parameter Regression Model B…….67

Figure 3.17 Diagnostic Plots for β-Parameter Regression Model C…….68

Figure 3.18 Diagnostic Plots for β-Parameter Regression Model D…….69

Figure 3.19 Diagnostic Plots for β-Parameter Regression Model 1……..72

Figure 3.20 Diagnostic Plots for β-Parameter Regression Model 2……..73

Figure 3.21 Diagnostic Plots for β-Parameter Regression Model 3……..74

Figure 3.22 Diagnostic Plots for β-Parameter Regression Model 4……..75

Figure 3.23 Diagnostic Plots for β-Parameter Regression Model 5……..76

Figure 4.1 Flowchart for Validation of Pseudo Fatigue Cracking Damage Model……...81

Figure 4.2 Cumulative Distribution of R^2 Associated with Expected β-Parameters…….83

Figure 4.3 Distribution of Error Between Expected and Predicted β-Parameters…….84

Figure 4.4 Predicted β-Parameters (Model 4) versus Expected β-Parameters……..85

Figure 4.5 Variations in Predicted and Expected β-Parameters – Regression Model 1…86

Figure 4.6 Variations in Predicted and Expected β-Parameters – Regression Model 2…87

Figure 4.7 Variations in Predicted and Expected β-Parameters – Regression Model 3…87

Figure 4.8 Variations in Predicted and Expected β-Parameters – Regression Model 4…88

Figure 4.9 Variations in Predicted and Expected β-Parameters – Regression Model 5…88

Figure 4.10 Cumulative Distribution of R^2 Values Indicating Goodness-of-Fit of Predicted Versus Measured Fatigue Damage Curves……91

Figure 4.11 Pseudo Fatigue Damage Model Validation: Percent of Load Cycles to Failure Simulated……..93

Figure 4.12 Pseudo Fatigue Damage Model Validation: Reduction in Initial AC Modulus……94

Figure 4.13 Pseudo Fatigue Damage Model Validation: Sample Predicted Versus Measured Fatigue Damage Curves……...…….99

CHAPTER 1

INTRODUCTION

1.1 Background

Bottom-up fatigue cracking has been studied for over six decades, making it the most-researched asphalt pavement distress (Shell, 2015). Fatigue is a progressive, permanent structural change that occurs under repeated stress or strain applications and which culminates in cracking after several repetitions (ASTM, 1963). The maximum stress or strain is less than the tensile strength of the material (Finn, 1967). Hveem's (1955) recognition of a strong link between pavement deflection and fatigue failure intensified research into fatigue cracking (e.g., Pell, 1962; Monismith et al., 1970; Highway Research Board, 1973). Today, the mechanism of bottom-up fatigue cracking is well-known: traffic loads induce repetitive flexural bending of asphalt concrete (AC) layer, which culminates in microcracks at the bottom where horizontal tensile strains are highest. The cracks develop into macrocracks and propagate to the surface to form a network in the wheel paths, as Figure 1.1 shows.

Figure 1.1 Bottom-up Fatigue Cracking

Bottom-up fatigue cracking has significant damaging effects: it weakens the structural capacity of AC layers; it allows water to percolate the pavement system to damage the AC material, as well as to minimize the load-spreading capacity of the unbound layers; and it triggers distresses such as raveling and potholes. Thus, fatigue cracking inhibits both the structural and functional performance of pavements. Reconstruction, although resource-

intensive, is the most effective rehabilitation strategy. Hence, fatigue analysis is a key component of a pavement design system.

Several methods for modeling fatigue performance are available. These methods – which may be based on empirical, phenomenological, dissipated energy, fracture mechanics and continuum damage mechanics concepts – differ in complexity and the targeted phase of the fatigue damage process. Traditionally, empirical models, which are mostly based on historical pavement performance, have been used to design against fatigue cracking. Because these models have no strong basis on fundamental material behavior theories, they have limited capability to fundamentally address fatigue cracking. Over-conservative designs and inability to adapt to advances in design inputs are major drawbacks of empirical fatigue models.

In contrast, phenomenological fatigue models combine empiricism and mechanics to provide better prediction of AC fatigue performance. These models correlate fatigue life to strain or stress repetitions through empirical constants. To develop such models, the effect of repetitive traffic loading is simulated by a laboratory fatigue test. A shift factor is used to adjust the resulting fatigue model to field conditions. Alternatively, a phenomenological fatigue model can be developed using data from instrumented pavements. The mechanistic-empirical (M-E) pavement design concept, which is gaining popularity in recent times, implements phenomenological fatigue modeling. In M-E fatigue analysis, critical tensile strains under the bottom of an AC layer are computed and are then used in a transfer function (phenomenological fatigue model) to predict fatigue cracking. Thus, a well-calibrated fatigue model is critical for a cost-effective design. Apart from the excessive calibration cost and inappropriateness of extensive extrapolation, phenomenological models typically lump fatigue lives related to crack initiation and crack propagation, which is considered a drawback (Aglan et al., 1993).

Several researchers (e.g., Van Dijk and Visser, 1977; SHRP, 1994; Ghuzlan and Carpenter, 2000) have attempted to utilize dissipated energy, defined as the energy loss per load cycle in a fatigue test, to provide a more fundamental characterization of fatigue damage. Dissipated energy, as a fatigue damage determinant, seems to have greater conceptual appeal, since it captures viscoelasticity (Abojaradeh et al., 2007). However, effective separation of its components (dissipated energy due to viscoelastic damping and that due to damage) is a challenge. Contrary to earlier research findings, it has been shown that using total dissipated energy for fatigue analysis is inaccurate (Ghuzlan and Carpenter, 2000). Instead, the ratio of dissipated energy change (RDEC), dissipated pseudostrain energy (DPSE) and rate of DPSE have been suggested. Regardless, Bhasin et al. (2009) noted these parameters also needed refinement to account for nonlinear viscoelastic energy dissipation and plastic deformation.

Another challenge is the elimination of mode-of-loading dependency of dissipated energy. Some researchers (e.g., Lytton, et al., 1993; Masad et al., 2008) have suggested the combination of fracture mechanics theory with the rate of DPSE could resolve this difficulty. Currently, the dissipated energy concept remains a laboratory fatigue characterization procedure, which is yet to be validated for routine pavement design purposes.

Fracture mechanics-based approaches, advanced by researchers in the 1970s (e.g., Majidzadeh et al., 1972; Majidzadeh and Ramsamooj, 1976; Germann and Lytton, 1979), correlate a driving force required to grow a crack of arbitrary dimensions to crack growth rate using a power law formulated by Paris et al. (1961). Under linear elastic conditions, the crack driving force may be the stress intensity factor or the energy release rate. Paris' law is empirical, does not consider crack initiation, and it is applicable only under linear elastic conditions. Regardless of these limitations, fracture mechanics methods provide a physical interpretation of damage, in terms of crack dimensions. In recent times, cohesive zone modeling (CZM), a nonlinear fracture mechanics-based technique, is gaining popularity. Despite its reported capability to analyze brittle, quasi-brittle and ductile cracking failures in asphalt pavements (Kim, 2011), several challenges hinder its routine application. CZM needs a finite element or discrete element simulation framework. Not only are these simulation tools unsuitable for routine use, the accuracy of the simulation results depends on the size and orientation of the cohesive zone elements (Kim, 2011). CZM requires measured fracture properties but, presently, no test method characterizes mixed-mode fracture, a common mechanism in asphalt pavements (Kim, 2011). To date, no field validation of cohesive zone fracture models seems to have been reported. Thus, CZM is unfit for immediate use in pavement design systems.

Beginning in the 1980s, there has been tremendous effort to characterize fatigue cracking using continuum damage mechanics. A notable application of this theory is Kim and Little's (1990) viscoelastic continuum damage (VECD) model, which is based on Schapery's (1987) viscoelastic constitutive theory. The simplified version of the VECD model (S-VECD) combines elastic-viscoelastic correspondence principle, continuum damage mechanics-based work potential theory and time-temperature superposition principle with growing damage (Wang et al., 2016). The S-VECD model has a characteristic fatigue damage curve that relates damage to material integrity (Underwood et al., 2012). A failure criterion, based on pseudostrain energy release rate, enables the application of the model to predict fatigue performance (Sabouri and Kim, 2014). Recently, the S-VECD model has been incorporated in a structural design system called Layered Viscoelastic Pavement Design for Critical Distresses (LVECD) (Wang et al., 2016). The program requires transfer functions to relate its predictions

to field performance. Despite the advanced material characterization, current continuum damage-based fatigue models are subject to the limitations of empirical transfer functions.

A major goal of asphalt pavement research is the development of fully-mechanistic fatigue models which will not rely on empirical transfer functions. While it may be desirable for such fatigue models to account for, in a unified manner, the effects of geometry, nonhomogeneities, anisotropy, healing, binder aging, and nonlinear material behavior (Desai, 2009), it is important to maintain a balance between implementation efficiency and model complexity. Thus, a fatigue cracking damage model that leans toward fully-mechanistic fatigue characterization, requires fewer inputs for fatigue performance prediction and that can be used routinely by practitioners is desirable.

1.2 Problem Statement

Although the need to design pavements to withstand bottom-up fatigue cracking has long been recognized, current fatigue models still need improvement. Fatigue cracking is a complex mechanism affected by traffic, structural and environmental factors. Fatigue damage itself changes the AC material properties which, in turn, affects the structural response of the pavement to traffic loads. Thus, the complexity of fatigue cracking has led to several analytical approaches, as described in the literature review.

While empirical models cannot fundamentally characterize the fatigue cracking mechanism, phenomenological models, which are developed for a specific site, require recalibration for significantly new conditions, and they rarely incorporate damage parameters. Dissipated energy-based methods may provide a more fundamental characterization of fatigue cracking damage, but there are concerns over improper separation of the dissipated energy components. Assuming the presence of crack a priori, the application of an empirical crack growth law, specialized computer modeling skills and fracture properties testing limitations are drawbacks of fracture mechanics-based methods for characterizing AC fatigue damage. Fatigue models based on viscoelasticity and continuum damage theories have improved understanding of AC fatigue behavior; however, their current applications involve rigorous mathematical derivations and complex simulation, as well as the need for transfer functions. These factors discourage the use of these models for routine pavement design. Thus, despite considerable progress in fatigue damage modeling, the current methods still need improvement.

In the foreseeable future, it is anticipated fully-mechanistic fatigue models, based on advanced material behavior theories, may become the basis for pavement design. Although such models may provide more accurate predictions of fatigue performance, their practical

usefulness may be limited if the models involve intricate mathematical equations and complex computer simulation. Thus, for practical purposes, there is a need for a simplified fatigue cracking damage analytical procedure that leans toward fully-mechanistic fatigue characterization, and yet realistically simulates fatigue damage of in-service pavements.

1.3 Objective

The objective of this study was to develop a recursive pseudo fatigue cracking damage model for asphalt pavements based on layered elastic theory. The proposed model has an orientation toward fully-mechanistic fatigue damage analysis. Despite the complexity of the fatigue cracking mechanism, a simple but effective analytical tool that can be used routinely by practitioners is desirable. Thus, the motivation was to formulate a practical fatigue cracking damage analytical procedure that requires limited design inputs.

1.4 Scope of Work

The primary components of this study were: literature review of common fatigue cracking modeling methods (Chapter 2), development of the pseudo fatigue cracking damage model (Chapters 3 and 4) and a discussion on the model's application in mechanistic pavement design procedures (Chapter 5). The development of the pseudo fatigue damage model involved three primary tasks: a search for an appropriate functional form of the model, model calibration and model validation. Bending beam fatigue testing was the platform for the model's development. Beam fatigue test data from 20 different asphalt mixtures constructed at the National Center for Asphalt Technology Pavement Test Track during the 2006, 2009 and 2012 research cycles were utilized. Statistical analysis was performed with Statistical Analysis System (version 9.0) and Minitab (version 18). The multilayered elastic analysis program, WESLEA for Windows (version 3.0), was utilized for structural analysis and running the proposed model.

CHAPTER 2

LITERATURE REVIEW

Dominant fatigue cracking modeling methods were reviewed to identify an appropriate analytical framework for the proposed pseudo fatigue cracking damage model. Also, several laboratory test methods for characterizing bottom-up fatigue cracking were considered to determine a fatigue characterization procedure which could provide a platform for the development of the proposed model.

2.1 Fatigue Modeling Methods

Fatigue performance prediction is a key component of pavement design systems. Fatigue modeling approaches continue to evolve in response to advances in design inputs and increasing knowledge of pavement structural performance. In the following subsections, a review of five categories of AC fatigue cracking damage modeling methods is presented.

2.1.1 Empirical Models

These models are mostly based on historical pavement performance, index material properties, or a combination of both factors. The AASHTO empirical design procedure (AASHTO, 1993), which was based on the AASHO Road Test (HRB, 1960), is a popular empirical design model, but it does not specifically design against fatigue cracking. Limitations of empirical models include limited or no dependence on fundamental material properties, difficulty in adapting to advances in design inputs and lack of flexibility to design against specific distresses. For example, the AASHTO empirical pavement design method (AASHTO, 1993) targets a certain terminal serviceability index, which corresponds to a composite pavement surface condition. The contribution of individual distresses, such as fatigue cracking, to the terminal condition is not clear. Empirical models may produce less cost-effective designs; hence, attention is shifting to more fundamental fatigue models.

2.1.2 Phenomenological Models

These models characterize AC fatigue damage based on stress or strain repetitions. Material homogeneity is assumed, and there is no separation of fatigue life during crack initiation or crack propagation. Incremental damage is determined as a function of historical damage, current state of damage, load cycle increment and material properties; damage accumulation is linear and quantified by a deterministic parameter (Ellyin, 1997). Domon and Metcalf (1965),

based on Burmister's (1943, 1945) layered elastic theory, pioneered the use of phenomenological modeling to study bottom-up fatigue cracking by developing theoretical design curves for a 3-layer pavement structure subjected to 18-kip load applications. They utilized horizontal tensile strains at the bottom of the AC layer, which Saal and Pell (1960) had earlier proposed as a fatigue damage determinant. Dormon and Metcalf's (1965) work influenced the current mechanistic-empirical (M-E) design concept, which is implemented in pavement design methods such as Shell (1978), Asphalt Institute (2008), and AASHTO Mechanistic-Empirical Pavement Design Guide (NCHRP, 2004). The goal of M-E fatigue analysis is to keep horizontal tensile strain at the bottom of the AC layer within tolerable limits.

Current state-of-the-practice fatigue modeling involves computation of critical tensile strains at the AC layer bottom for the materials, traffic and environmental conditions anticipated and entering them in a transfer function (phenomenological model) to predict fatigue cracking. The ratio of the expected number of load repetitions under a set of conditions and the corresponding predicted number of allowable load repetitions to failure constitutes an incremental fatigue damage. Miner's (1945) cumulative damage hypothesis linearly sums the incremental damage to provide the pavement fatigue life. According to Miner's (1945) hypothesis (Equation 1), fatigue life corresponds to the total number of load repetitions at which the sum of the incremental damage is unity. In practice, this corresponds to the number of load repetitions that produces a certain amount of fatigue cracking in the pavement.

$$\sum_{i=1}^{n}\left(\frac{n_i}{N_i}\right) = 1.0 \qquad (1)$$

Where:

n_i = Number of actual traffic load repetitions at strain level *i*

N_i = Number of allowable load repetitions to failure at strain level *i*

Fatigue transfer functions have the typical form shown in Equation 2. They are developed from laboratory fatigue tests and adjusted to field conditions by applying a shift factor. A shift factor is needed for reasons such as lateral wheel wander, rest periods between traffic load applications, healing of microcracks, asphalt binder aging, secondary AC mixture densification, environmental factors, and differences in geometry and test conditions in pavements compared to test specimens (Molenaar, 2007; Prowell, 2010; Mateos et al., 2011). The wide range of reported shift factors, typically between 0.1 and 100, is an indication of their

dependency on multiple factors, and hence the difficulty of their accurate determination (Pierce et al., 1993; Harvey et al., 1997; Adhikari et al., 2009; Prowell, 2010; Mateos et al., 2011). Alternatively, data from test sections can be used to calibrate transfer functions (El-Basyouny and Witczak, 2005; Timm and Newcomb, 2012). Field calibration is considered advantageous, as it incorporates actual traffic conditions, environmental effects, observed performance, and in-situ material characterization (Timm and Newcomb, 2012).

$$N_f = k_1 \left(\frac{1}{\varepsilon_t}\right)^{k_2} \left(\frac{1}{E}\right)^{k_3} \quad (2)$$

Where:

N_f = Number of load repetitions to fatigue failure

ε_t = Critical tensile strain at AC layer bottom

E = AC modulus

k_i = Calibration constants

Proper calibration of transfer functions is crucial for cost-effective pavement design. Due to their empirical nature, transfer functions are directly applicable to conditions pertaining to their calibration; undue extrapolation yields poor designs. Calibration of transfer functions is resource-intensive. The assumption that each load cycle consumes a portion of a pavement's fatigue life regardless of the load magnitude is inaccurate (NCHRP, 2013). Studies show the existence of AC fatigue endurance limit, a strain level below which no fatigue damage occurs or healable, for unlimited load repetitions (NCHRP, 2013). Thus, the AASHTO Mechanistic-Empirical Design Guide (NCHRP, 2004) allows the input of fatigue endurance limit.

Recent studies suggest the need for fatigue damage parameters in phenomenological fatigue models to improve predictions. For instance, Wen and Li (2013) formulated a fatigue model with the functional form in Equation 3 to include AC critical strain energy density as a fatigue damage parameter. They defined critical strain energy density as the area under an indirect tensile test (IDT)-measured stress-strain curve up to the peak stress.

$$N_f = k_1 \left(\frac{1}{\varepsilon_t}\right)^{k_2} \left(\frac{1}{E}\right)^{k_3} (CSED)^{k_4} h^{k_5} \quad (3)$$

Where:

N_f = Number of load repetitions to failure

ε_t = Critical tensile strain at AC layer bottom

E = AC mixture modulus

CSED = Critical strain energy density

h = AC layer thickness

k_i = Calibration constants

Also, Ullidtz (2005) formulated the strain-based phenomenological model in Equation 4, with a nonlinear relationship between fatigue damage and load repetitions. Miner's (1945) hypothesis was used for damage accumulation. Fatigue damage was defined as a relative reduction in AC modulus. The model, which was deemed useful for incremental-recursive pavement design, was found to reasonably predict fatigue damage, as observed in direct uniaxial fatigue testing and in accelerated loading facility test sections.

$$\text{Damage} = \left(\frac{E_i - E}{E_i}\right) = A(MN)^{\alpha}\left(\frac{resp}{resp_{ref}}\right)^{\beta}\left(\frac{E}{E_i}\right)^{\gamma} \quad (4)$$

Where:

E_i = Initial AC modulus

E = AC modulus

MN = 1 million load cycles

resp = Response (normal stress or strain; tensile or compressive)

$resp_{ref}$ = Reference response

A, α, β, γ = Constants

In a nutshell, phenomenological fatigue models, due to their utilization of mechanistic theory, can adapt to advances in design inputs to provide better characterization of fatigue performance compared with empirical models. However, the accuracy of their calibration and the recognized need for a damage parameter are some key issues that need attention.

2.1.3 Dissipated Energy-Based Models

Dissipated energy is the energy loss per load cycle in the fatigue testing of viscoelastic materials, such as AC mixtures. These materials trace different paths for the loading and unloading cycles, resulting in a hysteresis loop. The area of the stress-strain hysteresis loop

represents dissipated energy, which is calculated using Equation 5. It is assumed dissipated energy comprises viscoelastic energy dissipation and energy dissipation due to fatigue damage, although a portion is expended on mechanical work and heat generation (Rowe, 1993). Dissipated energy seems to have greater conceptual appeal as a fatigue damage determinant, since it captures viscoelasticity and correlates well to modulus reduction in fatigue testing (SHRP, 1994; Abojaradeh et al., 2007). Thus, dissipated energy-based models have been explored to gain understanding of AC fatigue behavior.

$$w_i = \pi \sigma_i \varepsilon_i \sin\phi_i \quad (5)$$

Where:

w_i = Dissipated energy in load cycle *i*, J/m^3

σ_i = Stress amplitude in load cycle *i*, Pa

ε_i = Strain amplitude in load cycle *i*, m/m

ϕ_i = Phase angle in load cycle *i*, degrees

Initial dissipated energy, total cumulative dissipated energy, dissipated energy ratio, ratio of dissipated energy change, dissipated pseudostrain energy and the rate of dissipated pseudostrain energy are typical parameters used to characterize fatigue damage. The Strategic Highway Research Program (SHRP, 1994) recommended initial dissipated energy as a fatigue damage determinant in phenomenological models of the form shown in Equation 2, but this approach is unpopular. Researchers (Van Dijk et al., 1972; Van Dijk, 1975; Van Dijk and Visser, 1977) hypothesized that total cumulative dissipated energy at failure was constant (material parameter) for different modes of loading. Consequently, Van Dijk and Visser (1977) proposed an empirical relationship between total cumulative dissipated energy to failure and load cycles to failure, as shown in Equation 6. As the name suggests, total cumulative dissipated energy lumps the portion of dissipated energy due to damage and that due to viscoelastic energy dissipation. Later studies (e.g., SHRP, 1994) found total cumulative dissipated energy was dependent on temperature and mode of loading. Because it grossly estimates energy dissipated in the fatigue damage process, this energy parameter is only effective in differentiating AC mixtures with considerably different fatigue damage resistance (Bhasin et al., 2009).

$$W_N = A(N_f)^z \quad (6)$$

Where:

W_N = Cumulative dissipated energy to failure, J/m^3

N_f = Fatigue life

A, z = Material parameters

Pronk (1995) defined dissipated energy ratio as cumulative dissipated energy up to the *i*-th load cycle divided by dissipated energy at the *i*-th load cycle. Without damage, the slope of dissipated energy ratio versus load cycles curve is unity. However, in case of damage, the curve exhibits three stages, which Bahia (2009) described as: (a) the first stage involves energy dissipation in viscoelastic damping; (b) the second stage is associated with crack initiation, which consumes energy beyond viscoelastic damping; and (c) crack propagation occurs in the final stage, accompanied by a significant increase in dissipated energy per load cycle.

The ratio of dissipated energy change (RDEC) was proposed to provide a more fundamental characterization of fatigue life (Carpenter and Jansen,1997; Ghuzlan and Carpenter, 2000). Ghuzlan and Carpenter (2000) defined RDEC as the relative change in dissipated energy, computed using Equation 7. A plot of RDEC versus load cycles has three regions (Ghuzlan and Carpenter, 2000): (a) the first region has a steep negative slope, suggesting a substantial portion of the dissipated energy is converted to damage due to reorientation of material constituents under loading; (b) the middle horizontal region signifies a steady-state fatigue damage; the incremental damage per cycle is constant; and (c) the last region exhibits a rapid increase in the rate of damage, indicating failure. Fatigue failure was defined as the number of load cycles corresponding to a sudden increase in RDEC. They named the constant value of RDEC in the steady-state region as the plateau value (PV) and suggested this parameter, which was deemed independent of loading mode, was a failure criterion.

$$\mathrm{RDEC_a} = \frac{\mathrm{DE_a} - \mathrm{DE_b}}{\mathrm{DE_a} * (\mathrm{b} - \mathrm{a})} \tag{7}$$

Where:

$RDEC_a$ = Ratio of dissipated energy change at cycle *a* compared with cycle, *b*

DE_a, DE_a = Dissipated energy for load cycles *a* and *b*, respectively

Although the PV has been shown to exhibit a strong relationship with fatigue life that is independent of testing mode (Ghuzlan and Carpenter, 2000; Shen and Carpenter, 2005;

Ghuzlan and Carpenter, 2006), concerns exist over the unique determination of PV from experimental data due to variability. Hence, Carpenter and Shen (2006), by defining PV as the RDEC which corresponds to a 50% reduction in AC modulus, formulated Equation 8 for determining the PV, based on a power curve fitting procedure. Later, Shen and Carpenter (2007) proposed a model of the general form in Equation 9 to predict PV from AC mixture properties and loading levels and related it to fatigue life, using Equation 10. They suggested the model could be calibrated to field conditions.

$$PV = \frac{1 - \left(1 + \frac{100}{N_{f50}}\right)^{m}}{100} \tag{8}$$

Where:

PV = Plateau value

m = Slope of dissipated energy versus load cycles power curve

N_{f50} = Fatigue life at 50% stiffness reduction

$$PV = k_1 \varepsilon^{k_2} S^{k_3} (VP)^{k_4} (GP)^{k_5} \tag{9}$$

Where:

ε = Tensile strain

S = Flexural stiffness

VP = AC mixture volumetric parameter

GP = Aggregate gradation parameter

k_i = Constants

$$VP = \frac{V_a}{V_a + V_b} \tag{9a}$$

$$GP = \frac{P_{NMS} - P_{PCS}}{P_{200}} \tag{9b}$$

Where:

V_a = Air voids, %

V_b = Asphalt binder content by volume, %

P_{NMS} = Percent aggregate passing nominal maximum size sieve

P_{PCS} = Percent aggregate passing primary control sieve

$$N_f = k_1(PV)^{k_2} \quad (10)$$

Where:

N_f = Load cycles to failure (corresponding to a sudden increase in RDEC)

PV = Predicted plateau value

k_1, k_2 = Constants

In contrast, Bhasin et al. (2009) have shown that PV and load cycles to failure (N_f) are dependent on testing mode; however, their product (PV x N_f) is a material constant independent of testing mode and load cycles to failure. Hence, they proposed the product of PV and load cycles to failure as a measure of fatigue cracking damage, provided nonlinear material response was negligible. To separate the components of dissipated energy, Schapery (1984) suggested that transforming physical strain to pseudostrain by the correspondence principle eliminates viscoelasticity energy dissipation. Hence, the area of the stress-pseudostrain hysteresis loop represents only energy dissipation due to damage. Many researchers (e.g., Kim et al., 1997; Arambula et al., 2007; Lytton, 2000; Si et al., 2002) have used dissipated pseudostrain energy (DPSE) to characterize fatigue damage. However, Bhasin et al. (2009) have found that DPSE, although was a better fatigue damage determinant than initial dissipated energy and total cumulative dissipated energy, was sensitive to mode of testing.

In a rather complex approach, the rate of DPSE has been utilized with fracture mechanics principles and material properties to evaluate AC fatigue performance (e.g., Lytton et al., 1993; Masad et al., 2008). The *J*-integral (energy per unit area of crack surface) has been employed as the crack driving force in Paris' law to formulate a crack growth index as a function of the rate of DPSE and material properties. Bhasin et al. (2009) found the crack growth index to be independent of testing mode, and it effectively characterized fatigue life of fine AC mixtures. Regardless, some researchers (e.g., Luo et al., 2013) suggest that since fatigue damage and plastic deformation may occur concurrently, DPSE due to fatigue damage must be separated from DPSE due to deformation to obtain a true fatigue model. Clearly, a major issue with dissipated energy-based fatigue models is the effective isolation of the dissipated energy components. Currently, dissipated energy is used for laboratory fatigue analysis and is yet to be validated for pavement structural design purposes.

2.1.4 Fracture Mechanics-Based Models

Griffith (1920) proposed the basic ideas of modern fracture mechanics in the 1920s, but it was in the late 1960s that some researchers (e.g., Majidzadeh et al., 1969, 1970, 1971) applied them to study AC fatigue behavior. Fracture mechanics theory assumes cracks are present a priori and propagate under repeated loading events. Although this assumption provides a physical interpretation of damage in terms of crack dimensions, it precludes the modeling of crack initiation. Fracture mechanics analysis has two approaches: the use of energy release rate and stress intensity factor. The energy release rate is the rate of change in potential energy with crack area for a linear elastic material, whereas stress intensity factor characterizes stress condition at the crack tip in a homogeneous, linear elastic material (Anderson, 2005). Both parameters, which are analogous, are the driving force for fracture; their critical value is fracture toughness, a parameter which indicates a material's resistance to fracture (Anderson, 2005). Fracture grows if the driving force is at least equal to fracture toughness.

Stress intensity factors, which are determined experimentally or numerically for complex situations, are affected by material properties, boundary conditions, testing conditions and crack configuration (Shukla, 2005). They are determined for three modes of loading that a crack may experience. As Figure 2.1 shows, in Mode I, the principal load is normal to the crack plane, leading to a tensile opening of the crack. Mode II is in-plane shear loading, which causes sliding of one crack surface against another. Mode III is out-of-plane shear loading, which tears the material apart. Asphalt pavements mostly exhibit Modes I and II cracking (Wang et al., 2013), although Mode III may also occur (Ameri et al., 2011).

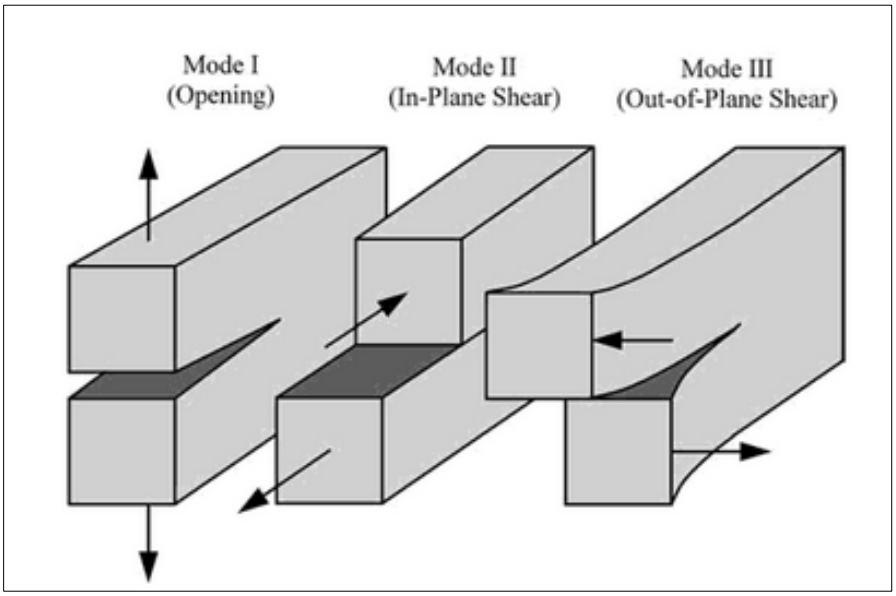

Figure 2.1 Crack Loading Modes in Fracture Mechanics (Anderson, 2005)

Paris et al. (1961) related stress intensity factor to the rate of crack growth (da/dN) under repeated stress application by postulating the power law in Equation 11, popularly known as Paris' law. Fatigue life is determined by integrating Paris' law from an assumed initial crack size to a critical size. The empirical nature of Paris' law and the assumption of an initial crack size are major concerns with this linear fracture mechanics-based approach to fatigue life characterization. For instance, Zhang et al. (2001a) measured crack growth rates in the laboratory and compared them with field performance. They found Paris' law inadequately characterized AC fatigue performance under typical field conditions.

$$\frac{da}{dN} = c(\Delta K)^n \qquad (11)$$

Where:

a	=	Crack size
N	=	Number of load repetitions
ΔK	=	Stress intensity factor range
c, n	=	Material constants

Fatigue life may be characterized as either a one- or two-phase fracture process. In the one-phase process, a single model characterizes both crack initiation and propagation. Researchers such as Majidzadeh et al. (1970, 1971) have utilized this approach. The two-phase process attempts to address the criticism that fracture mechanics-based methods combine fatigue life pertaining to crack initiation and crack propagation. For example, the Strategic Highway Research Program (SHRP, 1994) utilized a micro-fracture model and Paris' law to characterize fatigue life during crack initiation and crack propagation, respectively. The micro-fracture model utilized the energy equivalency concept to develop a relationship between modulus reduction and micro-crack growth. Li (1999) noted micro-fracture fatigue models inadequately characterize crack initiation, and hence utilized a phenomenological model to describe crack initiation and conventional fracture mechanics theory to model crack propagation. The crack size, which separated the crack initiation and crack propagation phases, was determined experimentally.

Linear elastic fracture mechanics is inapplicable when the crack tip exhibits nonlinear behavior such as plasticity, viscoelasticity and viscoplasticity. Instead, nonlinear fracture mechanics theory is deemed capable to address nonlinearity. Cohesive zone modeling (CZM),

introduced by Dugdale (1960) and Barenblatt (1962) in the 1960s, is gaining popularity as a nonlinear fracture mechanics theory for analyzing brittle, quasi-brittle and ductile crack failures, all of which may occur in asphalt pavements (Kim, 2011). A cohesive crack is a fictitious crack that transfers stress across its interface; crack growth occurs across an extended crack tip, with cohesive tractions resisting fracture (Kim, 2011). Park (2009) used Figure 2.2 to describe CZM as: (a) Stage I represents intact material condition; (b) Stage II is crack initiation stage; (c) Stage III describes nonlinear material softening that characterizes damage evolution; and (d) Stage IV signifies failure, with critical crack opening width representing new fracture surfaces. Fracture properties such as cohesive strength (σ_{max}), critical separation (δ), fracture energy and the shape of the traction-separation curve (softening curve in Stage III) must all be determined before CZM can be applied to characterize fatigue damage. Kim et al. (2005, 2006, 2007) have used CZM to study AC fatigue by using linear viscoelastic AC mixture properties and nonlinear viscoelastic fracture parameters in a finite element model. CZM has also been used to analyze AC moisture damage (Caro et al., 2010a, 2010b), reflective cracking (Baek and Al-Qadi, 2008) and thermal cracking (Kim and Buttlar, 2009).

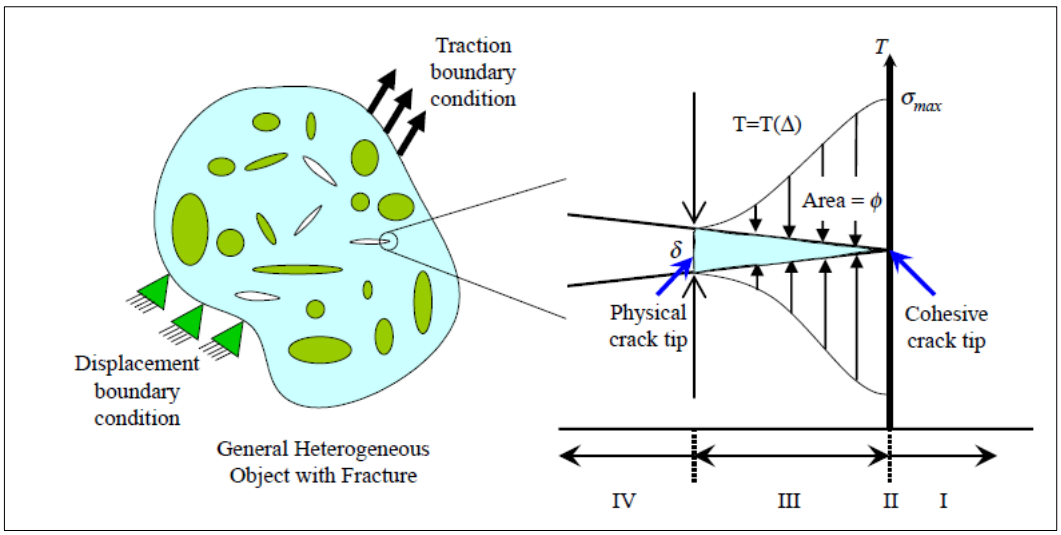

Figure 2.2 Illustration of the Cohesive Zone Model (Park, 2009)

Kim (2011) discussed three significant issues that may hinder the routine use of CZM: determination of fracture properties, computational efficiency and model validation. CZM require fracture properties, but current AC fracture test methods such as single-edge notched beam, disc-shaped compact tension and semi-circular bend characterize only Mode I (tensile opening) fracture; no laboratory test method has yet been developed for mixed-mode fracture (Modes I and II), although it is a common fracture mechanism in asphalt pavements. CZM is implemented within finite element or discrete element simulation framework. These simulation

tools are generally unsuitable for routine use due to the tremendous amount of computational time required. Also, the accuracy of the simulation results depends on the size and orientation of the cohesive zone elements. To date, no field validation of cohesive zone fracture models seems to have been reported.

To develop a more practical solution, recent studies by Zhang et al. (2001b) and Roque et al. (2002) have led to the development of a fatigue crack growth law based on damage limits, dissipated energy and nonlinear fracture mechanics, termed Hot Mix Asphalt (HMA) Fracture Mechanics. The model assumes lower and upper damage limits, defined by AC dissipated creep strain energy (DCSE) and fracture energy, respectively. Damage below the DCSE limit is healable; accumulated damage greater than the DCSE limit induces a non-healable macrocrack. A single load application can cause damage beyond the upper fracture limit. While linear fracture mechanics assumes stress at the crack tip approaches infinity, HMA Fracture Mechanics assumes the stress level cannot exceed the tensile strength of an AC mixture (Zhang et al., 2001b). Also, linear elastic fracture mechanics assumes continuous crack growth, but HMA Fracture Mechanics assumes a stepwise crack growth (Roque et al., 1999; Zhang et al., 2001b). The model predicts the length of the crack process zone (the area in front of the crack tip) for a crack subjected to one-dimensional uniform tension by using linear elastic fracture mechanics solutions for plane stress conditions; discontinuous crack growth is then modeled by increasing crack length by an amount equal to the length of each process zone (Sangpetngam et al., 2003). It is hypothesized cracks grow if the accumulated DCSE in the process zone exceeds the energy limits. Indirect tensile testing (IDT) provides the needed material properties: creep compliance parameters from the static creep test (AASHTO T 322); fracture energy and DCSE limits from the strength test (ASTM D6931) and resilient modulus test (ASTM D7369); and tensile strength from the strength test (ASTM D6931). Repeated loading leads to an accumulation of DCSE (damage); hence, depending on the mixture's DCSE limit and the rate of DCSE accumulation at the top and bottom of the AC layer, a pavement may experience bottom-up or top-down cracking (Zhang et al., 2001b; Roque et al., 2002).

Roque et al. (2004) developed a failure criterion called energy ratio (the ratio of DCSE limit and the minimum DCSE required to produce a 2-in. crack) to enable the implementation of HMA Fracture Mechanics in a pavement design system for top-down cracking design in Florida (Birgisson et al., 2006). No such criterion has yet been developed for bottom-up fatigue cracking. HMA Fracture Mechanics requires finite element simulation, although displacement discontinuity boundary element method could also be used (Sangpetngam et al., 2003). Sangpetngam et al. (2003) noted that simulating fatigue cracking with the finite element

method was complicated; improper meshing produced unreliable results and ordinary computers could not handle the computations involved. HMA Fracture Mechanics, which considers only tensile mode of cracking, has only been verified with data obtained from IDT testing for Superpave mixtures (Sangpetngam et al., 2003).

In summary, linear fracture mechanics-based fatigue models have limitations. Moreover, nonlinear fracture mechanics-based models require complex simulation and high computational power, making them unsuitable for routine pavement design applications. The combination of fracture mechanics theory and damage limits in the HMA Fracture Mechanics model seems to have simplified the characterization of fatigue cracking, but a failure criterion is yet to be validated for bottom-up fatigue cracking. Regardless, fracture mechanics-based approaches rely on the basic assumption that cracks are present a priori.

2.1.5 Continuum Damage Mechanics-Based Models

Kachanov (1958) originally postulated the continuum damage theory to describe creep loading-induced damage. The theory's success has resulted in its application to AC fatigue analysis. Kim et al. (2009) summarizes the basic ideas of the theory as: (a) a damaged body is represented as a homogenous continuum on a macroscopic scale; (b) damage causes reduction in modulus or strength; (c) the state of damage is described by damage parameters (internal state variables); and (d) modulus is determined as a function of internal state variables by fitting a theoretical model to experimental data.

Continuum damage theory has been used to analyze AC fatigue behavior under elastic, viscoelastic, plastic and viscoplastic conditions (Chehab et al., 2002, 2003; Chehab and Kim 2005; Darabi et al., 2011). Kim and Little's (1990) viscoelastic continuum damage (VECD) model, which development was influenced by Schapery's (1987) viscoelastic constitutive theory for materials with distributed damage is, perhaps, the most popular application of continuum damage theory for AC fatigue analysis. The simplified version of the VECD model (S-VECD) combines three key concepts (Wang et al., 2016): (a) elastic-viscoelastic correspondence principle, which allows viscoelastic solutions to be derived from their elastic counterparts by using pseudo-variables; (b) continuum damage mechanics-based work potential theory, which accounts for the effect of microcracking on constitutive behavior, and (c) time-temperature superposition principle with growing damage, which describes the effect of temperature on constitutive behavior. The S-VECD model predicts a fundamental damage evolution curve that relates cumulative damage to pseudosecant modulus, a material integrity parameter (Underwood et al., 2012). The integrity parameter is unity if there is no damage, but

it decreases as damage accumulates. The damage curve is deemed independent of loading mode (monotonic versus cyclic), temperature and strain amplitude (Daniel and Kim, 2002). Direct tension cyclic fatigue (AASHTO TP 107) and dynamic modulus |E*| tests provide data for using the S-VECD model. An energy-based failure criterion (G^R), defined as the average rate of pseudostrain energy release, represents the overall rate of damage accumulation (Sabouri and Kim, 2014). Thus, the failure criterion enables S-VECD to be used for predicting fatigue life, since it uniquely relates to load cycles to failure.

Recently, the S-VECD model has been incorporated in a pavement design program called Layered Viscoelastic Pavement Design for Critical Distresses (LVECD) (Wang et al., 2016). Fatigue life is quantified as a combination of microcrack initiation and propagation. Thus, cracking is not assumed to be initially present; the S-VECD model allows cracks to initiate and propagate freely (Wang et al., 2016). The LVECD program uses a strain-based phenomenological model of the general form in Equation 12.

$$N_f = \beta_1 k_1 \left(\frac{1}{\varepsilon_t}\right)^{\beta_2 k_2} \left(\frac{1}{E}\right)^{\beta_3 k_3} \quad (12)$$

Where:

N_f = Number of load repetitions to fatigue failure

ε_t = Tensile strain at critical location

E = AC mixture modulus

k_i = Material coefficients

β_i = Local calibration constants

The material coefficients are obtained from the S-VECD model and its accompanying failure criterion (G^R). The LVECD program, which utilizes the load equivalency concept, performs a 3-D finite element viscoelastic analysis with moving loads to determine critical tensile strains. Damage is computed incrementally for the design period, and Miner's (1945) hypothesis is used for damage accumulation, using damage area (number of nodes that experiences failure over total nodes in the AC layers) as a performance index. A transfer function, which is yet to be developed, converts the damage area into an equivalent field areal cracking (Wang et al., 2016). Despite the advanced material characterization embodied in current continuum damage-based fatigue models, fatigue life predictions are subject to the limitations of empirical transfer functions.

2.2 Laboratory Fatigue Characterization

The direct tension cyclic fatigue test (AASHTO TP 107), bending beam fatigue test (AASHTO T 321, ASTM D7460), Illinois flexibility index test (AASHTO TP 124), semi-circular bend test (ASTM D8044) and Texas overlay test (TexDOT Tex-248-F) are prominent examples of AC fatigue tests. Except for the first two, all the test methods are based on fracture mechanics theory, and their simulation of the fatigue cracking mechanism is unsuitable for phenomenological fatigue modeling. The bending beam fatigue test was considered appropriate for this study, since it simulates bottom-up fatigue cracking in a phenomenological approach. Developed by Deacon (1965), the bending beam fatigue test has historically been used to formulate phenomenological models to analyze bottom-up fatigue cracking (NCHRP, 2016). Figures 2.3 and 2.4 show the beam fatigue test apparatus and the dimensions of the test specimen, respectively.

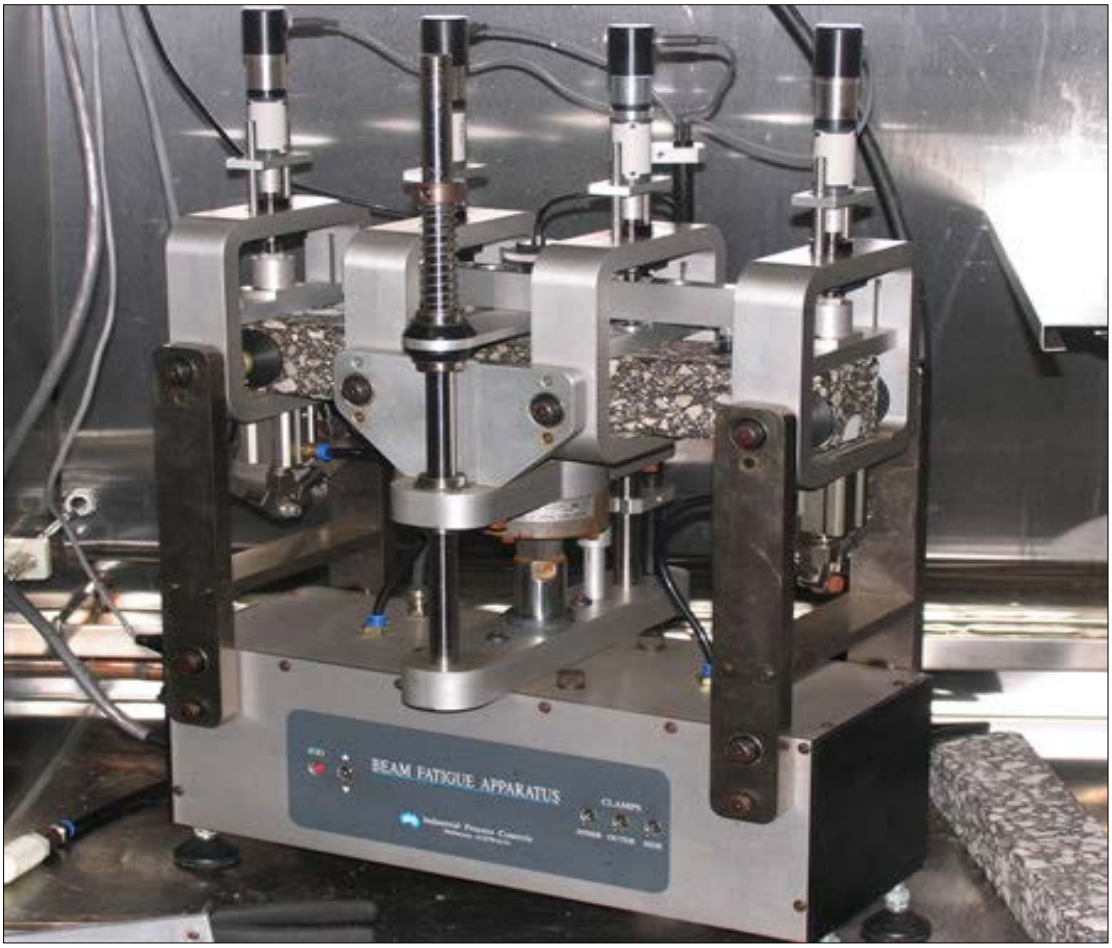

Figure 2.3 Bending Beam Fatigue Test Device (NCHRP, 2016)

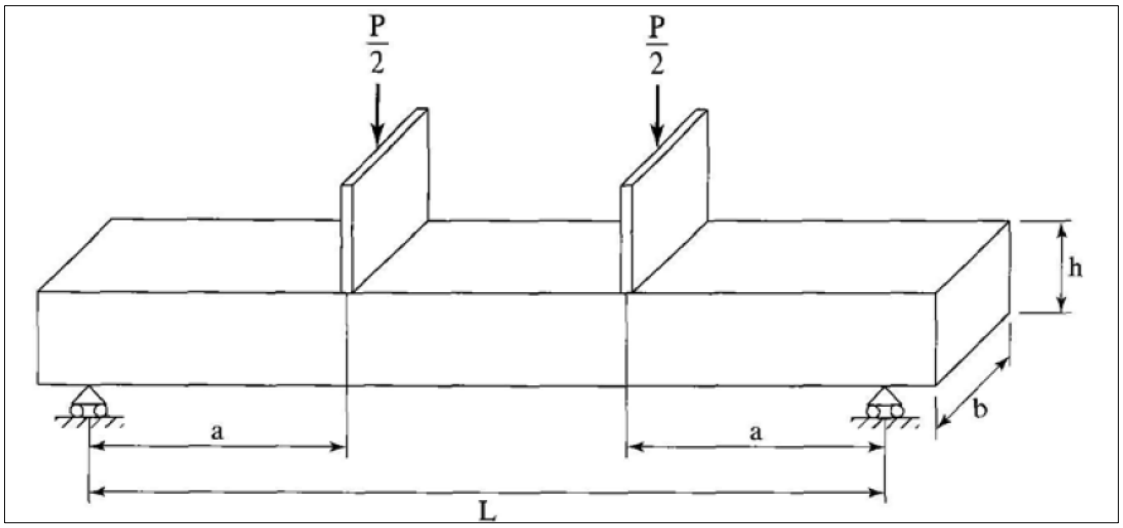

Figure 2.4 Dimensions of Bending Beam Fatigue Test Specimen (Huang, 2012)

Beam specimens (380 mm long by 63 mm wide by 50 mm thick), which may be sawed from laboratory or field compacted AC mixtures, are subjected to repeated flexural loading of haversine (ASTM D7460) or sinusoidal (AASHTO T 321) waveform at their third points. The loading frequency ranges from 5 to 10 Hz. The test is conducted at intermediate pavement temperatures, which are typically associated with fatigue cracking. To simulate bottom-up fatigue cracking, each load application deflects the beam by a certain amount, and a load of an appropriate magnitude forces the beam to its original position. The repeated flexural bending and relaxation produces a constant bending moment over the middle span of the beam, resulting in tensile strains at the bottom. Damage increases with load applications, leading to stiffness reduction as the number of load application increases.

Based on elastic theory, the stress, strain and flexural stiffness induced by load application are computed using Equations 13 through 15, respectively. Both AASHTO T321 and ASTM D7460 recommend the flexural stiffness (dynamic stiffness modulus) at the 50th load cycle be taken as the initial beam stiffness. AASHTO T321 defines failure as the load cycle at which the initial stiffness reduces by half, whereas ASTM D7460 defines failure as the number of load cycles corresponding to the peak of the curve of the product of normalized flexural stiffness and load cycles versus number of load cycles. For constant stress testing, failure corresponds to specimen fracture.

$$\sigma = \frac{3aP}{bh^2} \tag{13}$$

$$\varepsilon_t = \frac{12h\Delta}{3L^2 - 4a^2} \tag{14}$$

$$E_s = \frac{\sigma}{\varepsilon_t} = \frac{Pa(3L^2 - 4a^2)}{4bh^3\Delta} \quad (15)$$

Where:

σ	=	Maximum tensile stress, Pa.
a	=	Distance between the load and nearest support, m.
P	=	Dynamic load with half applied at each third point, N.
b, h	=	Specimen width and depth, respectively, m.
ε_t	=	Maximum tensile strain, m/m
Δ	=	Maximum deflection at beam center, m
L	=	Span length between supports, m
E_s	=	Flexural stiffness, Pa

Beam fatigue testing is performed in either a constant stress or constant strain mode. In a constant stress mode, the same stress is continuously applied, but strain increases with load repetitions. For a constant strain test, stress is decreased with the number of load repetitions to maintain a constant strain. Based on layered elastic analysis, Monismith and Deacon (1969) suggested a constant stress fatigue test better simulates fatigue behavior of AC layers greater than 6 in thick. For such pavements, the AC layer is the main load-carrying medium; as the layer weakens under repeated loading, strain level increases (Huang, 2012). However, Monismith and Deacon (1969) found constant strain fatigue test better characterizes fatigue behavior of AC layers of thickness 2 in. or less. Strain in thin AC layers is largely influenced by the underlying structure; AC modulus reductions play a less significant role (Huang, 2012). For intermediate thicknesses, a form of loading between the two modes was deemed applicable; hence, Monismith and Deacon (1969) proposed the mode factor concept to describe such conditions. Although constant strain and constant stress may represent the mode of loading in thin and thick pavements respectively, the SHRP A003-A researchers (Tangella et al., 1990; Tayebali et al., 1994) recommended constant strain testing for both pavement loading conditions, since constant stress and constant strain test data yielded similar pavement evaluation rankings (Tayebali et al., 1993; Tayebali et al., 1994; Harvey and Tsai,1996).

Beam fatigue testing provides basis for the development of phenomenological fatigue cracking modeling because flexural stiffness obtained from this test correlates linearly with compressive dynamic modulus (|E*|), which is generally accepted as an effective AC material property for

fatigue cracking analysis. Witczak and Root (1974) developed the relationship in Equation 16 to determine |E*| from beam fatigue testing. Recently, Adhikari et al. (2009) reported a strong linear relationship between |E*| and AC flexural stiffness (coefficient of determination was 0.99), with flexural stiffness being 30% lower than |E*|.

$$|E^*| = 0.18089f^{2.1456}E_0^{(14.6918f^{-0.01}-13.5739)} \quad (16)$$

Where:

|E*| = Compressive dynamic modulus, psi

f = Frequency at which |E*| is required, Hz

E_0 = Y-intercept of flexural stiffness versus stress curve, psi

Several studies (e.g., Deacon, 1965; Kallas and Puzinauskas, 1972) show that AC flexural stiffness versus load cycle curves typically exhibit three zones, as illustrated in Figure 2.5. AC stiffness decreases rapidly with load applications in the first zone; the middle zone shows a prolonged, gradual and nearly linear decrease in stiffness with load application; and the last zone shows a rapid decrease in stiffness toward failure conditions. The researchers noted the slope of the middle zone increased with increasing applied stress. Freeme and Marais (1973), based on constant strain fatigue testing of AC trapezoidal specimens, also reported a similar stiffness deterioration curve (Figure 2.6). They explained the gradual stiffness reduction zone in the middle zone was associated with crack initiation, and the final rapid stiffness reduction zone corresponded to crack propagation.

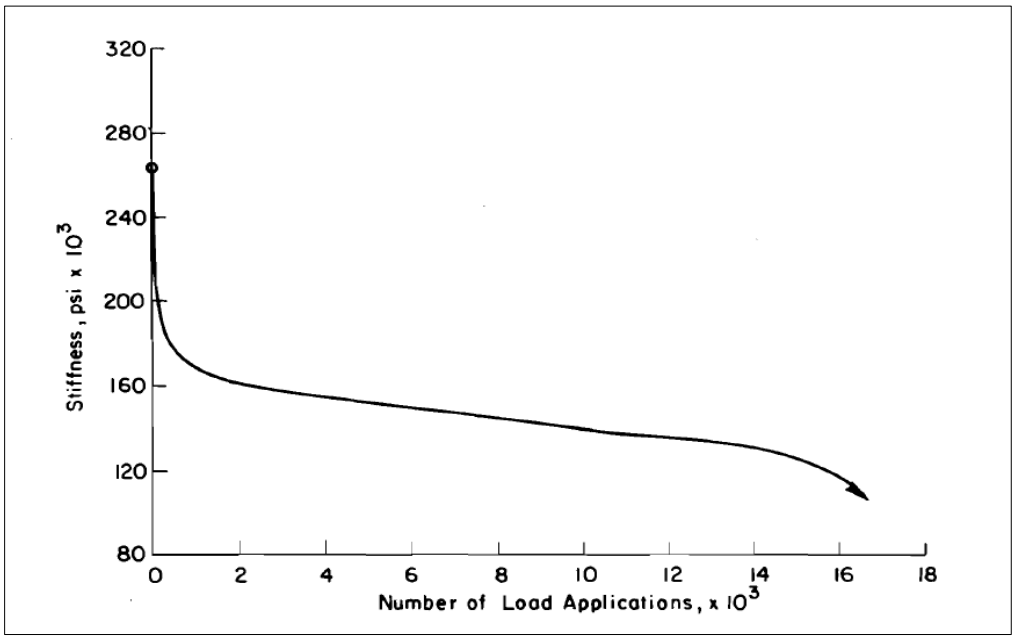

Figure 2.5 AC Stiffness Deterioration Curve (Deacon, 1965)

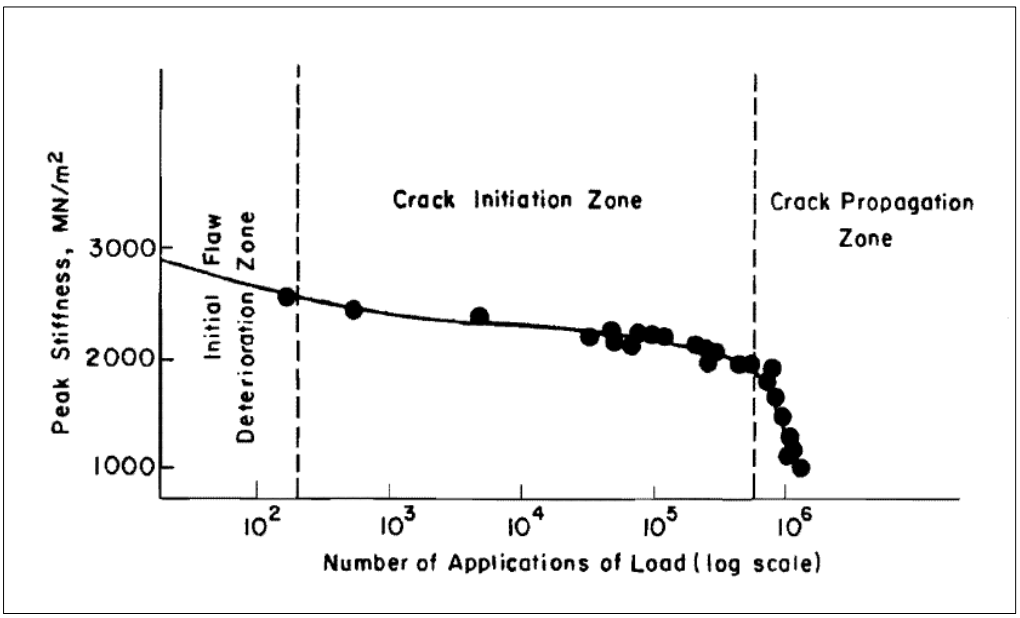

Figure 2.6 AC Stiffness Deterioration Curve (Freeme and Marais, 1973)

Freeme and Marais (1973) suggested the crack initiation point, which they recommended as the AC material's service life, be defined as the number of load repetitions corresponding to the intersection of the lines extrapolated from the crack initiation and propagation zones. They suggested the slope of the crack initiation and propagation zones were related to stiffness and load repetitions, according to Equation 17. They found the slope of the crack initiation zone was not significantly affected by temperature; the optimum slope was

recorded at 20°C. However, the slope of the crack propagation zone significantly increased as temperature decreased. No equation was reported for the determination of these slopes.

$$E = R\text{Log}\, N + E_i \quad (17)$$

Where:

E = AC flexural stiffness

R = Slope of the crack initiation (R_i) or crack propagation zone (R_p)

N = Number of load repetitions

E_i = AC stiffness at the first load application

Similarly, Adedimila and Kennedy (1975) studied AC fatigue behavior using indirect tensile testing and reported resilient modulus versus load cycle curves comprising three zones: (a) initial rapid drop in modulus for about 10% of fatigue life; (b) prolonged period of gradual decrease in modulus with increasing load cycles, representing between 10 and 80% of fatigue life; and (c) final rapid modulus reduction in the failure zone, corresponding to about 20% of fatigue life. Similar three-zone damage curves have been reported for test sections studied in accelerated testing facilities (Chen, 1998; Sebaaly et al., 1989; Ullidtz, 2005). Reasons attributed to the initial rapid drop in AC stiffness include structural flaws, rupture or reorientation of chemical bonds, adjustment to loading and secondary compaction (Freeme and Marais, 1973; Adedimila and Kennedy, 1975).

2.3 Summary of Literature Review

Common modeling approaches and laboratory test methods for characterizing bottom-initiated fatigue cracking were reviewed. A summary of the key findings are as follows:

- Empirical fatigue models, despite their straightforward application, do not fundamentally address the bottom-up fatigue cracking mechanism.
- Phenomenological modeling uses mechanistic analysis to improve fatigue performance prediction, but it is limited by the accuracy of transfer functions and non-inclusion of a damage parameter. Regardless, phenomenological modeling is a potential platform for future improvement in fatigue characterization due to its relative simplicity.
- Dissipated energy-based methods may provide a more fundamental fatigue analysis, but the effective separation of the dissipated energy components is a major challenge.

- Fatigue models premised on fracture mechanics theory provide physical interpretation of damage in terms of crack dimensions, but some consider the presence of crack a priori as a limitation. Complex simulation techniques, high computational power requirement and fracture property testing limitations are major drawbacks for routine application.
- Continuum damage theory-based models employ advanced material behavior theories, but current applications are subject to the limitations of empirical transfer functions.
- Beam fatigue testing simulates bottom-up fatigue cracking in a phenomenological approach and provides a typical three-zone damage curve like what has been observed in accelerated pavement test sections. The initial zone exhibits a rapid drop in stiffness, followed by a middle zone with a prolonged period of gradual decrease in stiffness; the last zone shows a rapid stiffness reduction toward failure conditions.
- To realistically simulate fatigue cracking damage, it is suggested phenomenological fatigue models incorporate a damage parameter to account for damage-induced changes in the AC.

CHAPTER 3

DEVELOPMENT OF PSEUDO FATIGUE CRACKING DAMAGE MODEL

As discussed in the literature review, mechanistic-empirical fatigue analysis is a two-step process: computation of critical tensile strains at the AC layer bottom and prediction of fatigue cracking, using empirical transfer functions. The key difference between the pseudo fatigue cracking damage model presented in this dissertation and conventional mechanistic-empirical fatigue models is that the current model does not utilize transfer functions. Instead, fatigue cracking is modeled as a function of deterioration in AC modulus in an incremental-recursive manner. It is assumed fatigue damage reduces AC modulus which, in turn, affects structural response. Accounting for AC modulus deterioration is a more realistic approach to model in-service fatigue cracking compared with mechanistic-empirical fatigue modeling methods which ignore damage. Due to the complexity of the field fatigue cracking phenomenon, the beam fatigue test, a well-known laboratory test method for simulating fatigue cracking, was adopted as a platform for the pseudo fatigue cracking damage model's development. The beam fatigue test has served as the foundation for fatigue damage modeling for over half a century. It was considered that if a model could be developed to successfully simulate measured beam fatigue damage curve in a layered elastic framework, then such a model could be expanded to simulate fatigue cracking under field conditions. The model development process is presented in the following subsections, starting with a description of data acquisition.

3.1 Data Acquisition

The National Center for Asphalt Technology (NCAT) Pavement Test Track (Figure 3.1), located at Opelika in Alabama, was the primary source of data. The oval-shaped Test Track is a 1.7-mile long full-scale, accelerated pavement testing facility comprising 46 test sections, each 200-ft. long. The test sections are classified as either structural or non-structural. The structural sections are instrumented with asphalt strain gauges, earth pressure cells and temperature sensors for collecting pavement performance data. The non-structural sections, which have no embedded instrumentation, are used for surface mixture performance evaluation and pavement preservation studies. A research cycle consists of a 1-year construction–forensic investigation period, followed by a 2-year performance monitoring period, during which manned triple-trailer trucks operating at a target speed of 45mph apply 10 million equivalent single-axle loads (ESALs). At the end of a research cycle, sections either remain in place for additional trafficking in the next cycle or are re-constructed for new experiments.

This study utilized beam fatigue test data from Superpave-designed base mixtures of 16 test sections constructed in the 2006, 2009 and 2012 research cycles; four sections were from 2006, eight from 2009 and four from 2012. The data were selected based on availability. Data from 12 test sections (Table 3.1), representing 75% of the available beam fatigue test data, were used for model calibration and data from the other four test sections (25%) constituted the validation dataset (Table 3.2). Out of the total of 158 beams, 117 (74%) were allocated for model calibration and 41 (26%) for model validation. As will be explained later, data from seven of the 158 beams were unsuitable for this study, thus reducing the sample size to 151. Of the 20 different asphalt mixtures, the calibration-validation data split was 75 to 25%. Tables 3.3 and 3.4 summarize mixture characteristics. Considering the beam fatigue test data originated from asphalt mixtures designed for a wide range of experimental objectives, the proportioning was carried out such that each dataset had a fair representation of research cycle, asphalt binder modification, recycled materials content and strain levels used in the beam fatigue testing.

Figure 3.1 NCAT Pavement Test Track

Table 3.1 Summary of Beam Fatigue Test Data Used for Model Calibration

Year	Number of Test Sections	Name of Test Sections	Number of Mixtures	Number of Beam Specimens Tested at Strain Level				Mixtures With Binder Modification	Asphalt Binder Modification	Number of Mixtures Containing RAP/RAS
				200 με	400 με	600 με	800 με			
2006	3	N9, S11, S12	3	0	8	0	9	1	SBS	0
2009	6	N5, N10, S8, S10, S11, S12	6	19	18	0	18	2	Shell Thiopave Trinidad Lake Asphalt	1
2012	3	N5, S5, S6	6	18	18	0	9	1	SBS	6
Total	**12**		**15**	**37**	**44**	**0**	**36**	**4**		**7**
				117						

Table 3.2 Summary of Beam Fatigue Test Data Used for Model Validation

Year	Number of Test Sections	Name of Test Sections	Number of Mixtures	Number of Beam Specimens Tested at Strain Level				Mixtures With Binder Modification	Asphalt Binder Modification	Number of Mixtures Containing RAP/RAS
				200 με	400 με	600 με	800 με			
2006	1	N10	1	-	3	-	3	-	-	-
2009	2	N7, N11	2	3	7	3	6	1	SBS	1
2012	1	S13	2	4	6	3	3	2	GTR, GTR	1
Total	**4**		**5**	**7**	**16**	**6**	**12**	**3**		**2**
				41						

Table 3.3 Summary Information on Mixtures Used for Model Calibration

Year	Test Section	Binder Grade (Modifier Type)	[a]Effective Binder (%)	RAP/RAS Content	NMAS (mm)	Bottom-Up Fatigue Cracking Performance
2006	N9	PG 64-22	7.0	None	12.5	No cracking in 2006, 2009 and 2012 Cycles
	S11	PG 67-22	5.0	None	19.0	Cracked in 2006 Cycle
	S12	PG 70-22 (SBS)	7.7	None	9.5	No cracking in 2006 Cycle
2009	N5	PG 67-22 (Shell Thiopave®)	5.8	None	19.0	No cracking in 2009 Cycle
	N10	PG 67-22	4.1	50% RAP	19.0	No cracking in 2009 Cycle. Cracked in 2012 Cycle
	S8	PG 67-22	4.4	None	19.0	No cracking in 2009 Cycle. Cracked in 2012 Cycle
	S10	PG 67-22	4.2	None	19.0	No cracking in 2009 Cycle. Cracked in 2012 Cycle
	S11	PG 67-22	4.5	None	19.0	No cracking in 2009 Cycle. Cracked in 2012 Cycle
	S12	PG 67-28 (Trinidad Lake Asphalt)	4.7	None	19.0	No cracking in 2009 Cycle. Unavailable 2012 Cycle
2012	S5 Intermediate Layer	PG 67-22	4.3	50% RAP	19.0	Cracked in 2012 Cycle
	S5 Intermediate Layer (Repave)	PG 67-22	4.3	50% RAP	19.0	Cracked in 2012 Cycle
	S6 Intermediate Layer	PG 67-22	4.3	25% RAP 5% PC-RAS	19.0	Cracked in 2012 Cycle
	N5	PG 67-22	4.1	35% RAP	19.0	Cracked in 2012 Cycle
	S5	PG 76-22	4.1	35% RAP	19.0	Cracked in 2012 Cycle
	S6	PG 76-22 (SBS)	4.8	25% RAP	19.0	Cracked in 2012 Cycle

Note: (a) Total Binder Content for 2006 Mixtures

Table 3.4 Summary Information on Mixtures Used for Model Validation

Year	Test Section	Binder Grade (Modifier Type)	[a]Effective Binder (%)	RAP/RAS Content	NMAS (mm)	Bottom-Up Fatigue Cracking Performance
2006	N10	PG 64-22	5.2	None	19.0	Cracked in 2006 Cycle
2009	N7	PG 88-22 (SBS)	4.2	None	19.0	No cracking in 2009 and 2012 Cycles
	N11	PG 67-22	4.0	50% RAP	19.0	No cracking in 2009 Cycle. Cracked in 2012 Cycle
2012	S13 Intermediate Layer	ARB12 (-30) (Ground Tire Rubber)	4.3	35% RAP	19.0	Cracked in 2012 Cycle
	S13 Base Layer	ARB20 (-16) (Ground Tire Rubber)	6.5	None	19.0	Cracked in 2012 Cycle

Note: (a) Total Binder Content for 2006 Mixtures

The 2006 structural test sections (N9, N10, S11) were designed mainly for the calibration of transfer functions, development of recommendations for mechanistic-based material characterization, characterization of pavement responses in rehabilitated pavements and determination of field-based fatigue endurance thresholds for perpetual pavements (Timm, 2009). The non-structural Section S12 was used to evaluate the effectiveness of a rich-bottom crack attenuating mixture at preventing reflective cracking (Willis et al., 2009). In the 2009 research cycle, five of the structural sections (N10, N11, S8, S10 and S11) were utilized to evaluate the performance of pavements constructed with warm-mix asphalt (WMA) technologies, high recycled asphalt pavement (RAP) contents, a combination of high RAP content and WMA (West et al., 2012; Vargas-Nordcbeck and Timm, 2013). Section N5 assessed pelletized sulfur technology (Thiopave®), while N7 sought to demonstrate the benefit of using highly modified binder in all structural layers (West et al., 2012). Section S12 used a conventional binder modified with 25% Trinidad Lake Asphalt (West et al., 2012). The structural study in the 2012 research cycle evaluated pavement performance and sustainability benefits of waste materials. Thus, the test sections (N5, S5, S6 and S13) incorporated RAP, recycled asphalt shingles and rubber-modified binder. The broad experimental objectives culminated in the use of both neat and modified binders, different binder contents and varying recycled material contents to achieve different fatigue performance characteristics.

3.1.1 Beam Fatigue Testing

Asphalt mixtures were sampled at the Test Track during construction of the test sections for beam fatigue testing. The mixtures were compacted with a kneading compactor to different target air void contents, depending on the experimental objectives. The 2006 and 2009 mixtures were compacted to 6.0 ± 1.0 percent air voids, except for two mixtures from 2009 (N5 and N7),

which were compacted to 7.0 ± 1.0 percent air voids. Also, the 2012 mixtures were compacted to 7.0 ± 1.0 percent air voids; however, the mixture for S13 was compacted to 11 ± 1.0 percent air voids. Beam specimens were cut to dimensions of 380 mm long by 50 mm thick by 63 mm wide and subjected to deflection-controlled haversine loading (ASTM D 7460) at a frequency of 10 Hz and at a test temperature of 20°C, except for the 2012 specimens, which underwent deflection-controlled sinusoidal loading (AASHTO T 321) under similar test conditions.

For each mixture, at least three replicate beam specimens were tested at a given strain level (200, 400, 600, 800με). Eight of the 20 mixtures were tested at two strain levels, while the remaining were tested at three strain levels. As Tables 3.1 and 3.2 indicate, 28% of the 158 beams were tested at 200με, 38% at 400με, 4% at 600με and 30% at 800με. The raw beam fatigue test data were used for the model development; there was no averaging in order to incorporate variability in the model building. Appendix A shows the number of replicate beams for each mixture and the strain levels at which they were tested. Depending on the research objectives, the beam specimens were tested to different failure points, such as 25, 30 and 50% reduction in the initial AC stiffness. However, 20 specimens tested at 200με and 3 tested at 400με did not reach failure point (50% reduction in the initial stiffness) after 12 million load cycles. The number of load cycles to failure was extrapolated, using either a single-stage or three-stage Weibull function, in accordance with the procedure developed under the NCHRP 09-38 project (NCHRP, 2010). In this study, failure was defined as number of load cycles corresponding to a 50% reduction in the initial AC stiffness. Appendix A shows the properties of each mixture (initial AC stiffness, binder grade, binder modification, binder content, recycled materials content) and fatigue performance characteristics (cycles to failure and field cracking). These pieces of information were assembled from various NCAT technical reports (e.g., Willis et al., 2009; Timm et al., 2009; Timm et al., 2012a; Timm et al., 2012b; West et al., 2012; Timm et al., 2013; Vargas-Nordcbeck and Timm, 2013; Timm et al., 2014).

Figures 3.2 and 3.3 present coefficient of variation (COV) of the initial AC stiffness and fatigue lives to show the variation in the beam fatigue test data, respectively. Comparatively, the initial AC stiffness had lower COV, generally increasing with strain level. While the high variability in the fatigue lives indicated wide-ranging fatigue performance characteristics, test variability could also be a related factor. The extrapolated fatigue lives contributed to the extremely high COV. By omitting the extrapolated fatigue lives corresponding to the 200με strain level, the COV drastically reduced from 332, 315 and 64% to 59, 61 and 46% for the full, calibration and validation datasets, respectively. However, at the 400με strain level, the deletion of the extrapolated fatigue lives caused a slight increase in

the COV values: they rose from 207, 258 and 149% to 224, 282 and 155 for the full, calibration and validation datasets, respectively. The beam specimens tested at 600 and 800με strain levels all failed; no fatigue life extrapolation was done.

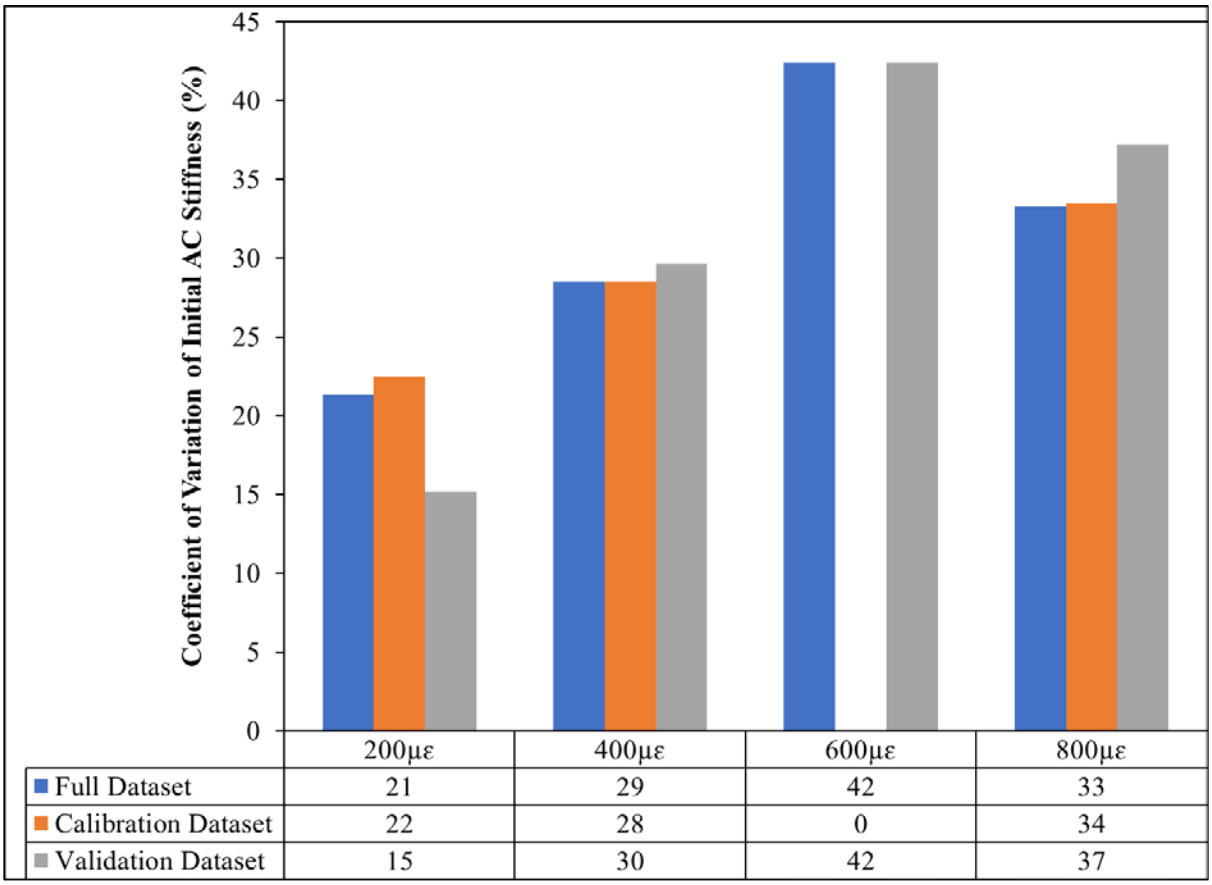

	200με	400με	600με	800με
Full Dataset	21	29	42	33
Calibration Dataset	22	28	0	34
Validation Dataset	15	30	42	37

Figure 3.2 Coefficient of Variation of Initial AC Stiffness in Beam Fatigue Testing

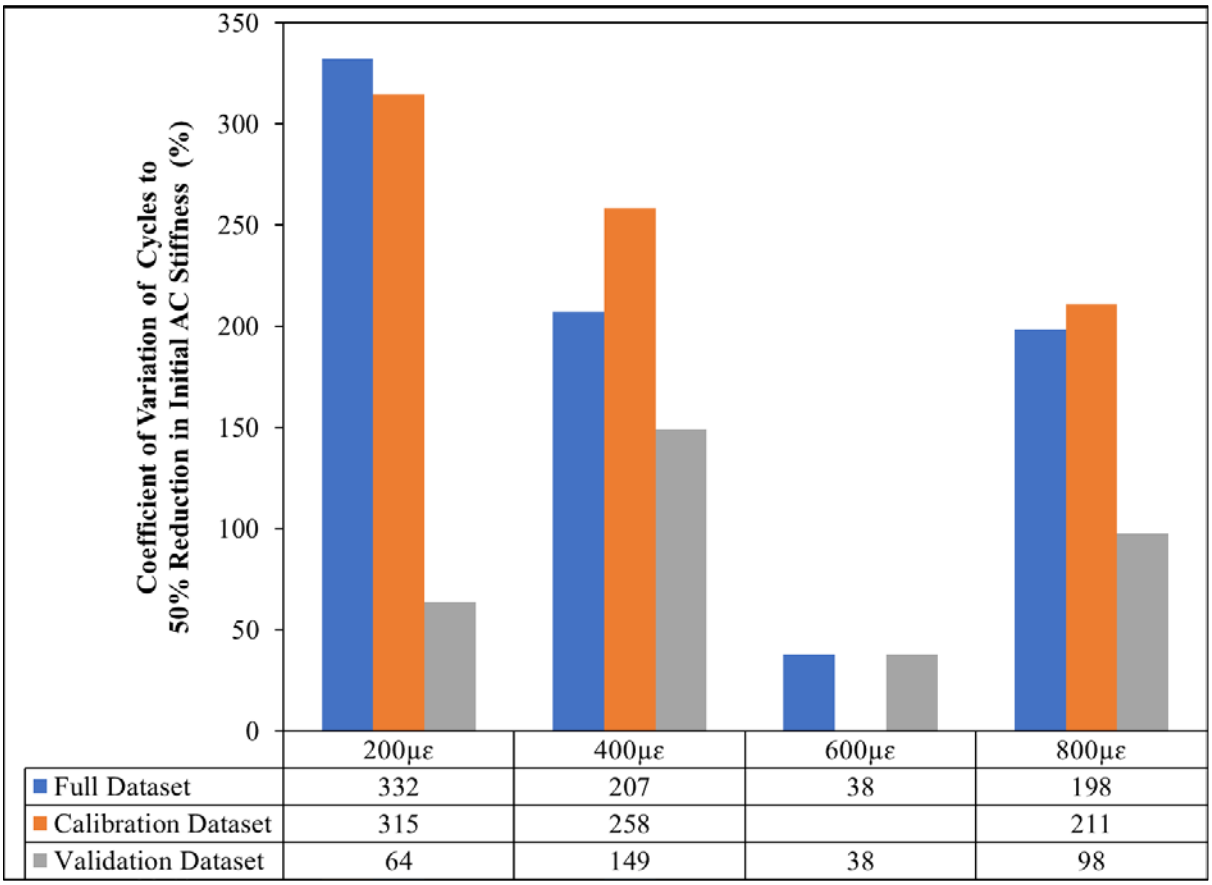

	200με	400με	600με	800με
Full Dataset	332	207	38	198
Calibration Dataset	315	258		211
Validation Dataset	64	149	38	98

Figure 3.3 Coefficient of Variation of Load Cycles to Failure in Beam Fatigue Testing

Figures 3.4 through 3.6 illustrate variability of beam fatigue test results for replicate beam specimens tested at the same strain level. In Figure 3.4, while Beams A and B survived 12 million applications of 200με without reaching a 50% decrease in the initial stiffness, the initial stiffness of Beam C reduced to 25% after approximately 4.7 million repetitions of 200με. Although the replicate beams in Figure 3.5 were all tested at 400με to 25% reduction in the initial stiffness, notice the significant difference in the fatigue lives of Beams A and B versus that of Beam C; the fatigue life of Beam C is twice that of Beam B. The specimens in Figure 3.6 were tested at 800με, Beams A and B to 30% reduction in the initial stiffness and Beam C to a 30% reduction. Interestingly, while the fatigue curves of Beams B and C are overlapping, that of Beam A seems to be an outlier. These examples highlight the variable nature of beam fatigue test data. In summary, this variability analysis is a useful reference for discussing the robustness of the proposed pseudo fatigue damage model.

The cases presented above are not isolated, as variability of beam fatigue test data is well-recognized. For instance, the NCHRP 09-38 project, based on a limited round robin testing, suggested the coefficient of variation of the logarithm of the fatigue lives of properly

conducted beam fatigue tests at normal strain levels for within- and between-laboratory variability is 5.4 and 6.8%, respectively. The difference between the logarithm of fatigue lives (logarithm of fatigue life of Sample 1 minus logarithm of fatigue life of Sample 2) of two properly conducted tests should not exceed 0.69 for a single operator or 0.89 between two laboratories (NCHRP, 2010). It should be noted that the beam fatigue test data used to build the pseudo fatigue damage model were not subjected to these precision statistics.

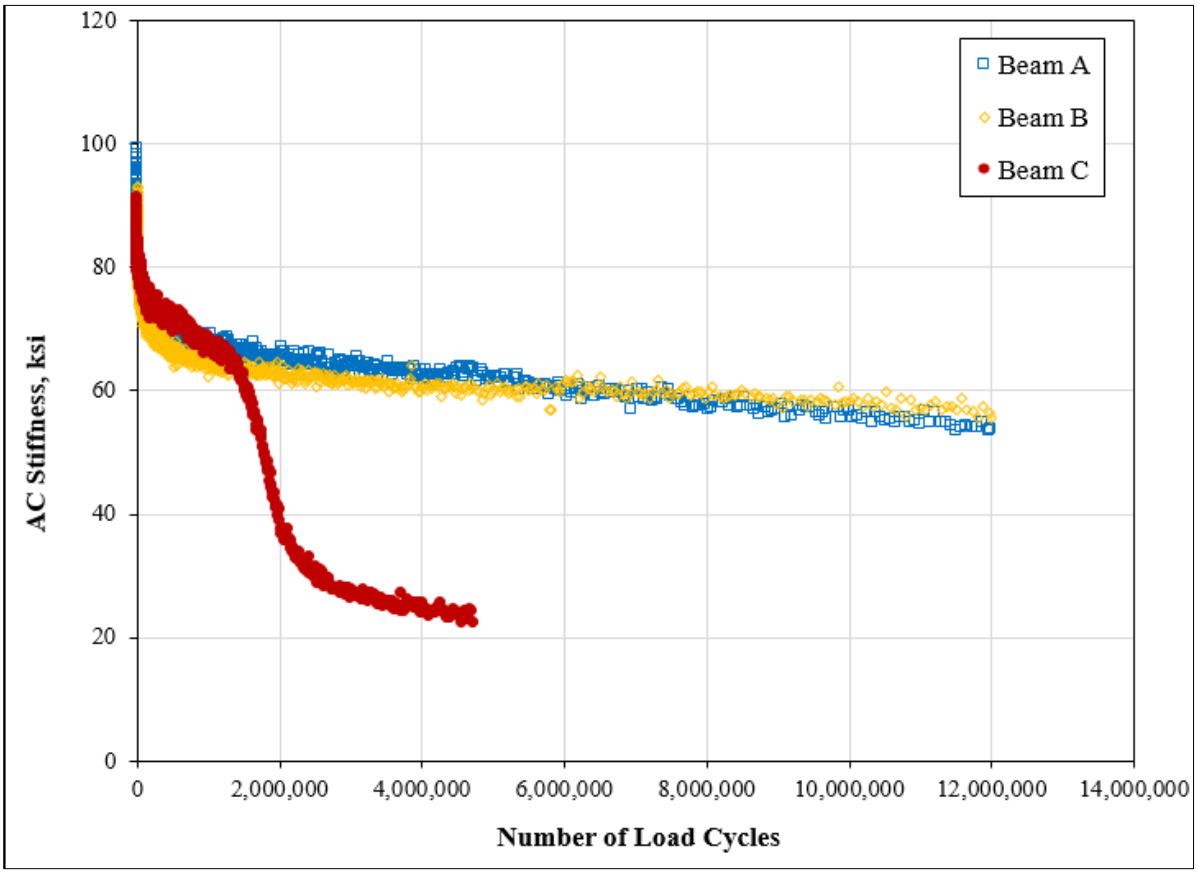

Figure 3.4 Fatigue Curves of Three Replicate Beams Tested at 200με (2009 Section N5)

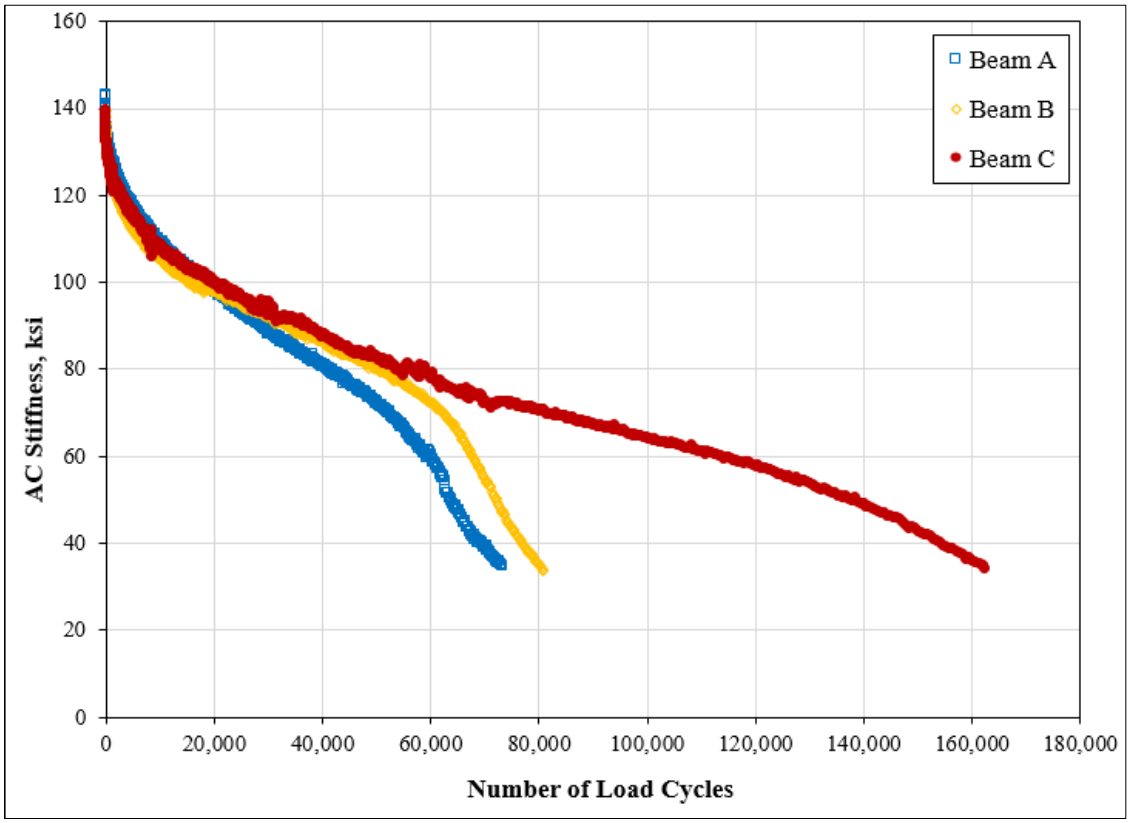

Figure 3.5 Fatigue Curves of Three Replicate Beams Tested at 400με (2012 Section N5)

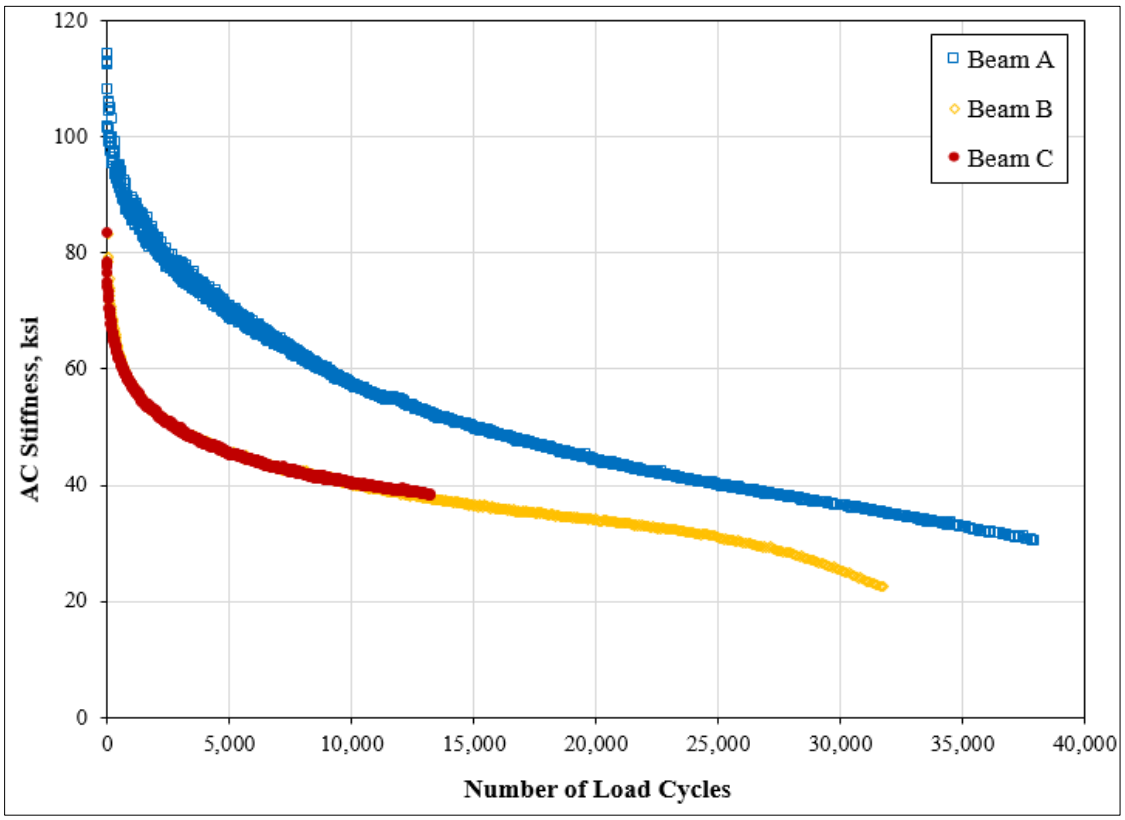

Figure 3.6 Fatigue Curves of Three Replicate Beams Tested at 800με (2006 Section S11)

3.1.2 Prediction of Fatigue Endurance Limits

Fatigue endurance limit (FEL), an asphalt mixture property often determined from laboratory fatigue testing, has an enormous impact on pavement structural design. It is a level of strain below which no fatigue damage accumulation occurs. A wide range of endurance limits has been reported. For instance, Monismith and McLean (1972) first reported fatigue endurance limit of 70με; Nishizawa et al. (1997) analyzed in-service pavements and reported 200με; Wu et al. (2004), through falling weight deflectometer backcalculation, obtained values between 96 and 158με; Bhattacharjee et al. (2009) reported values ranging from 115 to 250με, based on uniaxial fatigue testing; a value of 100με has also been suggested (Carpenter et al., 2003; Thompson and Carpenter, 2006). Recently, research at the NCAT Test Track indicates pavements can withstand a distribution of strains without accumulating fatigue damage (Willis and Timm, 2009). FEL is an important parameter used for the computation of damage by the proposed pseudo fatigue damage model because critical tensile strains at the bottom of the AC layer that exceed the FEL of the AC mixture is an indication of the level of fatigue damage.

For this study, two methods of determining FEL were evaluated: the healing-based approach proposed by the NCHRP 9-44A project (NCHRP, 2013) and the traffic capacity analysis approach developed under NCHRP 09-38 (NCHRP, 2010). Both procedures rely on beam fatigue and uniaxial compression-tension testing, but attention was focused on beam fatigue testing. The NCHRP 9-44A procedure investigated the relationship between FEL and AC mixture properties, specimen loading conditions and temperature. The phenomenon of AC healing featured prominently in the analysis. Fatigue endurance limit was considered to emanate from a balance between damage and healing during rest periods between load applications. A plot of stiffness ratio (stiffness at load cycle *i* divided by initial stiffness) versus load cycles for a fatigue test conducted without a rest period was found to be steeper than a fatigue test conducted with a rest period. It was suggested that, if full healing occurs after each load cycle, there should be no damage accumulation and stiffness ratio should remain unity.

The NCHRP 9-44A researchers conducted a comprehensive factorial design for beam fatigue testing (AASHTO T 321) of 19-mm Superpave mixtures involving three binder grades (PG 58-28, PG 64-22 and PG 76-16), two binder contents (4.2 and 5.2%), two air void contents (4.5 and 9.5%), three strain levels (low, medium and high), three temperatures (40, 70 and 100 ^{o}F) and four rest periods (0, 1, 5 and 10s) to obtain data from 468 beam specimens. The data were used to develop a regression model to relate stiffness ratio to binder grade, binder content, air voids, temperature, initial strain, load cycles and rest period. However, initial stiffness

emerged as a surrogate for binder content, air voids, binder grade and temperature. If stiffness ratio is set to one, the strain variable becomes the fatigue endurance limit.

The final model, with an adjusted coefficient of determination (R^2) of 0.891, is shown in Equation 18 (NCHRP, 2013). Load cycles was found to have a minor effect on stiffness ratio (and hence on endurance limit), particularly for rest periods greater than 1s. This was considered a validation of the assumption of complete healing during rest periods. Hence, the researchers used 200,000 load cycles for predicting FEL. The threshold rest period for healing was identified to range from 5 to 10s, for a loading duration of 0.1s; reportedly, a rest period greater than this range achieved no additional healing in the laboratory. It was noted that FEL should increase with decreasing AC stiffness (material becomes ductile) and longer rest period.

$$\begin{aligned} SR = {} & 2.0844 - 0.1386\text{Log}(E_0) - 0.4846\text{Log}(\varepsilon_t) - 0.2012\text{Log}(N) \\ & + 1.4103\text{Tanh}(0.8471RP) + 0.0320\text{Log}(E_o) * \text{Log}(\varepsilon_t) - 0.0954\text{Log}(E_0) \\ & * \text{Tanh}(0.7154RP) - 0.4746\text{Log}(\varepsilon_t) * \text{Tanh}(0.6574RP) + 0.0041\text{Log}(N) \\ & * \text{Log}(E_0) + 0.0557\text{Log}(N) * \text{Log}(\varepsilon_t) + 0.0689\text{Log}(N) \\ & * \text{Tanh}(0.2594RP) \end{aligned} \quad (18)$$

Where:

SR	=	Stiffness ratio
E_o	=	Initial flexural beam stiffness, ksi
ε_t	=	Applied tensile microstrain (tensile portion of the tension-compression loading cycle, or half peak-to-peak)
RP	=	Rest period between load cycle, s
N	=	Number of load cycles

The definition of fatigue endurance limit – a strain level below which no fatigue damage accumulates over an infinite number of load cycles – suggests it is impractical to test beam specimens to an infinite number of load cycles. Consequently, the NCHRP 09-38 procedure (NCHRP, 2010), based on traffic capacity analysis and a laboratory-field shift factor of 10, suggested that beam fatigue testing to 50 million load cycles represented 500 million design traffic load repetitions in a 40-year pavement service life. This practical definition of a long-life pavement was recommended for predicting fatigue endurance limit.

The NCHRP 09-38 methodology for predicting FEL is straightforward. Beam fatigue testing is conducted on three replicate beam specimens to determine load cycles to failure (corresponding to 50% reduction in initial stiffness) at three strain levels (e.g., 300, 500 and

700με). Preferably, all nine specimens should be tested to failure. Strain is plotted versus load cycles to failure in a log-log space. A linear regression equation is fitted and used to predict strain (FEL) for a fatigue life of 50 million cycles. Finally, 95% lower bound FEL is computed using Equation 19 (NCHRP, 2010). Notice that this procedure predicts FEL at a single temperature, but FEL is a temperature-dependent AC material property (NCHRP, 2010).

$$\text{Endurance Limit} = \hat{y}_0 - t_\alpha s\sqrt{1 + \left(\frac{1}{n}\right) + \frac{(x_0 - \bar{x})^2}{S_{xx}}} \quad (19)$$

Where:

$\hat{y}_0$ = Logarithm of predicted fatigue endurance limit

t_α = One-sided critical *t* value for *n*-2 degrees of freedom and $\alpha = 0.05$

s = Standard error from regression analysis

n = Number of beam samples

$S_{xx} = \sum_{i=1}^{n}(x_i - \bar{x})^2$

x_i = Logarithm of fatigue lives

$\bar{x}$ = Average of logarithm of fatigue lives

x_0 = $\text{Log}\ (50{,}000{,}000) = 7.69897$

Figure 3.7 compares the fatigue endurance limits computed using the NCHRP 9-44A and NCHRP 09-38 procedures for the 20 asphalt mixtures comprising the dataset for this study. Appendix B presents the full set of the fatigue endurance limits. The NCHRP 9-44A-derived endurance limits corresponded to rest periods of 5, 8 and 10s and load cycles of 200,000. The endurance limits obtained for rest periods of 10 and 20s were practically the same, as suggested by the researchers. The endurance limits were averaged for the number of specimens tested. On the average, the endurance limits obtained from the NCHRP 09-38 procedure were 60, 37 and 34% greater than those derived from the NCHRP 9-44A procedure corresponding to 5, 8 and 10s, respectively. A paired *t*-test at 5% significance level ($\alpha = 0.05$) confirmed the differences were significant (p-values of < 0.000, 0.005 and 0.008, respectively).

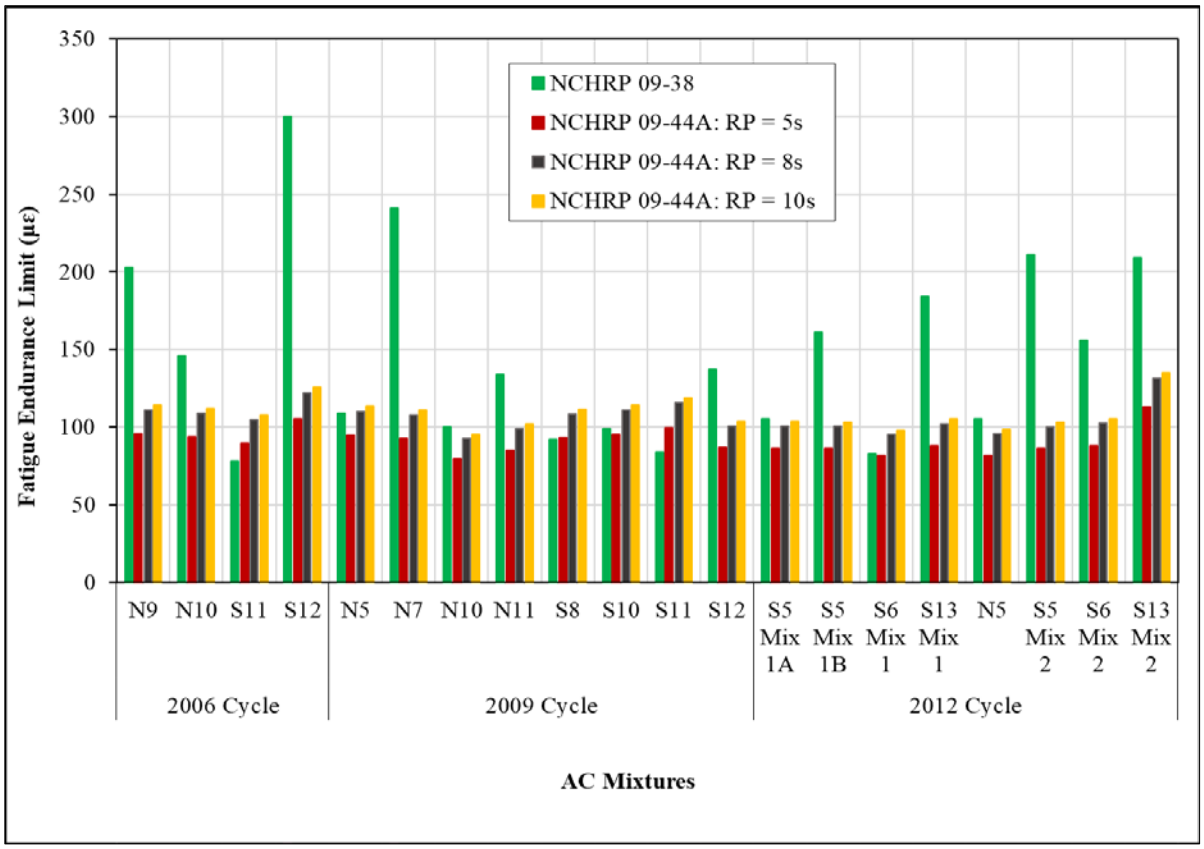

Figure 3.7 Fatigue Endurance Limits from NCHRP 9-44A and NCHRP 09-38 Models

Mixtures from Sections N9 and S12 (2006 research cycle), N7 (2009 research cycle) and S13 intermediate layer and S5 base layer (2012 research cycle) had prominently high FELs. The averaged endurance limits of these five mixtures determined using the NCHRP 09-38 method exceeded their NCHRP 9-44A counterparts by 142, 109 and 103% for rest periods of 5, 8 and 10s, respectively. As seen in Tables 3.3 and 3.4, Section N9 had rich-bottom mixture produced with unmodified PG 64-22 at 7% binder content. Similarly, S12 incorporated a rich-bottom mixture (crack attenuating mixture) with 7.7% of SBS-modified PG 70-22 binder. The mixture in Section N7 was produced with SBS-modified PG 88-22 binder at 4.2% effective binder content. The intermediate base mixture for S13, which contained 35% RAP, utilized 4.3% effective content of GTR-modified binder. Also, the mixture for S5 base consisted of 4.1% effective binder content of PG 76-22 and 35% RAP. Considering field performance, Sections N9, S12 and N7 survived 30, 10 and 20 million ESALs, respectively, without experiencing bottom-up fatigue cracking (Willis and Timm, 2009). However, Sections S5 and S13 cracked within their research cycles. It may be suggested that the high FEL influenced the good field fatigue performance. Hence, it appears the NCHRP 09-38 procedure for the

prediction of FEL better captures the effects of binder modification, rich-bottom layer and recycled materials.

Studies (e.g., Goodrich, 1988; Asphalt Pavement Alliance, 2002; Lee et al., 2002; Von Quintus, 2004) show that binder modification and rich mixtures improve fatigue performance, and this is reflected in the high endurance limits predicted by the NCHRP 09-38 procedure. As previously noted, the NCHRP 9-44A researchers indicated FEL increases with longer rest periods. This trend is noticeable in Figure 3.7. The intermediate mixture for S13 and base mixture for S5 recorded high initial stiffness values due to the 35% RAP and the binder grade. Because the NCHRP 9-44A model predicts low endurance limits for high-modulus mixtures, the endurance limits of S13 and S5 were lower. Based on these findings, it was concluded the laboratory-measured fatigue endurance limits obtained from the NCHRP 09-38 procedure would be used for calibrating the pseudo fatigue cracking damage model.

3.2 Description of Pseudo Fatigue Cracking Damage Model

The proposed pseudo fatigue cracking damage model is a strain-based phenomenological model that employs layered elastic theory for bottom-initiated fatigue cracking analysis. Typical of phenomenological fatigue models, the model does not separate crack initiation and crack propagation. The term ‘pseudo’ indicates there is no physical representation of damage in terms of crack size, as it is the case with fracture mechanics-based models. Instead, fatigue damage is simulated as a function of AC modulus deterioration. The model’s fundamental assumption, which is shared by continuum damage-based models, is that fatigue damage reduces AC modulus. Although fatigue damage, aging, temperature and load duration (vehicle speed) could all affect in-situ AC modulus, the current model considers only damage; the other effects may be accounted for when the model is implemented in a pavement design system.

Fatigue damage is defined as a reduction in AC modulus due to traffic loading. A key question is: how can AC modulus reduction in a pavement system be simulated in an incremental-recursive manner using layered elastic theory? Finding an answer to this question will be a significant step toward addressing a major limitation of conventional M-E fatigue cracking damage modeling: non-inclusion of fatigue damaging effect on AC modulus. Thus, the proposed model combines the advantages of the widely-used layered elastic theory and the effect of damage on AC modulus. The operation of the model is straightforward: layered elastic theory is used to analyze a pavement structure to determine maximum horizontal tensile strain (critical strain) at the AC layer bottom. The critical strain is then utilized to adjust the AC modulus to reflect the amount of fatigue damage. Thus, incremental fatigue damage becomes

a function of historical damage, current damage, load cycle increment and tensile structural response. In general, the proposed pseudo fatigue cracking damage model is an incremental-recursive mechanistic procedure that predicts fatigue performance by using changes in tensile structural response as a fatigue damage determinant to modify AC modulus.

3.3 Formulation of Pseudo Fatigue Cracking Damage Model

Prior to the formulation of the pseudo fatigue cracking damage model, there was a need to select material response and structural analysis models. Although AC is a viscoelastic material, elastic modulus was adopted due to its simplicity and reasonable accuracy to characterize AC response to traffic loading. Consequently, layered elastic theory was selected for structural analysis to determine critical tensile strains. Layered elastic theory assumes (Huang, 2012): (a) pavement layers are homogeneous, isotropic, infinite in areal extent and linearly elastic, which allows characterization by elastic modulus and Poisson's ratio; (b) layer thicknesses are finite, except for the subgrade; (c) traffic load is applied over a circular area; and (d) continuity conditions are satisfied at layer interfaces. WESLEA, a windows-based program that utilizes layered elastic theory to determine pavement responses, was selected for the structural analysis.

3.3.1 Preliminary Specifications of Pseudo Fatigue Cracking Damage Model

The search for a functional form of the pseudo fatigue cracking damage model followed the iterative process in Figure 3.8. The goal was to determine a recursive model that could reasonably predict beam fatigue damage curve. As noted previously, beam fatigue testing was the foundation for the development of the pseudo fatigue cracking damage model. In the iterative process, WESLEA analyzed a pavement structure to determine critical tensile strain at the AC layer bottom. If the critical strain exceeded a threshold strain (fatigue endurance limit), the AC layer was considered to have incurred fatigue damage, and the modulus was reduced by a certain quantum, as determined by the pseudo fatigue cracking damage model. The adjusted AC modulus was then used in the subsequent structural analysis to determine critical strain at the AC layer bottom. If the critical strain was greater than the fatigue endurance limit, the amount of damage was computed, and the AC modulus was reduced, as per the amount determined by the pseudo fatigue model. This recursive process continued until the AC modulus reached a failure criterion. In this study, failure was defined as a 50% reduction in the initial AC modulus; however, in this preliminary investigation, the target was to simulate the full beam fatigue curve. A plot of AC modulus versus load cycles represented a fatigue damage curve for the simulated pavement structure.

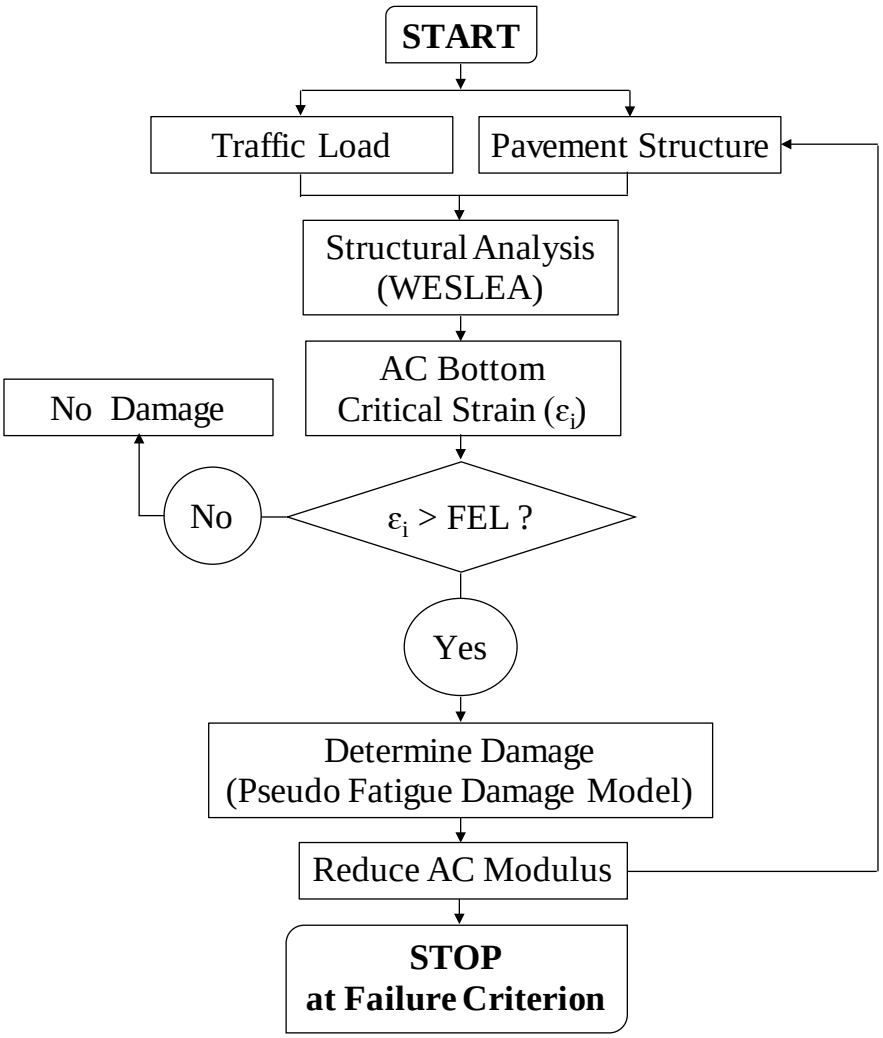

Figure 3.8 Flowchart for Executing Preliminary Pseudo Fatigue Damage Models

Nine trial pseudo fatigue cracking damage models were evaluated to predict fatigue damage curves for the typical 3-layer pavement structure in Table 3.5 by implementing the iterative process in Figure 3.8. The AC modulus of 1,412 ksi was the initial stiffness obtained from beam fatigue testing of the AC mixture constructed on Section N5 at the NCAT Test Track during the 2012 research cycle. An 18-kip steer axle, with a tire inflation pressure of 100 psi, was simulated. From the WESLEA analysis, the axle load induced an initial critical strain of 200με at the AC layer bottom when the pavement was in an undamaged condition; this strain value corresponded to the value used in the beam fatigue testing. By this arrangement, the beam fatigue test was conceptually simulated in a layered elastic pavement system. The beam fatigue testing was conducted in accordance with AASHTO T 321. The constant strain of 200με was applied at a frequency of 10 Hz for 6,442,250 cycles and at a test temperature 20°C. The AC mixture contained 35% RAP and unmodified PG 67-22 binder at an effective content of 4.1 %.

Table 3.5 Pavement Simulated with Pseudo Fatigue Cracking Damage Models

Layer	Thickness (in.)	Modulus (ksi)	Poisson's Ratio
Asphalt Concrete	6.5	1,412	0.35
Granular Base	10.0	15	0.40
Subgrade Soil	Infinite	5	0.45

Table 3.6 summarizes the trial models and their performance characteristics. The unknown model parameters were beta (β) and fatigue endurance limit. The β-parameter was idealized as a fatigue damage related parameter and fatigue endurance limit as fatigue damage resistant parameter, and hence both needed accurate determination. However, in this preliminary investigation, fatigue endurance limit was assumed to be 100με, while the β-parameter was varied until the corresponding fatigue damage curve matched the measured fatigue curve. The quality of fit was measured with coefficient of determination, computed using Equation 20.

$$R^2 = 1 - \frac{\sum_{i=1}^{n}\left(E_m - E_p\right)^2}{\sum_{i=1}^{n}(E_m - \overline{E}_m)^2} \quad (20)$$

Where:

R^2 = Coefficient of determination

E_m = Measured AC stiffness, psi

Ep = Predicted AC stiffness, psi

$\overline{E}_m$ = Average of measured AC stiffness, psi

n = Number of iterations

As Table 3.6 shows, early attempts at formulating a functional form for the pseudo fatigue cracking damage model centered on finding an expression (Models 1 through 3) for calculating a modulus reduction factor based on AC mixture property (fatigue endurance limit) and mechanistic pavement response (critical tensile strain at the AC layer bottom). The fatigue damage curves obtained from the modulus-reduction-factor models showed weak correlation with measured fatigue curves, hence a new generation of pseudo fatigue cracking damage models were explored. Through continuous searching, it was found that models with the general form in Equation 21 demonstrated potential for predicting beam fatigue curves.

$$E_i = E_0 - (\text{Damage})_i \quad (21)$$

Where:

E_i = AC modulus at load cycle *i*

E_o = Initial AC modulus

Damage = AC modulus deduct to account for fatigue damage at load cycle *i*

Models 4 through 9 in Table 3.6 show expressions for calculating AC modulus deduct values, which could be considered as the amount of fatigue damage. Damage was determined based on the quantum by which critical tensile strains exceeded fatigue endurance limit, number of load cycles, and a fatigue damage related parameter (β-parameter). The number of load cycles is a power function of strain ratio (α-factor), which is a ratio of critical strain at load cycle *i* and fatigue endurance limit, in the case of Models 5 through 9. In Model 4, the α-factor is the difference between the critical strain and fatigue endurance limit normalized to the fatigue endurance limit. Thus, by raising load cycles to a power function of critical strain and fatigue endurance limit helps to capture the effect of damage accumulation due to repetitive traffic loading.

Table 3.6 Performance of Trial Pseudo Fatigue Cracking Damage Models

No.	Model Functional Form	Variable Definition	Model Description	Performance Characteristics
1	$MRF = \left(\frac{\varepsilon_0}{\varepsilon_i}\right)^{\beta}$	MRF = AC modulus reduction factor ε_0 = Fatigue endurance limit, με ε_i = Critical strain at load cycle *i*, με β = Fatigue damage parameter	AC modulus reduction factor (damage) is computed as a function of fatigue endurance limit, critical strain and β-parameter	Faster modulus deterioration. Model unable to reasonably predict beam fatigue curve
2	$MRF = \beta\left\{1 - \left(\frac{\varepsilon_i - \varepsilon_0}{\varepsilon_0}\right)\right\}$	MRF = AC modulus reduction factor ε_i = Critical strain at load cycle *i*, με ε_0 = Fatigue endurance limit, με β = Fatigue damage parameter	AC modulus reduction factor (damage) is computed as a function of fatigue endurance limit, critical strain and β-parameter	Model fails to function for critical strains of at least twice the fatigue endurance limit
3	$MRF = \beta\left\{1 - \left(\frac{\varepsilon_i - \varepsilon_{i-1}}{\varepsilon_i}\right)\right\}$	MRF = AC modulus reduction factor ε_i = Critical strain at load cycle *i*, με ε_{i-1} = Critical strain at load cycle *i*-1, με β = Fatigue damage parameter	AC modulus reduction factor (damage) is a function of normalized difference between successive critical strain and β-parameter	For larger load cycles, the strain ratio exceeds one and MRF becomes negative
4	$E_i = E_o - \beta Log(N^{\alpha})$ $\alpha = \left(\frac{\varepsilon_i - \varepsilon_0}{\varepsilon_0}\right)$	E_i = AC modulus at load cycle *i*, psi E_o = Initial AC modulus, psi β = Fatigue damage parameter N = Load cycle ε_i = Critical strain at load cycle *i*, με ε_0 = Fatigue endurance limit, με	AC modulus deduct (damage) is determined based on number of load cycles, fatigue endurance limit, critical strain and β-parameter	Model reasonably predicts initial zone of beam fatigue curve; fast modulus deterioration in middle zone
5	$E_i = E_o - \beta Log(N^{\alpha})$ $\alpha = \left(\frac{\varepsilon_i}{\varepsilon_0}\right)$	E_i = AC modulus at load cycle *i*, psi E_o = Initial AC modulus, psi β = Fatigue damage parameter N = Load cycle ε_i = Critical strain at load cycle *i*, με ε_0 = Fatigue endurance limit, με	AC modulus deduct (damage) is determined based on number of load cycles, fatigue endurance limit, critical strain and β-parameter	Model reasonably predicts initial zone of beam fatigue curve; modulus deterioration in middle zone is faster than in Model 4

Table 3.6 cont'd

No.	Model Functional Form	Variable Definition	Model Description	Performance Characteristics
6	$E_i = E_o - \alpha_1 \beta Log(N^{\alpha_2})$ $\alpha_1 = \left(\frac{\varepsilon_i - \varepsilon_0}{\varepsilon_0}\right)$ $\alpha_2 = \left(\frac{\varepsilon_i}{\varepsilon_0}\right)$	E_i = AC modulus at load cycle *i* E_o = Initial AC modulus, psi β = Fatigue damage parameter N = Load cycle ε_i = Critical strain at load cycle *i*, με ε_0 = Fatigue endurance limit, με	AC modulus deduct (damage) is determined as a function of load cycles, fatigue endurance limit, critical strain and β-parameter	Model reasonably predicts initial zone and some portion of middle zone of beam fatigue curve. The α_1 factor decays AC modulus faster than required
7	$E_i = E_o - k\beta Log(N^{\alpha_2})$ $k = 1 + Log(\alpha_1)$ $\alpha_1 = \left(\frac{\varepsilon_i - \varepsilon_0}{\varepsilon_0}\right)$ $\alpha_2 = \left(\frac{\varepsilon_i}{\varepsilon_0}\right)$	E_i = AC modulus at load cycle *i*, psi E_o = Initial AC modulus, psi β = Fatigue damage parameter N = Load cycle ε_i = Critical strain at load cycle *i*, με ε_0 = Fatigue endurance limit, με	AC modulus deduct (damage) is determined as a function of load cycles, fatigue endurance limit, critical strain and β-parameter	Model reasonably predicts beam fatigue curve, except for the tertiary zone. Model shows potential and was selected for further investigation
8	$E_i = E_o - k\beta Log(N^{\alpha_2})$ $k = 1 + Ln(\alpha_1)$ $\alpha_1 = \left(\frac{\varepsilon_i - \varepsilon_0}{\varepsilon_0}\right)$ $\alpha_2 = \left(\frac{\varepsilon_i}{\varepsilon_0}\right)$	E_i = AC modulus at load cycle *i*, psi E_o = Initial AC modulus, psi β = Fatigue damage parameter N = Load cycle ε_i = Critical strain at load cycle *i*, με ε_0 = Fatigue endurance limit, με	AC modulus deduct (damage) is determined as a function of load cycles, fatigue endurance limit, critical strain and β-parameter	Model deteriorates AC modulus faster than Model 7. It reasonably predicts beam fatigue curve, except for the tertiary zone. Model 8 was noted for further investigation

Table 3.6 cont'd

No.	Model Functional Form	Variable Definition	Model Description	Performance Characteristics
9	$E_i = E_o - {\alpha_1}^{0.5}\beta Log(N^{\alpha_2})$ $\alpha_1 = \left(\frac{\varepsilon_i - \varepsilon_0}{\varepsilon_0}\right)$ $\alpha_2 = \left(\frac{\varepsilon_i}{\varepsilon_0}\right)$	E_i = AC modulus at load cycle *i*, psi E_o = Initial AC modulus, psi β = Fatigue damage parameter N = Load cycle ε_i = Critical strain at load cycle *i*, με ε_0 = Fatigue endurance limit, με	AC modulus deduct (damage) is determined as a function of number of load cycles, fatigue endurance limit, critical strain and β-parameter	Model's predictive power is weaker than those of Models 7 and 8

The predictions of Models 4 and 5 did not compare favorably with measured fatigue curves. To regulate the fast modulus deterioration observed in their predictions, an α_1-factor (normalized strain differential) was introduced in Model 6 to capture the influence of the strain condition at the bottom of the AC layer and fatigue damage resistance of the AC material, but this intervention resulted in a minor improvement in the model's predictions. Consequently, a k-factor was incorporated in Models 7 and 8 to better regulate damage accumulation. The k-factor is one plus the logarithm of the normalized difference between critical strain and fatigue endurance limit. Model 7 uses logarithm to base 10 in the k-factor, thus making its damage accumulation rate slower than that of Model 8, which utilizes natural logarithm. Model 9 took the square root of the normalized strain differential (α_1-factor) to regulate fatigue damage, but this approach was less successful compared with the use of the k-factors in Models 7 and 8.

The formulation of the pseudo fatigue cracking damage models was intended to capture the effect of growing fatigue damage due to recursive load applications, a missing component in most conventional mechanistic-empirical fatigue modeling methods. The calibration of the models involved determining a predictive equation for β-parameter. A properly calibrated model, coupled with well-characterized design inputs, could provide a simplified mechanistic procedure for characterizing fatigue cracking damage without the use of transfer functions.

3.3.2 Performance of Preliminary Pseudo Fatigue Cracking Damage Models

The preliminary investigation identified Models 7 and 8 as strong potential pseudo fatigue cracking damage models. This conclusion was based on the reasonable match between their predicted damage curves and beam fatigue curves. As Figure 3.9 shows, in simulating the pavement cross-section in Table 3.5, β-parameters of 22,000 and 17,800 reasonably fitted Models 7 and 8, respectively, to the measured fatigue curve, assuming fatigue endurance limit of 100με. Both predicted curves had an initial rapid stiffness reduction zone, followed by a prolonged, gradual stiffness reduction zone, but failed to adequately capture the tertiary zone of the measured fatigue curve. Coefficient of determination (R^2), which measured the quality of fit, were 76 and 90% for Models 7 and 8, respectively. Based on these preliminary results, Models 7 and 8 were selected for further investigation as pseudo fatigue cracking damage models. Clearly, the β-parameter has an important influence on the predictive capability of the models, and so its accurate determination would be paramount to the utility of the final pseudo fatigue cracking damage model.

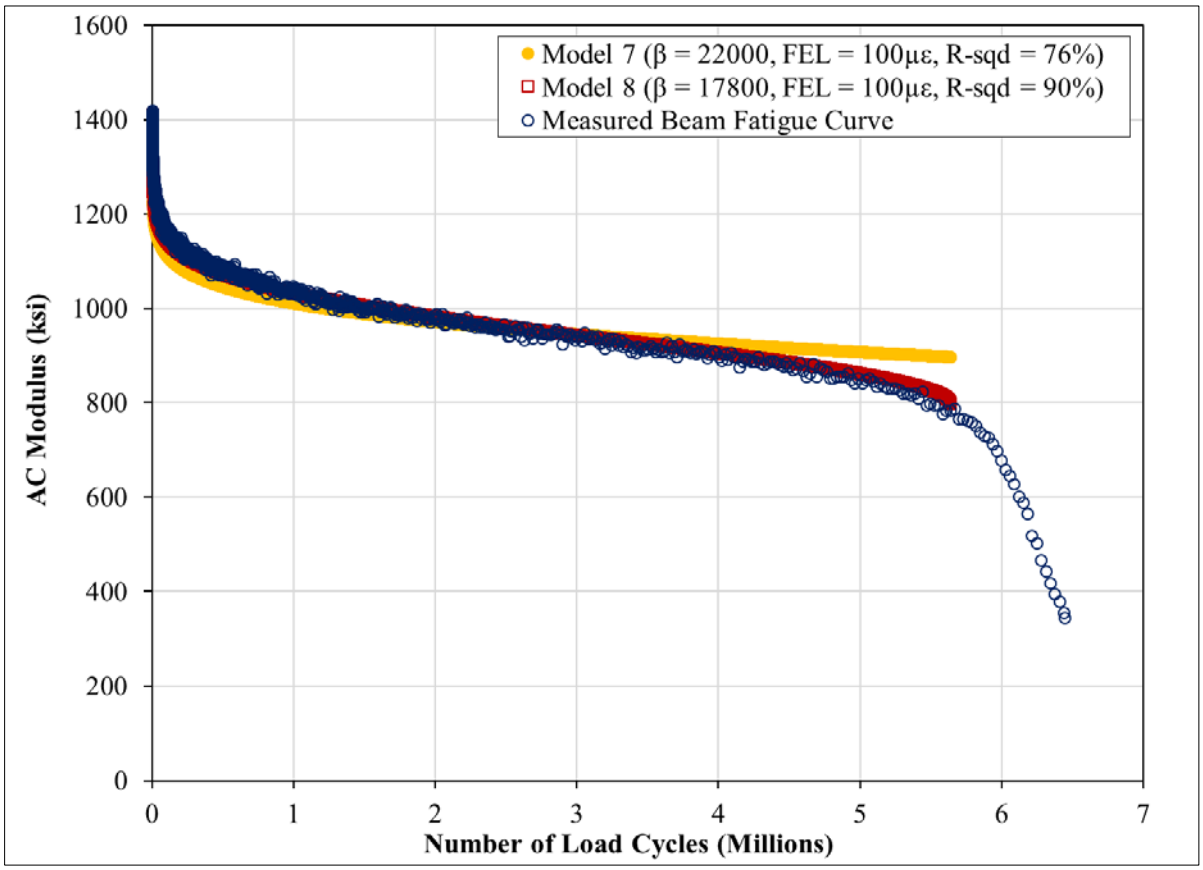

Figure 3.9 Measured Beam Fatigue Curve versus Predicted Fatigue Curves

3.3.3 Selected Pseudo Fatigue Cracking Damage Model

Based on their preliminary performance, Models 7 and 8 were further scrutinized prior to calibration using the entire data set. The models are merged in Equation 22 for easy reference. Model 7 differs from 8 only in terms of the use of logarithm to base 10 in the k-factor versus the use of natural logarithm in the k-factor of Model 8.

$$E_i = E_o - k\beta Log(N^{\alpha_2}) \quad (22)$$

$$\text{For Model 7:} \quad k = 1 + Log(\alpha_1) \quad (22a)$$

$$\text{For Model 8:} \quad k = 1 + Ln(\alpha_1) \quad (22b)$$

$$\alpha_1 = \left(\frac{\varepsilon_i - \varepsilon_0}{\varepsilon_0}\right) \quad (22c)$$

$$\alpha_2 = \left(\frac{\varepsilon_i}{\varepsilon_0}\right) \quad (22d)$$

Where:

k	=	Adjustment factor dependent on normalized strain differential (α_1)
β	=	Fatigue damage parameter
N	=	Number of load cycles
ε_i	=	Tensile strain at AC layer bottom at load cycle *i*, με
ε_0	=	Fatigue endurance limit, με
E_i	=	AC modulus at load cycle *i*, psi
E_o	=	Initial AC modulus, psi

For a pavement subjected to traffic load, three separate strain conditions can exist at the bottom of the AC layer: critical tensile strain is greater than, equal to, or less than the fatigue endurance limit. If the critical strain exceeds the endurance limit, fatigue damage is incurred, and the AC modulus is correspondingly adjusted by the k-factor, as a function of the α_1-factor. This strain condition is feasible, particularly under truck traffic. However, in the rare scenario where the critical strain is exactly equal to twice the endurance limit, the influence of the k-factor diminishes since the α_1-term becomes unity and the logarithm of one is zero. Consequently, damage accumulation is influenced by the β-parameter and load cycles raised to the power of α_2-factor. Theoretically, the critical strain may be equal to the endurance limit, in which case the α_1-term becomes zero and the k-factor is rendered invalid. The k-factor could also be invalidated if the critical strain is less than the endurance limit (negative α_1-factor) in situations such as light wheel load application. The models' response to cases in which critical strains are equal to or less than the endurance limit is non-accumulation of fatigue damage. In other words, the models only address cases in which fatigue endurance limit is exceeded, and the pavement is expected to accumulate fatigue damage. Hence, the models address concerns over conventional mechanistic-empirical fatigue modeling approaches which assume cumulative damage occurs where each load cycle, regardless of the load magnitude, consumes a portion of the pavement's fatigue life (NCHRP, 2013). The proposed pseudo fatigue damage models incorporate the fatigue endurance limit concept into mechanistic pavement design.

A close examination of Models 7 and 8 revealed that if the logarithm of the α_1-factor returned a value less than negative one, the k-factor became a negative value, causing AC modulus to increase with load repetitions, a situation which violated the assumption of fatigue

damage. This was an artifact of the models' structure, and to address this issue, the following question was posed: what minimum normalized strain differential (α_1-factor) would cause fatigue damage? The question was answered for Models 7 and 8 by solving Equations 23 and 24, respectively.

$$\text{For Model 7:} \quad k = 1 + \text{Log}(\alpha_1) > 0 \tag{23}$$

$$\text{For Model 8:} \quad k = 1 + \text{Ln}(\alpha_1) > 0 \tag{24}$$

Considering that $\alpha_1 = \left(\frac{\varepsilon_i - \varepsilon_0}{\varepsilon_0}\right)$, Equations 23 and 24 simplify to Equations 25 and 26, respectively:

$$\text{For Model 7:} \quad \left(\frac{\varepsilon_i}{\varepsilon_0}\right) > 1.10 \tag{25}$$

$$\text{For Model 8:} \quad \left(\frac{\varepsilon_i}{\varepsilon_0}\right) > 1.37 \tag{26}$$

According to Equations 25 and 26, Models 7 and 8 accumulate damage if critical tensile strains at the AC layer bottom exceed fatigue endurance limit by 10 and 37%, respectively. These findings suggested Model 7 was more versatile than Model 8, and so it was selected as the best candidate for calibration. It is important to differentiate the utility of Model 7 from the perpetual pavement design concept. Perpetual pavement design prevents bottom-up fatigue cracking by incorporating materials and layer thicknesses to maintain critical tensile strains at the bottom of the AC layer below the fatigue endurance limit. Model 7 characterizes fatigue damage accumulation once critical tensile strains exceed the fatigue endurance limit by 10%.

3.4 Calibration of Pseudo Fatigue Cracking Damage Model

The calibration of the selected pseudo fatigue cracking damage model (Model 7) was a two-step process: (a) application of Model 7 to the calibration dataset in Table 3.1 (117 beam fatigue test results from 15 asphalt mixtures) to determine the unknown fatigue damage parameters (β-parameters), and (b) utilizing the β-parameters to develop a regression equation for prediction of β-parameters as a function of AC material properties and strain conditions. Upon successful

formulation of the β-parameter regression model, it would be incorporated in Model 7 to obtain a fully functional pseudo fatigue cracking damage model.

3.4.1 Determination of β-Parameters

Following the same procedure used in the preliminary investigation of the functional form of the pseudo fatigue cracking damage model (Sub-section 3.3.1), 3-layer pavement structures were developed such that the system produced an initial critical tensile strain at the AC layer bottom equal to the strain level used in the beam fatigue testing. For instance, if the strain level in the fatigue test was 200με, the pavement system (material properties, thicknesses and load) resulted in an initial critical strain at the AC layer bottom equal to 200με. The AC layer moduli corresponded to the initial beam stiffness values measured at the 50th load cycle in the fatigue test. This arrangement was analogous to simulating beam fatigue test in a layered elastic system. A steer axle, with a tire inflation pressure of 100 psi, was utilized in the structural analysis, which was conducted with WESLEA. A total of 117 pavement cross-sections were formulated to represent each of the 117 fatigue test results. Summary information on the simulated cross-sections are presented in Table 3.7; detailed information is available in Appendix C.

Table 3.7 Pavement Cross-Sections Simulated for Determination of β-Parameters

Layer	Thickness (in.)	Modulus (ksi)	Poisson's Ratio
Asphalt Concrete	6	475 – 1700	0.35
Granular Base	7 – 10	6 – 10	0.40
Subgrade Soil	Infinite	2 – 5	0.45

The pseudo fatigue cracking damage model (Model 7) was used to simulate the 117 pavement structures by executing the flowchart in Figure 3.10. In brief, WESLEA analyzes a pavement structure to determine critical tensile strain at the AC layer bottom. At first, the initial critical strain will be equal to the strain level in the beam fatigue test. If the critical strain exceeds the fatigue endurance limit, the AC layer incurs fatigue damage, and the modulus is reduced by an amount equal to $k\beta Log(N^{\alpha_2})$, as found in Model 7 (Equation 22). The reduced AC modulus is then used in the subsequent structural analysis to determine critical strain at the AC bottom. If the next critical strain exceeds the endurance limit, the amount of damage is computed as per $k\beta Log(N^{\alpha_2})$, and the AC modulus is reduced. This incremental recursive process continues until the AC modulus reaches a failure criterion. The failure point was defined as a 50% reduction in the initial AC modulus. The number of model iterations was equal to the number

of load cycles to 50% reduction in the initial AC modulus, as determined by beam fatigue testing. The exception was specimens that survived 12 million load cycles without reaching failure point. For those specimens, the model iterations ended at 12 million, to match the terminating load cycle in the beam fatigue test. A fatigue damage curve (AC modulus versus load cycles) was plotted for each of the 117 simulated pavement cross-sections. For each cross-section, the β-parameter was varied until there was a best match between the predicted and measured fatigue damage curves. The quality of fit was objectively assessed by using coefficient of determination, calculated by using Equation 20.

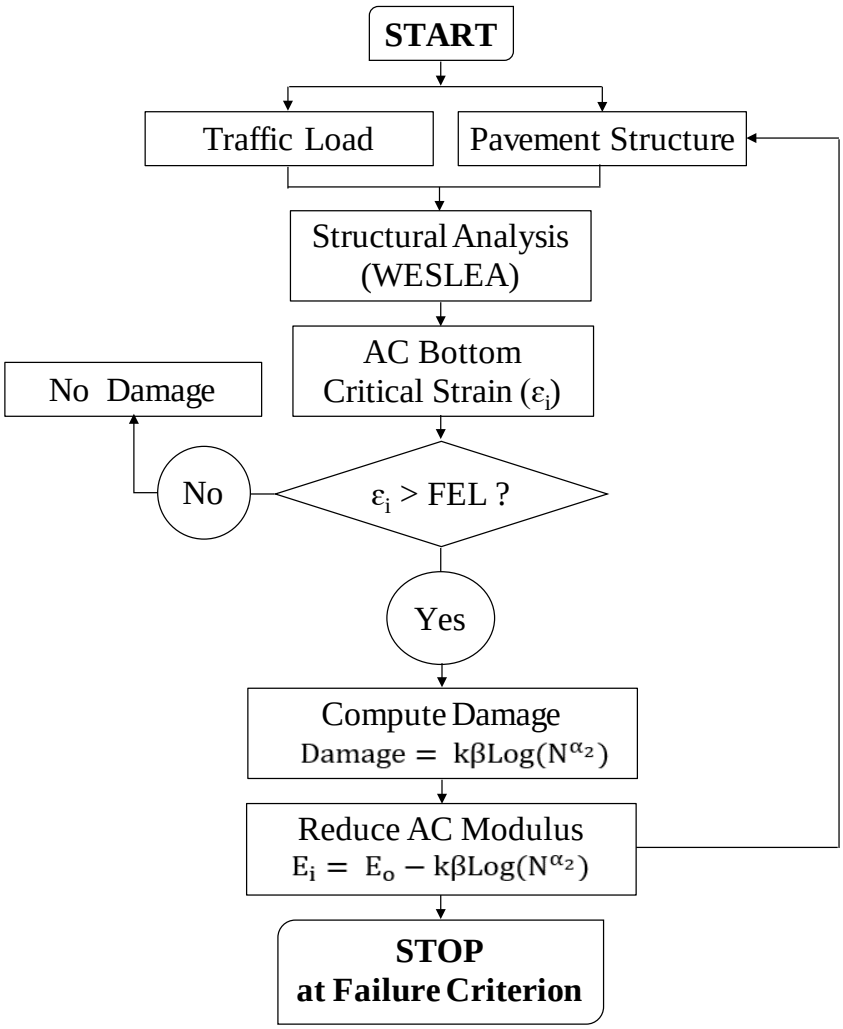

Figure 3.10 Flowchart for Executing Pseudo Fatigue Cracking Damage Model

Out of the 117 beam fatigue test results comprising the calibration dataset, the pseudo fatigue damage model (Model 7) was inapplicable to three (Section S5 base mixture in 2012 research cycle) because the endurance limit of 211με exceeded the beam fatigue test strain

level of 200με, which is the strain level that corresponds to the initial critical strain at the bottom of the AC layer. For those cases, the α_1-factor (Equation 22c) in Model 7 became a negative value, rendering the k-factor (Equation 22a) invalid. The physical interpretation of this scenario is that no damage accumulation occurred because the critical strain was less than the endurance limit. Hence, the sample size of the calibration dataset reduced to 114.

Figure 3.11 shows the cumulative distribution of the coefficient of determination values for the measured versus predicted fatigue damage curves. Overall, the goodness-of-fit was high, notwithstanding the large variations in the beam fatigue test data. For instance, 80% of the 114 pairs of fatigue damage curves had coefficient of determination of at least 70%, indicating the capability of the pseudo fatigue damage model to predict fatigue curves over a wide range of strain conditions. As the figure shows, a similar trend was observed when the pairs of fatigue curves were analyzed on a strain-by-strain basis.

Sample plots of measured versus predicted fatigue curves are presented in Figure 3.12 for beam fatigue testing at 200, 400 and 800με. Both specimens tested at 200με survived 12 million load cycles without reaching the failure point of 50% reduction in the initial AC stiffness. Notice the pseudo fatigue damage model replicated the fatigue test results with high coefficient of determination of 94 and 97%. The beam fatigue testing at 400με was terminated at 25% reduction in the initial AC modulus but, as previously noted, the model iterations were ended when the initial AC modulus decreased by half. Notice the good match between the measured and predicted fatigue damage curves, as evidenced by coefficient of determination of 85%. In the 2006 research cycle, the beam specimen for Section N9 was tested at 800με to 50% reduction in the initial stiffness, whereas the specimen for Section S12 was tested at the same strain level, but up to 30% decrease in the initial stiffness. The predicted fatigue damage curves showed good agreement with the measured fatigue curves, coefficient of determination being 91 and 90%, respectively.

Although not all the predicted fatigue damage curves closely matched the measured curves as the examples in Figure 3.12 did, the high quality-of-fit evident in the error distribution (Figure 3.11) suggested the functional form of the pseudo fatigue damage model was appropriate for simulating beam fatigue test results; the limiting factor would be the β-parameter. Thus, a proper β-parameter estimation procedure was needed to ensure high predictive capability of the pseudo fatigue damage model. The good matching results also provided a critical first-step confirmation toward developing a full model capable of simulating live-traffic field conditions.

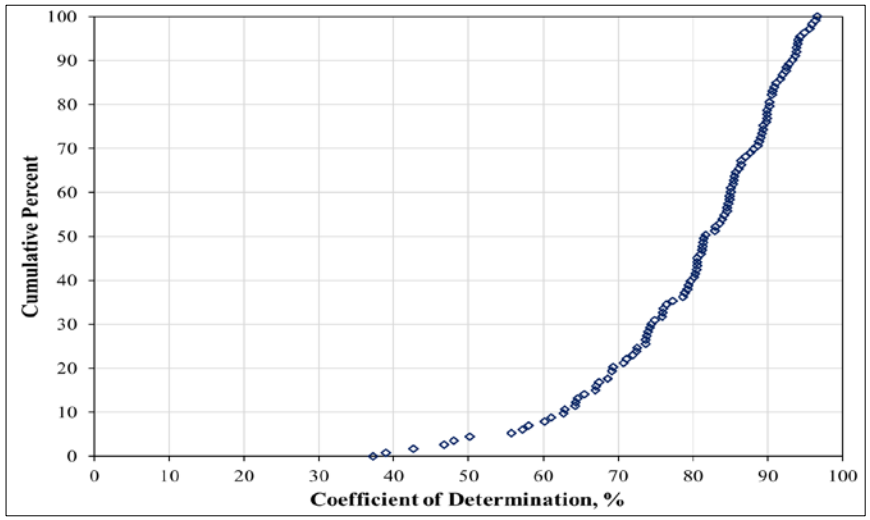

(a)

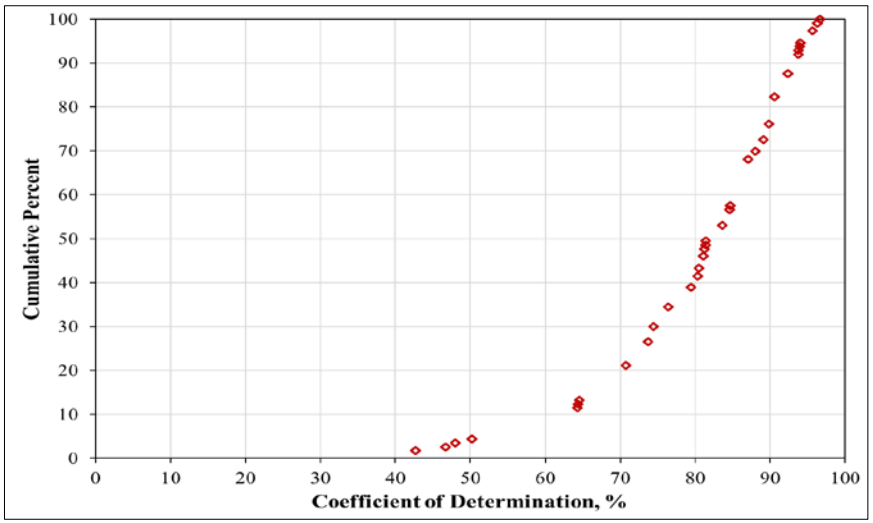

(b)

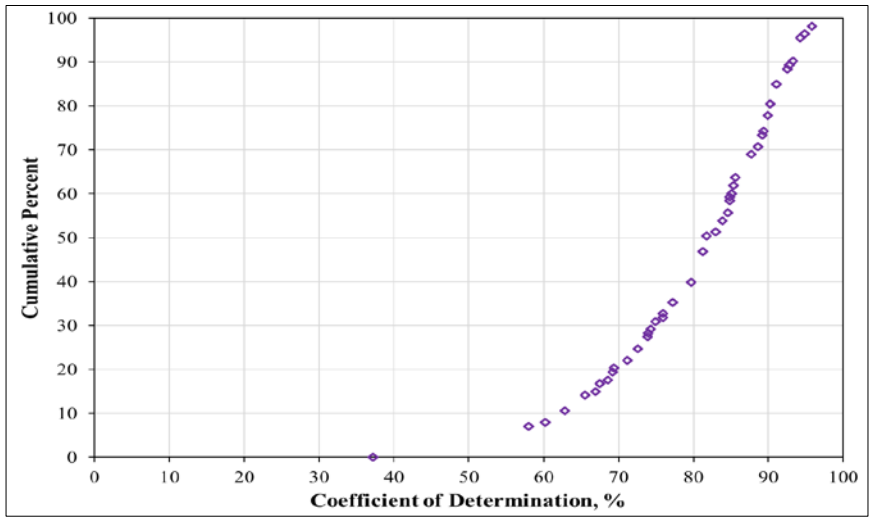

(c)

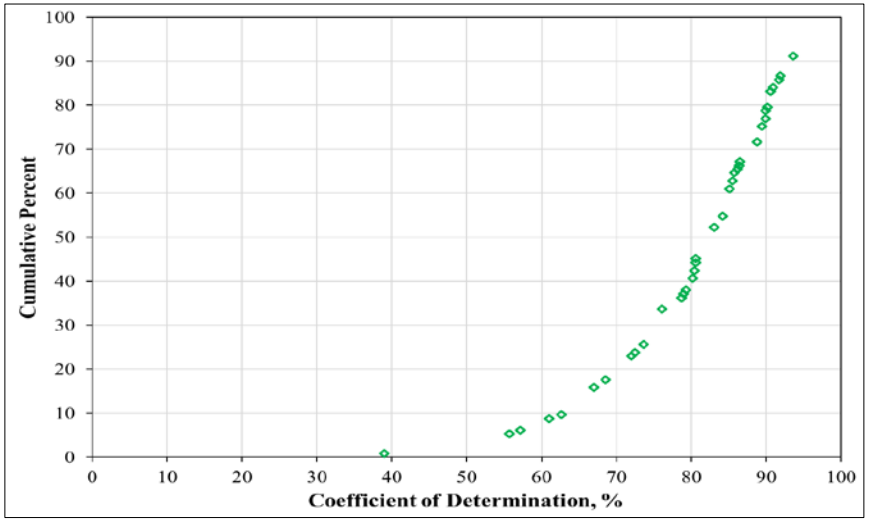

(d)

Figure 3.11 Cumulative Distribution of Coefficient of Determination Values: (a) All Strain Levels (b) 200με (c) 400με (d) 800με

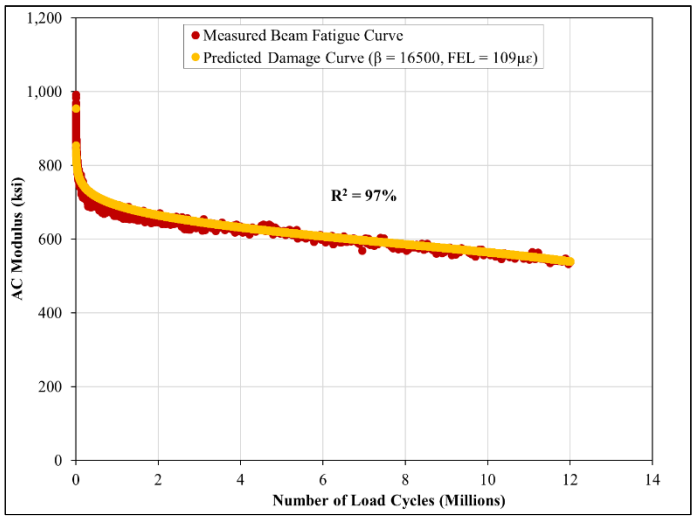

2009 Section N5: Beam Tested at 200με

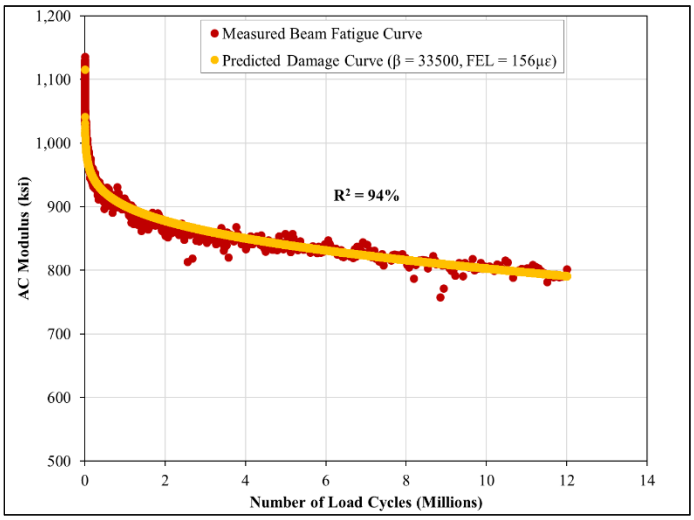

2012 Section S6: Beam Tested at 200με

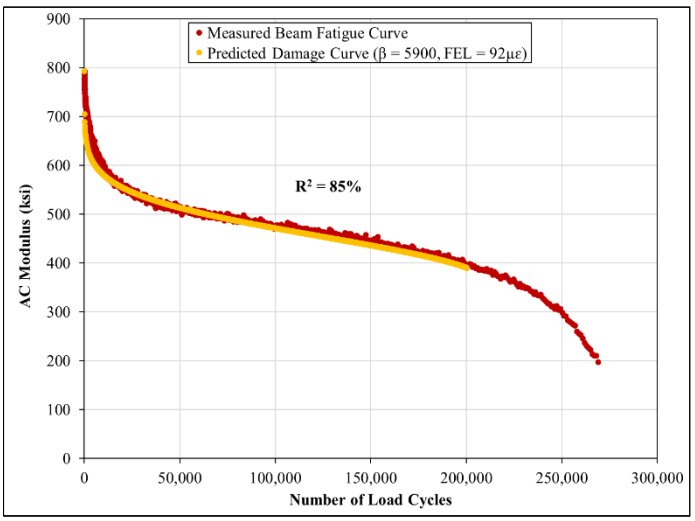

2009 Section S8: Beam Tested at 400με

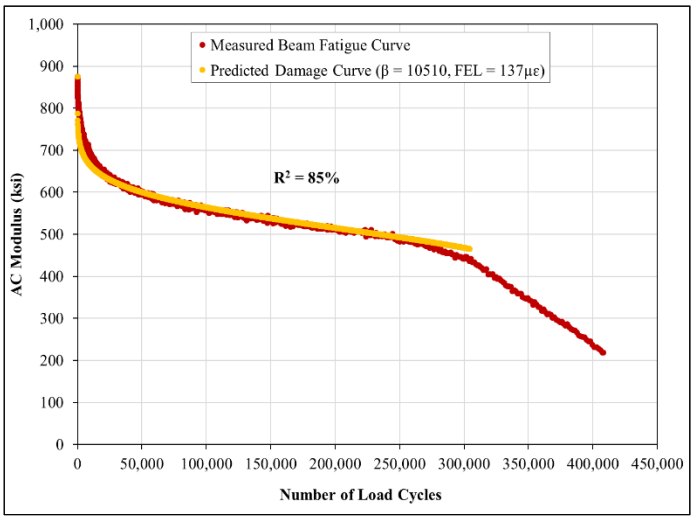

2009 Section S12: Beam Tested at 400με

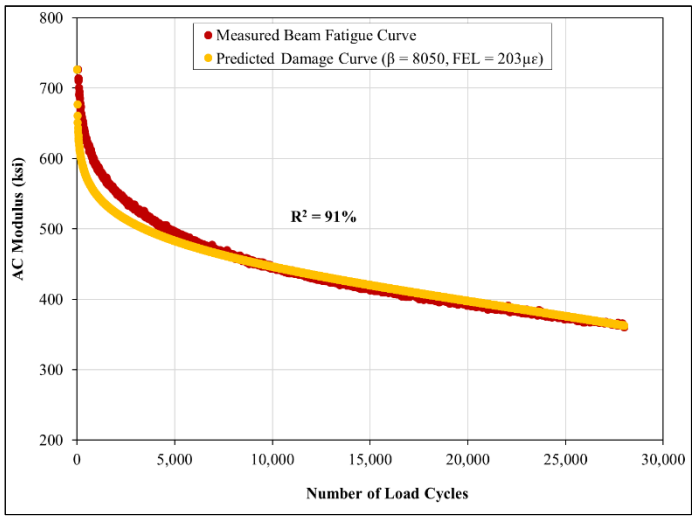

2006 Section N9: Beam Tested at 800με

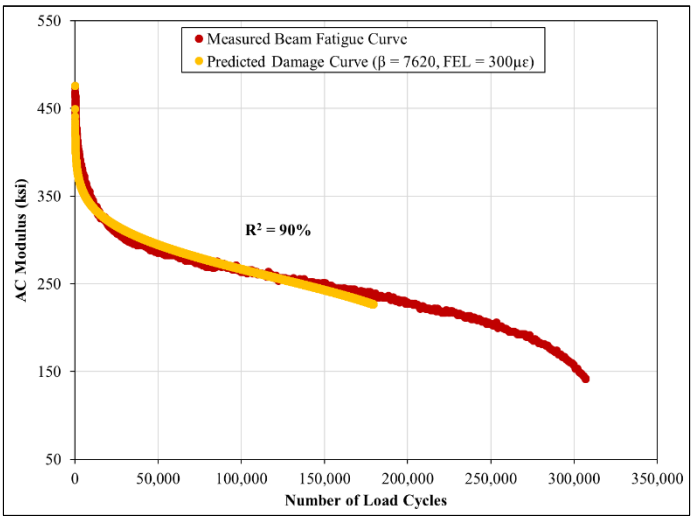

2006 Section S12: Beam Tested at 800με

Figure 3.12 Sample Plots of Beam Fatigue Versus Predicted Damage Curves

3.4.2 Formulation of β-Parameter Regression Model

The second phase of the pseudo fatigue cracking damage model calibration process was to formulate a regression equation to predict the fatigue damage parameter, β-parameter, as a function of AC material properties and strain condition. Being able to estimate β-parameter from easily-obtained data was a crucial step toward achieving the objective of this study: developing a simplified fatigue cracking damage model. The output of the first phase was a set of 114 β-parameters determined by trial-and-error. These β-values yielded the best correlation between the measured and predicted fatigue damage curves. According to the pseudo fatigue damage model (repeated in Equation 27), the β-parameter is a unique damage accumulation parameter that links the model's damage accumulation with that of beam fatigue test. In this phase of the calibration process, a multiple linear regression model was developed to predict β-parameter as a function of material properties and strain conditions.

$$E_i = E_o - k\beta Log(N^{\alpha_2}) \quad (27)$$

The iterative regression process shown in Figure 3.13 provided a framework for formulating the β-parameter regression model. The finalized regression model satisfied the fundamental assumptions of ordinary least square regression analysis and fitted the available data well. Each step of the regression process is discussed next, except for the validation process, which is extensively covered in Chapter 4.

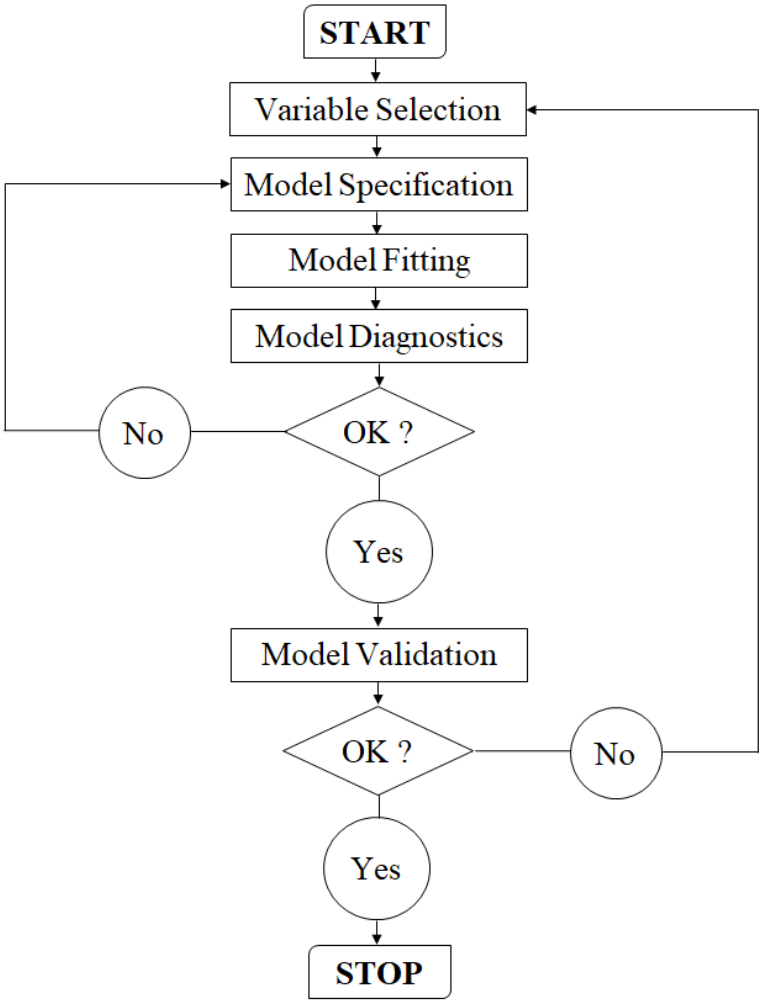

Figure 3.13 Regression Process for Formulating β-Parameter Model

Variable Selection

There was no clear-cut theory on how the β-parameter was associated with fatigue damage accumulation, since this was a newly-developed and original model. Therefore, several AC mixture properties that are known to influence fatigue behavior were considered as potentially relevant predictor variables. For instance, Epps and Monismith (1972) – in discussing the effects of binder stiffness, binder content, aggregate type, aggregate gradation and air void content on fatigue behavior – concluded that binder stiffness and air void content were the most influential factors. On the contrary, Maupin and Freeman (1976) found a 1.0% increase in binder content significantly improved fatigue life. In studying the effects of air voids and binder content on fatigue life, Harvey and Tsai (1996) noted that several combinations of these AC mixture properties could yield similar voids filled with asphalt (VFA), leading them to caution against the use of VFA in fatigue damage predictions. In developing their healing-based fatigue endurance limit model, the NCHRP 9-44A researchers noted that while binder grade, binder

content and air voids could all affect fatigue performance, the initial stiffness from beam fatigue testing could serve as a surrogate (NCHRP, 2013).

NCAT technical reports and Test Track construction records were consulted for data on the 15 asphalt mixtures comprising the calibration dataset (Table 3.1). Air void data for individual beam fatigue test specimens for the 2009 research cycle were not readily available, and so volumetric properties such as VFA and voids in mineral aggregate (VMA) could not be determined. Therefore, air voids, VMA and VFA were excluded as potential predictor variables for β-parameter; their exclusion was not expected to adversely affect the accuracy of the β-parameter model because the initial AC stiffness could be considered as a surrogate. Table 3.6 shows the potentially relevant variables selected for the regression analysis. Apart from AC mixture properties, load-related factors (strain level and axle load) were considered as predictors. The strain levels were those utilized in the fatigue testing of the calibration data, which also represented the initial critical tensile strain at the bottom of the AC layer. The axle loads were those used for the structural analysis (WESLEA) of the pavement structures developed for the generation of the 114 β-parameters (Table 3.7).

Table 3.8 Potentially Relevant Variables for β-Parameter Regression Model

Variable	Definition
BETA	Response variable
STR	Strain level in beam fatigue test (initial critical tensile strain at AC bottom), με
E_0	Initial AC modulus from beam fatigue testing, ksi
FEL	Fatigue endurance limit determined using NCHRP 09-38 Method, με
PGD	Difference between binder performance grades (e.g., for PG 70-22, PGD = 92)
RAP	Recycled asphalt pavement material content, %
NMAS	Nominal maximum aggregate size, mm
P4	Percent passing No. 4 sieve
P200	Percent passing No. 200 sieve
AC	Asphalt binder content, %
LOAD	Axle load used in structural analysis (WESLEA), kips

To examine the strength of the linear relationship among the variables, a correlation matrix (Appendix E) was generated with Statistical Analysis System (SAS). Low Pearson correlation coefficients were verified with scatter plots to ensure the relationship was nonlinear. The response variable (BETA) was strongly correlated with strain (STR), producing a correlation coefficient of -0.6358. Although BETA was weakly correlated with initial AC modulus (E_0), fatigue endurance limit (FEL), binder performance grade difference (PGD),

recycled asphalt pavement (RAP) material content and axle load (LOAD) with correlation coefficients of 0.4702, 0.2966, 0.3256, 0.4513 and -0.4311, respectively, the strength of the linear correlation was significant; p-values at 5% significant level were < 0.0001, 0.0014, 0.0004, < 0.0001 and < 0.0001, respectively. Pairwise scatter plots did not show a nonlinear relationship. Consequently, STR, E_0, FEL, PGD, RAP and LOAD constituted a reduced set of predictor variables for BETA. However, E_0 and RAP were strongly associated, likewise STR and LOAD; their correlation coefficients were 0.7265 and 0.8515, respectively.

Collinearity, defined as the existence of a linear relationship between two predictor variables, has adverse effects on the results of regression analysis. It prohibits estimation of the unique effects of predictor variables, produces sensitive regression coefficients that change erratically in response to slight changes in data or the model and generates large sampling errors of regression coefficients, which affect hypothesis testing and forecasting (Chatterjee and Hadi, 2012). Consequently, RAP and LOAD were dropped in favor of their counterparts. The regression analysis proceeded to develop a relation between BETA and the downsized predictors, in the form of Equation 28. The scatter diagram in Figure 3.14 illustrates the pairwise correlation between the selected predictor variables (STR, E_0, FEL, PGD), as well as between each predictor variable and the response variable (BETA). The plot is diagonally symmetrical, the upper half reflects the lower. The plots labeled 1 through 4 show the correlation between BETA and STR, E_0, FEL and PGD, respectively. Strong linear trend, such as in Plot 1, was preferable; nonetheless BETA was significantly correlated to all the predicted variables. Plots 5 through 7 illustrate the relationship between STR and E_0, FEL and PGD, respectively. In Plots 8 and 9, the association between E_0 and FEL and PGD, respectively, is shown. Lastly, Plot 10 demonstrates the correlation between FEL and PGD. As expected, there was no strong linear relationship among the predictor variables. Note that ε_0 in the pseudo fatigue model (Table 3.6) and FEL both refer to AC fatigue endurance limit.

$$\text{BETA} = \text{f}\,(\text{STR}, \text{E}_0, \text{FEL}, \text{PGD}) \qquad (28)$$

Where:

BETA	=	Fatigue damage related parameter
STR	=	Strain level, με
E_0	=	Initial AC modulus, ksi
FEL	=	Fatigue endurance limit, με
PGD	=	Difference in binder performance grades

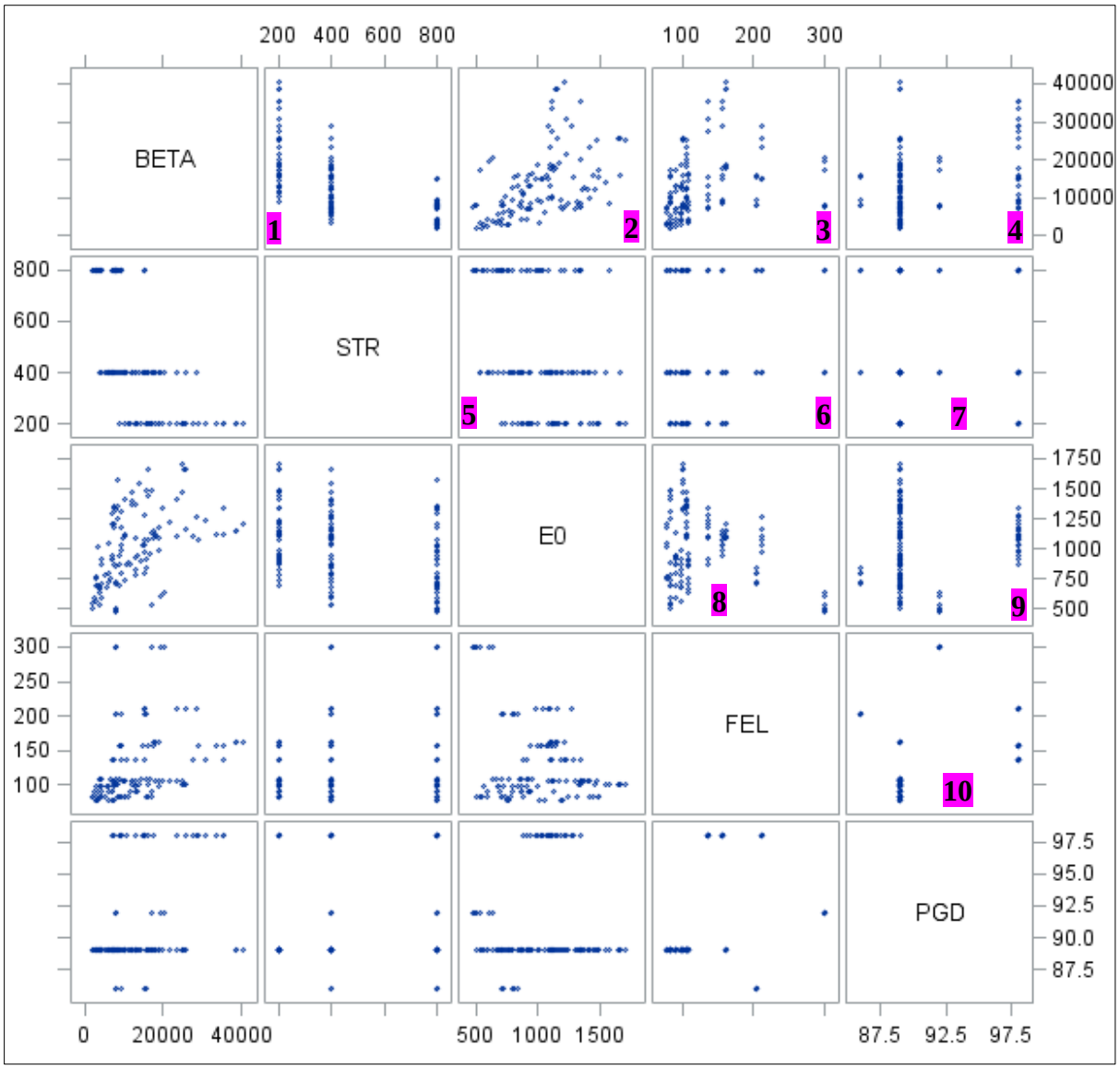

Figure 3.14 Pairwise Scatter Plots of Selected β-Parameter Predictor Variables

Model Specification and Fitting

The search for a suitable regression model that could best relate BETA to STR, E_0, FEL, PGD followed an iterative process. Generally, for *n* observations on a response variable Y and *p* predictor variables, X_1, X_2…, X_p, the relationship between Y and X_1, X_2…, X_p is represented by the multiple linear regression model in Equation 29.

$$Y = \beta_0 + \beta_1 X_1 + \beta_2 X_2 + \cdots + \beta_p X_p + \varepsilon \quad (29)$$

Where:

$\beta_0, \beta_1, \beta_2, \ldots, \beta_p$ = Regression coefficients (parameters)

ε = Random error

The SAS statistical package was utilized to fit the regression models (estimate their coefficients) by implementing the most common linear regression coefficient estimation technique: the ordinary least squares (OLS) method. Regression coefficients are estimates of the true population parameters; hence, to obtain best estimates, the following underlying OLS assumptions for linear regression were verified (Chatterjee and Hadi, 2012):

- The regression model is linear in its parameters (linearity assumption).
- The errors (ε) are random variables with a normal distribution (normality assumption), mean of zero, common variance (constant variance assumption) and are independent of each other (independent errors assumption)
- The predictor variables are linearly independent of each other (non-collinear) and are non-random. The values of the predictor variables have no measurement errors.

The quality of regression analysis results depends on satisfying the above assumptions. For instance, statistical hypothesis testing and confidence interval estimation are based on the normality assumption, and so non-normality invalidates these standard tests. Unequal error variance results in regression coefficients that lack maximum precision; their estimated standard errors may give a false sense of accuracy (Chatterjee and Hadi, 2012). The adverse effects of collinearity have already been mentioned. While the assumption of error-free predictor values is hardly satisfied in practice, the linearity, normality and constant variance assumptions were verified as part of the model diagnosis.

Model Diagnostics

After fitting a regression model, diagnostic plots from the SAS output were reviewed to detect model deficiencies, as well as evaluate goodness-of-fit and predictive capability. To detect model deficiencies, residual (error) plots were examined for gross violations of the OLS assumptions. The linearity and normality assumptions were verified by examining plots of residuals versus predicted values, observed versus predicted values, residuals versus each of the predictors and normal quantile plots of the residuals. For normally distributed residuals, the normal quantile plot should fall close to the diagonal line of equality. Nonlinearity existed if the observed versus predicted values plot was asymmetrically distributed along the equality line. The residual versus predicted value plot was expected to be symmetrically distributed about a horizontal axis, with an approximately constant variance. Also, plots of residuals against each of the predictor variables should have a random scatter of points around a horizontal line. The shape of the histogram of the residuals indicated departure from normality.

Non-independence of the error terms is a common phenomenon with time series data or data measured in a certain sequence. However, to test for non-time-series violations of independence, plots of residuals versus predictor variables were examined to ensure the residuals were randomly and symmetrically distributed about zero. Constancy of error variance was verified by examining plots of residuals versus predicted values and of residuals versus predictor variables. Discernible patterns such as residuals that increase with predicted values (funnel-shaped distribution) or residuals that systematically increase in one direction was an indication that the variance of the residuals was not constant.

Influential outliers over-determine the model fit, and so plots of studentized residuals (residuals divided by their estimated standard deviation) against predicted values were examined to detect outliers in the response variable. Response variable values with studentized residuals larger than 2 or 3 standard deviations away from zero are considered outliers (Chatterjee and Hadi, 2012). On the other hand, leverage was used to identify outliers in the predictor variables. Observations with leverage greater than two times the number of model coefficients divided by the number of observations are typically considered outliers (Kutner et al., 2008; Chatterjee and Hadi, 2012). For a large sample size, leverage greater than 0.5 is considered very high, but those between 0.2 and 0.5 are moderate (Kutner et al., 2008). Thus, a studentized residual versus leverage plot simultaneously detects outliers in both the response and predictor variables. Cook's distance, which is the difference between the regression coefficients obtained from the full data and those obtained by deleting the *i*-th observation, was used to measure the influence of outliers. Observations with Cook's distance greater than unity are often considered influential (Chatterjee and Hadi, 2012).

If a fitted model satisfies the OLS assumptions, then the coefficient of determination (R^2), which is the proportion of the total variability in the response variable accounted for by the model, is a valid statistic for measuring the goodness-of-fit of the model and for assessing its predictive capability. Because R^2 increases with the number of predictor variables, an adjusted R^2 is the preferred measure of goodness-of-fit for models with unequal number of predictors. Adjusted R^2 accounts for the number of predictors such that the inclusion of a predictor in a model is rewarded (R^2 increases) if it sufficiently improves the model fit or penalized (R^2 decreases) if its explanatory benefit is minimal. Predicted R^2 was used to evaluate the predictive power of the β-parameter regression models. In calculating predicted R^2, a statistical package deletes a data point, fits a regression model and evaluates its ability to predict the deleted observation. The process is repeated for all data points. An overfitted regression model (one with excessive number of predictors) has predicted R^2 distinctly smaller than the

ordinary R^2. Alternatively, the standard error of estimate (SEE) of the model (square root of mean squared error (MSE)) may be used as a measure of goodness-of-fit: a small SEE indicates a good model fit. In summary, by employing several diagnostic plots, a parsimonious regression model was formulated for estimating β-parameter.

3.4.3 Preliminary β-Parameter Regression Models

Four linear regression models were fitted to the 114 calibration data points (Table 3.1) by incorporating various combinations of the selected variables (STR, E_0, FEL and PGD). Table 3.9 presents the models and their diagnostic issues, which were summarized from the SAS-generated residual plots in Figures 3.15 through 3.18. Appendix F provides explanatory notes on the residual plots, using Figure 3.15 as an example. Model A utilized all four selected variables, but Model B excluded PGD, in search for model simplicity. Model C replaced E_0 with RAP due to their high correlation; their coefficient of correlation was 0.7265. In Model D, the interaction term RAP*AC substituted for E_0, since both RAP and AC had strong correlation with E_0, but a weak correlation between them. The correlation coefficient of E_0 and AC was -0.5499 and that of RAP and AC was -0.4766.

The diagnostic plots indicated considerable violations of the constant variance, linearity and normality OLS linear regression assumptions. However, there was no statistical evidence to suggest the presence of influential outliers, in both the response and predictor variables. Although the regression coefficients were significant and the models' predictive capability was high (adjusted R^2 ranged between 71 and 73%), the model fits were considered inadequate due to the violations of the regression assumptions. Another key finding was that the elimination of PGD, as a predictor variable, had no significant effect on the regression results, hence PGD was dropped, and the subsequent model building proceeded with only STR, E_0 and FEL.

Table 3.9 Preliminary β-Parameter Regression Models

Model	Multiple Linear Regression Model	Significance of Coefficients	Adjusted R^2	[a]SEE	Model Fit Issues Summarized from SAS Diagnostic Plots
A	$BETA = \beta_0 + \beta_1(STR) + \beta_2(E_0) + \beta_3(FEL) + \beta_4(PGD)$	Significant (p-values < 0.05)	0.7293	4,579	1. Residuals versus predicted values plots show unsymmetrical point distribution about horizontal line; indicative of unstable error variance
					2. Residuals versus predictor variables plots show a fairly random scatter of points about horizontal line, suggesting some stability in error variance
					3. Observed versus predicted values plot reveals strong nonlinearity at the tails
					4. Normal quantile plot of residuals indicates departure from normality at the tails
					5. Residuals histogram shows generally normal distribution of residuals (errors)
					6. Plot of studentized residuals against predicted values suggest few outliers in response variable (few studentized residuals exceed 3 standard deviations from zero)
					7. Plot of studentized residuals against leverage indicate few outliers in response variable but none in predictor variables (leverage values less than 0.5)
					8. Outliers not influencial; Cook's distance less than unity.
B	$BETA = \beta_0 + \beta_1(STR) + \beta_2(E_0) + \beta_3(FEL)$	Significant (p-values < 0.05) Intercept not significant (p-value = 0.9417)	0.7116	4,726	1. Residuals versus predicted values plots show similar trend as in Model A
					2. Residuals versus predictor variables plots exhibits similar trend as in Model A
					3. Observed versus predicted values plot has similar trend as in Model A
					4. Normal quantile plot of residuals shows similar trend as in Model A
					5. Residuals histogram has similar shape as in Model A
					6. Plot of studentized residuals against predicted values suggest fewer outliers in response variable (few studentized residuals close to 3 standard deviations from zero)
					7. Plot of studentized residuals against leverage values indicate fewer outliers in response variable but none in predictor variables (leverage values less than 0.5)
					8. Outliers not influencial; Cook's distance less than unity
C	$BETA = \beta_0 + \beta_1(STR) + \beta_2(RAP) + \beta_3(FEL) + \beta_4(PGD)$	Significant (p-values < 0.05)	0.7301	4,573	1. Residuals versus predicted values plots has slight improvement over the trend in Model A
					2. Residuals versus predictor variables plots show similar trend as in Model A
					3. Observed versus predicted values plot has slight improvement over the trend in Model A
					4. Normal quantile plot of residuals shows slight improvement over the trend in Model A
					5. Residuals histogram has slight deterioration over the shape in Model A
					6. Plot of studentized residuals vs. predicted values shows slight improvement over the trend in Model
					7. Plot of studentized residuals against leverage exhibit slight improvement over the trend in Model B
					8. Outliers not influencial; slight increases in Cook's distance but still less than unity
D	$BETA = \beta_0 + \beta_1(STR) + \beta_2(RAP * AC) + \beta_3(FEL) + \beta_4(PGD)$	Significant (p-values < 0.05)	0.7289	4,583	1. Residuals versus predicted values plots have similar trend as in Model C
					2. Residuals versus predictor variables plots show similar trend as in Model C
					3. Observed versus predicted values plot has similar trend as in Model C
					4. Normal quantile plot of residuals demonstrates similar trend as in Model C
					5. Residuals histogram has similar shape as in Model C
					6. Plot of studentized residuals against predicted values shows similar trend as in Model C
					7. Plot of studentized residuals against leverage values has similar trend as in Model C
					8. Outliers not influencial, similar characteristics as in Model C

Note: (a) SEE: standard error of estimate of regression model

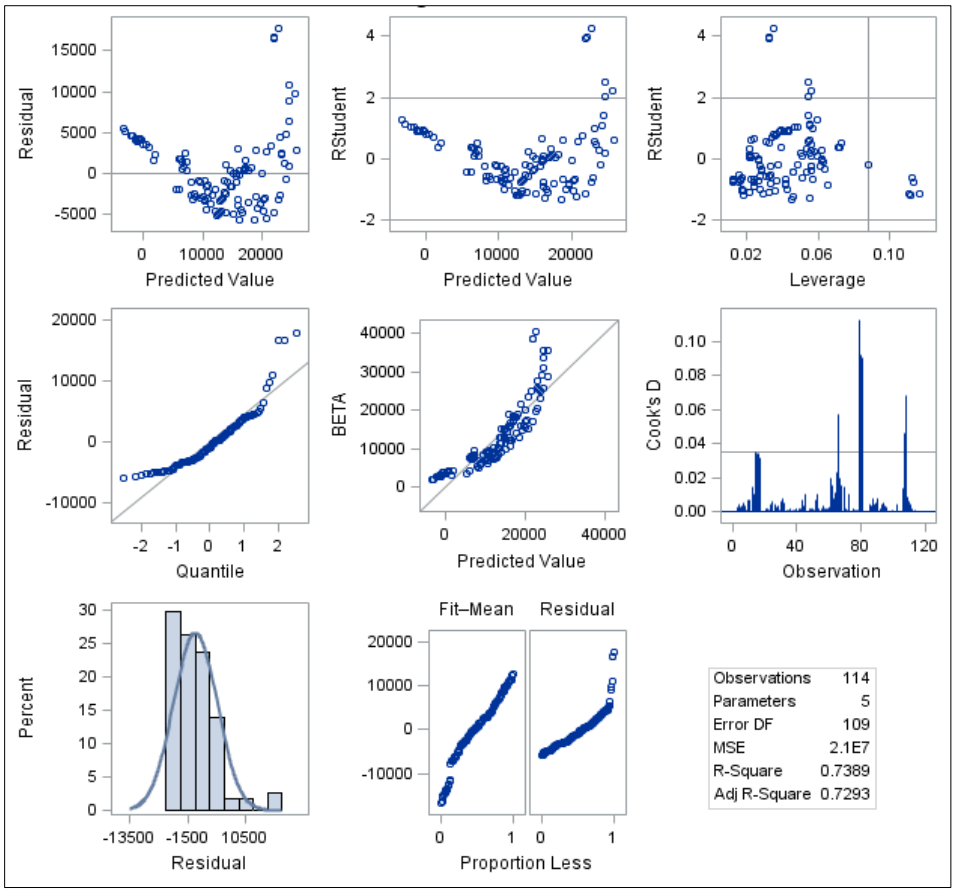

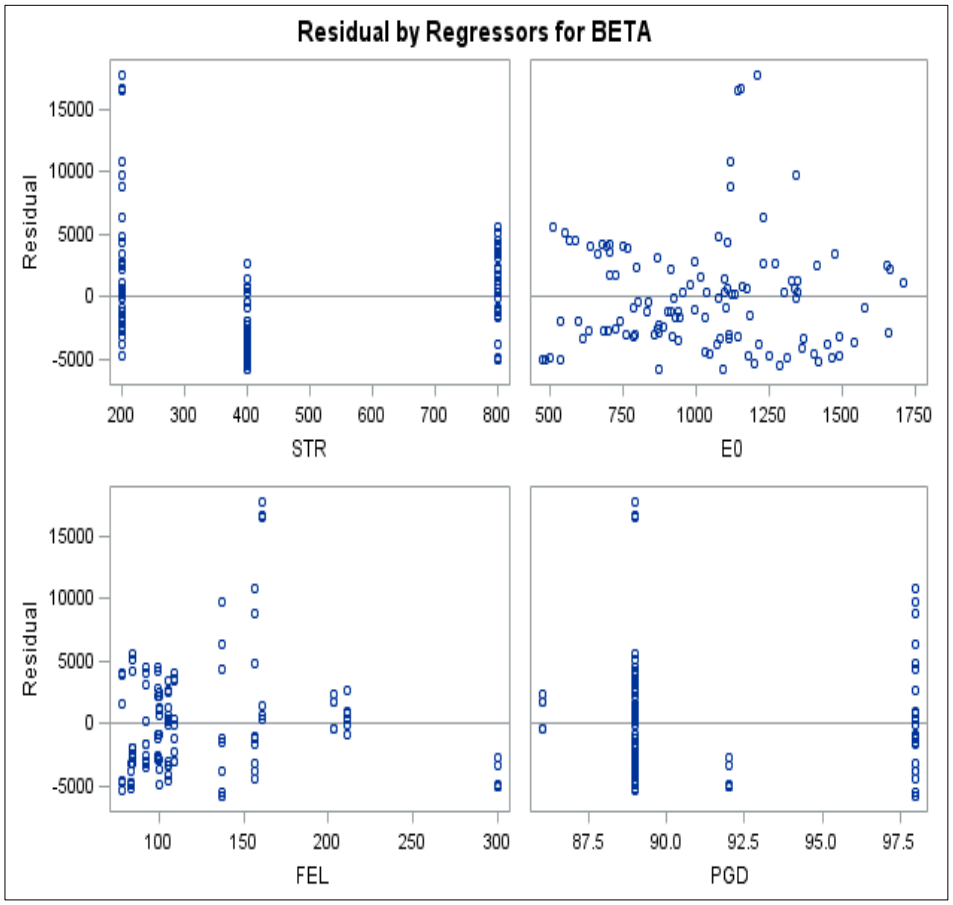

Figure 3.15 Diagnostic Plots for β-Parameter Regression Model A

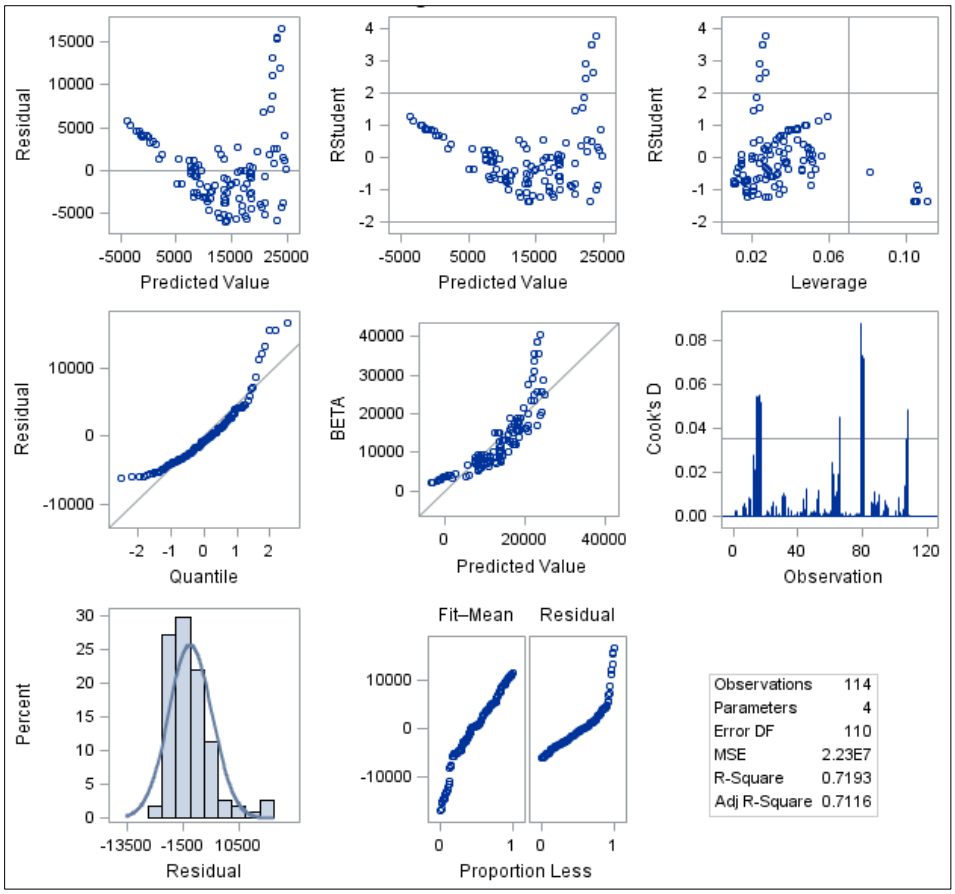

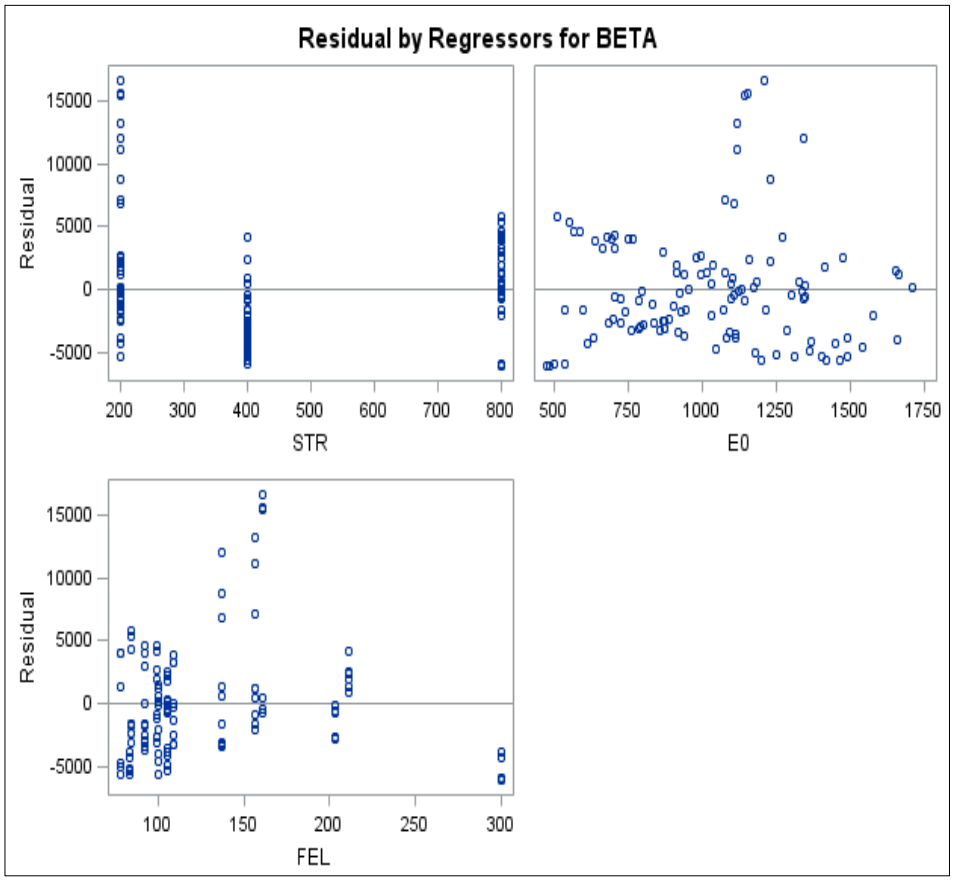

Figure 3.16 Diagnostic Plots for β-Parameter Regression Model B

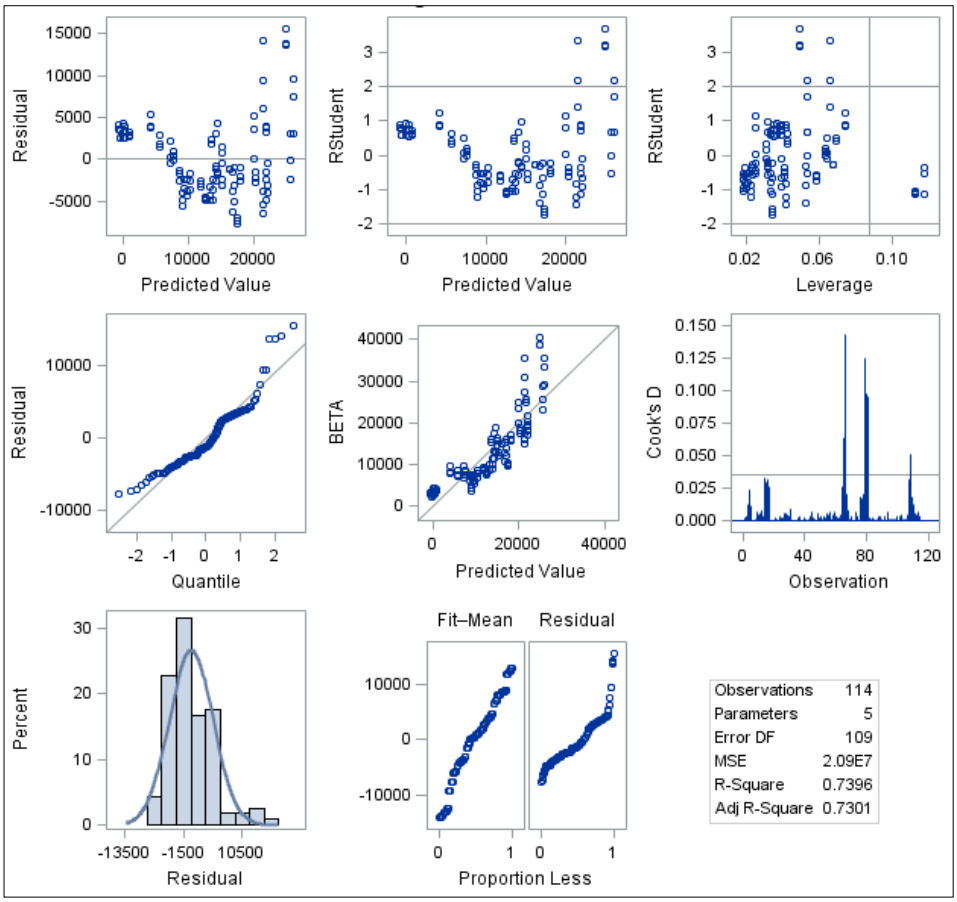

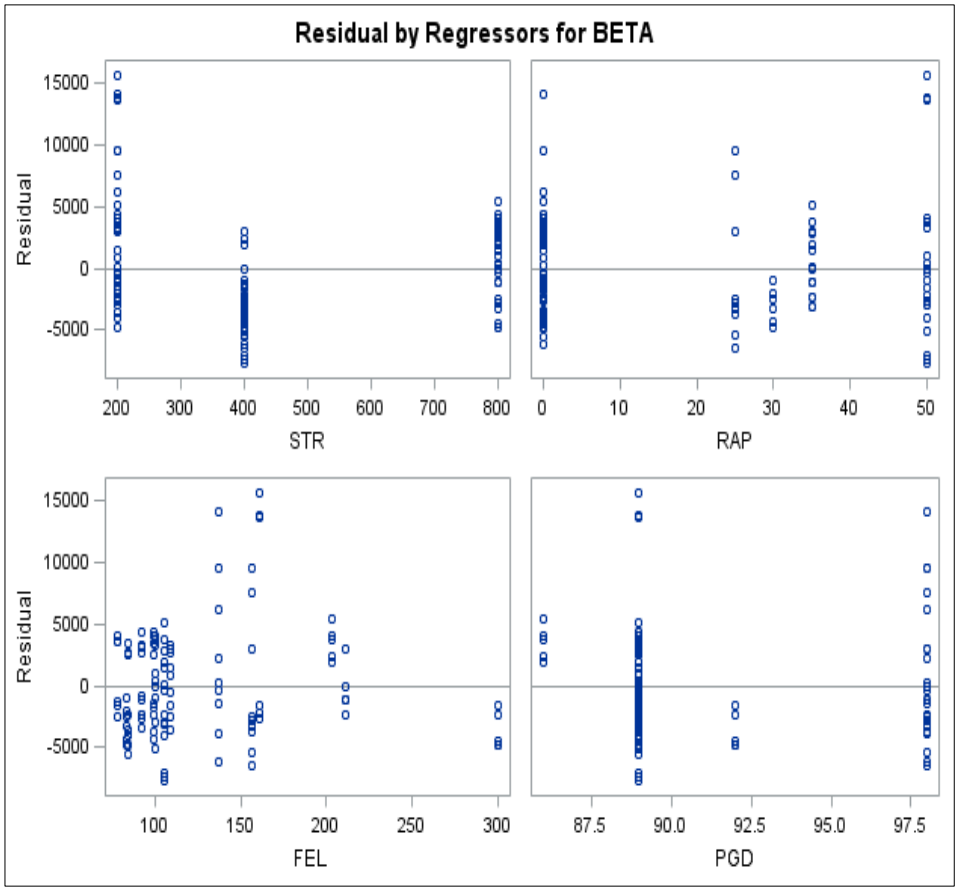

Figure 3.17 Diagnostic Plots for β-Parameter Regression Model C

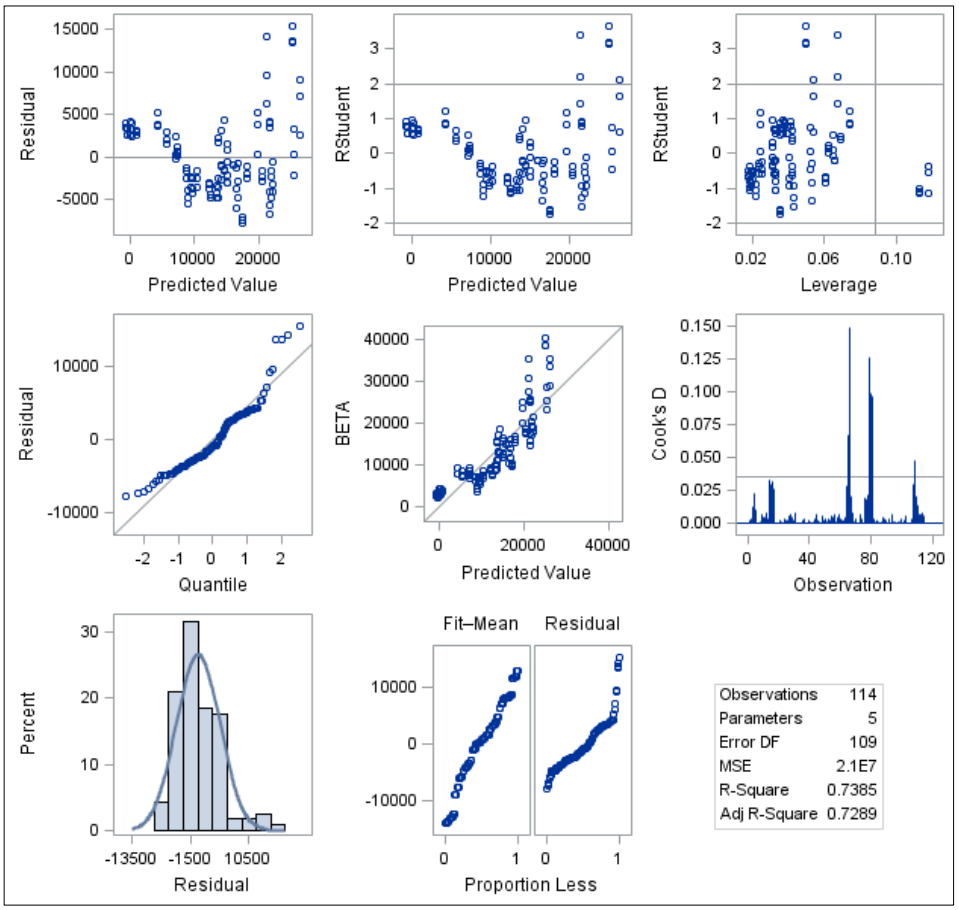

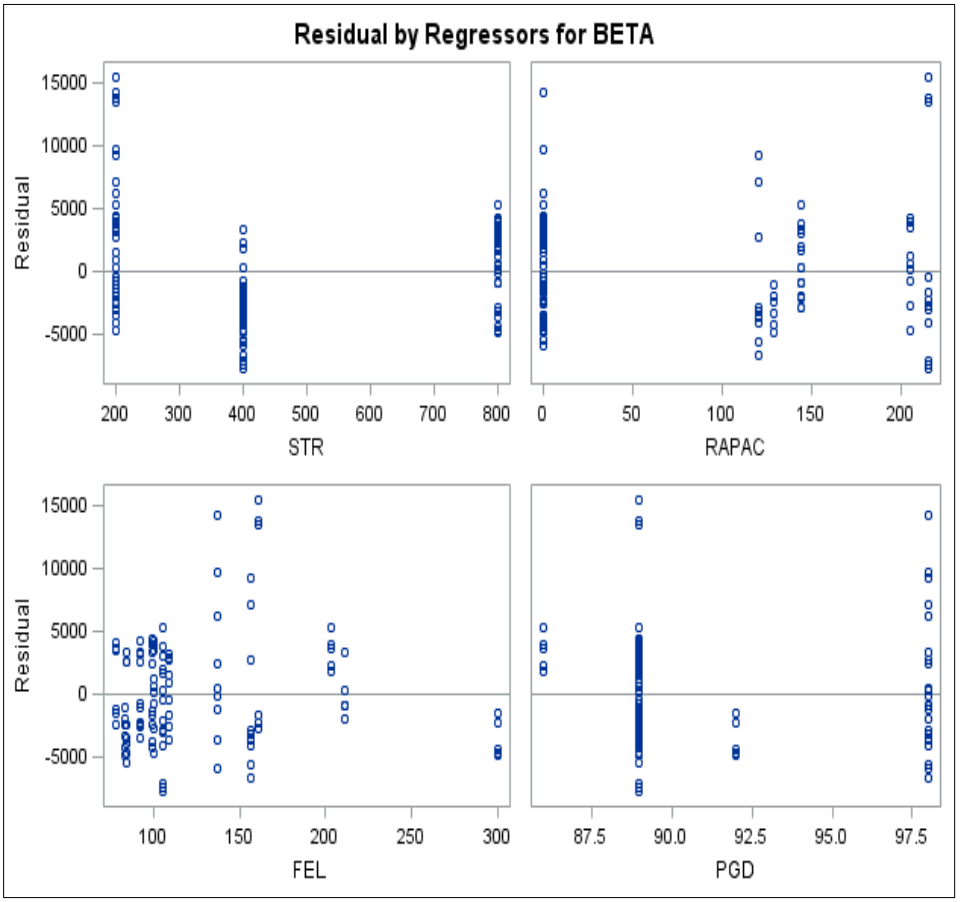

Figure 3.18 Diagnostic Plots for β-Parameter Regression Model D

3.4.4 New Generation of β-Parameter Regression Models

Logarithmic and reciprocal (inverse) variable transformations were investigated as remedial measures to address the nonlinearity, non-normality and unequal variance associated with the preliminary β-parameter regression models. It is well-known that logarithmic transformation minimizes variability, stabilizes error variance and normalizes errors. Apart from variable transformation, polynomial regression, a special case of linear multiple regression, was employed to model the interaction effects of the predictor variables on the response variable. Because polynomial regression is a special case of linear regression, the diagnostic plots were applicable. The Minitab statistical software was used to fit the polynomial regression model, but the diagnostic plots were generated with SAS. Minitab followed an automatic stepwise regression analysis procedure in which predictor variables with the highest correlation to the response variable were first included in the model. The resulting best fit model incorporated linear and quadratic terms of the predictor variables and their two-way interaction terms. Table 3.10 shows the functional forms of the five new β-parameter regression models investigated.

Table 3.10 New Generation of β-Parameter Regression Models

Model	Regression Model	Model Description
1	$\text{Ln (BETA)} = \beta_0 + \beta_1(\text{STR}) + \beta_2(E_0) + \beta_3(\text{FEL})$	Natural log transformation of response variable BETA
2	$\text{Ln (BETA)} = \beta_0 + \beta_1(E_0) + \beta_2\left(\frac{1}{\text{STR}}\right) + \beta_3\left(\frac{1}{\text{FEL}}\right)$	Natural log transformation of response variable BETA and inverse transformation of STR and FEL predictor variables
3	$\text{Ln (BETA)} = \beta_0 + \beta_1(\text{Ln } E_0) + \beta_2\left(\frac{1}{\text{STR}}\right) + \beta_3\left(\frac{1}{\text{FEL}}\right)$	Natural log transformation of response variable BETA and ACM predictor variable. Inverse transformation of STR and FEL predictor variables
4	$\text{Ln (BETA)} = \beta_0 + \beta_1(\text{Ln STR}) + \beta_2(\text{Ln } E_0) + \beta_3(\text{Ln FEL})$	Natural log transformation of all variables
5	$\text{BETA} = \beta_0 + \beta_1(\text{STR}) + \beta_2(E_0) + \beta_3(\text{FEL}) + \beta_4(\text{STR})^2 + \beta_5(\text{STR} * E_0) + \beta_6(\text{STR} * \text{FEL}) + \beta_7(E_0 * \text{FEL})$	Polynomial regression incorporating linear and quadratic terms of the predictor variables and their two-way interaction terms

The diagnostic plots for the new β-parameter regression models, presented in Figures 26 through 30, show significant improvements over those from the preliminary models. Notice that the enhancement in Model 5 was more visible in the plot of the observed versus predicted values (Figure 3.23), where the points fell reasonably close to the line of equality to signify satisfaction of the linearity and normality assumptions. Overall, the plots of the residuals against the predicted values had no systematic pattern. The residuals were randomly distributed about the horizontal axis, falling within a narrow band parallel to the horizontal axis. Plots of the residuals versus each of the predictor variables showed a random scatter of points about the horizontal axis. These trends in the residual plots suggested there was no marked evidence of

unequal error variance in the transformed models. Nonlinearity was not an issue as the observed versus predicted values plots were symmetrical along the equality line. The normality assumption was satisfied because the normal quantile plot fell close to the equality line, which was also confirmed by the histogram of residuals, which indicated no gross departure from normality. The studentized residuals versus leverage and Cook's distances indicated no outliers. Evidently, the violations of the OLS regression assumptions were addressed by the variable transformation and the polynomial regression.

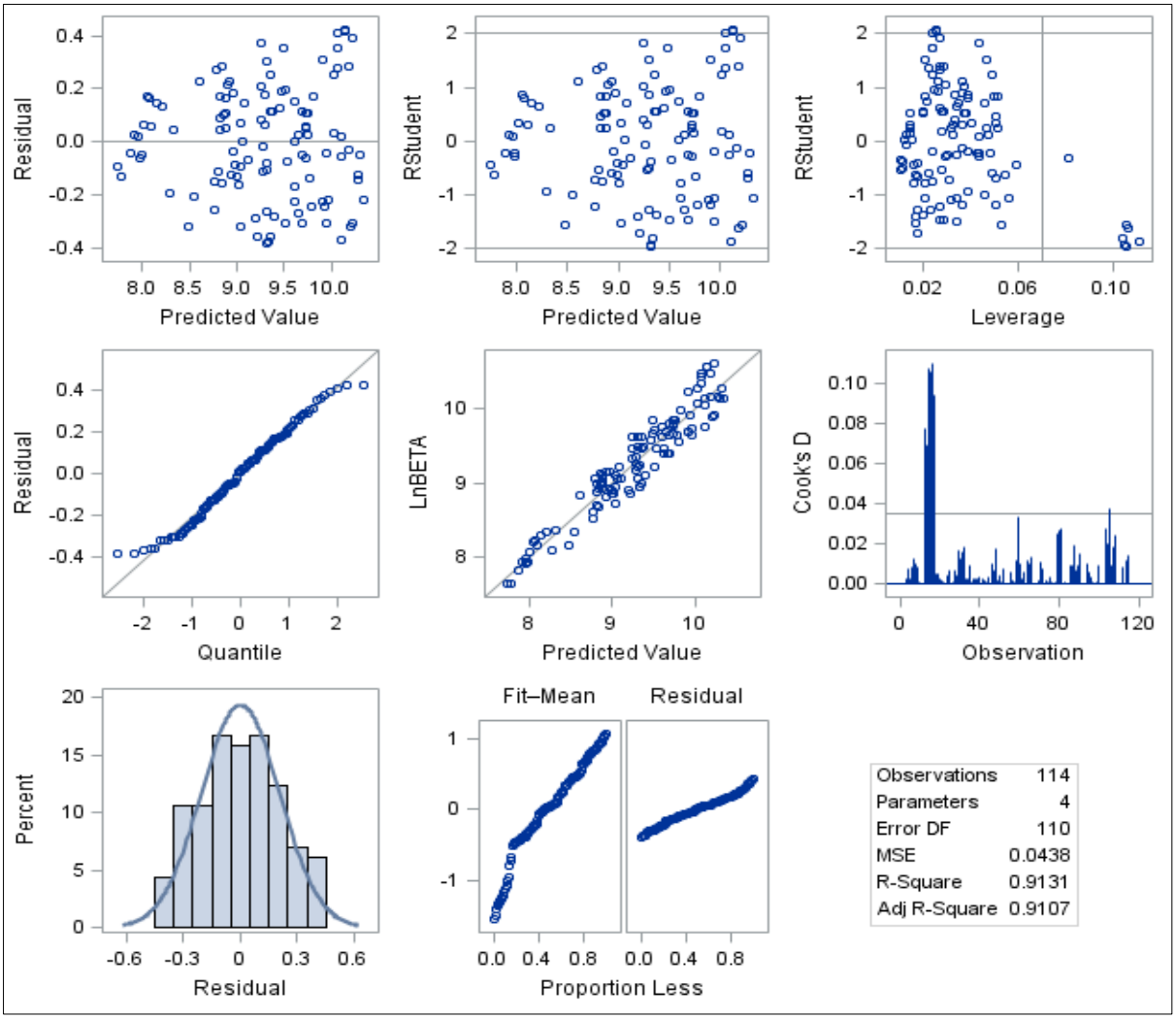

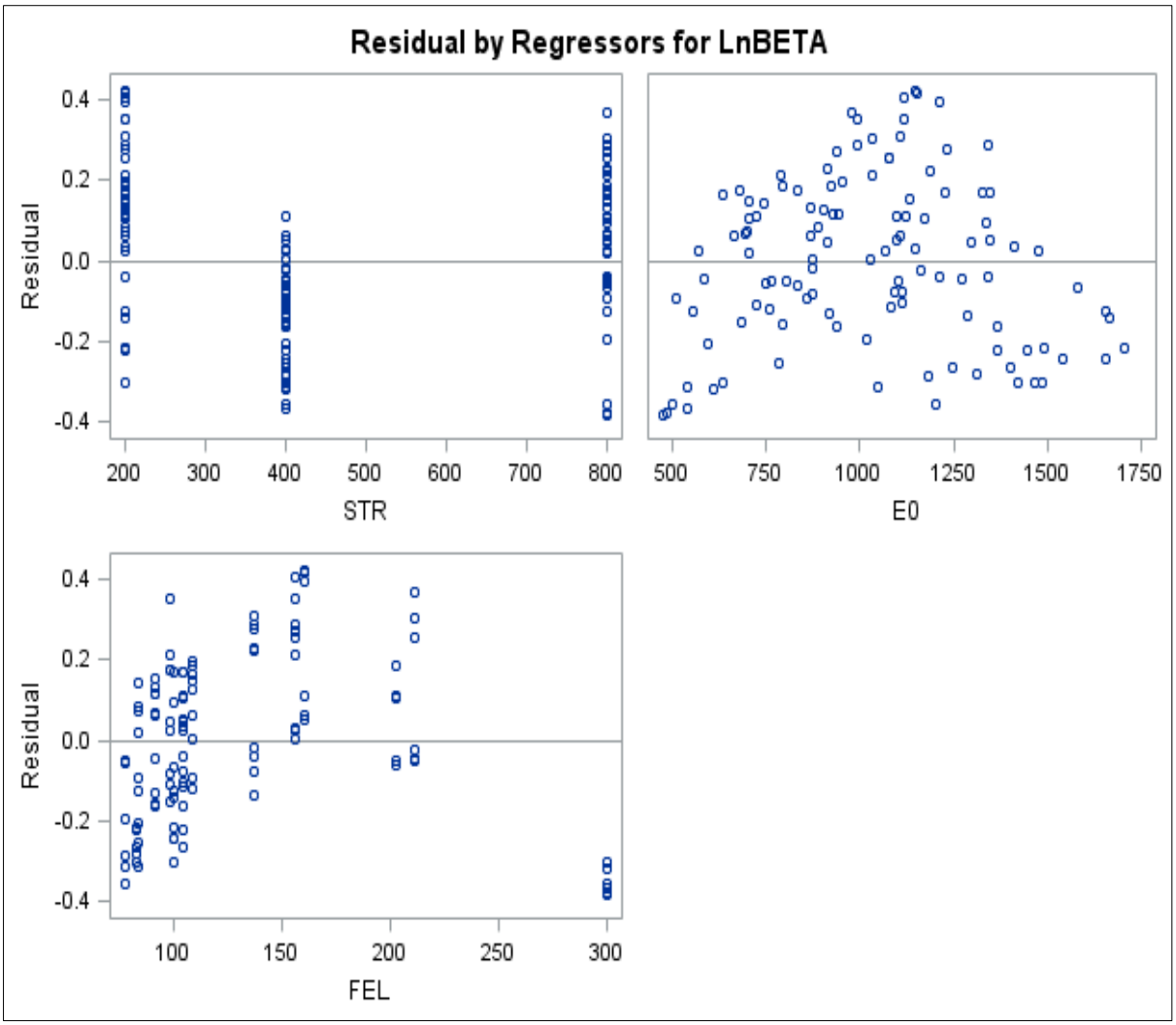

Figure 3.19 Diagnostic Plots for β-Parameter Regression Model 1

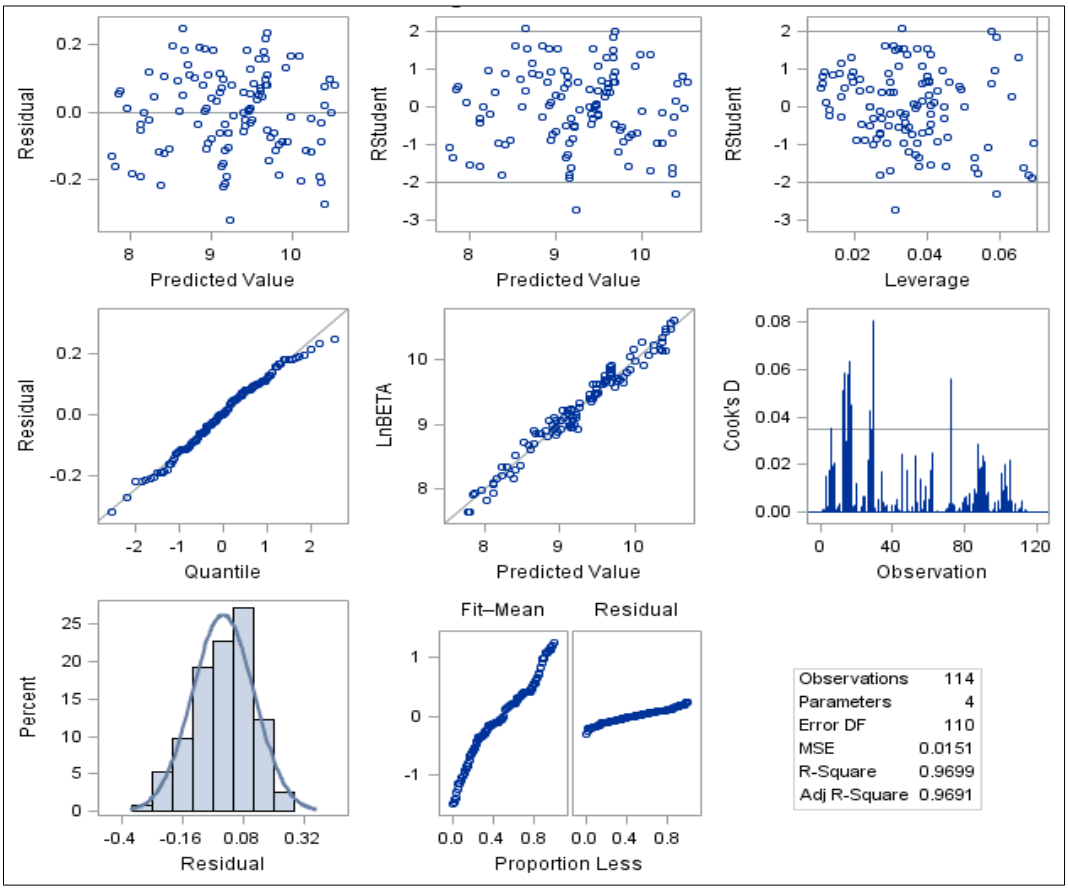

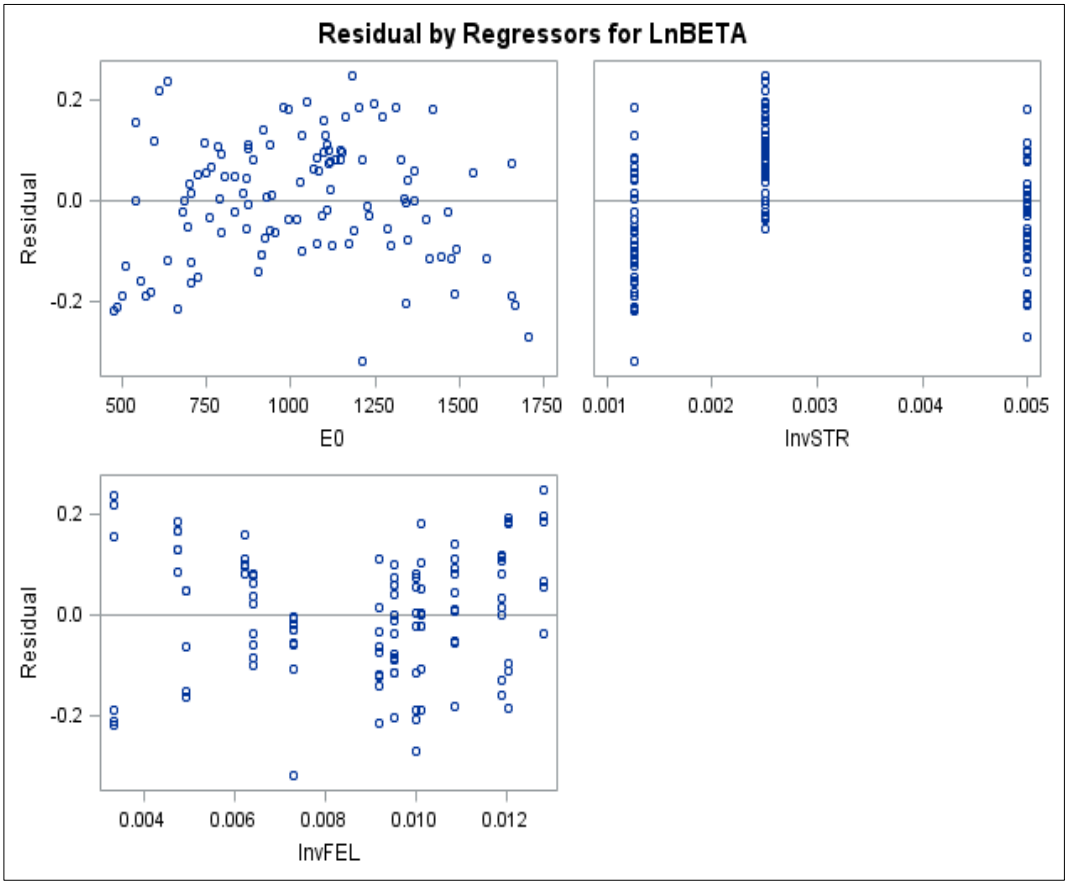

Figure 3.20 Diagnostic Plots for β-Parameter Regression Model 2

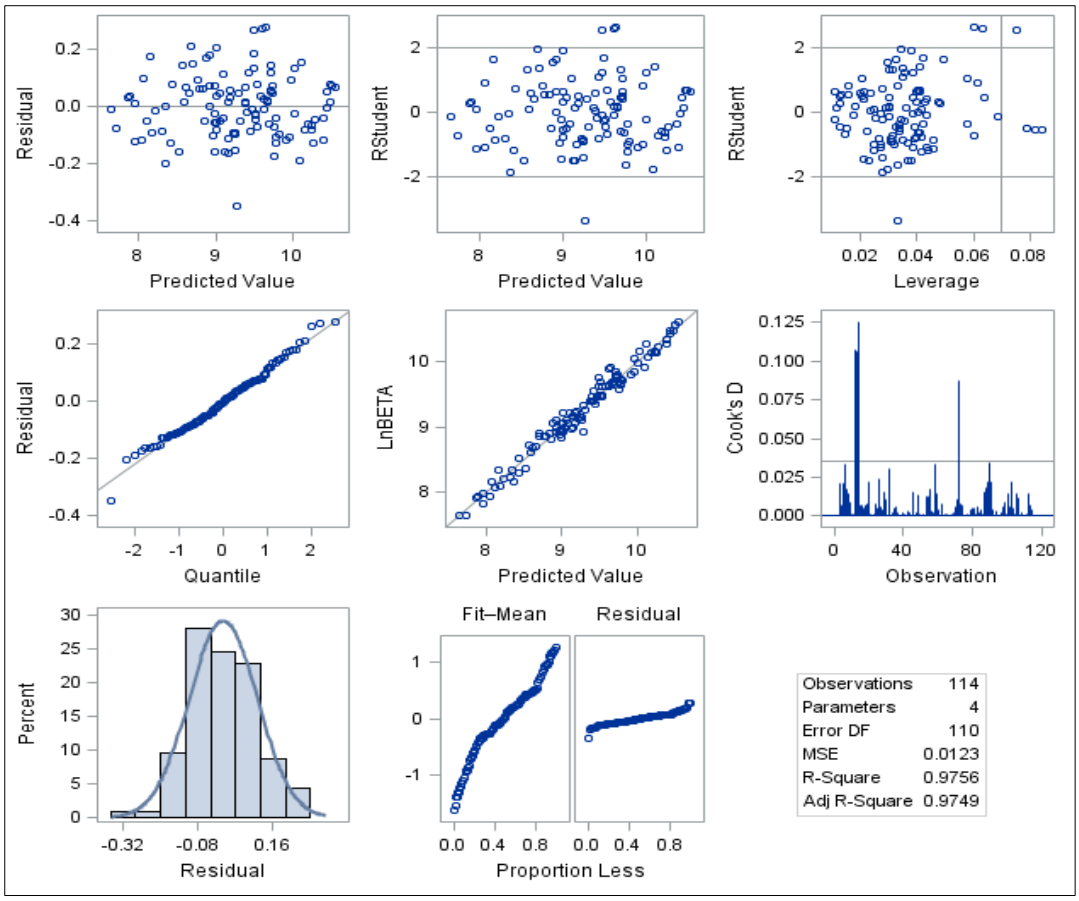

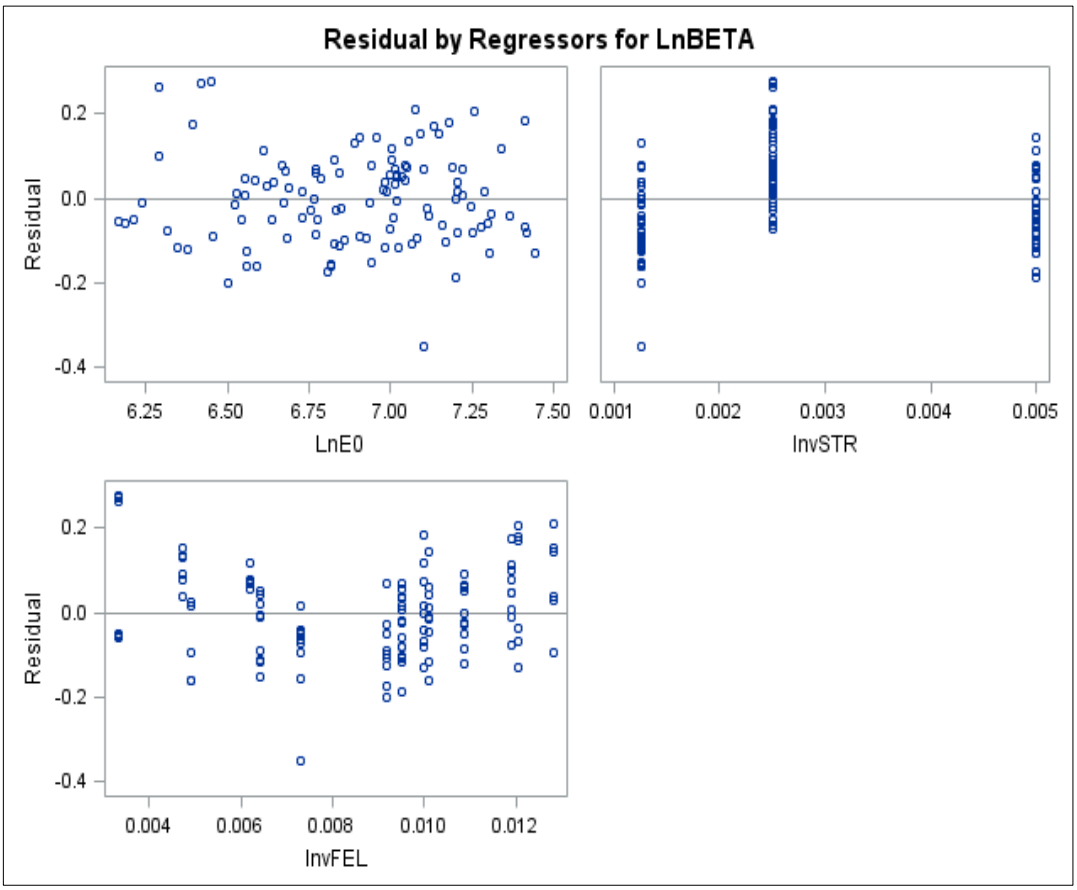

Figure 3.21 Diagnostic Plots for β-Parameter Regression Model 3

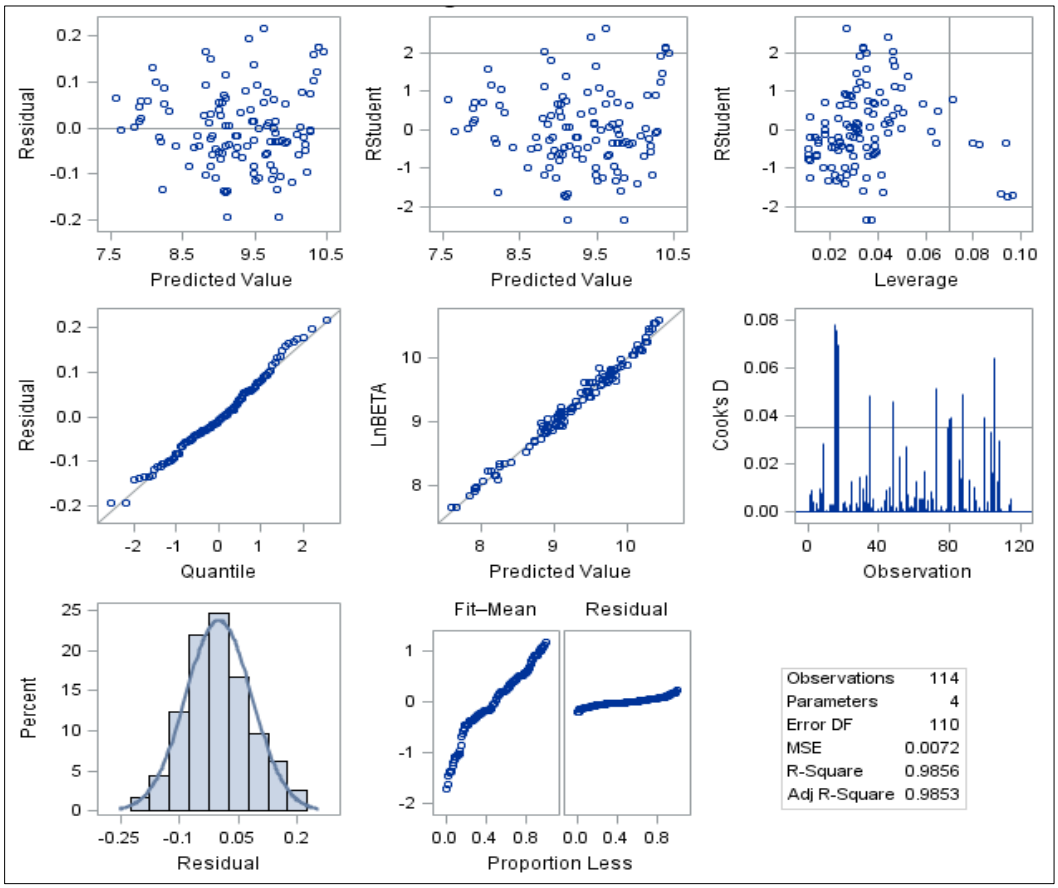

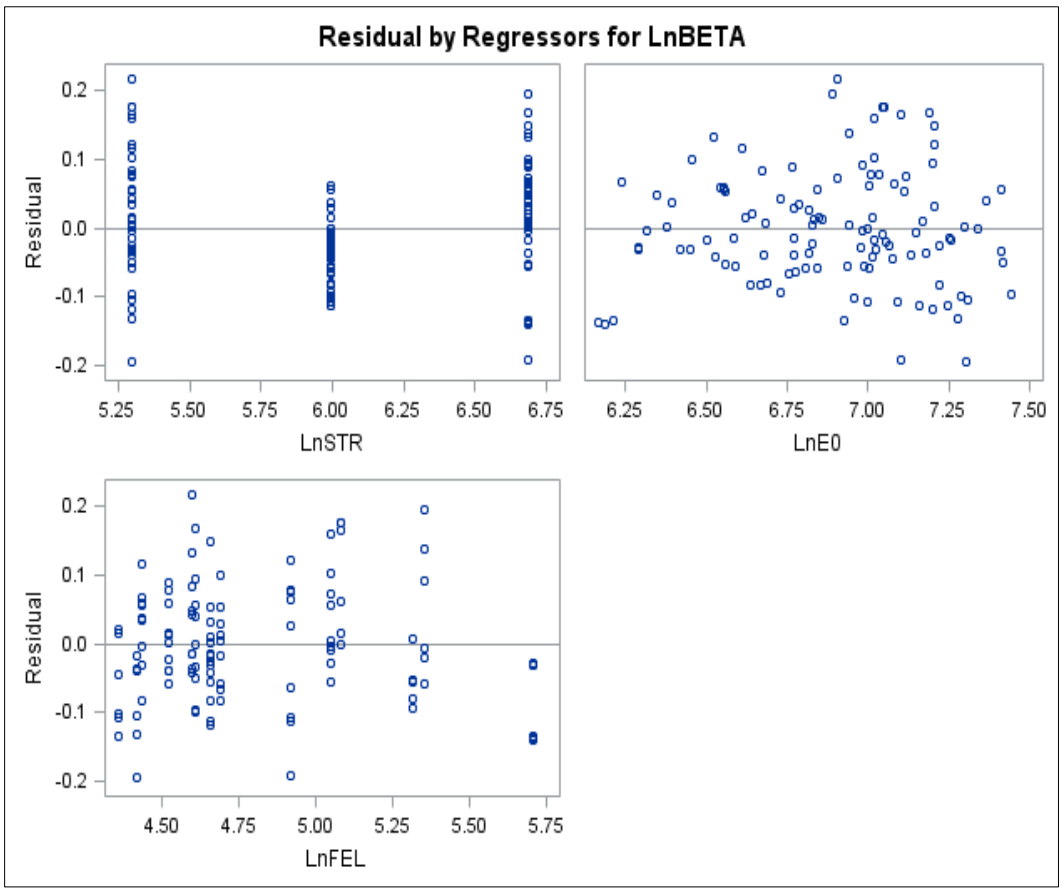

Figure 3.22 Diagnostic Plots for β-Parameter Regression Model 4

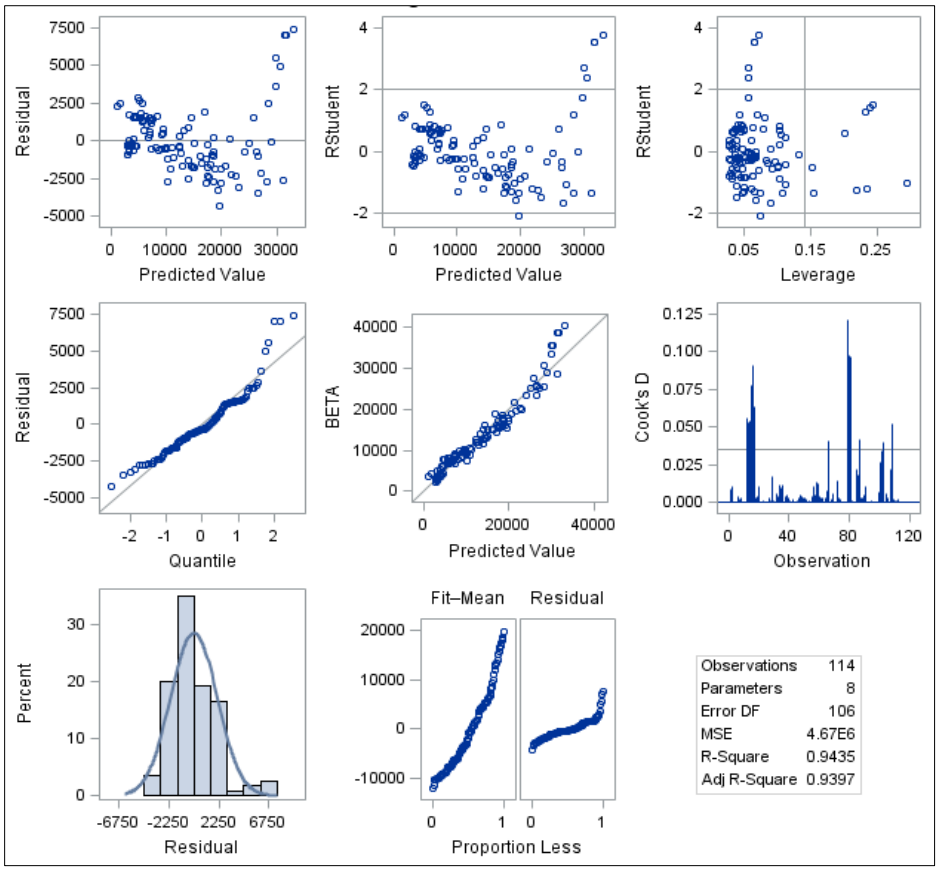

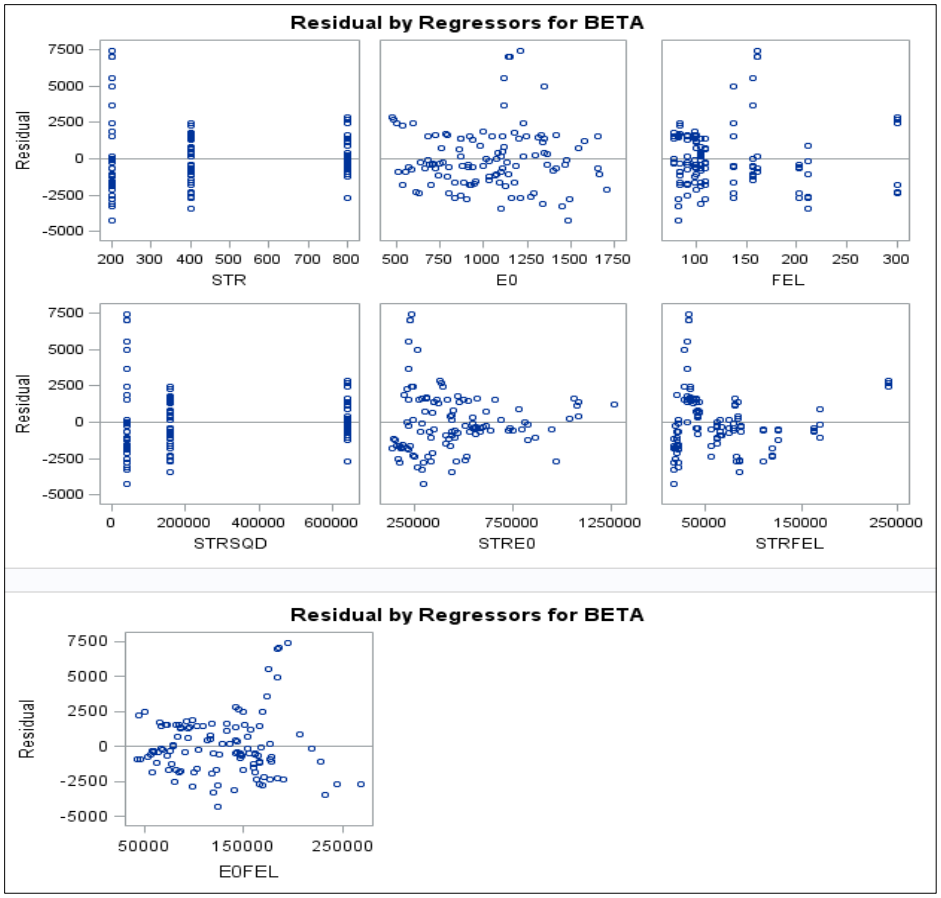

Figure 3.23 Diagnostic Plots for β-Parameter Regression Model 5

The satisfaction of the OLS regression assumptions provided confidence in the regression analysis results. Tables 3.11 through 3.15 present the regression coefficients and goodness-of-fit measures. All the regression coefficients were statistically significant ($\alpha = 0.05$), and the standard errors were reasonable. The only exception was that the coefficient of E_0 in Model 5 (Table 3.15) was not significant (p-value of 0.1670), but the variable was maintained in the regression model because its interaction with strain level (STR) was significant. A considerable proportion of the total variation in the response variable (BETA) was explained by the models, after accounting for the number of predictor variables (adjusted R^2 ranged between 91 and 99%). The models' predictive capabilities were correspondingly high: predicted R^2 were between 91 and 98%. The proximity of the three types of R^2 was an indication of the parsimony of the models, since overfitted models (those with excessive number of predictors) have predicted R^2 distinctly smaller than the other types of R^2.

Based on the results of the residual analysis and the regression parameters, it was concluded the five models had been adequately fitted and any one of them was acceptable for predicting β-parameter, as a function of AC material properties (AC modulus and fatigue endurance limit) and loading condition (strain level). Judging from the coefficient of determination, Model 4 was the preferred choice. However, instead of selecting this model for validation, it was decided to subject all five to the validation exercise and to select the best-performing model from the validation results.

Table 3.11 Regression Coefficients for β-Parameter Model 1
Ln(BETA) = f (STR, E_0, FEL)

Variable	Regression Coefficient	Standard Error	P-Value	95% Confidence Limits	
				Lower	Upper
Intercept	7.91681	0.11452	< 0.0001	7.68986	8.14376
STR	-0.00179	0.00008727	< 0.0001	-0.00196	-0.00162
E_0	0.00119	0.00007230	< 0.0001	0.00104	0.00133
FEL	0.00758	0.00037312	< 0.0001	0.00684	0.00832
N = 114	R^2 = 0.91311	Adjusted R^2 = 0.91074		Predicted R^2 = 0.90515	SEE = 0.20919

Table 3.12 Regression Coefficients for β-Parameter Model 2
Ln(BETA) = f (E_0, 1/STR, 1/FEL)

Variable	Regression Coefficient	Standard Error	P-Value	95% Confidence Limits	
				Lower	Upper
Intercept	8.86471	0.05319	< 0.0001	8.75930	8.97011
E_0	0.00101	0.00004135	< 0.0001	0.00092777	0.00109
InvSTR	295.07026	8.25567	< 0.0001	278.70946	311.43107
InvFEL	-166.62279	4.44642	< 0.0001	-175.43455	-157.81103
N = 114	R^2 = 0.96993	Adjusted R^2 = 0.96911		Predicted R^2 = 0.96732	SEE = 0.12304

Table 3.13 Regression Coefficients for β-Parameter Model 3
Ln(BETA) = f (LnE_0, 1/STR, 1/FEL)

Variable	Regression Coefficient	Standard Error	P-Value	95% Confidence Limits	
				Lower	Upper
Intercept	3.02384	0.24226	< 0.0001	2.54373	3.50394
LnE_0	0.99932	0.03625	< 0.0001	0.92748	1.07116
InvSTR	290.29245	7.48205	< 0.0001	275.46479	305.12012
InvFEL	-165.83146	4.00247	< 0.0001	-173.76342	-157.89949
N = 114	R^2 = 0.97559	Adjusted R^2 = 0.97492		Predicted R^2 = 0.97353	SEE = 0.11086

Table 3.14 Regression Coefficients for β-Parameter Model 4
Ln(BETA) = f (LnSTR, LnE_0, LnFEL)

Variable	Regression Coefficient	Standard Error	P-Value	95% Confidence Limits	
				Lower	Upper
Intercept	0.73461	0.27814	0.0095	0.18340	1.28582
LnSTR	-0.81541	0.01589	< 0.0001	-0.84691	-0.78392
LnE_0	1.08514	0.02828	< 0.0001	1.02910	1.14118
LnFEL	1.24489	0.02311	< 0.0001	1.19910	1.29069
N = 114	R^2 = 0.98565	Adjusted R^2 = 0.98526		Predicted R^2 = 0.98445	SEE = 0.08503

Table 3.15 Regression Coefficients for β-Parameter Model 5
BETA = f (STR, E_0, FEL)

Variable	Regression Coefficient	Standard Error	P-Value	95% Confidence Limits	
				Lower	Upper
Intercept	8208.03325	3028.02287	0.0078	2204.68341	14211
STR	-57.86279	7.42353	< 0.0001	-72.58066	-43.14492
E_0	3.02754	2.17574	0.1670	-1.28607	7.34115
FEL	67.93529	18.21441	0.0003	31.82344	104.04714
STR*STR	0.07083	0.00568	< 0.0001	0.05957	0.08210
STR*E_0	-0.01708	0.00308	< 0.0001	-0.02318	-0.01097
STR*FEL	-0.16031	0.01888	< 0.0001	-0.19775	-0.12288
E_0*FEL	0.14498	0.01449	< 0.0001	0.11625	0.17371
N = 114	R^2 = 0.94347	Adjusted R^2 = 0.93974		Predicted R^2 = 0.93298	SEE = 2160.45481

3.5 Summary of Pseudo Fatigue Cracking Damage Model Development

- A pseudo fatigue cracking damage model was formulated on the platform of beam fatigue testing. It is a simple strain-based phenomenological model that implements incremental-recursive fatigue damage accumulation in WESLEA, a layered elastic analysis program.
- Nine trial functional forms of the pseudo fatigue damage cracking model were evaluated to identify which of them could reasonably predict beam fatigue damage curves, quantifying the goodness-of-fit between predicted and measured fatigue damage curves by coefficient of determination.
- After identifying the best-performing model (Model 7), it was calibrated with 114 beam fatigue test results obtained from 15 different plant-produced asphalt mixtures. These mixtures incorporated modified and unmodified binders, different binder contents and recycled materials meant to achieve a wide range of fatigue performance characteristics.
- Fatigue endurance limit was a key model input. Two sets of fatigue endurance limits were determined with the procedures recommended by NCHRP 9-44A and NCHRP 09-38. The laboratory-measured endurance limits obtained from the NCHRP 09-38 procedure better captured the effects of binder modification, rich-bottom mixtures and recycled materials, so they were used for calibrating the pseudo fatigue cracking damage model.
- The calibration exercise involved using Model 7 to iteratively simulate 114 pavement structures to determine a set of 114 β-parameters that produced the best match between the

predicted and measured fatigue damage curves. The β-parameter was idealized as a fatigue damage parameter that bridged predicted and measured fatigue curves.

- The cumulative distribution of the coefficient of determination for the 114 pairs of measured versus predicted fatigue curves showed high quality of fit, notwithstanding the large variations in the beam fatigue test data. This was an indication that the functional form of the pseudo fatigue cracking damage model was appropriate, and the accuracy of its predictions would be influenced by the quality of the β-parameters.
- The 114 β-parameters were used as values of a response variable to develop a linear multiple regression model for predicting β-parameter as a function of easily-obtained data. Initially, 10 potentially relevant predictor variables, comprising AC mixture properties and strain levels, were considered.
- Nine β-parameter regression models were investigated. The five best performing models – which contained strain level, initial AC modulus and fatigue endurance limit as predictor variables – satisfied the fundamental assumptions of ordinary least square linear regression analysis to provide the best model fit to the observed data.
- Out of the five best performing β-parameter regression models, Model 4 was outstanding. It incorporated natural logarithm of β-parameter as a dependent variable and natural logarithm of strain, initial AC modulus and fatigue endurance limit as predictor variables to yield an adjusted R^2 of 98.53%.
- The strain variable in the β-parameter regression model represents the initial critical tensile strain at the bottom of the AC layer. The pseudo fatigue cracking damage model initiates damage accumulation if the initial critical strain exceeds 10% of the fatigue endurance limit.

CHAPTER 4

VALIDATION OF PSEUDO FATIGUE CRACKING DAMAGE MODEL

The validation process sought to evaluate the capability of the pseudo fatigue cracking damage model to predict fatigue damage curves for an independent set of beam fatigue test results. The validation results determined whether the proposed fatigue cracking damage model was a reasonable mathematical representation of the beam fatigue damage process in a layered elastic system. As the flowchart in Figure 4.1 shows, the validation exercise was executed in two phases: validation of the five best β-parameter regression models and the validation of the full pseudo fatigue cracking damage model.

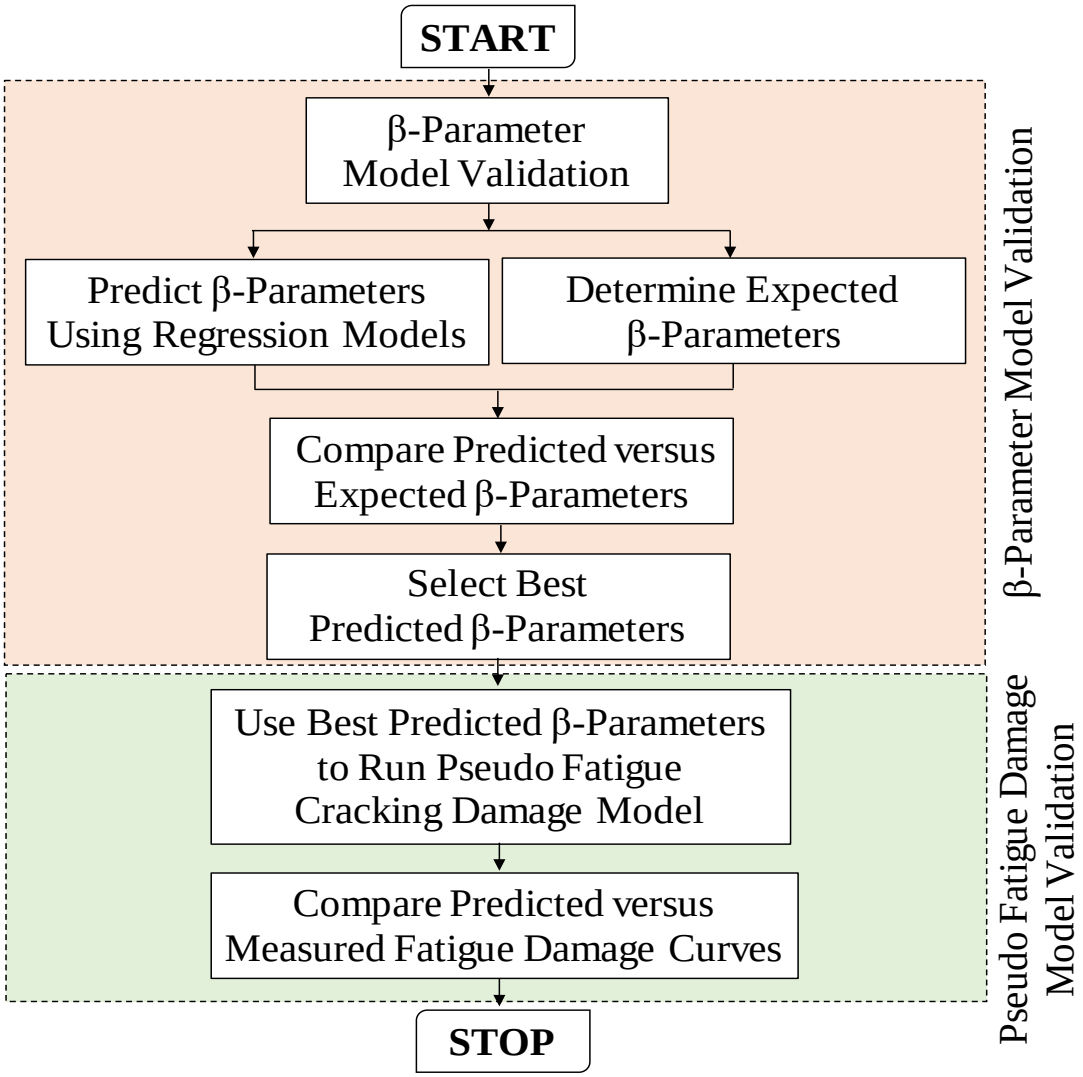

Figure 4.1 Flowchart for Validation of Pseudo Fatigue Cracking Damage Model

4.1 Validation of β-Parameter Regression Models

The validation dataset comprised of 41 beam fatigue test results, as summarized in Table 3.2. The validation process involved using the β-parameter regression models to predict β-parameters for a given inputs of strain, initial AC modulus and fatigue endurance limit and comparing the predicted β-parameters against expected β-parameters. The expected β-parameters, which may be considered as 'measured' β-parameters, were values that provided the best agreement between predicted and measured fatigue curves. The same process used to generate β-parameters for the model calibration was also employed to generate the expected β-parameters. Briefly, 41 pavement cross-sections were formulated to represent each of the beam fatigue test results; summary information on these cross-sections is shown in Table 4.1, while the details are presented in Appendix D. The cross-sections incorporated the initial AC stiffness from the beam fatigue tests. The initial critical strain at the AC layer bottom equaled the strain level used to generate the corresponding beam fatigue test data.

Following the flowchart in Figure 3.10, the pseudo fatigue cracking damage model (Model 7) simulated the 41 pavement structures to generate fatigue damage curves, which were then compared with the measured beam fatigue curves. Notice that the number of iterations was the same as the number of load cycles to failure in the beam fatigue tests, except for extrapolated cycles to failure, in which case iterations ended at 12 million, the number of load cycles for beam fatigue test specimens that did not reach the 50% AC stiffness reduction failure point. After several trials, β-parameters that yielded the best match between the predicted and measured fatigue curves, as determined by R^2, were identified and denoted as expected β-parameters. Figure 4.2 shows the cumulative distribution of the R^2 values associated with the expected β-parameters. The high R^2 values, regardless of the high variation in the fatigue test data, indicated the robustness of the pseudo fatigue damage model. For instance, 80% of the R^2 values were better than 80%.

Table 4.1 Summary Information on Cross-Sections Simulated for Model Validation

Layer	Thickness (in.)	Modulus (ksi)	Poisson's Ratio
Asphalt Concrete	6	350 – 1400	0.35
Granular Base	8 – 10	8 – 10	0.40
Subgrade Soil	Infinite	3 – 5	0.45

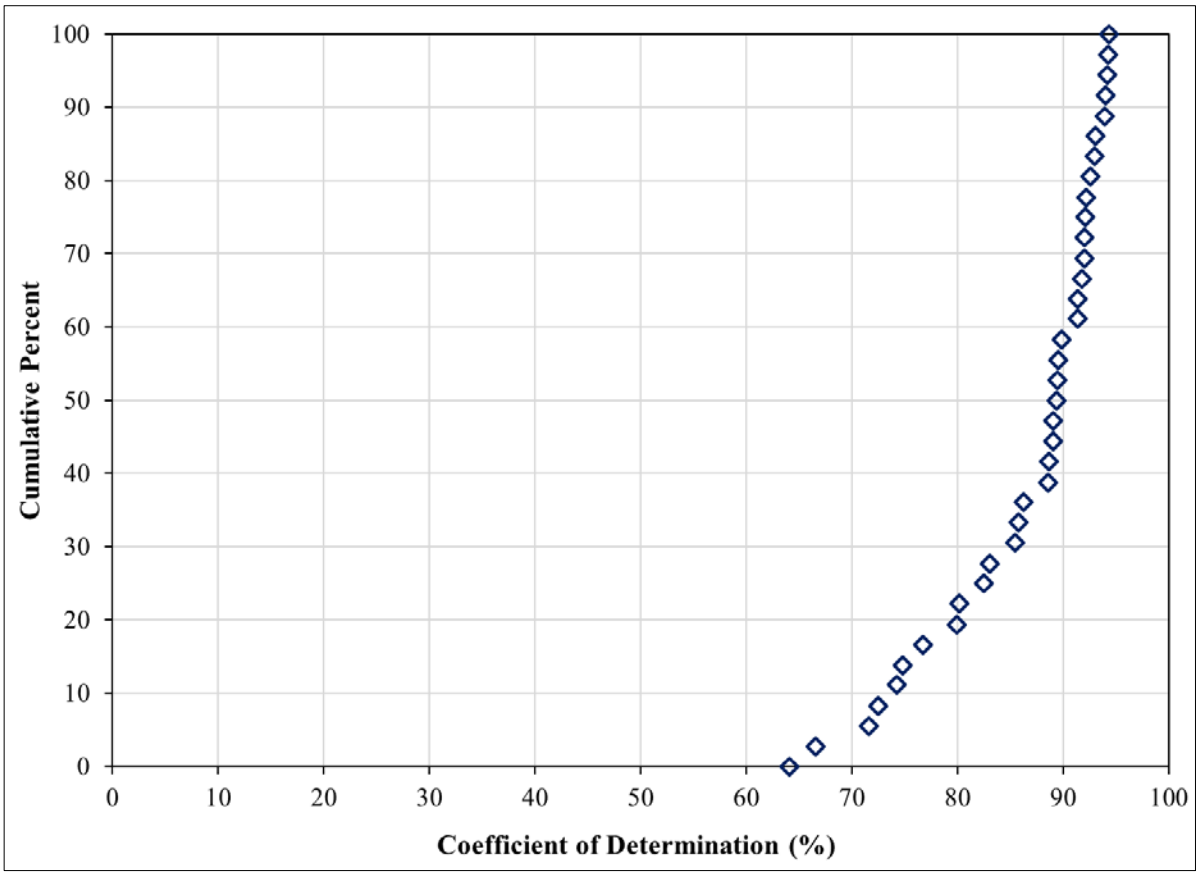

Figure 4.2 Cumulative Distribution of R^2 Associated with Expected β-Parameters

Out of the 41 measured fatigue curves, expected β-parameters could not be found for four (Section S13 intermediate base mixture in the 2012 research cycle), thus reducing the sample size of the validation dataset to 37. For those four cases, the strain level used in the beam fatigue testing was 200με, and the AC mixture's fatigue endurance limit was 184με, resulting in a strain ratio of 1.09. In the application of the pseudo fatigue cracking damage model, this implies the initial critical tensile strain at the AC layer bottom exceeded the fatigue endurance limit by only 9%. According to Equation 25, the initial critical strain must exceed the fatigue endurance limit by 10% for the initiation of damage accumulation. Violating this threshold, the natural logarithm of the α_1-factor in the pseudo fatigue damage model (Equation 22a) became smaller than negative one. Consequently, the k-term reduced to a negative value, and the AC modulus increased with load cycles, instead of decreasing.

Next, the five best β-parameter regression models (Tables 3.11 through 3.15) were used to predict five sets of 37 β-parameters, using the validation data. Recall the model inputs were the strain level, initial AC modulus and fatigue endurance limit. The percent error between the expected and predicted β-parameters was computed using Equation 30 and developed into the cumulative distribution plot in Figure 4.3 to determine which of the β-parameter regression

models provided a more accurate prediction. Evidently, Model 4, which employed natural logarithm of all variables, yielded better predictions; the errors between the predicted and expected β-parameters were within a range of ±20%, with nearly an equal split between over- and under predicted values. Figure 4.4 shows the predicted β-parameters from Model 4 versus the expected β-parameters. On the average, the predicted β-parameters were larger than the expected β-parameters by 1%, with a strong correlation between them (R^2 value of 95.86%). The plots for the remaining regression models, which also showed strong correlation between the predicted and expected β-parameters, are shown in Appendix G. Again, Model 4 is validated as the preferred β-parameter prediction equation.

$$\text{Percent Error} = 100\left(\frac{\beta_{expected} - \beta_{predicted}}{\beta_{expected}}\right) \quad (30)$$

Where:

Error = Percent error between expected and predicted β-parameters

$\beta_{expected}$ = Expected β-parameter

$\beta_{predicted}$ = Predicted β-parameter

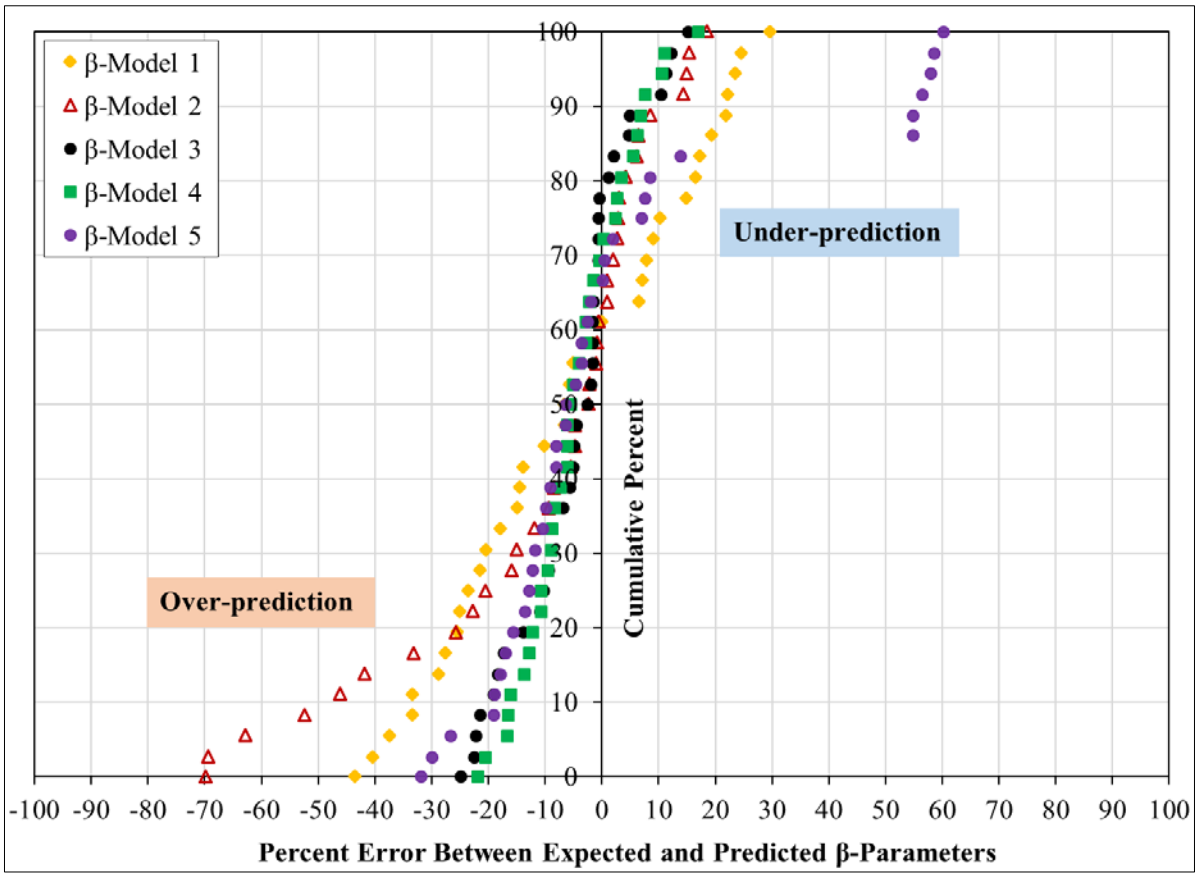

Figure 4.3 Distribution of Error Between Expected and Predicted β-Parameters

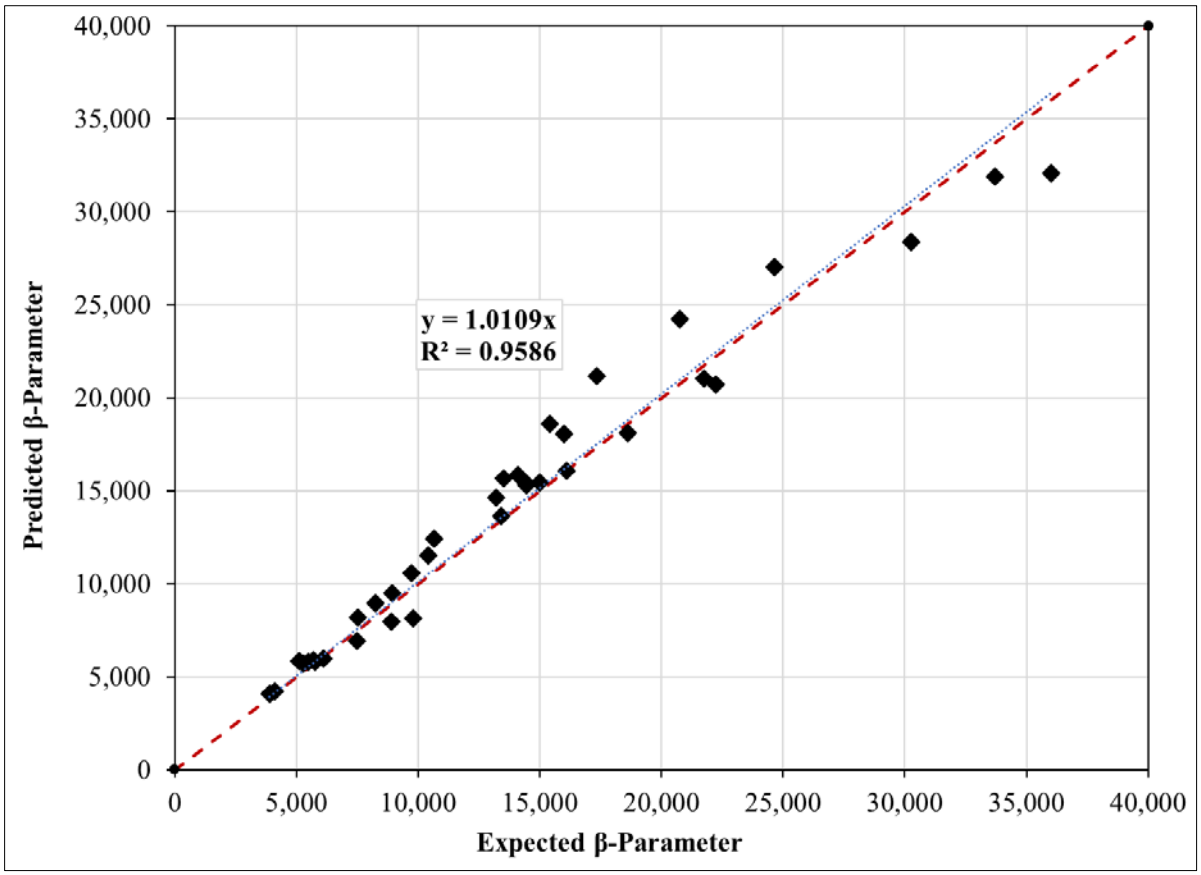

Figure 4.4 Predicted β-Parameters (Model 4) versus Expected β-Parameters

To ascertain if the variations in the predicted and expected β-parameters were in harmony, and whether the expected β-parameters fell within 95% confidence limits of the predicted β-parameters, Figures 4.5 through 4.9 were prepared for β-parameter regression Models 1 through 5, respectively. The confidence band was determined based on the 95% confidence limits for the β-parameter regression coefficients shown in Tables 3.11 through 3.15. Overall, the variations in the predicted β-parameters corresponded with those in the expected β-parameters, except for the unusual trend observed in the last six data points in Figure 4.6 (over-prediction by Model 2) and Figure 4.9 (under-prediction by Model 5). The effect of these six unusual β-parameters was evident in the error distribution shown in Figure 4.3.

As seen in Table 3.10, Model 2 related the natural logarithm of the response variable (BETA) to the initial AC modulus (E_0) and the inverses of strain level (1/STR) and fatigue endurance limit (1/FEL). Model 5 implemented polynomial regression, incorporating linear and quadratic terms of the predictor variables and their two-way interaction terms. Despite their good data fit, polynomial regression models could produce inaccurate predictions when extrapolated beyond the range of the calibration data (Kutner et al., 2008); this seems to be a reason for the negative lower bound β-parameters, which could not be shown in Figure 4.9.

Considering the predictions of both Models 2 and 5 on the same six data points were unusual, it was necessary to examine these data points to identify underlying reasons, if any.

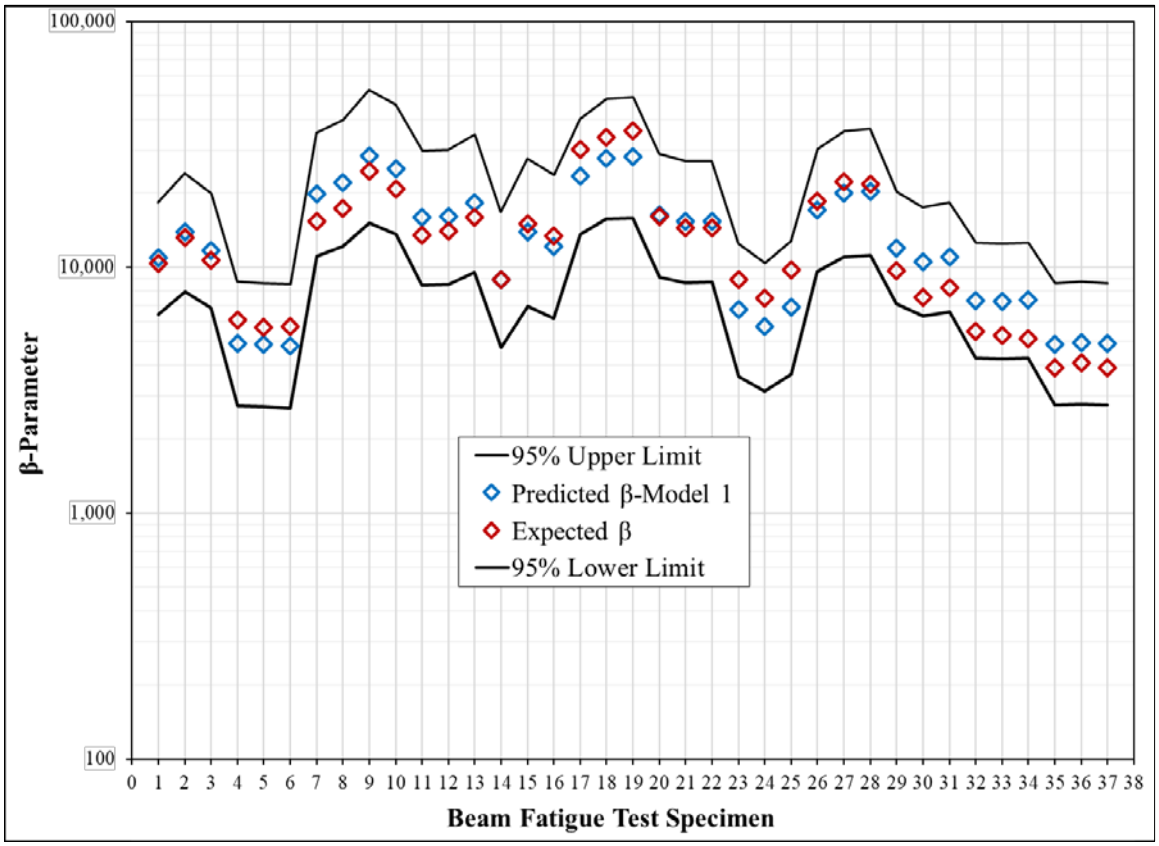

Figure 4.5 Variations in Predicted and Expected β-Parameters – Regression Model 1

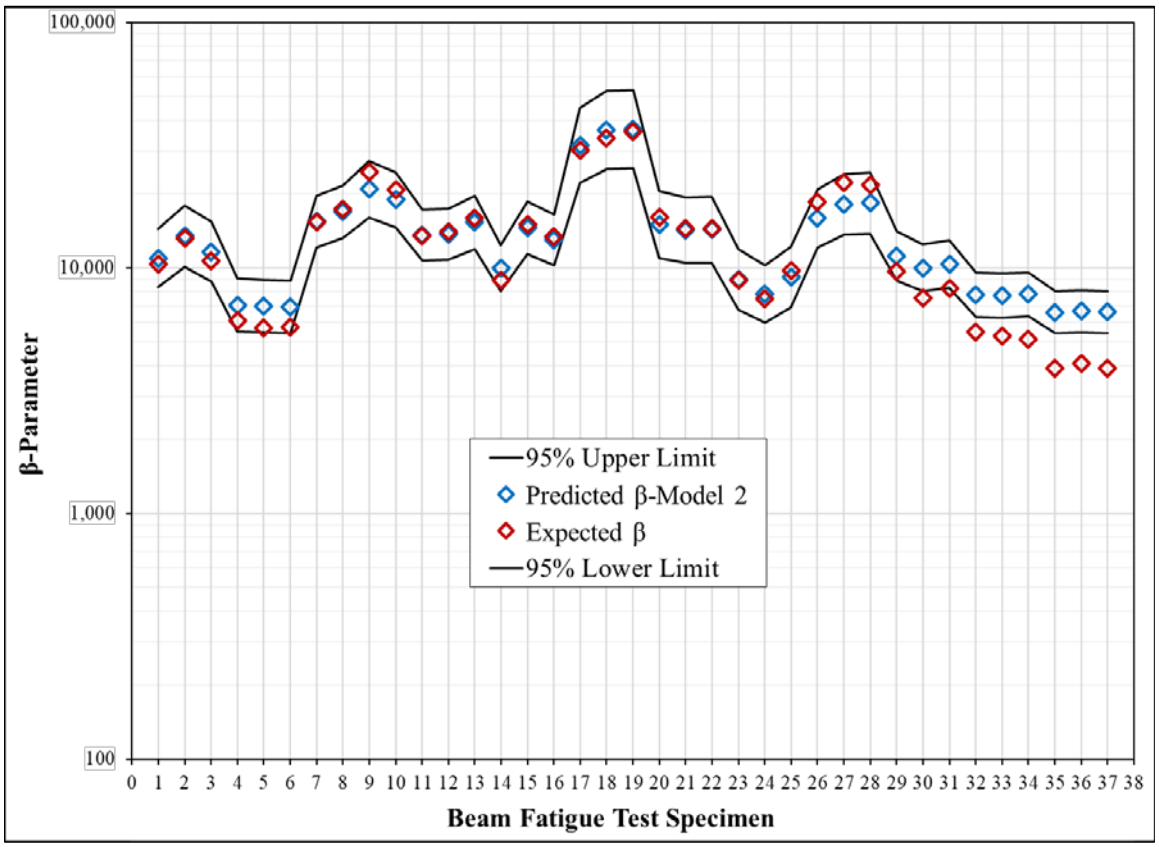

Figure 4.6 Variations in Predicted and Expected β-Parameters – Regression Model 2

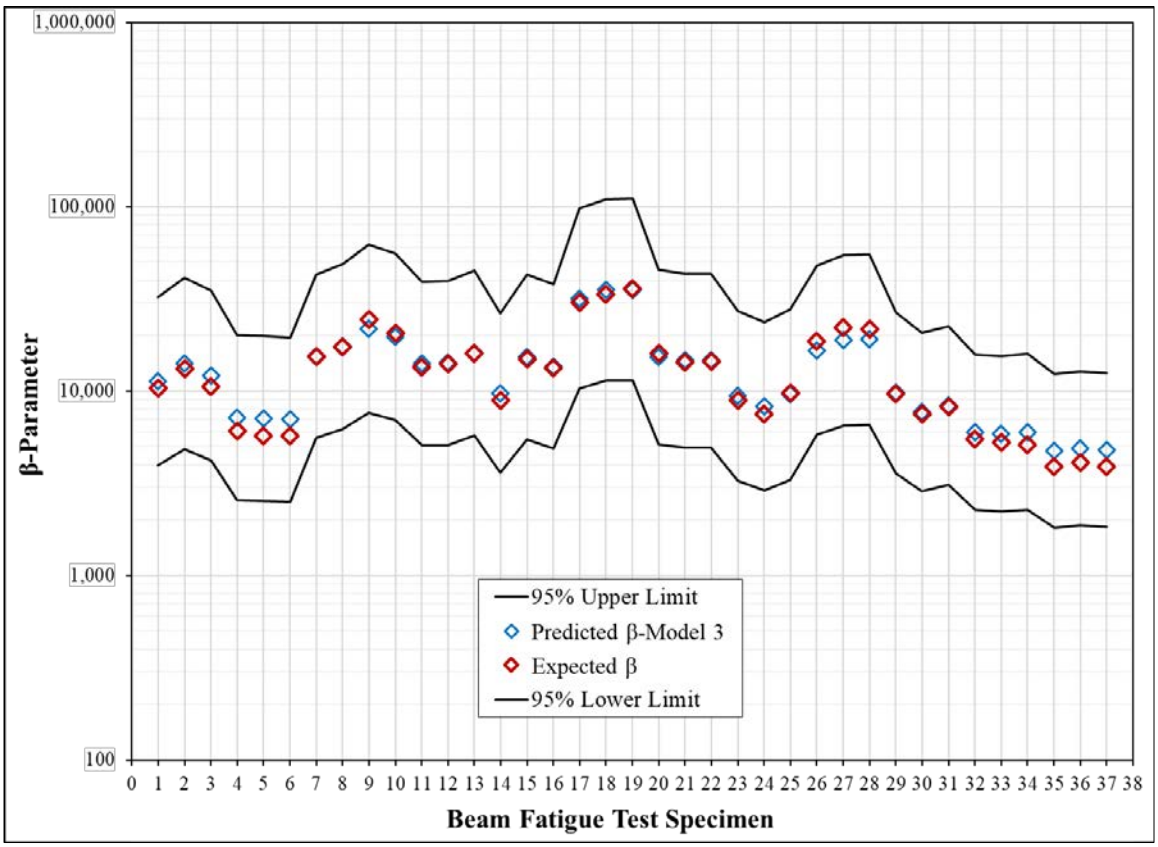

Figure 4.7 Variations in Predicted and Expected β-Parameters – Regression Model 3

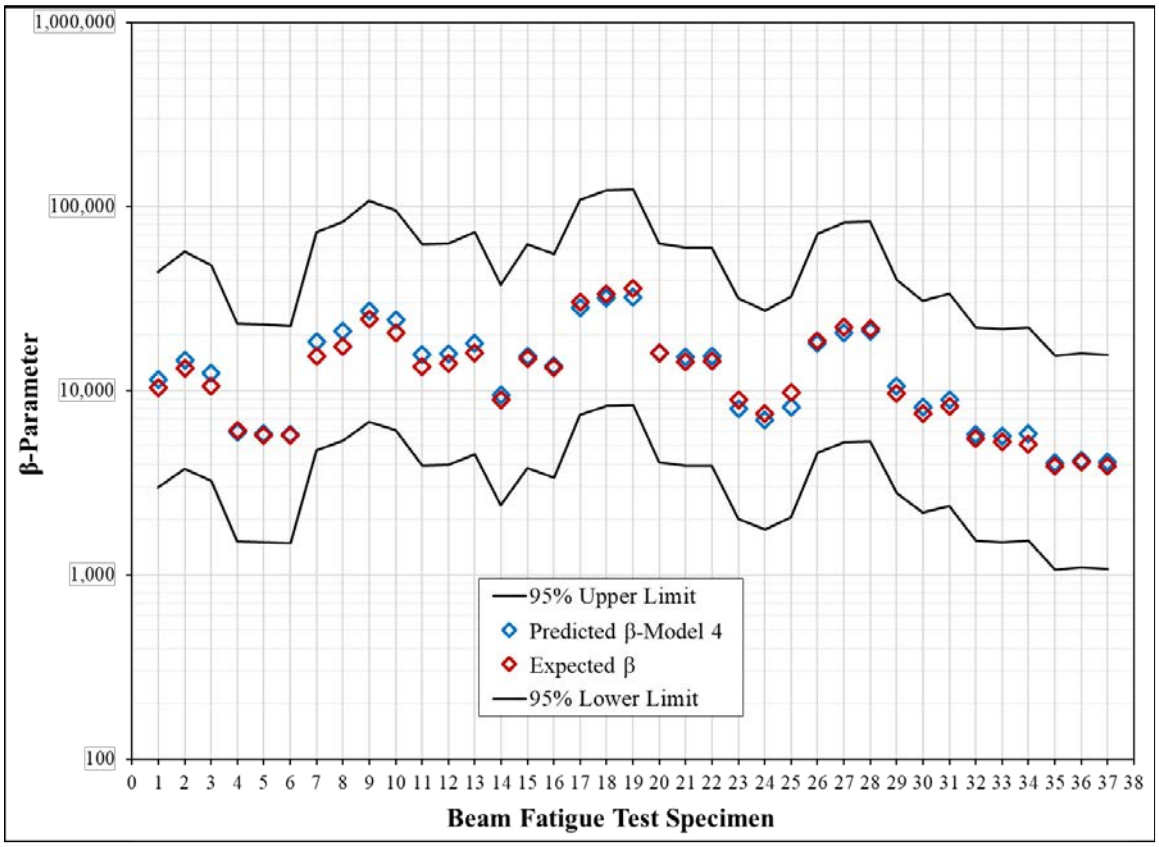

Figure 4.8 Variations in Predicted and Expected β-Parameters – Regression Model 4

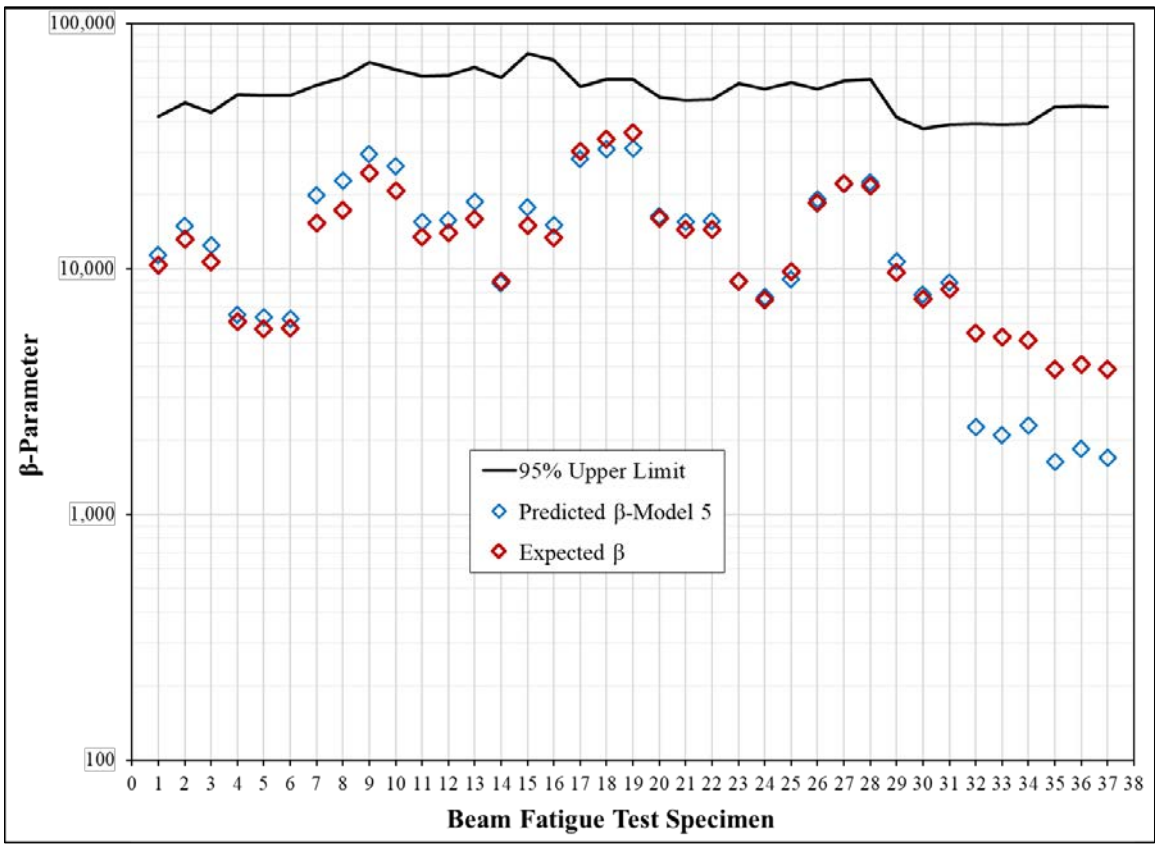

Figure 4.9 Variations in Predicted and Expected β-Parameters – Regression Model 5

Appendix A shows the last six validation data points originated from the base mixture of Section S13, tested at 600 and 800με during the 2012 research cycle. The three replicate beams tested at 600με had initial stiffness of 398, 391 and 400 ksi, and the corresponding stiffness for those tested at 800με were 356, 367 and 359 ksi. These stiffness values were the lowest in both the calibration and validation datasets. According to Appendix B, the fatigue endurance limit of the AC mixture for S13 (209με) ranked second among the validation dataset, next to 2009 Section N7's value of 241με. Overall, S13 ranked fourth, preceded by 300με (2006, S12), 241με (2009, N7) and 211με (2012, S5 base). N7 recorded a higher initial AC stiffness than S13; they were 845, 853 and 963 ksi for the beams tested at 600με and 661, 1,034 and 923ksi for those tested at 800 με.

Interestingly, while Models 2 and 5 produced less accurate β-parameters for the last six data points of S13 (Specimens 32 through 37 in Figures 4.6 and 4.9, respectively), both models yielded reasonably accurate β-parameters for another set of six data points from N7 (Specimens 11 through 16 in Figures 4.6 and 4.9, respectively). For both sets of data points, the strain levels (STR) for fatigue testing were the same (600 and 800με), and the endurance limits (FEL) were high (209με for S13 and 241με for N7). The major difference between S13 and N7 was the initial AC moduli (E_0): the average values for N7 were 2.2 and 2.4 times higher than those for S13 at strain levels of 600 and 800 με, respectively. Put together, the validation results suggested β-parameter regression Models 2 and 5 exhibited low prediction capability for high FEL–low modulus inputs, but handled high FEL–high modulus inputs reasonably well. While Figures 4.5 and 4.7 indicate Models 1 and 3, respectively, provided reasonably accurate predictions for the full range of variable inputs, Model 4 (Figure 4.8), overall, exhibited superior predictive performance. Notice, too, Model 4 handled both high FEL-high modulus (Specimens 11 through 16) and high FEL–low modulus (Specimens 32 through 37) inputs reasonably well.

Finally, variance inflation factors (VIFs), which indicate the presence of collinearity in the predictor variables of a regression model, were computed using SAS to provide statistical confirmation for the scatter plots' (Figure 3.14) indication that the predictor variables in Model 4 (LnSTR, LnE_0 and LnFEL) were not collinear. Recall collinearity causes wrong signs of regression coefficients, among other adverse effects. The VIFs for LnSTR, LnE_0 and LnFEL were 1.17433, 1.19603 and 1.06307, respectively; none exceeded 10, a typical criterion for collinearity (Chatterjee and Hadi, 2012). In conclusion, the regression analysis results confirmed β-parameter regression Model 4 as the most preferred option.

4.2 Validation of Pseudo Fatigue Cracking Damage Model

Per the flowchart in Figure 4.1, the second phase of the model validation process was to incorporate the predicted β-parameters in the pseudo fatigue cracking damage model to predict fatigue damage curves. By comparing these curves with the measured fatigue curves, it would be possible to assess how reasonably well the proposed fatigue cracking damage model simulates the fatigue damage process in beam fatigue testing within a linear elastic system.

Model 4 provided the most accurate β-parameters for validating the pseudo fatigue damage model. However, to provide basis for comparison, the β-parameters obtained from the other four regression models were also utilized. The 37 pavement structures (Table 4.1, Appendix D) formulated for validating the β-parameter regression models were simulated with the pseudo fatigue damage model, incorporating the predicted β-parameters to generate fatigue damage curves. The iterative procedure in Figure 3.10 was followed. Here, too, the number of iterations was set to the number of load cycles to failure in the corresponding fatigue tests or 12 million cycles, if failure point was not reached. After the simulations, 37 fatigue damage curves were generated for each of the five β-parameter regression models.

To evaluate how well the pseudo fatigue damage model utilized the predicted β-parameters to simulate beam fatigue damage in a layered elastic framework, the predicted damage curves were compared with measured fatigue curves, using R^2 (Equation 20) to measure the goodness-of-fit. Five sets of R^2 cumulative distribution plots were prepared, one for each of the β-parameter regression models. The R^2 cumulative distribution plots demonstrated the comparative performance of the β-parameter regression models and, by extension, the pseudo fatigue cracking damage model. The higher the R^2 value, the better the agreement between the predicted and measured fatigue curves which, in turn, meant: (a) the β-parameter regression models provided better predictions, and (b) the pseudo fatigue cracking damage model properly utilized the β-parameter predictions to simulate the damage accumulation in beam fatigue testing using layered elastic theory.

4.3 Results of Pseudo Fatigue Cracking Damage Model Validation

Figure 4.10 shows the cumulative distribution of R^2, signifying the quality of fit of the predicted versus measured fatigue damage curves. Two key pieces of information are noteworthy. First, notice the overall capability of the pseudo fatigue cracking damage model to simulate beam fatigue damage, as evident in the decent R^2 values. In general, predictions that incorporated β-parameters from β-Model 4 provided the largest R^2 values. As seen in the figure, 70% of the predictions produced R^2 of at least 60%. Predictions with lower R^2 values were generally

related to variability in the beam fatigue test data. These validation results are significant considering the large variations in the fatigue test data used for the analysis. Clearly, an accurate estimation of β-parameters is essential for the pseudo fatigue cracking damage model to reasonably predict beam fatigue curves, at least up to a failure point of 50% reduction in the initial AC modulus, which typically represents the initial zone of rapid stiffness deterioration and the middle zone of gradual decrease in stiffness. Secondly, β-parameter regression Model 4 distinguished itself, among the other candidates, as the most accurate model, thus confirming the earlier conclusions.

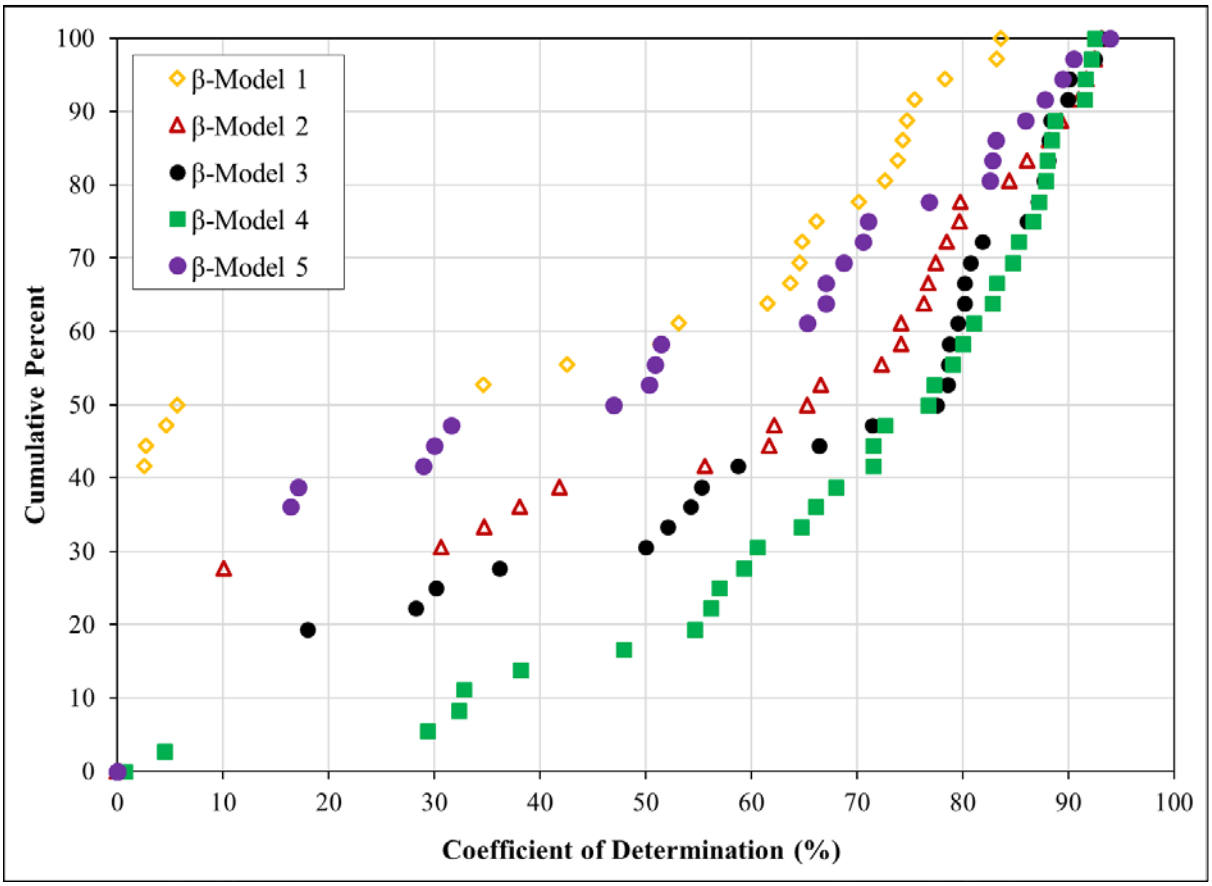

Figure 4.10 Cumulative Distribution of R^2 Values Indicating Goodness-of-Fit of Predicted Versus Measured Fatigue Damage Curves

Apart from the goodness-of-fit analysis, the validation results were examined to identify other performance characteristics of the pseudo fatigue cracking damage model. While all the expected β-parameters and those used for model calibration ensured the pseudo fatigue damage model simulated the full number of load cycles to failure recorded in the beam fatigue tests, the predicted β-parameters could not facilitate this for all pavement cross-sections simulated in the validation process. Recall the expected β-parameters and those used for model calibration were not predicted; they were identified, through trial-and-error, as values that yielded the best

match between measured and predicted fatigue damage curves. In contrast, the β-parameters used to validate the pseudo fatigue damage model were predicted using the regression models. Consequently, a key model performance-related question was: what percent of the beam fatigue tests' load cycles to failure was simulated by the pseudo fatigue damage model?

Figure 4.11 shows the distribution of percent of load cycles to failure from beam fatigue testing simulated by the pseudo fatigue damage model during the validation. The percent of load cycles to failure was calculated as the total number of model iterations divided by number of load cycles to failure in the beam fatigue test multiplied by 100. Three beam specimens survived 12 million load cycles in the fatigue testing without reaching failure; accordingly, the pseudo fatigue damage model was set to perform 12 million iterations. Hence, in computing the percent of load cycles to failure, the number of load cycles to failure was taken as 12 million. Ideally, the predicted β-parameters should enable iterations equal to the number of load cycles to failure (to yield percent of load cycles to failure of 100) and, in addition, ensure the predicted and measured fatigue curves reasonably match.

In interpreting Figure 4.11, it should be noted that, if all other model inputs were held constant, lower percent of load cycles to failure indicates the β-parameters were large (faster damage accumulation), and so the pseudo fatigue damage model could only predict a small portion of the measured fatigue curve. However, higher percent of load cycles to failure indicates the predicted β-parameters were adequate to allow the pseudo fatigue damage model to run many iterations (slower damage accumulation) to cover sizable portion of the measured fatigue curve. Either of the two scenarios could have different implications on the quality of fit of the predicted and measured fatigue curves, so the information in Figure 4.11 should be juxtaposed with the goodness-of-fit plot in Figure 4.10. For instance, a small or large β-parameter could produce either a good or poor match of the fatigue damage curves.

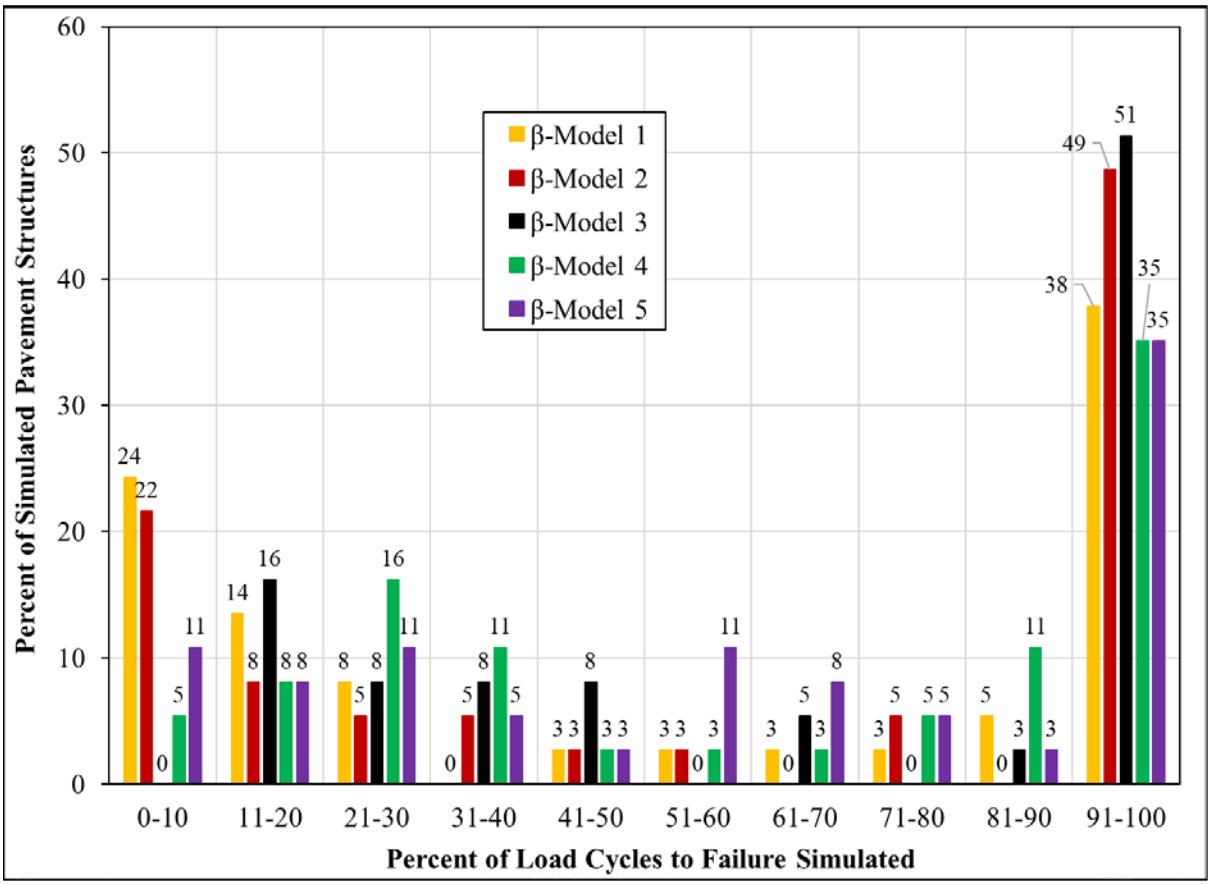

Figure 4.11 Pseudo Fatigue Damage Model Validation: Percent of Load Cycles to Failure Simulated

A different approach used to evaluate the performance of the pseudo fatigue damage model was to identify the AC modulus remaining at the end of the pseudo fatigue damage model's iterations and expressed it as percentage of the initial AC modulus (Figure 4.12). Preferably, there should be an exactly 50% reduction in the initial AC modulus at the end of model iterations to conform to the failure point of the beam fatigue testing. Practically, the modulus reduction could hover around 50%. Keeping all other model inputs constant, lower percent reduction in initial AC modulus implies fewer iterations of the pseudo fatigue damage model (large β-parameter, faster damage accumulation), whereas higher percent reduction means many model iterations (small β-parameter, slower damage accumulation).

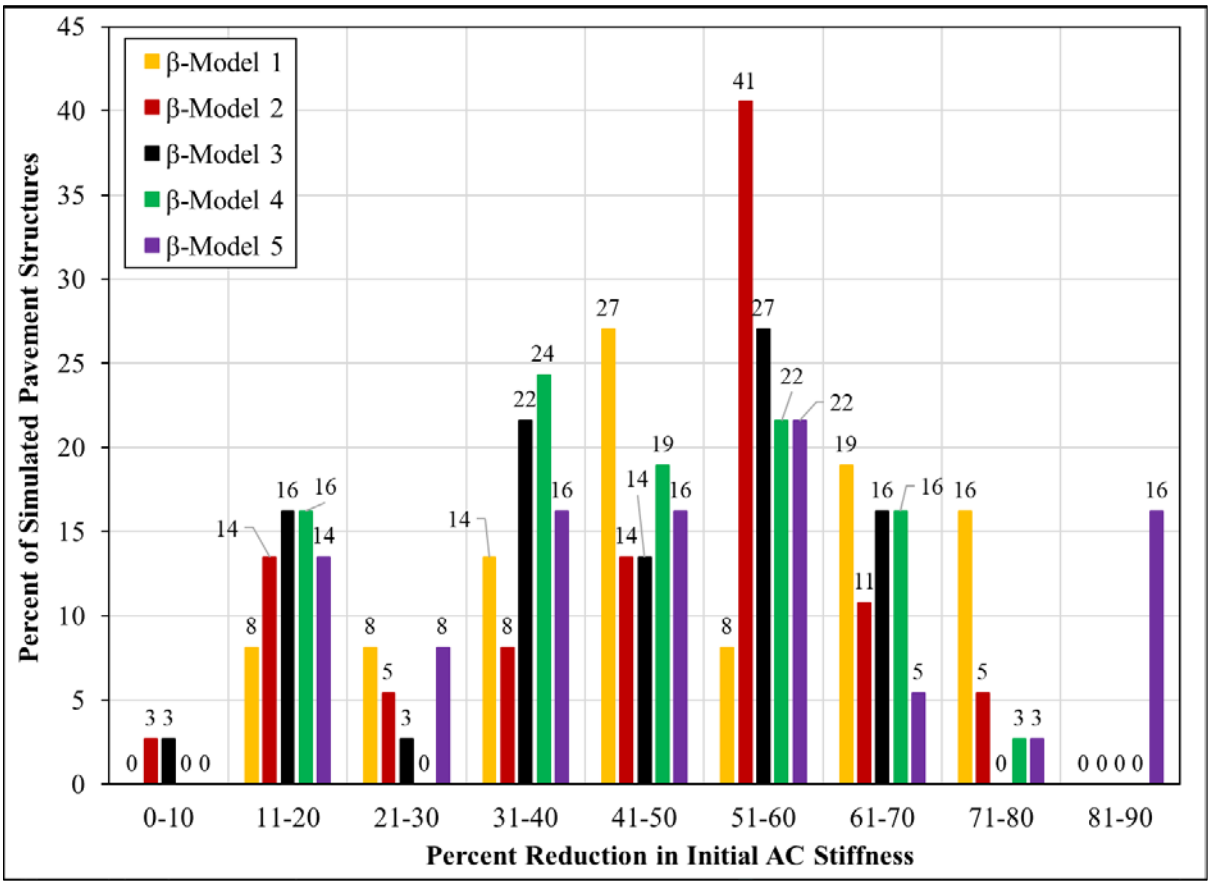

Figure 4.12 Pseudo Fatigue Damage Model Validation: Reduction in Initial AC Modulus

Perhaps an intuitive approach to present the same information in Figure 4.12 is to categorize the percent reduction in initial AC modulus as low (0-30%), medium (61-60%) and high (61-90%), as shown in Table 4.2. Recall the low category indicates large β-parameters that produced faster damage accumulation. The medium category implies β-parameters that yielded generally good damage accumulation rate (ideal reduction is 50% to match the failure point in beam fatigue testing) and the high category denotes small β-parameters that caused a slower damage accumulation rate.

For each β-parameter regression model, most of the simulated pavements had percent reduction in initial AC modulus in the medium category, with Model 4 topping followed by both Models 2 and 3. If all other factors were held constant, Models 2, 3 and 5 produced the largest β-parameters: 22% of the pavements they simulated recorded modulus reduction in the 0-30% range. This was followed by both Models 1 and 4, with 16% of their results falling in the same range. In the high category, Models 2 and 3 had the least number of small β-parameters (slow damage accumulation), followed by Models 4, 5 and 1. The combined effect of these results shows the predicted fatigue curves produced with β-parameters from Model 4 provided the best agreement with the beam fatigue test data, as confirmed by the error

distribution in Figure 4.10. Examples of predicted (incorporating β-parameter Model 4 predictions) versus measured fatigue damage curves are shown in Figure 4.13. Overall, the pseudo fatigue model reasonably predicted the measured fatigue curves, as evident in the cumulative distribution of R^2 (Figure 4.10). Cases in which the entire beam fatigue curve could not be predicted were traced to AC mixtures with high FEL (exceeding 200με) and low AC modulus. Examples of such cases are shown in Figures 4.13 (c and e). The mixture contained 6.5% (effective) of GTR-modified binder, and the beams were compacted to 10–12 % air void content, yielding an initial AC modulus between 300 and 500 ksi, while the FEL was estimated as 209με. It seems high FEL–low modulus combination produces large β-parameters, which result in partial simulation of the measured fatigue curve. In Figure 4.13 (g), the large FEL of 241 caused no major problem in fully simulating the measured fatigue curve when it was combined with the relatively high initial AC modulus of 923 ksi. Considering the variability of beam fatigue test data, these exceptional cases could not constitute an invalidation of the pseudo fatigue model since, for most cases, the beam fatigue curves were predicted with reasonable accuracy. Recall it was high FEL–low modulus inputs that caused β-parameter regression Models 2 and 5 to produce inaccurate β-parameter predictions. Overall, the validation showed the pseudo fatigue model (along with β-parameter regression model 4) was a good representation, in a layered elastic system, of the damage accumulation process in beam fatigue testing.

Table 4.2 Reduction in Initial AC Modulus in Pseudo Fatigue Damage Model Validation

Percent Reduction in Initial AC Modulus	Percent of Simulated Pavement Cross-Sections				
	β-Model 1	β-Model 2	β-Model 3	β-Model 4	β-Model 5
0 - 30 (Low)	16	22	22	16	22
31 - 60 (Medium)	49	62	62	65	54
61 - 90 (High)	35	16	16	19	24

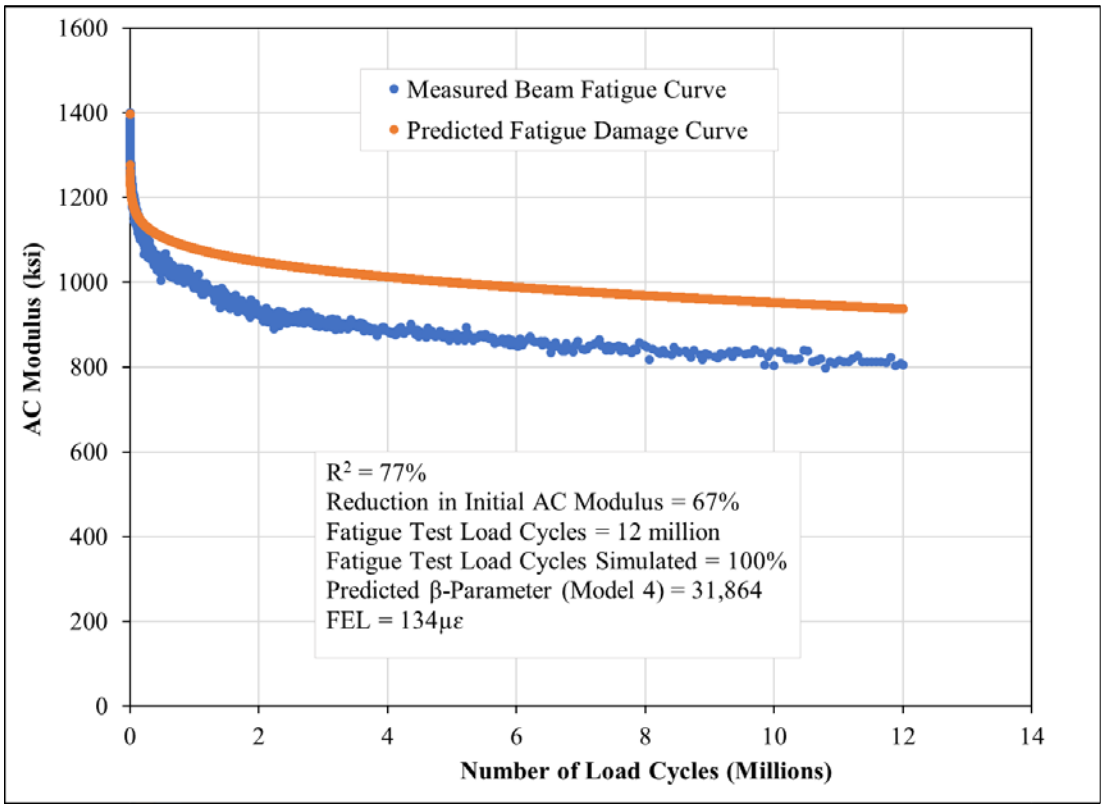

(a) Beam Specimen N11-3-6 from 2009 Research Cycle Tested at 200με

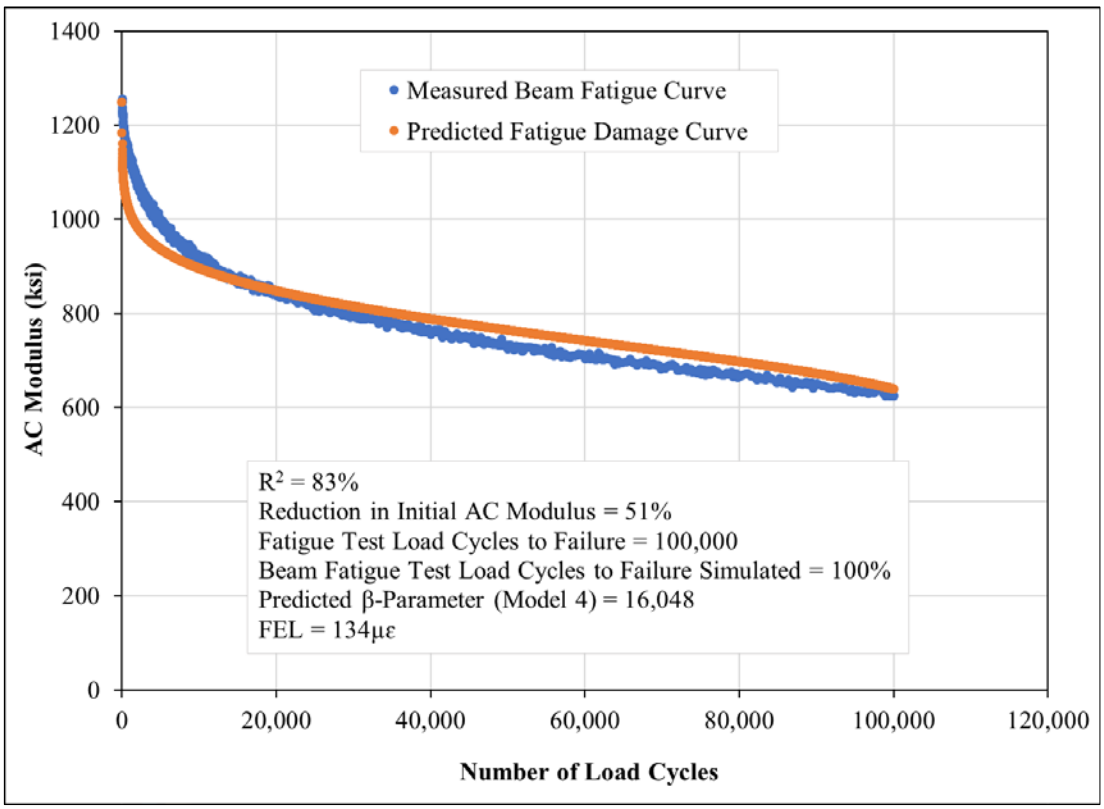

(b) Beam Specimen N11-3-2 from 2009 Research Cycle Tested at 400με

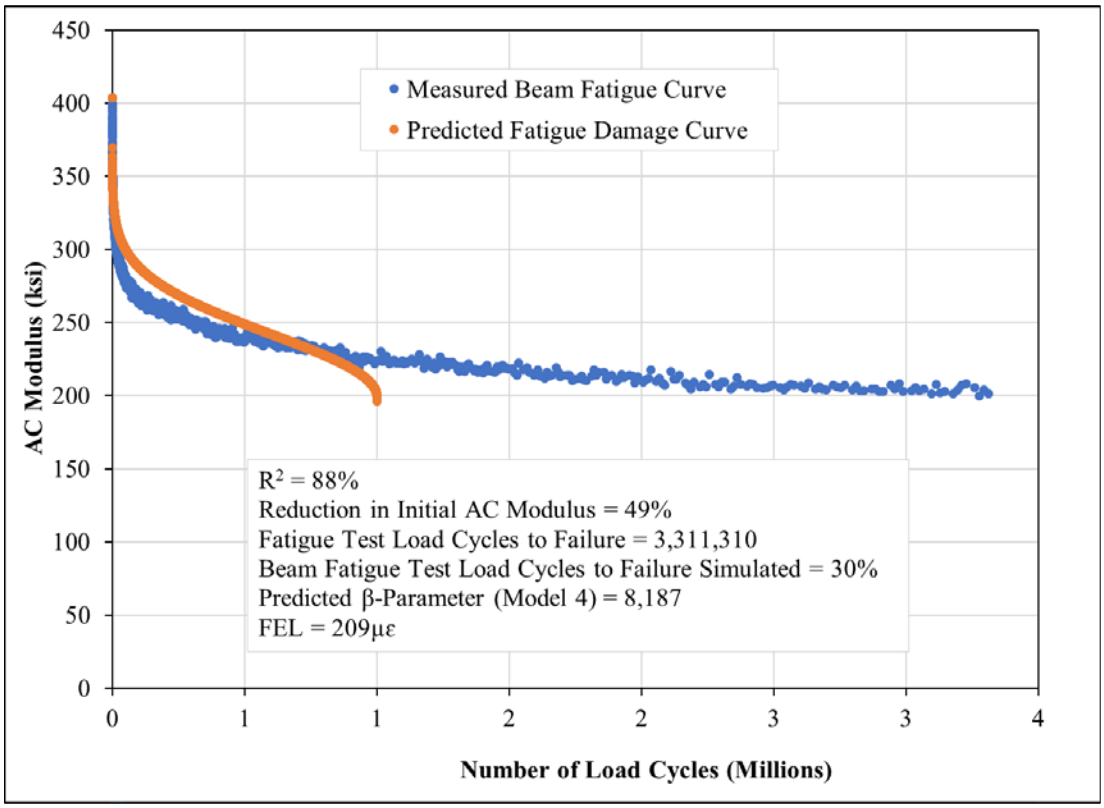

(c) Beam Specimen S13-3-4 from 2012 Research Cycle Tested at 400με

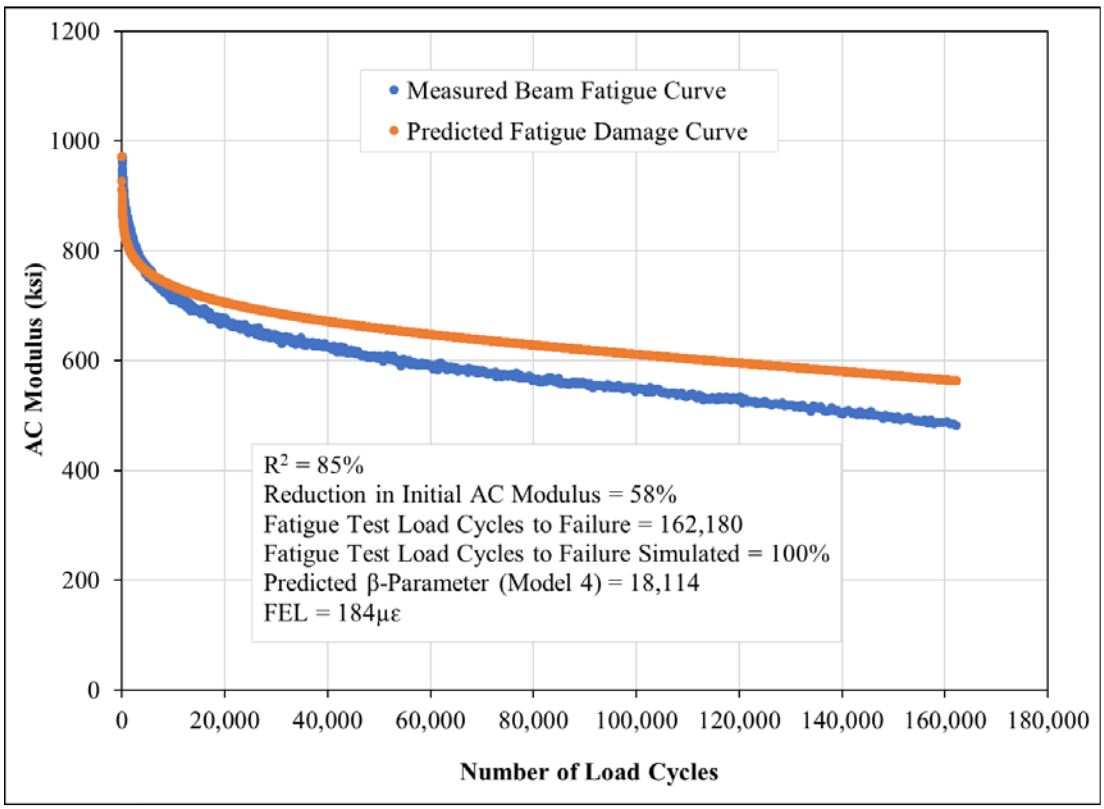

(d) Beam Specimen S13-2-7 from 2012 Research Cycle Tested at 400με

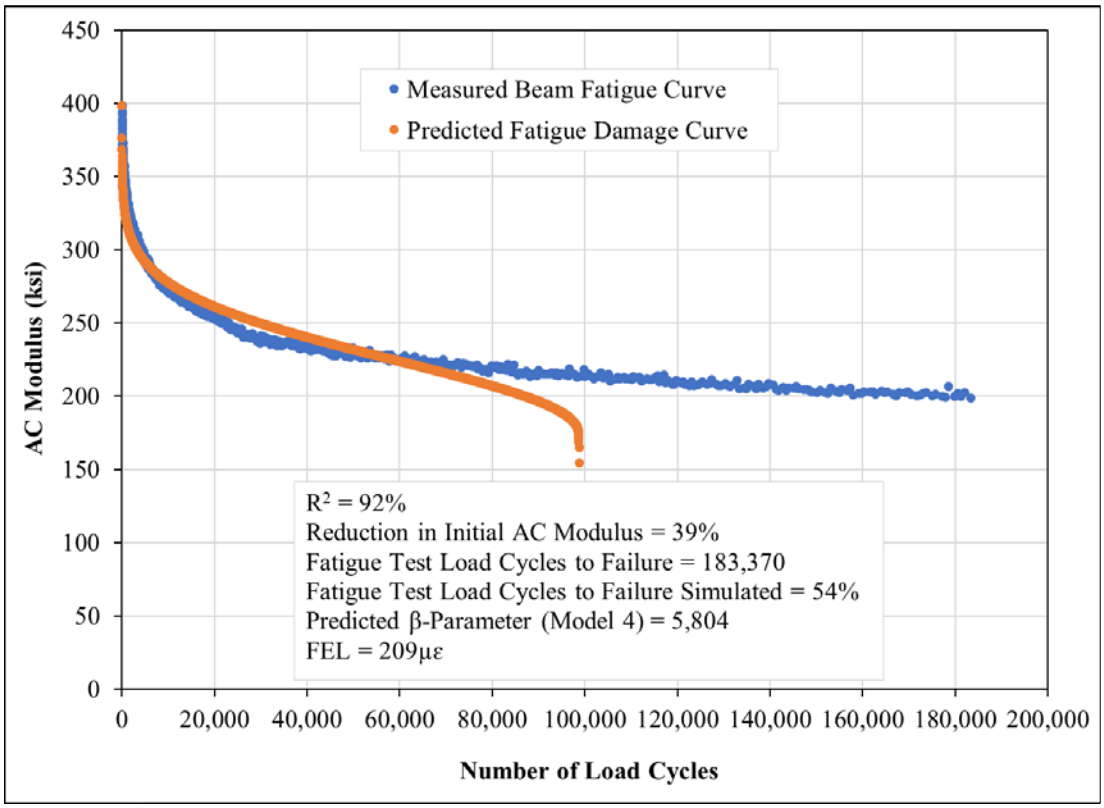

(e) Beam Specimen S13-3-6 from 2012 Research Cycle Tested at 600με

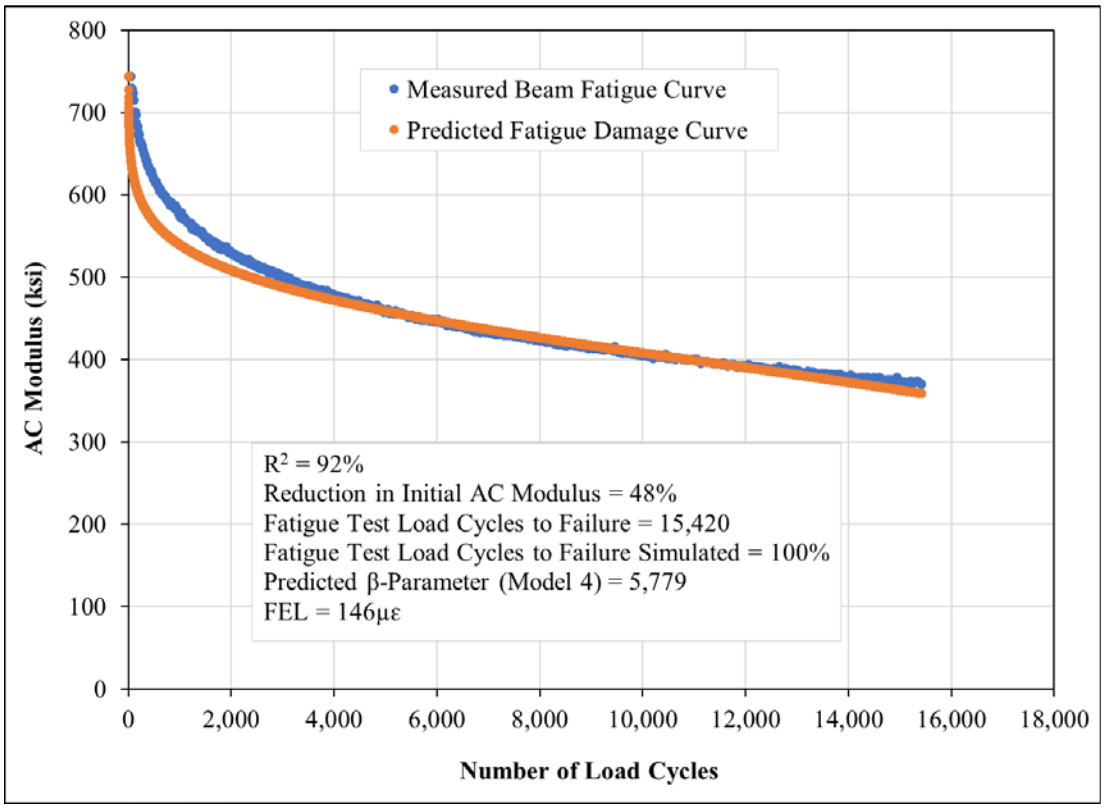

(f) Beam Specimen N10-3-3 from 2006 Research Cycle Tested at 800με

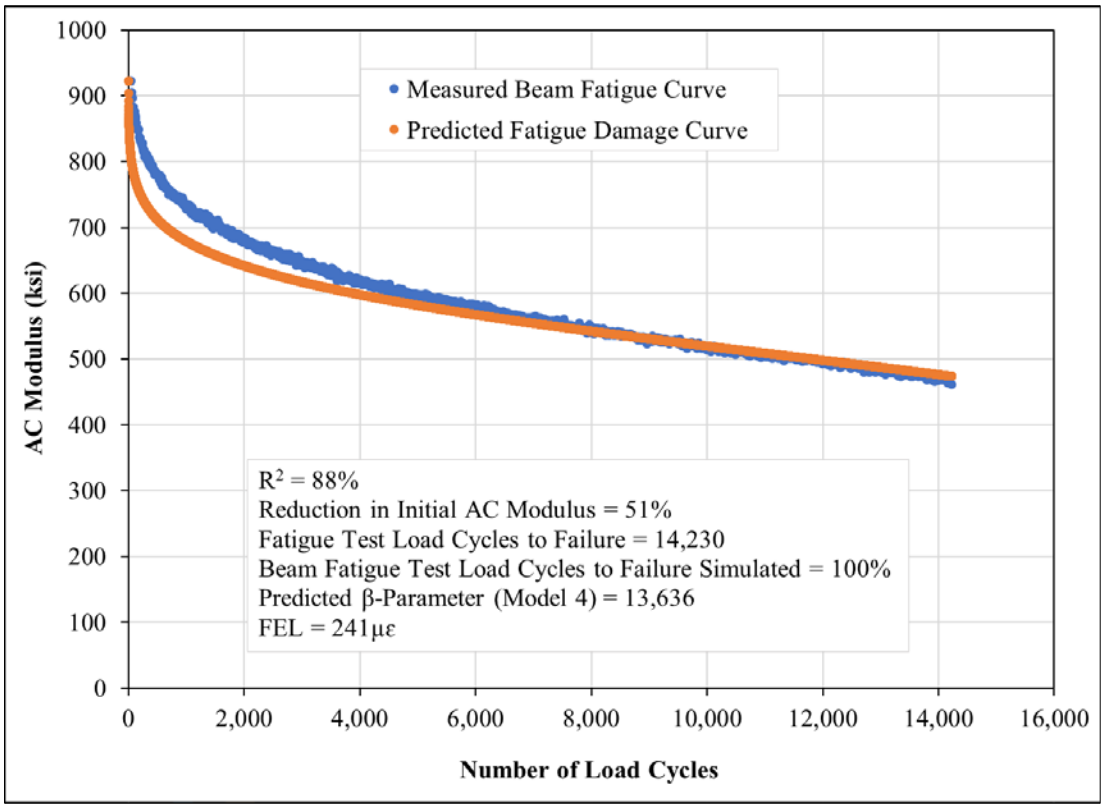

(g) Beam Specimen N7-3-10 from 2009 Research Cycle Tested at 800με

Figure 4.13 Pseudo Fatigue Damage Model Validation: Sample Predicted Versus Measured Fatigue Damage Curves

4.4 Summary of Pseudo Fatigue Cracking Damage Model Validation

- The validation process evaluated the capability of the pseudo fatigue cracking damage model to predict fatigue damage curves of 36 new beam fatigue test results. Rather than using only outstanding model (Model 4), all the five best performing β-parameter regression models were used to compute β-parameters as a function of strain, initial AC modulus and fatigue endurance limit for the validation exercise. This was considered necessary in order to have basis for comparison of the validation results and to confirm earlier conclusions about β-parameter regression Model 4.
- The computed β-parameters were utilized in the pseudo fatigue damage model to predict fatigue damage curves, which were then compared with measured beam fatigue curves.
- By analyzing the error distribution and goodness-of-fit indicators, it was found the pseudo fatigue cracking damage model, in conjunction with β-parameter regression Model 4, yielded predictions that provided the best match with measured fatigue damage curves.

- To further evaluate the performance of the pseudo fatigue cracking damage model, the number of model iterations and the percent of the initial AC modulus remaining after simulating a pavement structure were analyzed. Preferably, these two statistics should be similar to the measured beam fatigue life and half of the initial beam stiffness, respectively. Overall, the pseudo fatigue cracking damage model predictions, incorporating β-parameters computed from regression Model 4, produced the best match with measured fatigue data.
- In conclusion, the validation exercise showed that pseudo fatigue cracking damage model (along with β-parameter regression Model 4) was a reasonable mathematical representation, in a layered elastic system, of the damage accumulation process in beam fatigue testing. This was demonstrated by the high goodness-of-fit between measured and predicted fatigue damage curves (70% of the simulation results recorded R^2 of at least 60%), and the shape of the predicted fatigue curves conformed to that of a typical beam fatigue curve (initial rapid modulus reduction, followed by a steady, prolonged modulus reduction).

CHAPTER 5

INCORPORATION OF PSEUDO FATIGUE CRACKING DAMAGE MODEL IN MECHANISTIC PAVEMENT DESIGN

The pseudo fatigue cracking damage model was developed based on beam fatigue testing in which temperature and loading conditions were uniform. However, the application of the model in mechanistic pavement design would involve dealing with a wide range of traffic and material conditions. This section of the dissertation discusses ideas for incorporating the pseudo fatigue damage model in mechanistic pavement design procedures. NCHRP (2010) categorizes mechanistic-empirical pavement design procedures for bottom-up fatigue cracking as follows:

- **Procedures Based on Equivalent Axle Load and Equivalent Temperature Concepts**
  The cumulative damage concept is applied to determine fatigue damage over the design period of a pavement structure. Equivalent temperature is determined on annual or monthly basis. The layered elastic program, DAMA, adopts this procedure (Asphalt Institute, 1991).

- **Procedures Based on Axle Load Spectra and Equivalent Temperature Concepts**
  These procedures also quantify fatigue damage by using the cumulative damage concept, but consider the full spectrum of axle load distribution. Equivalent temperature is determined on annual or monthly basis. The multilayered elastic-based perpetual pavement design program, PerRoad, implements this approach (Timm, 2008).

- **Procedures Based on Axle Load Spectra and Pavement Temperatures Determined at Several Pavement Depths over certain Time Intervals**
  The increment damage concept is used to determine the amount of fatigue damage within specific time intervals and at specific depths in the pavement structure. The AASHTO Mechanistic-Empirical Pavement Design Guide (MEPDG) is an example of a design system that incorporates this technique (ARA, 2007). MEPDG uses the Enhanced Integrated Climatic Model to compute hourly temperatures at specific pavement depths, which are then averaged into monthly values. These monthly average temperatures are used, along with other inputs, to determine monthly incremental fatigue damage indices, which are aggregated over the design period to predict area of fatigue cracking at each depth interval.

All three categories of mechanistic-empirical design procedures employ maximum horizontal tensile strain at the bottom of the AC layer as a fatigue damage determinant in

transfer functions to characterize damage accumulation using Miner's hypothesis. Notice that Version 4.3 of PerRoad, released in 2017, has an option to use cumulative strain distribution at the AC layer bottom for controlling fatigue cracking instead of depending on transfer functions. A distinguishing feature of the pseudo fatigue cracking model is its non-reliance on transfer functions, although the model also utilizes critical tensile strain at the bottom of the AC layer as a fatigue damage determinant. The MEPDG's analytical approach is complicated and would not serve the objective of the proposed fatigue damage model. The incorporation of the pseudo fatigue cracking damage model in the first two categories of pavement structural design approaches is discussed below.

5.1 Design Based on Equivalent Axle Load and Equivalent Temperature Concepts

For a pavement cross-section under investigation, the key inputs of the pseudo fatigue cracking damage model are the initial critical strain at the AC layer bottom (STR), initial AC modulus (E_0) and fatigue endurance limit (FEL). These inputs are required to compute the fatigue damage related β-parameter, using regression Model 4. Also, the initial critical strain is needed to initiate damage accumulation; its value must exceed the asphalt mixture's fatigue endurance limit by 10%. Based on a highway agency's asphalt mixture design and performance testing practices, pavement design policies and pavement performance experience, the selection of the design AC modulus and fatigue endurance limit should not be problematic. For instance, agencies may have catalogs of fatigue endurance limits for their commonly-used AC mixtures. The equivalent temperature represents a single temperature for which annual or seasonal damage equals the cumulative damage determined at monthly or more frequent intervals (NCHRP, 2010). The equivalent temperature, along with a typical loading frequency (e.g., 10 Hz), may be entered on an AC mastercurve to determine design modulus.

The equivalent single axle load (ESAL) concept is a simplified approach for characterizing the pavement-damaging effects of different axle types and loads over a pavement's design life. A typical reference axle load is 18kips, but this may be changed based on the traffic characteristics of the project road. With all design inputs known, a trial pavement cross-section is formulated such that the critical strain induced by the reference load at the AC layer bottom exceeds the mixture's fatigue endurance limit by 10%. The pseudo fatigue cracking damage model simulates the pavement structure to determine its fatigue life, which is then compared with the design ESALs. If necessary, the cross-section is modified to achieve an acceptable fatigue life. At this current stage of the pseudo fatigue damage model's development, there is no claim the predicted fatigue life will exactly match with the design

ESALs. Field validation, which is beyond the scope of this study, will indicate suggestions for either fine-tuning the model or developing a shift factor, or both, as well as correlating the model's predictions to amount of fatigue cracking.

5.2 Design Based on Axle Load Spectra and Equivalent Temperature Concepts

The utilization of the pseudo fatigue cracking damage model in mechanistic pavement design procedures that depend on axle load spectra and equivalent temperature concepts is like those procedures based on equivalent axle load and equivalent temperature concepts, except that the critical strain is calculated at the equivalent temperature for each axle type and load in the spectra. Consequently, changes in the critical tensile strain (and hence fatigue damage) correspond to the actual loads on the axle types (steer, single, tandem or tridem). While the use of axle load spectra is a more realistic traffic characteristic approach for fatigue damage analysis, a key issue is how to simulate actual traffic conditions to generate pavement responses. PerRoad uses Monte Carlo simulation to address this issue by randomly generating strain responses based on the percentage of each axle load for each axle configuration. In applying Monte Carlo simulation to the pseudo fatigue damage model, generated strain responses that are below the fatigue endurance limit will be neglected, since they do not induce fatigue damage, whereas those greater than the endurance limit by 10% enter the pseudo fatigue damage model for the computation of damage over time.

AC moduli of in-service pavements experience seasonal changes due to temperature variations. A simplified approach to account for the seasonal effects is to use design AC modulus adjusted utilizing an equivalent annual temperature. To be robust, equivalent seasonable temperatures could be utilized for the AC modulus adjustment. For instance, PerRoad, in lieu of user-defined seasonal AC moduli, allows input of mean seasonal air temperatures, which are converted to mean seasonal pavement temperatures by using Equation 31 (Witczak, 1972). Seasonal AC moduli are then predicted as a function of pavement temperature and binder performance grade (PG) from a temperature-modulus equation of the form shown in Equation 32; the constants k_1 and k_2 are selected based on binder PG grade. Alternatively, the pavement temperatures could be used in AC modulus mastercurves to estimate seasonal moduli. Having determined seasonal AC moduli, Monte Carlo simulation can be employed to select AC moduli to compute critical strain responses. Thus, fatigue damage accumulation can be predicted while accounting for changes in traffic conditions and seasonal effects on AC modulus.

$$\mathrm{MMPT} = \mathrm{MMAT}\left(1 + \frac{1}{\mathrm{Z}+4}\right) - \left(\frac{34}{\mathrm{Z}+4}\right) + 6 \quad (31)$$

Where:

MMPT = Mean monthly pavement temperature, °F

MMAT = Mean monthly air temperature, °F

Z = Pavement depth below surface, in. (PerRoad uses upper one-third)

$$\mathrm{E_{AC}} = \mathrm{k_1 e^{k_2 MMPT}} \quad (32)$$

Where:

E_{AC} = AC modulus, psi

MMPT = Mean monthly pavement temperature, °F

k_1, k_2 = Binder PG-based regression coefficients

CHAPTER 6

SUMMARY, CONCLUSIONS AND RECOMMENDATIONS

Several models, with diverse levels of sophistication, exist for analyzing bottom-up fatigue cracking damage in asphalt pavements. However, a key feature missing in most them is that damage-induced changes in the asphalt concrete material is unaccounted for. Moreover, the complicated nature of most of these models hinder their routine application. The use of transfer functions in conventional mechanistic-empirical fatigue models presents another set of challenges, including calibration issues and problematic fatigue performance predictions. For a simplified and a more realistic analysis of fatigue cracking damage, this study attempted to develop a recursive fatigue damage model that incorporates damage-induced changes in AC material and which does not depend on transfer functions. The proposed pseudo fatigue cracking damage model is a significant advancement toward full-mechanistic fatigue characterization, a major goal of asphalt pavement research. Key findings, conclusions and recommendations drawn from the study are as follows:

6.1 Summary and Conclusions

- Among current bottom-up fatigue cracking analytical procedures such as empirical techniques, dissipated energy-based models, fracture mechanics-based models and continuum damage-based models, a phenomenological model that incorporates damage-induced changes in AC, although unpopular, is a simple, but a viable option to realistically simulate fatigue cracking damage without the need for transfer functions.
- The pseudo fatigue cracking damage model is a strain-based phenomenological model that implements the incremental-recursive damage accumulation concept. It is described as pseudo because there is no physical representation of crack dimensions. The key model assumptions are that fatigue damage deteriorates AC modulus, and the maximum horizontal tensile strain at the bottom of the AC layer is a fatigue damage determinant.
- The development of the pseudo fatigue cracking model was based on beam fatigue testing, a widely-accepted laboratory test method for simulating bottom-initiated fatigue cracking. The model, which employs layered elastic theory, was implemented in WESLEA, a multilayered pavement structural analysis program.
- After investigating nine trial functional forms (Table 3.6), Model 7, shown in Equation 33, emerged as the most suitable representation of the pseudo fatigue cracking damage model.

$$E_i = E_o - k\beta Log(N^{\alpha_2}) \quad (33)$$

$$k = 1 + Log(\alpha_1) \quad (33a)$$

$$\alpha_1 = \left(\frac{\varepsilon_i - \varepsilon_0}{\varepsilon_0}\right) \quad (33c)$$

$$\alpha_2 = \left(\frac{\varepsilon_i}{\varepsilon_0}\right) \quad (33d)$$

Where:

k	=	Adjustment factor dependent on normalized strain differential (α_1)
β	=	Fatigue damage parameter, determined using Equation 34
N	=	Number of load cycles
ε_i	=	Critical tensile strain at AC layer bottom at load cycle i, με
ε_0	=	Fatigue endurance limit, με
E_i	=	AC modulus at load cycle i, psi
E_o	=	Initial AC modulus, psi

- A key output of the model calibration process was a well-fitted linear regression model for predicting an influential model parameter, β-parameter, which was idealized as a fatigue damage related parameter. The regression model predicted β-parameter as a function of AC material properties (initial AC modulus and fatigue endurance limit) and strain condition (initial critical tensile strain at the AC layer bottom, which must exceed the fatigue endurance limit by 10%).
- Out of the nine β-parameter regression models evaluated (Tables 3.9 and 3.10), Model 4, shown in Equation 34, satisfied the classic assumptions of ordinary least square linear regression analysis to provide the most accurate predictions; hence, it was selected for incorporation in the pseudo fatigue cracking damage model. The adjusted and predicted coefficient of determination (R^2) values were 98.53 and 98.45%, respectively.

$$Ln(BETA) = 0.73461 - 0.81541 * LnSTR + 1.08514 * LnE_0 + 1.24489 * LnFEL \quad (34)$$

Where:

BETA = β-parameter

STR = Initial critical tensile strain at AC layer bottom, με

E_0 = Initial AC modulus, ksi

FEL = Fatigue endurance limit, με

- Estimates of fatigue endurance limit were obtained from beam fatigue test data, utilizing the procedure recommended by NCHRP 09-38. Fatigue endurance limit is estimated based on 50 million fatigue test load applications, which correspond to 500 million design load repetitions in a 40-year pavement service life.
- The validation exercise showed the pseudo fatigue cracking damage model was a reasonable mathematical representation of the damage accumulation process in beam fatigue testing, particularly up to a 50% reduction in the initial AC modulus. The goodness-of-fit between the measured and predicted fatigue damage curves was high (70% of the simulation results recorded R^2 of at least 60%), and the shape of the predicted fatigue curves conformed to that of a typical beam fatigue curve (initial rapid modulus reduction, followed by a prolonged, steady modulus reduction). While the functional form is suitable, the capability of the pseudo fatigue cracking damage model to accurately predict measured beam fatigue curves is influenced by the accuracy of the β-parameters. Notice, too, that beam fatigue test data may be highly variable, and the pseudo fatigue damage model may appear to provide inaccurate predictions.

6.2 Recommendations

These cover four thematic areas: (a) prediction of fatigue endurance limit as an asphalt mixture property, (b) improvements in the pseudo fatigue cracking damage model, (c) field validation of the pseudo fatigue damage model, and (d) incorporation of the pseudo fatigue damage model in mechanistic pavement design procedures.

(a) Prediction of Fatigue Endurance Limit

The National Cooperative Highway Research Project (NCHRP) 9-38 methodology, which determines fatigue endurance limit at a single temperature, was adopted for model development in this study. The endurance limits were determined using beam fatigue test data measured at a single temperature of 20°C. The endurance limits of the 15 asphalt mixtures used for model calibration ranged from 78 to 300με, whereas those of the five mixtures utilized for model validation were between 134 and 241με. It is believed that fatigue endurance limit is

temperature-dependent. Other laboratory test protocols such as the uniaxial fatigue test are being studied for determination of endurance limit. Recent research at the NCAT Pavement Test Track shows that pavements can experience strain distributions, which include strain levels that exceed laboratory-measured endurance limits at a single temperature, and yet accumulate no fatigue damage (Willis and Timm, 2009). Consequently, using strain distributions to control bottom-up fatigue cracking has been suggested. Thus, future efforts to incorporate the pseudo fatigue damage model in mechanistic pavement design systems should consider proven techniques for determining fatigue endurance limits and/or field-measured strain thresholds. As the concept of fatigue endurance limit gains popularity, many agencies may have started developing catalogs of endurance limits for their typical asphalt base mixtures.

(b) Improvements in Pseudo Fatigue Cracking Damage Model

The model was calibrated primarily to a failure criterion of 50% reduction in the initial AC modulus. This failure point essentially covered the initial and middle zones of a typical beam fatigue curve. Recall that a typical fatigue damage curve has three zones: the initial zone exhibits a rapid drop in modulus, followed by a middle zone with a prolonged period of gradual decrease in modulus; the last zone shows a rapid modulus reduction toward failure conditions. Future improvements in the pseudo fatigue damage model may involve modifying the equation to predict damage beyond the current failure criterion, with the goal of capturing the last zone of a fatigue damage curve.

The model development process strongly suggested the functional form of the pseudo fatigue cracking model was appropriate. However, increasing the sample size of the calibration data may further improve the accuracy of the model parameters, and hence the predictive capability of the pseudo fatigue damage model.

(c) Field Validation of Pseudo Fatigue Cracking Damage Model

Beam fatigue test data, measured under uniform laboratory conditions, were used in the formulation of the fatigue damage model. However, in-service pavements experience a range of field conditions. Therefore, prior to its application in mechanistic pavement design systems, it would be necessary to perform field validation to compare the model's predictions with field fatigue performance. The validation would require traffic, mixture design, construction and falling weight deflectometer data for pavement sections with fatigue cracking. The cross-sections would be simulated by the pseudo fatigue model to generate fatigue damage curves,

which would be compared with field-measured modulus deterioration curves. The field validation results will influence model modifications.

(d) Incorporation of Pseudo Fatigue Cracking Damage Model in Design Procedures

Upon field validation, the proposed fatigue cracking damage model could be incorporated in mechanistic pavement design procedures. For a given pavement system, the key model inputs will be fatigue endurance limit, initial AC modulus, initial critical tensile strain at the bottom of the AC layer and a failure criterion. The model could be incorporated in both mechanistic design procedures that rely on equivalent axle load and equivalent temperature concepts and those that are based on axle load spectra and equivalent temperature concepts. Using an equivalent annual or seasonal temperature for pavement design seems to provide some justification to use a single fatigue endurance limit.

REFERENCES

1. AASHTO (1993). *Guide for Design of Pavement Structures*. American Association of State Highway and Transportation Officials, Washington, D.C.

2. AASHTO T 322 (2007). *Standard Method of Test for Determining the Creep Compliance and Strength of Hot Mix Asphalt (HMA) Using the Indirect Tensile Test Device*. American Association of State Highway and Transportation Officials, Washington, D.C.

3. AASHTO TP 107 (2016). *Standard Method of Test for Determining the Damage Characteristic Curve of Asphalt Mixtures from Direct Tension Cyclic Fatigue Tests.* American Association of State Highway and Transportation Officials, Washington, D.C.

4. AASHTO T 321 (2014). *Standard Method of Test for Determining the Fatigue Life of Compacted Asphalt Mixtures Subjected to Repeated Flexural Bending.* American Association of State Highway and Transportation Officials, Washington, D.C.

5. AASHTO TP 124 (2016). *Standard Method of Test for Determining the Fracture Potential of Asphalt Mixtures Using Semicircular Bend Geometry (SCB) at Intermediate Temperature.* American Association of State Highway and Transportation Officials, Washington, D.C.

6. Abojaradeh, M. A., Witczak, M. W., Mamlouk, M. S. and Kaloush, K. E. (2007). Validation of Initial and Failure Stiffness Definitions in Flexure Fatigue Test for Hot Mix Asphalt. *Journal of Testing and Evaluation*, Vol. 35, No. 1, pp. 95–102.

7. Adedimila, A. S. and Kennedy, T. W. (1975). *Fatigue and Resilient Characteristics of Asphalt Mixtures by Repeated-Load Indirect Tensile Test.* Research Report No. 183-5, Texas State Department of Highways and Public Transportation, Austin, Texas.

8. Adhikari, S., Shen, S. and You, Z. (2009). Evaluation of Fatigue Models of Hot-Mix Asphalt Through Laboratory Testing. *Transportation Research Record: Journal of the Transportation Research Board*, No. 2127, Transportation Research Board of the National Academies, Washington, D.C., pp. 36–42.

9. Aglan, H. A. and Figueroa, J. L. (1993). Damage-Evolution Approach to Fatigue Cracking in Pavements. *Journal of Engineering Mechanics*, Vol. 119, No. 6, pp. 1243–1259.

10. Applied Research Associates (ARA) (2004). *Guide for Mechanistic-Empirical Design of New and Rehabilitated Pavement Structures*, Champaign, Illinois.

11. Arambula, E., Masad, E. and Martin, A. E. (2007). Moisture Susceptibility of Asphalt Mixtures with Known Field Performance: Evaluated with Dynamic Analysis and Crack Growth Model. *Transportation Research Record: Journal of the Transportation Research Board*, No. 2001, Transportation Research Board of the National Academies, Washington, D.C., pp. 20–28.

12. Asphalt Institute (1991). *Computer Program DAMA (CP-1/1991 Revision). Pavement Structural Analysis Using Multi-Layered Elastic Theory*. Asphalt Institute, Lexington, KY

13. Asphalt Institute (2008). *Thickness Design: Asphalt Pavements for Highways and Street*, Manual Series No. 1, Ninth Edition, The Asphalt Institute, Lexington, KY.

14. Asphalt Pavement Alliance (APA) (2002). *Perpetual Pavements: A Synthesis. APA 101*. Lanham, Maryland.

15. Ameri, M., Mansourian, A., Khavas, M. H., Aliha, M.R.M. and Ayatollahi, M.R. (2011). Cracked Asphalt Pavement Under Traffic Loading-A 3D Finite Element Analysis. *Engineering Fracture Mechanics*. Vol. 78, No. 8, pp. 1817–1826.

16. ASTM D7369 (2011). *Standard Test Method for Determining the Resilient Modulus of Bituminous Mixtures by Indirect Tension Test.* American Society for Testing and Materials, West Conshohocken, PA.

17. ASTM D6931 (2012). *Standard Test Method for Indirect Tensile (IDT) Strength of Bituminous Mixtures*. American Society for Testing and Materials, West Conshohocken, PA.

18. ASTM D8044 (2016). *Standard Test Method for Evaluation of Asphalt Mixture Cracking Resistance using the Semi-Circular Bend Test (SCB) at Intermediate Temperatures.* American Society for Testing and Materials, West Conshohocken, PA.

19. ASTM D7460 (2010). *Standard Test Method for Determining Fatigue Failure of Compacted Asphalt Concrete Subjected to Repeated Flexural Bending*. American Society for Testing and Materials, West Conshohocken, PA.

20. ASTM (1963). *A Guide for Fatigue Testing and the Statistical Analysis of Fatigue Data*. Special Technical Publication 9l-A, Second Edition, American Society for Testing and Materials, West Conshohocken, PA.

21. Anderson, T. L. (2005). *Fracture Mechanics: Fundamentals and Applications*. CRC Press, Taylor & Francis Group, Third Edition, Boca Raton, FL.

22. Baek, J. and Al-Qadi, I. L. (2008). Mechanism of Overlay Reinforcement to Retard Reflective Cracking Under Moving Vehicular Loading. In: *6th RILEM International Conference on Cracking in Pavements*. Chicago, IL: CRC Press, pp. 563–573.

23. Bahia, H. U. (2009). Modeling of Asphalt Binder Rheology and Its Application to Modified Binders. In Y. R. Kim, ed., *Modeling of Asphalt Concrete*, American Society of Civil Engineers, Reston, VA., pp. 11–56.

24. Barenblatt, G. I. (1962). The Mathematical Theory of Equilibrium Cracks in Brittle Fracture. *Advances in Applied Mechanics,* Vol. 7, pp. 55–129.

25. Bhasin, A., Branco, V.T.F.C., Masad, E. and Little, D. N. (2009). Quantitative Comparison of Energy Methods to Characterize Fatigue in Asphalt Materials. *Journal of Materials in Civil Engineering*, Vol. 21, No. 2, pp. 83–92.

26. Bhattacharjee, S., Swamy, A. and Daniel, J. (2009). Application of Elastic–Viscoelastic Correspondence Principle to Determine Fatigue Endurance Limit of Hot-Mix Asphalt. *Transportation Research Record: Journal of the Transportation Research Board*, No. 2126, Transportation Research Board of the National Academies, Washington, D.C., pp. 12–18.

27. Birgisson, B., Wang, J. and Roque, R. (2006). *Implementation of the Florida Cracking Model into the Mechanistic-Empirical Pavement Design*. Final Report, Florida Department of Transportation, Tallahassee, Florida.

28. Burmister, D. M. (1943). The Theory of Stresses and Displacements in Layered Systems and Applications to the Design of Airport Runways. In: *Highway Research Board*, Vol. 23, pp. 126–144.

29. Burmister, D. M. (1945). The General Theory of Stresses and Displacements in Layered Soil Systems. *Journal of Applied Physics*, Vol. 16, pp. 84–94, 126–127, 296–302.

30. Caro, S., Masad, E., Bhasin, A. and Little, D. (2010a). Micromechanical Modeling of the Influence of Material Properties on Moisture-Induced Damage in Asphalt Mixtures. *Construction and Building Materials*, Vol. 24, No. 7, pp. 1184–1192.

31. Caro, S., Masad, E., Bhasin, A. and Little, D. (2010b). Coupled micromechanical model of moisture-induced damage in asphalt mixtures. *Journal of Materials in Civil Engineering*, Vol. 22, No. 4, pp. 380–388.

32. Carpenter, S., Ghuzlan, H. K. and Shen, S. (2003). Fatigue Endurance Limit for Highway and Airport Pavements. *Transportation Research Record: Journal of the Transportation Research Board*, No. 1832, Transportation Research Board of the National Academies, Washington, D.C., pp. 131–138.

33. Carpenter, S. H., and Jansen, M. (1997). Fatigue Behavior Under New Aircraft Loading Conditions. In: *Aircraft/Pavement Technology: In the Midst of Change, Airfield Pavement Conference*, American Society of Civil Engineers, New York, pp. 259–271.

34. Carpenter, S. H., and Shen, S. (2006). A Dissipated Energy Approach to Study HMA Healing in Fatigue. *Transportation Research Record: Journal of the Transportation Research Board*, No. 1970, Transportation Research Board of the National Academies, Washington, D.C., pp. 178–185.

35. Chatterjee, S. and Hadi, A. S. (2012). *Regression Analysis by Example.* Fifth Edition. John Wiley & Sons, Inc., New Jersey.

36. Chehab, G.R., Kim, Y. R., Schapery, R. A., Witczak, M. W. and Bonaquist, R. (2002). Time-Temperature Superposition Principle for Asphalt Concrete Mixtures with Growing Damage in Tension State. *Journal of the Association of Asphalt Paving Technologists*, Vol. 71, pp. 559–593.

37. Chehab, G. R, Kim, Y. R., Schapery, R. A., Witczak, M. W. and Bonaquist, R. (2003). Characterization of Asphalt Concrete in Uniaxial Tension Using a Viscoelastoplastic Continuum Damage Model. *Journal of the Association of Asphalt Paving Technologists*, Vol. 72, pp. 315–355.

38. Chehab, G.R. and Kim, Y.R. (2005). Viscoelastoplastic Continuum Damage Model Application to Thermal Cracking of Asphalt Concrete. *Journal of Materials in Civil Engineering*, Vol. 17, No. 4, pp. 384–392.

39. Chen, D-H. (1998) Pavement Distress Under Accelerated Trafficking. *Transportation Research Record: Journal of the Transportation Research Board*, No. 1630, Transportation Research Board of the National Academies, Washington, D.C., pp. 120–129.

40. Daniel, J. S. and Kim, Y. R. (2002). Development of a Simplified Fatigue Test and Analysis Procedure Using a Viscoelastic Continuum Damage Model. *Journal of the Association of Asphalt Paving Technologists*, Vol. 71, pp. 619–650.

41. Darabi, M. K., Al-Rub, R. K. A., Masad, E. A., Huang, C-W. and Little, D. N. (2011). A Thermo-Viscoelastic-Viscoplastic-Viscodamage Constitutive Model for Asphaltic Materials. *International Journal of Solids and Structures*, Vol. 48, Issue 1, pp. 191–207.

42. Deacon, J. A. (1965). *Fatigue of Asphalt Concrete*. PhD. University of California, Berkeley, California.

43. Desai, C. S. (2009). Unified Disturbed State Constitutive Modeling of Asphalt Concrete. In Y. R. Kim, ed., *Modeling of Asphalt Concrete*, American Society of Civil Engineers, Reston, VA. pp. 205–244.

44. Dormon, G.M., and Metcalf, C. T. (1965). Design Curves for Flexible Pavements Based on Layered System Theory. *Transportation Research Record: Journal of the Transportation Research Board*, No. 71, Transportation Research Board of the National Academies, Washington, D.C., pp. 69–84.

45. Dugdale, D. S. (1960). Yielding of Steel Sheets Containing Slits. *Journal of the Mechanics and Physics of Solids*. Vol. 8, Issue 2, pp. 100–104.

46. El-Basyouny, M. M. and Witczak, M. (2005). Calibration of Alligator Fatigue Cracking Model for 2002 Design Guide. *Transportation Research Record: Journal of the Transportation Research Board*, No. 1919, Transportation Research Board of the National Academies, Washington, D.C., pp. 77–86.

47. Ellyin, F. (1997). *Fatigue Damage, Crack Growth and Life Prediction*. Chapman & Hall, London.

48. Epps, J. A. and Monismith, C. L. (1972). Fatigue of Asphalt Concrete Mixtures-Summary of Existing Information. In: *ASTM STP 508: Fatigue of Compacted Bituminous Aggregate Mixtures*. American Society for Testing and Materials, Coshocken, PA, pp. 19–45

49. Finn, F. N. (1967). *Factors Involved in the Design of Asphaltic Pavement Surfaces*. Highway Research Board, National Cooperative Highway Research Program Report No. 39, Washington, D.C.

50. Freeme, C. R. and Marais, C. P. (1973). *Thin Bituminous Surfaces: Their Fatigue Behavior and Prediction*. Special Report 140, Highway Research Board, Washington, D.C.

51. Germann, P.F. and Lytton, R.L. (1979). *Methodology for Predicting the Reflection Cracking Life of Asphalt Concrete Overlays*. Report No. TT-2-8-75-207-5, Texas Transportation Institute, College Station, Texas.

52. Ghuzlan K. A. and Carpenter, S. H. (2000). Energy-Derived, Damage-Based Failure Criterion for Fatigue Testing. *Transportation Research Record: Journal of the Transportation Research Board*, No. 1723, Transportation Research Board of the National Academies, Washington, D.C., pp. 141–149.

53. Ghuzlan, K. A. and Carpenter, S. H. (2006). Fatigue Damage Analysis is Asphalt Concrete Mixtures Using the Dissipated Energy Approach. *Canadian Journal of Civil Engineering*, Vol 33., No. 7, pp. 890–901.

54. Goodrich, J. L. (1988). Asphalt and Polymer Modified Asphalt Properties Related to the Performance of Asphalt Concrete Mixes. In: *Association of Asphalt Paving Technologists Technical Sessions*, Vol. 57, Williamsburg, VA, pp. 116–175.

55. Griffith, A. A. (1921). The Phenomena of Rupture and Flow in Solids. *Philosophical Transactions of the Royal Society of London*, Series A, No. 221, pp. 163–198.

56. Harvey, J. T., Deacon, J. A., Tayebali, A. A. and Leahy, R. B. (1997). A Reliability-Based Mix Design and Analysis System for Mitigating Fatigue Distress. In: *8th International Conference on Asphalt Pavements*, Vol. 1, University of Washington, Seattle, WA, pp. 301–323.

57. Harvey, J. T. and Tsai, B. W. (1996). Effects of Asphalt Content and Air Void Content on Mix Fatigue and Stiffness. *Transportation Research Record: Journal of the Transportation Research Board* No. 1543, Transportation Research Board, Washington, D.C., pp. 38–45.

58. Highway Research Board (1962). *The AASHO Road Test*. Report 7, Special Report 61-G. Highway Research Board, Washington, D.C.

59. Highway Research Board (1973). *Structural Design of Asphalt Concrete Pavements to Prevent Fatigue Cracking*. Special Report 140, National Research Council, National Academy of Sciences, National Academy of Engineering Washington, D.C.

60. Huang, Y. H. (2012). *Pavement Analysis and Design*. Second Edition. Pearson Prentice Hall, Upper Saddle River, N. J.

61. Hveem, F. N. (1955). *Pavement Deflections and Fatigue Failures*. Bulletin 114, Highway Research Board, National Research Council, Washington, D. C.

62. Kachanov, L. M. (1958). Time of the Rupture Process under Creep Conditions. *Izvestiia Akademii Nauk SSSR, Otdelenie Teckhnicheskikh Nauk*, Vol. 8, pp. 26–31.

63. Kallas, B. F. and Puzinauskas, V. P. (1972). Flexural Fatigue Tests on Asphalt Paving Mixtures. In: *Fatigue of Compacted Bituminous Aggregate Mixtures*, ASTM Special Publication 508. American Society for Testing and Materials, Philadelphia, PA. pp. 47–65.

64. Kim, Y. R., Lee, H. Y., and Little, D. N. (1997). Fatigue Characterization of Asphalt Concrete using Viscoelasticity and Continuum Damage Theory. *Journal of the Association of Asphalt Paving Technologists*, Vol. 66, pp. 520–569.

65. Kim, Y., Allen, D. H. and Little, D. N. (2005). Damage-Induced Modeling of Asphalt Mixtures Through Computational Micromechanics and Cohesive Zone Fracture. *Journal of Materials in Civil Engineering*, Vol. 17, No. 5, pp. 477–484.

66. Kim, Y., Allen, D. H. and Little, D. N. (2006). Computational Model to Predict Fatigue Damage Behavior of Asphalt Mixtures Under Cyclic Loading. *Transportation Research Record: Journal of the Transportation Research Board*, No. 1970, Transportation Research Board of the National Academies, Washington, D.C., pp. 196–206.

67. Kim, Y., Allen, D. H. and Little, D. N. (2007). Computational Constitutive Model for Predicting Nonlinear Viscoelastic Damage and Fracture Failure of Asphalt Concrete Mixtures. *International Journal of Geomechanics*, Vol. 7, No. 2, pp. 102–110.

68. Kim, Y. R., Underwood, S. Chehab, G. R., Daniel, J. S., Lee, H. J. and Yun, T. Y. (2009). VEPCD Modeling of Asphalt Concrete with Growing Damage. In Y. R. Kim, ed., *Modeling of Asphalt Concrete*, American Society of Civil Engineers, Reston, VA., American Society of Civil Engineers, pp. 163–200.

69. Kim, H. and Buttlar, W.G. (2009). Finite Element Cohesive Fracture Modeling of Airport Pavements at Low Temperatures. *Cold Regions Science and Technology*, Vol. 57, Issues 2-3, pp. 123–130.

70. Kim, Y-R. (2011). Cohesive Zone Model to Predict Fracture in Bituminous Materials and Asphaltic Pavements: State-of-the-Art Review. *International Journal of Pavement Engineering*, Vol. 12, No. 4, pp. 343–356.

71. Kim, Y. R and Little, D. N. (1990). One-Dimensional Constitutive Modeling of Asphalt Concrete. *Journal of Engineering Mechanics*, Vol. 116, No. 4, pp. 751–772.

72. Kutner, M. H., Nachtsheim, C. J., and Neter, J. (2008). *Applied Linear Regression Models.* Fourth Edition. McGraw-Hill Education, New York.

73. Lee, H. J., Choi, J. Y., Zhao Y. and Kim Y. R. (2002). Laboratory Evaluation of the Effects of Aggregate Gradation and Binder Type on Performance of Asphalt Mixtures. In: *Ninth International Conference on Asphalt Pavements*, Copenhagen, Denmark.

74. Li, Y. (1999). *Asphalt Pavement Fatigue Cracking Modeling*. PhD. LSU Historical Dissertations and Theses, Louisiana State University.

75. Luo, X., Luo, R. and Lytton, R. L. (2013). Characterization of Fatigue Damage in Asphalt Mixtures Using Pseudostrain Energy. *Journal of Materials in Civil Engineering*, Vol. 25, No. 2, pp. 208–218.

76. Lytton, R. L., Uzan, J., Fernando, E. G., Roque, R., Hiltmen, D., and Stoffels, S. (1993). *Development and Validation of Performance Prediction Models and Specifications for Asphalt Binders and Paving Mixtures*. SHRP Report No. A-357, Strategic Highway Research Program, National Research Council, Washington, D.C.

77. Lytton, R. L. (2000). Characterizing Asphalt Pavement for Performance. *Transportation Research Record: Journal of the Transportation Research Board*, No. 1723, Transportation Research Board of the National Academies, Washington, D.C., pp. 5–16.

78. Majidzadeh, K., Kauffmann, E., and Saraf, C. (1972). Analysis of Fatigue of Paving Mixtures from the Fracture Mechanics Viewpoint. In: *Fatigue of Compacted Bituminous Aggregate Mixtures*, ASTM Special Publication 508. American Society for Testing and Materials, Philadelphia, PA. pp. 67–83.

79. Majidzadeh, K., Kaufmann, E. M. and Ramsamooj, D.V. (1971). Application of Fracture Mechanics in the Analysis of Pavement Fatigue. *Journal of the Association of Asphalt Pavement Technologists*, Vol. 40, pp. 227–246.

80. Majidzadeh, K. and Ramsamooj, D. (1976). *Application of Fracture Mechanics for Improved Design of Bituminous Concrete*. Report No. FHWA-RD-76-91, Federal Highway Administration, Washington, D. C.

81. Majidzadeh, K., Ramsamooj, D. V. and Fletcher, T. A. (1969). Analysis of Fatigue of a Sand-Asphalt Mixture. *Journal of the Association of Asphalt Paving Technologists*, Vol. 38, pp. 495–518.

82. Majidzadeh, K., Kaufmann, E.M., Ramsamooj, D.V. and Chan. A.T. (1970). *Analysis of Fatigue and Fracture of Bituminous Paving Mixtures*. US Bureau of Public Roads. Research and Development, Report No. 2546.

83. Masad, E., Branco, V.T.F.C., Little, D. N. and Lytton, R. L. (2008). A Unified Method for the Analysis of Controlled-Strain and Controlled-Stress Fatigue Testing. *International Journal of Pavement Engineering*, Vol. 9, Issue 4, pp. 233-246.

84. Mateos, A., Ayuso, J. P. and Jáuregui, B. C. (2011). Shift Factors for Asphalt Fatigue from Full-Scale Testing. *Transportation Research Record: Journal of the Transportation Research Board*, No. 2225, Transportation Research Board of the National Academies, Washington, D.C., pp. 128–136.

85. Maupin, G. W. Jr. and Freeman Jr., J. R. (1976). *Simple Procedure for Fatigue Characterization of Bituminous Concrete*. Final Report No. FHWA-RD-76-102, Federal Highway Administration, Washington, D.C.

86. Miner, M. A. (1945). Cumulative Damage in Fatigue. *Journal of Applied Mechanics*, Vol. 12, No. 9, pp. A159-A164.

87. Molenaar, A. A. A. (2007). Prediction of Fatigue Cracking in Asphalt Pavements: Do We Follow the Right Approach? *Transportation Research Record: Journal of the Transportation Research Board*, No. 2001, Transportation Research Board of the National Academies, Washington, D.C., pp. 155–162.

88. Monismith, C. L. and Deacon J. A. (1969). Fatigue of Asphalt Paving Mixtures. *Journal of Transportation Engineering*, Vol. 95, No. TE2, pp 317–346.

89. Monismith, C. L. and McLean, D. B. (1972). Structural Design Considerations. *Journal of Association of Asphalt Paving Technologists*, Vol. 41, pp. 12–31.

90. Monismith, C. L., Secor, K. E. and Blackmer, E. W. (1970). Asphalt Mixture Behavior in Repeated Flexure. *Journal Association of Asphalt Paving Technologists*. Vol. 39, pp. 188-222.

91. NCHRP (2004). *Mechanistic-empirical Design of New and Rehabilitated Pavement Structures*. National Cooperative Highway Research Program (NCHRP) Project 1-37A. Transportation Research Board, Washington, D. C.

92. NCHRP (2010). *Validating the Fatigue Endurance Limit for Hot Mix Asphalt*. National Cooperative Highway Research Program (NCHRP) Report 646, Transportation Research Board, Washington, D. C.

93. NCHRP (2013). *Laboratory Validation of an Endurance Limit for Asphalt Pavements*. National Cooperative Highway Research Program (NCHRP) Report 762, Transportation Research Board, Washington, D. C.

94. NCHRP (2016). *Performance Specifications for Asphalt Mixtures*. National Cooperative Highway Research Program Synthesis 492, Transportation Research Board, Washington, D. C.

95. Nishizawa, T., Shimeno, S. and Sekiguchi, M. (1997). Fatigue Analysis of Asphalt Pavements with Thick Asphalt Mixture Layer. In: *8th International Conference on Asphalt Pavements*, Vol. 2. University of Washington, Seattle, WA, pp. 969–976.

96. Paris, P. C., Gomez, M. P. and Anderson, W. E. (1961). A Rational Analytic Theory of Fatigue. *The Trend in Engineering*, Vol. 13, pp. 9–14.

97. Park, K. (2009). *Potential-Based Fracture Mechanics using Cohesive Zone and Virtual Internal Bond Modeling*. Ph.D. University of Illinois, Urbana Champaign, IL.

98. Pell, P. S. (1962). Fatigue Characteristics of Bitumen and Bituminous Mixes. In: *1st International Conference on the Structural Design of Asphalt Pavements*, Ann Arbor, Michigan, pp. 43–48.

99. Pierce, L. M., Jackson, N. C. and Mahoney, J. P. (1993). Development and Implementation of a Mechanistic, Empirically Based Overlay Design Procedure for Flexible Pavements. *Transportation Research Record: Journal of the Transportation Research Board*, No. 1388, Transportation Research Board of the National Academies, Washington, D.C., pp. 120–128.

100. Pronk, A. C. (1995). *Evaluation of the Dissipated Energy Concept for the Interpretation of Fatigue Measurements in the Crack Initiation Phase.* Report No. P-DWW-95-501, The Road and Hydraulic Engineering Division, Ministry of Transport, Public Works and Water Management, The Netherlands.

101. Prowell, B. D. (2010). Estimate of Fatigue Shift Factors Between Laboratory Tests and Field Performance. *Transportation Research Record: Journal of the Transportation Research Board*, No. 2181, Transportation Research Board of the National Academies, Washington, D.C., pp. 117–124.

102. Roque, R., Birgisson B., Drakos, C. and Dietrich, B. (2004). Development and Field Evaluation of Energy-Based Criteria for Top-Down Cracking Performance of Hot Mix Asphalt. *Journal of the Association of Asphalt Paving Technologists*, Vol. 73, pp. 229–260.

103. Roque, R., Birgisson, B., Sangpetngam, B. and Zhang, Z. (2002). Hot Mix Asphalt Fracture Mechanics: A Fundamental Crack Growth Law for Asphalt Mixtures. *Journal of the Association of Asphalt Paving Technologists*, Vol. 71, pp. 816–828.

104. Roque, R., Zhang, Z. and Sankar, B. (1999). Determination of Crack Growth Rate Parameters of Asphalt Mixtures Using the Superpave™ Indirect Tension Test (IDT). *Journal of the Association of Asphalt Paving Technologists*, Vol. 68, pp. 404–433.

105. Rowe, G. M. (1993). Performance of Asphalt Mixtures in the Trapezoidal Fatigue Test. *Journal of the Association of Asphalt Paving Technologists*, Vol. 62, pp. 344–384.

106. Saal, R. N. J. and Pell, P. S. (1960). Fatigue of Bituminous Road Mixes. *Kolloid Zeitschrift*, Vol. 171, No. 1, pp. 61–71.

107. Sabouri, M. and Kim, Y. R. (2014). Development of a Failure Criterion for Asphalt Mixtures Under Different Modes of Fatigue Loading. *Transportation Research Record: Journal of the Transportation Research Board*, No. 2447, Transportation Research Board of the National Academies, Washington, D.C., pp. 117–125.

108. Sangpetngam, B., Birgisson, B. and Roque, R. (2003). Development of Efficient Crack Growth Simulator Based on Hot-Mix Asphalt Fracture Mechanics. *Transportation Research Record: Journal of the Transportation Research Board*, No. 1832, Transportation Research Board of the National Academies, Washington, D.C., pp. 105–112.

109. Schapery, R. A. (1987). Deformation and Fracture Characterization of Inelastic Composite Materials Using Potentials. *Polymer Engineering and Science*, Vol. 27, No. 1, pp. 63–76.

110. Schapery, R. A. (1984). Correspondence Principles and Generalized *J*-integral for Large Deformation and Fracture Analysis of Viscoelastic Media. *International Journal of Fracture Mechanics*, Vol. 25, No. 3, pp. 194–223.

111. Sebaaly, P., Tabatabaee, N., Bonaquist, R. and Anderson, D. (1989). Evaluating Structural Damage of Flexible Pavements Using Cracking and Falling Weight Deflectometer Data. *Transportation Research Record: Journal of the Transportation Research Board*, No. 1227, Transportation Research Board of the National Academies, Washington, D.C., pp. 44–52.

112. Shell (2015). *Shell Bitumen Handbook*, Sixth Edition, Shell International Petroleum Company Limited.

113. Shen, S. and Carpenter, S. H. (2005). Application of the Dissipated Energy Concept in Fatigue Endurance Limit Testing. *Transportation Research Record: Journal of the Transportation Research Board*, No. 1929, Transportation Research Board of the National Academies, Washington, D.C., pp. 165–473.

114. Shen, S. and Carpenter, S. H. (2007). Development of an Asphalt Fatigue Model Based on Energy Principles. *Journal of the Association of Asphalt Paving Technologists*, Vol. 76, pp. 525–574.

115. Shukla, A. (2005). *Practical Fracture Mechanics in Design*. Second Edition, Marcel Dekker, New York.

116. Si, Z., Little, D. N. and Lytton, R. L. (2002). Characterization of Microdamage and Healing of Asphalt Concrete Mixtures. *Journal of Materials in Civil Engineering*, Vol. 14, No. 6, pp. 461–470.

117. SHRP (1994). *Fatigue Response of Asphalt-Aggregate Mixes*. Report No. SHRP-A-404, Strategic Highway Research Program, National Research Council, Washington, D. C.

118. TxDOT (2017). *TxDOT Designation: Tex-248-F. Test Procedure for Overlay Test.* Construction Division, Texas Department of Transportation.

119. Tangella, S. C. S. R., Craus, J., Deacon, J. A. and Monismith, C. L. (1990). *Summary Report on Fatigue Response of Asphalt Mixtures*. TM-UCB-A-003A-89-3, Strategic Highway Research Program, Project A003-A, University of California, Berkley, CA.

120. Tayebali, A. A., Deacon, J. A., Coplantz, J. S., Harvey, J. T., and Monismith, C. L. (1994). *Fatigue Response of Asphalt-Aggregate Mixes: Part I Test Method Selection*. SHRP A-404 Strategic Highway Research Program, National Research Council, Washington, DC.

121. Tayebali, A. A., Deacon, J. A., Coplantz, J. S. and Monismith, C. L. (1993). Modeling Fatigue Response of Asphalt-Aggregate Mixtures. *Journal of Association of Asphalt Paving Technologists,* Vol. 62, Austin, TX, pp. 385–421.

122. Thompson, M. R. and Carpenter, S. H. (2006). Considering Hot-Mix-Asphalt Fatigue Endurance Limit in Full-Depth Mechanistic-Empirical Pavement Design. In: *International Conference on Perpetual Pavement*, Columbus, OH.

123. Timm, D. H. (2008). PerRoad Computer Program. Auburn University, Auburn, AL.

124. Timm, D.H. (2009). *Design, Construction, and Instrumentation of the 2006 Test Track Structural Study*. NCAT Report 09-01, National Center for Asphalt Technology, Auburn University, Auburn, AL.

125. Timm, D. H. and Newcomb, D. E. (2012). Calibration of Flexible Pavement Performance Equations for Minnesota Road Research Project. *Transportation Research Record: Journal of the Transportation Research Board*, No. 1853, Transportation Research Board of the National Academies, Washington, D.C., pp. 134–141.

126. Timm, D. H., Robbins, M. M., Willis, J. R., Tran, N., Taylor, A. J. (2012a). *Evaluation of Mixture Performance and Structural Capacity of Pavements Utilizing Shell Thiopave®. Phase II: Construction, Laboratory Evaluation and Full-Scale Testing of Thiopave® Test Sections.* Final NCAT Report 12-07. National Center for Asphalt Technology, Auburn University, Auburn, AL.

127. Timm, D. H., Robbins, M. M, Willis, J. R., Tran, N., Taylor, A. J. (2012b). *Field and Laboratory Study of High-Polymer Mixtures at the NCAT Test Track*. Interim NCAT Report 12-08. National Center for Asphalt Technology, Auburn University, Auburn, AL.

128. Timm, D. H., Robbins, M. M, Willis, J. R., Tran, N., Taylor, A. J. (2013). *Field and Laboratory Study of High-Polymer Mixtures at the NCAT Test Track.* Final NCAT Report 13-03. National Center for Asphalt Technology, Auburn University, Auburn, AL.

129. Timm, D. H., Robbins, M. M, Willis, J. R., Tran, N., Taylor, A. J. (2014). *Field and Laboratory Study of Trinidad Lake Asphalt Mixtures at the NCAT Test Track.* NCAT Report 14-05. National Center for Asphalt Technology, Auburn University, Auburn, AL.

130. Timm, D., Tran, N., Taylor, A., Robbins, M., and Powell, B. (2009). *Evaluation of Mixture Performance and Structural Capacity of Pavements Utilizing Shell Thiopave®. Phase I: Mix Design, Laboratory Performance Evaluation and Structural Pavement Analysis and Design.* NCAT Report 09-05, National Center for Asphalt Technology, Auburn University, Auburn, AL.

131. Ullidtz, P. (2005). Simple Model for Pavement Damage. *Transportation Research Record: Journal of the Transportation Research Board*, No. 1905, Transportation Research Board of the National Academies, Washington, D.C., pp. 128–137.

132. Underwood, B. S., Baek, C. and Kim, Y.R. (2012). Simplified Viscoelastic Continuum Damage Model as Platform for Asphalt Concrete Fatigue Analysis. *Transportation*

Research Record: Journal of the Transportation Research Board, No. 2296, Transportation Research Board of the National Academies, Washington, D.C., pp. 36–45.

133. Van Dijk, W., Moreaud, H., Quedeville, A. and Ugé, P. (1972). The Fatigue of Bitumen and Bituminous Mixes. In: *3rd International Conference on the Structural Design of Asphalt Pavements*, London, Vol. 1, pp. 354–366.

134. Van Dijk, W. (1975). Practical Fatigue Characterization of Bituminous Mixes. *Journal of the Association of Asphalt Paving Technologists*, Vol. 44, pp. 38–74.

135. Van Dijk, W., and Visser, W. (1977). The Energy Approach to Fatigue for Pavement Design. *Journal of the Association of Asphalt Paving Technologists*, Vol. 46, pp. 1–40.

136. Vargas-Nordcbeck, A. and Timm, D. H. (2013). *Physical and Structural Characterization of Sustainable Asphalt Pavement Sections at the NCAT Test Track*. NCAT Report 13-02, National Center for Asphalt Technology, Auburn University, Auburn, AL.

137. Von Quintus, H. (2004). *Quantifications of the Effects of Polymer-Modified Asphalt for Reducing Pavement Distress*. ER-215, Asphalt Institute, Lexington, KY

138. Wang, Y., Norouzi, A. and Kim, Y. R. (2016). Comparison of Fatigue Cracking Performance of Asphalt Pavements Predicted by Pavement ME and LVECD Programs. *Transportation Research Record: Journal of the Transportation Research Board*, No. 2590, Transportation Research Board of the National Academies, Washington, D.C., pp. 44–55.

139. Wang, H., Ozer, H., Al-Qadi, I. L. and Duate, C. A. (2013). Analysis of Near-Surface Cracking under Critical Loading Conditions Under Uncracked and Cracked Pavement Models. *Journal of Transportation Engineering*, Vol. 139, No. 10, pp. 992–1000.

140. Wen, H. and Li, X. (2013). Development of a Damage-Based Phenomenological Fatigue Model for Asphalt Pavements. *Journal of Materials in Civil Engineering*, Vol. 25, No. 8, pp. 1006–1012.

141. West, R., Timm, D., Willis, R., Powell, B., Tran, N., Watson, D., Sakhaeifar, M., Brown, R., Vargas-Nordcbeck, A., Leiva Villacorta, F., Guo, X., and Nelson, J. (2012). *Phase IV NCAT Pavement Test Track Findings*. NCAT Draft Report 12-10, National Center for Asphalt Technology, Auburn University, Auburn, AL.

142. Willis, J. R. and Timm, D. H. (2009). *Field-Based Strain Thresholds for Flexible Perpetual Pavement Design*. NCAT Report 09-09. National Center for Asphalt Technology, Auburn University, Auburn, AL.

143. Willis, R., Timm, D., West, R., Powell, B., Robbins, M., Taylor, A., Smit, A., Tran, N., Heitzman, M. and Bianchini, A. (2009). *Phase III NCAT Test Track Findings*. NCAT Report 09-08. National Center for Asphalt Technology, Auburn University, Auburn, AL.

144. Witczak, M.W. (1972). Design of Full Depth Asphalt Airfield Pavements. In: Third International Conference on the Structural Design of Asphalt Pavements, Vol. I. London.

145. Witczak, M. W. and Root, R. E. (1974). Summary of Complex Modulus Laboratory Test Procedures and Results. *Fatigue and Dynamic Testing of Bituminous Mixtures*. ASTM Special Publication 561. American Society for Testing and Materials, Philadelphia, PA, pp. 67–94.

146. Wu, Z., Siddique, Z. Q. and Gisi, A. J. (2004). Kansas Turnpike — An Example of Long Lasting Asphalt Pavement. In: *International Symposium on Design and Construction of Long Lasting Asphalt Pavements*. National Center for Asphalt Technology, Auburn, AL, pp. 857–876.

147. Zhang, Z., Roque, R. and Birgisson, B. (2001a). Evaluation of Laboratory-Measured Crack Growth Rate for Asphalt Mixtures. *Transportation Research Record: Journal of the Transportation Research Board*, No. 1767, Transportation Research Board of the National Academies, Washington, D.C., pp. 67–75.

148. Zhang, Z., Roque, R., Birgisson, B., and Sangpetngam, B. (2001b). Identification and Verification of a Suitable Crack Growth Law. *Journal of the Association of Asphalt Paving Technologists*, Vol. 70, pp. 206–241.

APPENDICES

APPENDIX A

AC Mixture Properties & Fatigue Performance Characteristics

Table A1. AC Mixture Properties and Fatigue Performance Characteristics - Model Calibration Data

Test Section (Year)	Strain Level	Beam ID	Initial Stiffness (ksi)	[a]Cycles to 50% Initial Stiffness	Binder Grade (Modifier)	[b]Effective Binder (%)	RAP/RAS Content	NMAS (mm)	Bottom-Up Fatigue Cracking Performance
N9 (2006)	400	N9-5-2	804	1,483,020	PG 64-22	7.0	None	12.5	No cracking in 2006, 2009 and 2012 Cycles
	400	N9-5-6	836	1,672,290					
	800	N9-5-4	727	28,000					
	800	N9-5-7	797	15,790					
	800	N9-5-12	704	31,010					
S11 (2006)	400	S11-3-2	1,181	135,840	PG 67-22	5.0	None	19.0	Cracking in 2006 Cycle
	400	S11-3-3	1,201	282,130					
	400	S11-3-4	1,049	299,310					
	800	S11-3-5	1,016	14,300					
	800	S11-3-6	751	13,350					
	800	S11-3-7	765	13,210					
S12 (2006)	400	S12-2-3	612	13,881,233	PG 70-22 (SBS)	7.7	None	9.5	No cracking in 2006 Cycle
	400	S12-2-5	634	11,625,870					
	400	S12-2-7	539	24,626,856					
	800	S12-2-9	485	194,980					
	800	S12-2-10	476	179,190					
	800	S12-2-11	500	181,970					
N5 (2009)	200	N5-4-1	954	24,700,000	PG 67-22 (Shell Thiopave®)	5.8	None	19.0	No cracking in 2009 Cycle
	200	N5-4-4	923	54,400,000					
	200	N5-4-9	904	1,895,730					
	400	N5-4-5	762	415,270					
	400	N5-4-6	858	292,860					
	400	N5-4-8	872	81,490					
	800	N5-4-2	705	8,910					
	800	N5-4-3	637	6,810					
	800	N5-4-7	666	6,410					

Table A1. Cont'd

Test Section (Year)	Strain Level	Beam ID	Initial Stiffness (ksi)	[a]Cycles to 50% Initial Stiffness	Binder Grade (Modifier)	[b]Effective Binder (%)	RAP/RAS Content	NMAS (mm)	Bottom-Up Fatigue Cracking Performance
N10 (2009)	200	N10-3-3	1,664	15,200,000	PG 67-22	4.1	50% RAP	19.0	No cracking in 2009 Cycle. Cracking in 2012 Cycle
	200	N10-3-4	1,654	9,797,400					
	200	N10-3-10	1,707	3,328,290					
	400	N10-3-2	1,543	31,060					
	400	N10-3-6	1,465	112,630					
	400	N10-3-9	1,656	13,480					
	800	N10-3-1	1,339	3,230					
	800	N10-3-5	1,579	2,950					
	800	N10-3-11	1,328	690					
S8 (2009)	200	S8-3-2	870	26,179,413	PG 67-22	4.4	None	19.0	No cracking in 2009 Cycle. Cracking in 2012 Cycle
	200	S8-3-5	1,134	2,165,480					
	200	S8-3-7	943	6,953,800					
	200	S8-3-8	929	5,994,840					
	400	S8-3-1	793	200,290					
	400	S8-3-4	939	217,930					
	400	S8-3-9	921	143,430					
	800	S8-3-3	694	7,900					
	800	S8-3-6	867	4,300					
	800	S8-3-10	588	17,550					
S10 (2009)	200	S10-3-1	789	4,233,170	PG 67-22	4.2	None	19.0	No cracking in 2009 Cycle. Cracking in 2012 Cycle
	200	S10-3-4	835	7,134,000					
	200	S10-3-11	995	365,870					
	400	S10-3-3	724	159,710					
	400	S10-3-6	683	265,050					
	400	S10-3-10	873	135,410					
	800	S10-3-5	681	3,620					
	800	S10-3-7	570	7,000					
	800	S10-3-8	915	17,240					

Table A1. Cont'd

Test Section (Year)	Strain Level	Beam ID	Initial Stiffness (ksi)	[a]Cycles to 50% Initial Stiffness	Binder Grade (Modifier)	[b]Effective Binder (%)	RAP/RAS Content	NMAS (mm)	Bottom-Up Fatigue Cracking Performance
S11 (2009)	200	S11-3-1	743	1,764,680	PG 67-22	4.5	None	19.0	No cracking in 2009 Cycle. Cracking in 2012 Cycle
	200	S11-3-6	702	4,786,300					
	200	S11-3-7	887	4,641,580					
	400	S11-3-4	598	114,370					
	400	S11-3-8	539	185,490					
	400	S11-3-9	786	298,530					
	800	S11-3-2	513	9,160					
	800	S11-3-5	554	15,130					
	800	S11-3-10	703	7,220					
S12 (2009)	200	S12-3-1	1,107	75,095,892	PG 67-28 (Trinidad Lake Asphalt)	4.7	None	19.0	No cracking in 2009 Cycle
	200	S12-3-7	1,232	40,247,181					
	200	S12-3-8	1,344	4,570,880					
	400	S12-3-2	875	304,320					
	400	S12-3-6	1,093	458,840					
	400	S12-3-9	1,288	416,860					
	800	S12-3-4	1,186	5,310					
	800	S12-3-5	913	8,780					
	800	S12-3-10	1,213	3,400					
S5 Intermediate (2012)	200	S5-2-2	1,122	14,315,233	PG 67-22	4.3	50% RAP	19.0	Cracking in 2012 Cycle
	200	S5-2-4	1,173	3,194,800					
	200	S5-2-6	1,229	4,168,690					
	400	S5-2-1	1,111	118,390					
	400	S5-2-3	1,115	107,560					
	400	S5-2-5	1,084	151,350					

Table A1. Cont'd

Test Section (Year)	Strain Level	Beam ID	Initial Stiffness (ksi)	[a]Cycles to 50% Initial Stiffness	Binder Grade (Modifier)	[b]Effective Binder (%)	RAP/RAS Content	NMAS (mm)	Bottom-Up Fatigue Cracking Performance
S5 Intermediate (Repave) (2012)	200	S5-2 REP-5	1,212	13,017,312	PG 67-22	4.3	50% RAP	19.0	Cracking in 2012 Cycle
	200	S5-2 REP-6	1,153	138,612,244					
	200	S5-2 REP-7	1,146	109,912,621					
	400	S5-2 REP-1	1,097	154,880					
	400	S5-2 REP-3	1,098	74,890					
	400	S5-2 REP-8	1,110	125,410					
S6 Intermediate (2012)	200	S6-2-1	1,447	1,183,940	PG 67-22	4.3	25% RAP 5% PC-RAS	19.0	Cracking in 2012 Cycle
	200	S6-2-2	1,491	2,499,060					
	200	S6-2-3	1,488	7,356,420					
	400	S6-2-4	1,249	101,930					
	400	S6-2-5	1,313	84,030					
	400	S6-2-6	1,420	61,500					
N5 (2012)	200	N5-3-3	1,340	3,311,310	PG 67-22	4.1	35% RAP	19.0	Cracking in 2012 Cycle
	200	N5-3-5	1,412	5,964,240					
	200	N5-3-6	1,475	3,940,530					
	400	N5-3-7	1,402	52,210					
	400	N5-3-8	1,365	63,580					
	400	N5-3-9	1,367	86,870					
	800	N5-3-11	1,349	3,320					
	800	N5-3-12	1,299	2,890					
	800	N5-3-13	1,349	1,120					

Table A1. Cont'd

Test Section (Year)	Strain Level	Beam ID	Initial Stiffness (ksi)	[a]Cycles to 50% Initial Stiffness	Binder Grade (Modifier)	[b]Effective Binder (%)	RAP/RAS Content	NMAS (mm)	Bottom-Up Fatigue Cracking Performance
S5 Base (2012)	200	S5-3-5	1,188	3,813,919,261	PG 76-22	4.1	35% RAP	19.0	Cracking in 2012 Cycle
	200	S5-3-9	1,242	1,518,222,439					
	200	S5-3-10	1,323	258,131,813					
	400	S5-3-3	1,161	336,250					
	400	S5-3-7	1,101	582,100					
	400	S5-3-8	1,272	260,010					
	800	S5-3-2	1,035	3,160					
	800	S5-3-4	1,078	2,710					
	800	S5-3-6	980	1,190					
S6 Base (2012)	200	S6-3-1	1,078	979,320,923	PG 76-22 (SBS)	4.8	25% RAP	19.0	Cracking in 2012 Cycle
	200	S6-3-5	1,116	882,466,180					
	200	S6-3-6	1,120	11,733,950					
	400	S6-3-4	1,030	248,310					
	400	S6-3-7	1,070	211,340					
	400	S6-3-9	1,146	105,110					
	800	S6-3-2	1,032	3,730					
	800	S6-3-3	939	5,440					
	800	S6-3-8	995	4,240					

Notes: (a) Fatigue lives exceeding 12 million were extrapolated using Weibull function (b) Total Binder Content for 2006 Mixtures

Table A2. AC Mixture Properties and Fatigue Performance Characteristics - Model Validation Data

Test Section (Year)	Strain Level	Beam ID	Initial Stiffness (ksi)	[a]Cycles to 50% Initial Stiffness	Binder Grade (Modifier)	[b]Effective Binder (%)	RAP/RAS Content	NMAS (mm)	Bottom-Up Fatigue Cracking Performance
N10 (2006)	400	N10-3-5	834	562,660	PG 64-22	5.2	None	19.0	Cracking in 2006 Cycle
	400	N10-3-6	1,039	497,170					
	400	N10-3-7	894	1,191,490					
	800	N10-3-1	764	11,410					
	800	N10-3-2	753	21,400					
	800	N10-3-3	743	15,420					
N7 (2009)	400	N7-3-3	729	12,000,000	PG 88-22 (SBS)	4.2	None	19.0	No cracking in 2009 and 2012 Cycles
	400	N7-3-4	821	11,510,940					
	400	N7-3-6	1,029	1,685,250					
	400	N7-3-8	930	4,935,520					
	600	N7-3-1	845	287,290					
	600	N7-3-7	853	195,730					
	600	N7-3-9	963	186,920					
	800	N7-3-2	661	86,870					
	800	N7-3-5	1,034	20,890					
	800	N7-3-10	923	14,230					
N11 (2009)	200	N11-3-4	1,254	53,100,000	PG 67-22	4.0	50% RAP	19.0	No cracking in 2009 Cycle. Cracking in 2012 Cycle
	200	N11-3-6	1,396	54,500,000					
	200	N11-3-7	1,404	4,501,250					
	400	N11-3-2	1,249	100,000					
	400	N11-3-5	1,197	149,050					
	400	N11-3-8	1,199	124,920					
	800	N11-3-1	1,104	2,530					
	800	N11-3-3	970	3,060					
	800	N11-3-9	1,125	2,110					

Table A2. Cont'd

Test Section (Year)	Strain Level	Beam ID	Initial Stiffness (ksi)	[a]Cycles to 50% Initial Stiffness	Binder Grade (Modifier)	[b]Effective Binder (%)	RAP/RAS Content	NMAS (mm)	Bottom-Up Fatigue Cracking Performance
S13 Intermediate (2012)	200	S13-2-1	1,242	8,791,440	ARB12 (-30) (GTR)	4.3	35% RAP	19.0	Cracking in 2012 Cycle
	200	S13-2-6	1,018	72,022,743					
	200	S13-2-8	932	67,444,191					
	200	S13-2-9	1,117	36,358,596					
	400	S13-2-7	970	162,180					
	400	S13-2-10	1,098	78,020					
	400	S13-2-12	1,113	128,820					
S13 Base (2012)	400	S13-3-3	511	2,121,610	AZ20 (-16) (GTR)	6.5	None	19.0	Cracking in 2012 Cycle
	400	S13-3-4	403	3,311,310					
	400	S13-3-5	438	2,657,320					
	600	S13-3-6	398	183,370					
	600	S13-3-9	391	228,200					
	600	S13-3-10	400	428,210					
	800	S13-3-2	356	58,280					
	800	S13-3-7	367	48,850					
	800	S13-3-8	359	68,300					

Notes: (a) Fatigue lives exceeding 12 million were extrapolated using Weibull function (b) Total Binder Content for 2006 Mixtures

APPENDIX B

Fatigue Endurance Limits Determined Using NCHRP 9-44A & NCHRP 09-38 Procedures

Table B. Fatigue Endurance Limits Determined Using NCHRP 9-44A and NCHRP 09-38 Procedures

Test Section (Year)	Strain Level	Beam ID	Initial Stiffness (ksi)	Binder Grade (Modifier)	[a]Effective Binder (%)	NCHRP 9-44A Procedure								FEL (με) Using NCHRP 09-38 Procedure
						FEL (με) at Rest Period of				Average FEL (με) at Rest Period of				
						5s	8s	10s	20s	5s	8s	10s	20s	
N9 (2006)	400	N9-5-2	804	PG 64-22	7.0	95	110	113	115	96	111	114	116	203
	400	N9-5-6	836			94	109	112	114					
	800	N9-5-4	727			97	113	116	118					
	800	N9-5-7	797			95	110	113	115					
	800	N9-5-12	704			98	114	117	119					
N10 (2006)	400	N10-3-5	834	PG 64-22	5.2	94	109	112	114	94	109	112	114	146
	400	N10-3-6	1,039			88	103	106	108					
	400	N10-3-7	894			92	107	110	112					
	800	N10-3-1	764			96	111	115	117					
	800	N10-3-2	753			96	112	115	117					
	800	N10-3-3	743			97	112	115	117					
S11 (2006)	400	S11-3-2	1,181	PG 67-22	5.0	85	99	102	104	90	105	108	110	78
	400	S11-3-3	1,201			85	99	102	104					
	400	S11-3-4	1,049			88	103	106	107					
	800	S11-3-5	1,016			89	103	107	108					
	800	S11-3-6	751			96	112	115	117					
	800	S11-3-7	765			96	111	115	117					
S12 (2006)	400	S12-2-3	612	PG 70-22 (SBS)	7.7	102	118	121	123	105	122	125	127	300
	400	S12-2-5	634			101	117	120	122					
	400	S12-2-7	539			105	122	125	127					
	800	S12-2-9	485			108	125	129	131					
	800	S12-2-10	476			108	126	129	131					
	800	S12-2-11	500			107	124	128	130					

Table B. Cont'd

Test Section (Year)	Strain Level	Beam ID	Initial Stiffness (ksi)	Binder Grade (Modifier)	[a]Effective Binder (%)	NCHRP 9-44A Procedure								FEL (με) Using NCHRP 09-38 Procedure
						FEL (με) at Rest Period of				Average FEL (με) at Rest Period of				
						5s	8s	10s	20s	5s	8s	10s	20s	
N5 (2009)	200	N5-4-1	954	PG 67-22 (Shell Thiopave®)	5.8	90	105	108	110	95	110	113	115	109
	200	N5-4-4	923			91	106	109	111					
	200	N5-4-9	904			92	107	110	112					
	400	N5-4-5	762			96	111	115	117					
	400	N5-4-6	858			93	108	111	113					
	400	N5-4-8	872			93	108	111	113					
	800	N5-4-2	705			98	114	117	119					
	800	N5-4-3	637			101	117	120	122					
	800	N5-4-7	666			99	115	119	121					
N7 (2009)	400	N7-3-3	729	PG 88-22 (SBS)	4.2	97	113	116	118	93	108	111	113	241
	400	N7-3-4	821			94	109	113	114					
	400	N7-3-6	1,029			89	103	106	108					
	400	N7-3-8	930			91	106	109	111					
	600	N7-3-1	845			93	108	112	114					
	600	N7-3-7	853			93	108	111	113					
	600	N7-3-9	963			90	105	108	110					
	800	N7-3-2	661			100	116	119	121					
	800	N7-3-5	1,034			89	103	106	108					
	800	N7-3-10	923			91	106	109	111					
N10 (2009)	200	N10-3-3	1,664	PG 67-22	4.1	78	91	94	95	80	93	96	97	100
	200	N10-3-4	1,654			78	91	94	95					
	200	N10-3-10	1,707			77	90	93	95					
	400	N10-3-2	1,543			80	93	95	97					
	400	N10-3-6	1,465			81	94	97	98					
	400	N10-3-9	1,656			78	91	94	95					
	800	N10-3-1	1,339			83	96	99	101					
	800	N10-3-5	1,579			79	92	95	96					
	800	N10-3-11	1,328			83	96	99	101					

Table B. Cont'd

Test Section (Year)	Strain Level	Beam ID	Initial Stiffness (ksi)	Binder Grade (Modifier)	[a]Effective Binder (%)	NCHRP 9-44A Procedure								FEL (με) Using NCHRP 09-38 Procedure
						FEL (με) at Rest Period of				Average FEL (με) at Rest Period of				
						5s	8s	10s	20s	5s	8s	10s	20s	
N11 (2009)	200	N11-3-4	1,254	PG 67-22	4.0	84	98	101	103	85	99	102	104	134
	200	N11-3-6	1,396			82	95	98	100					
	200	N11-3-7	1,404			82	95	98	100					
	400	N11-3-2	1,249			84	98	101	103					
	400	N11-3-5	1,197			85	99	102	104					
	400	N11-3-8	1,199			85	99	102	104					
	800	N11-3-1	1,104			87	101	104	106					
	800	N11-3-3	970			90	105	108	110					
	800	N11-3-9	1,125			87	101	104	105					
S8 (2009)	200	S8-3-2	870	PG 67-22	4.4	93	108	111	113	93	108	112	113	92
	200	S8-3-5	1,134			86	101	104	105					
	200	S8-3-7	943			91	105	109	110					
	200	S8-3-8	929			91	106	109	111					
	400	S8-3-1	793			95	110	114	115					
	400	S8-3-4	939			91	106	109	111					
	400	S8-3-9	921			91	106	109	111					
	800	S8-3-3	694			98	114	118	119					
	800	S8-3-6	867			93	108	111	113					
	800	S8-3-10	588			103	119	123	125					
S10 (2009)	200	S10-3-1	789	PG 67-22	4.2	95	110	114	116	96	111	114	116	99
	200	S10-3-4	835			94	109	112	114					
	200	S10-3-11	995			89	104	107	109					
	400	S10-3-3	724			97	113	116	118					
	400	S10-3-6	683			99	115	118	120					
	400	S10-3-10	873			93	108	111	113					
	800	S10-3-5	681			99	115	118	120					
	800	S10-3-7	570			103	120	124	126					
	800	S10-3-8	915			91	106	109	111					

Table B. Cont'd

Test Section (Year)	Strain Level	Beam ID	Initial Stiffness (ksi)	Binder Grade (Modifier)	[a]Effective Binder (%)	NCHRP 9-44A Procedure								FEL (με) Using NCHRP 09-38 Procedure
						FEL (με) at Rest Period of				Average FEL (με) at Rest Period of				
						5s	8s	10s	20s	5s	8s	10s	20s	
S11 (2009)	200	S11-3-1	743	PG 67-22	4.5	97	112	115	117	100	116	119	121	84
	200	S11-3-6	702			98	114	117	119					
	200	S11-3-7	887			92	107	110	112					
	400	S11-3-4	598			102	119	122	124					
	400	S11-3-8	539			105	122	125	127					
	400	S11-3-9	786			95	111	114	116					
	800	S11-3-2	513			106	123	127	129					
	800	S11-3-5	554			104	121	124	126					
	800	S11-3-10	703			98	114	117	119					
S12 (2009)	200	S12-3-1	1,107	PG 67-28 (Trinidad Lake Asphalt)	4.7	87	101	104	106	87	101	104	105	137
	200	S12-3-7	1,232			85	98	101	103					
	200	S12-3-8	1,344			83	96	99	101					
	400	S12-3-2	875			93	108	111	113					
	400	S12-3-6	1,093			87	101	105	106					
	400	S12-3-9	1,288			84	97	100	102					
	800	S12-3-4	1,186			85	99	102	104					
	800	S12-3-5	913			92	106	110	111					
	800	S12-3-10	1,213			85	99	102	103					
S5 Intermediate (2012)	200	S5-2-2	1,122	PG 67-22	4.3	87	101	104	106	87	101	104	105	105
	200	S5-2-4	1,173			86	100	103	104					
	200	S5-2-6	1,229			85	98	101	103					
	400	S5-2-1	1,111			87	101	104	106					
	400	S5-2-3	1,115			87	101	104	106					
	400	S5-2-5	1,084			87	102	105	107					

Table B. Cont'd

Test Section (Year)	Strain Level	Beam ID	Initial Stiffness (ksi)	Binder Grade (Modifier)	[a]Effective Binder (%)	NCHRP 9-44A Procedure								FEL (με) Using NCHRP 09-38 Procedure
						FEL (με) at Rest Period of				Average FEL (με) at Rest Period of				
						5s	8s	10s	20s	5s	8s	10s	20s	
S5 Intermediate (Repave) (2012)	200	S5-2 REP-5	1,212	PG 67-22	4.3	85	99	102	103	86	100	103	105	161
	200	S5-2 REP-6	1,153			86	100	103	105					
	200	S5-2 REP-7	1,146			86	100	103	105					
	400	S5-2 REP-1	1,097			87	101	104	106					
	400	S5-2 REP-3	1,098			87	101	104	106					
	400	S5-2 REP-8	1,110			87	101	104	106					
S6 Intermediate (2012)	200	S6-2-1	1,447	PG 67-22	4.3	81	94	97	99	82	95	98	100	83
	200	S6-2-2	1,491			80	94	96	98					
	200	S6-2-3	1,488			80	94	96	98					
	400	S6-2-4	1,249			84	98	101	103					
	400	S6-2-5	1,313			83	97	100	101					
	400	S6-2-6	1,420			81	95	98	99					
S13 Intermediate (2012)	200	S13-2-1	1,242	ARB12 (-30) (GTR)	4.3	84	98	101	103	88	102	105	107	184
	200	S13-2-6	1,018			89	103	106	108					
	200	S13-2-8	932			91	106	109	111					
	200	S13-2-9	1,117			87	101	104	106					
	400	S13-2-7	970			90	105	108	110					
	400	S13-2-10	1,098			87	101	104	106					
	400	S13-2-12	1,113			87	101	104	106					
N5 (2012)	200	N5-3-3	1,340	PG 67-22	4.1	83	96	99	101	82	96	99	100	105
	200	N5-3-5	1,412			81	95	98	99					
	200	N5-3-6	1,475			81	94	97	98					
	400	N5-3-7	1,402			82	95	98	100					
	400	N5-3-8	1,365			82	96	99	100					
	400	N5-3-9	1,367			82	96	99	100					
	800	N5-3-11	1,349			82	96	99	101					
	800	N5-3-12	1,299			83	97	100	102					
	800	N5-3-13	1,349			82	96	99	101					

Table B. Cont'd

Test Section (Year)	Strain Level	Beam ID	Initial Stiffness (ksi)	Binder Grade (Modifier)	[a]Effective Binder (%)	NCHRP 9-44A Procedure								FEL (με) Using NCHRP 09-38 Procedure
						FEL (με) at Rest Period of				Average FEL (με) at Rest Period of				
						5s	8s	10s	20s	5s	8s	10s	20s	
S5 Base (2012)	200	S5-3-5	1,188	PG 76-22	4.1	85	99	102	104	86	100	103	105	211
	200	S5-3-9	1,242			84	98	101	103					
	200	S5-3-10	1,323			83	97	99	101					
	400	S5-3-3	1,161			86	100	103	105					
	400	S5-3-7	1,101			87	101	104	106					
	400	S5-3-8	1,272			84	98	100	102					
	800	S5-3-2	1,035			89	103	106	108					
	800	S5-3-4	1,078			88	102	105	107					
	800	S5-3-6	980			90	104	108	109					
S6 Base (2012)	200	S6-3-1	1,078	PG 76-22 (SBS)	4.8	88	102	105	107	88	102	105	107	156
	200	S6-3-5	1,116			87	101	104	106					
	200	S6-3-6	1,120			87	101	104	106					
	400	S6-3-4	1,030			89	103	106	108					
	400	S6-3-7	1,070			88	102	105	107					
	400	S6-3-9	1,146			86	100	103	105					
	800	S6-3-2	1,032			89	103	106	108					
	800	S6-3-3	939			91	106	109	111					
	800	S6-3-8	995			89	104	107	109					
S13 Base (2012)	400	S13-3-3	511	AZ20 (-16) (GTR)	6.5	106	123	127	129	113	131	135	137	209
	400	S13-3-4	403			113	131	135	137					
	400	S13-3-5	438			111	128	132	134					
	600	S13-3-6	398			113	131	135	137					
	600	S13-3-9	391			114	132	136	138					
	600	S13-3-10	400			113	131	135	137					
	800	S13-3-2	356			117	135	139	141					
	800	S13-3-7	367			116	134	138	140					
	800	S13-3-8	359			116	135	139	141					

Notes: (a) Total Binder Content for 2006 Mixtures

APPENDIX C

Pavement Cross-Sections Simulated for Model Calibration

Table C: Pavement Cross-Sections Simulated for Model Calibration

Test Section (Year)	Strain Level	Beam ID	FEL (με) (NCHRP 09-38)	Modulus (ksi)			Thickness (in.)		Load (lbs)	[a]Beam Fatigue Life	Simulation Results			
				AC	GB	Soil	AC	GB			End Modulus (psi)	% Initial Modulus	β-Param	R^2
N9 (2006)	400	N9-5-2	203	804	10	3	6	8	19,000	1,483,020	394,815	49	15,390	93
	400	N9-5-6		836	10	3	6	8	19,820	1,672,290	419,889	50	15,860	95
	800	N9-5-4		727	8	3	6	8	49,900	28,000	362,938	50	8,050	91
	800	N9-5-7		797	8	3	6	8	55,500	15,790	381,247	48	9,450	86
	800	N9-5-12		704	8	3	6	8	48,100	31,010	335,262	48	7,800	90
S11 (2006)	400	S11-3-2	78	1,181	8	3	6	8	28,050	135,840	557,866	47	7,370	83
	400	S11-3-3		1,201	8	3	6	8	28,580	282,130	581,408	48	7,050	85
	400	S11-3-4		1,049	8	3	6	8	24,600	299,310	513,427	49	6,125	84
	800	S11-3-5		1,016	8	3	6	8	73,400	14,300	619,729	61	3,250	67
	800	S11-3-6		751	8	3	6	8	51,800	13,350	368,273	49	2,720	91
	800	S11-3-7		765	8	3	6	8	52,900	13,210	366,095	48	2,790	94
S12 (2006)	400	S12-2-3	300	612	10	5	6	10	16,350	12,000,000	350,535	57	19,550	93
	400	S12-2-5		634	10	5	6	10	17,000	11,625,870	348,883	55	20,358	93
	400	S12-2-7		539	10	5	6	10	14,150	12,000,000	323,354	60	17,100	96
	800	S12-2-9		485	8	3	6	8	31,560	194,980	222,036	46	7,750	92
	800	S12-2-10		476	8	3	6	8	30,910	179,190	226,727	48	7,620	90
	800	S12-2-11		500	8	3	6	8	32,650	181,970	221,772	44	8,050	92
N5 (2009)	200	N5-4-1	109	954	10	5	6	10	9,480	12,000,000	539,522	57	16,500	97
	200	N5-4-4		923	10	5	6	10	9,150	12,000,000	546,269	59	15,800	96
	200	N5-4-9		904	10	5	6	10	8,950	1,895,730	670,175	74	14,500	64
	400	N5-4-5		762	8	3	6	8	17,260	415,270	358,293	47	6,685	91
	400	N5-4-6		858	8	3	6	8	19,680	292,860	406,583	47	7,725	90
	400	N5-4-8		872	8	3	6	8	20,050	81,490	453,208	52	8,650	73
	800	N5-4-2		705	8	3	6	8	48,200	8,910	351,547	50	4,000	85
	800	N5-4-3		637	8	3	6	8	42,910	6,810	308,952	49	3,750	86
	800	N5-4-7		666	8	3	6	8	45,120	6,410	407,753	61	3,500	74

Table C: Cont'd

Test Section (Year)	Strain Level	Beam ID	FEL (με) (NCHRP 09-38)	Modulus (ksi)			Thickness (in.)		Load (lbs)	[a]Beam Fatigue Life	Simulation Results			
				AC	GB	Soil	AC	GB			End Modulus (psi)	% Initial Modulus	β-Param	R^2
N10 (2009)	200	N10-3-3	100	1,664	10	5	6	10	17,430	12,000,000	891,332	54	25,500	85
	200	N10-3-4		1,654	10	5	6	10	17,320	9,797,400	858,459	52	25,708	84
	200	N10-3-10		1,707	10	5	6	10	17,940	3,328,290	1,183,596	69	25,000	50
	400	N10-3-2		1,543	8	3	6	8	37,850	31,060	943,636	61	14,000	67
	400	N10-3-6		1,465	8	3	6	8	35,680	112,630	875,579	60	12,000	37
	400	N10-3-9		1,656	8	3	6	8	40,950	13,480	1,043,683	63	16,000	69
	800	N10-3-1		1,339	8	3	6	7	99,800	3,230	706,859	53	7,500	76
	800	N10-3-5		1,579	6	2	6	7	97,360	2,950	845,804	54	8,500	79
	800	N10-3-11		1,328	8	3	6	7	98,800	690	855,088	64	8,000	56
S8 (2009)	200	S8-3-2	92	870	10	5	6	10	8,580	12,000,000	521,499	60	11,500	96
	200	S8-3-5		1,134	10	5	6	10	11,410	2,165,480	593,249	52	17,225	79
	200	S8-3-7		943	10	5	6	10	9,350	6,953,800	504,292	53	13,250	90
	200	S8-3-8		929	10	5	6	10	9,200	5,994,840	533,244	57	13,000	91
	400	S8-3-1		793	8	3	6	8	18,030	200,290	390,247	49	5,900	85
	400	S8-3-4		939	8	3	6	8	21,740	217,930	437,011	47	6,960	74
	400	S8-3-9		921	8	3	6	8	21,270	143,430	449,973	49	7,050	90
	800	S8-3-3		694	8	3	6	8	47,280	7,900	356,473	51	3,200	85
	800	S8-3-6		867	8	3	6	8	61,070	4,300	469,160	54	4,200	80
	800	S8-3-10		588	8	3	6	8	39,240	17,550	291,534	50	2,525	86
S10 (2009)	200	S10-3-1	99	789	10	5	6	10	7,730	4,233,170	414,296	53	12,780	89
	200	S10-3-4		835	10	5	6	10	8,210	7,134,000	440,296	53	13,050	88
	200	S10-3-11		995	10	5	6	10	9,900	365,870	581,881	58	18,800	74
	400	S10-3-3		724	8	3	6	8	16,320	159,710	373,360	52	6,000	80
	400	S10-3-6		683	8	3	6	8	15,310	265,050	322,681	47	5,485	85
	400	S10-3-10		873	8	3	6	8	20,060	135,410	443,557	51	7,350	81
	800	S10-3-5		681	8	3	6	8	46,320	3,620	365,703	54	3,700	80
	800	S10-3-7		570	8	3	6	8	37,880	7,000	320,467	56	2,800	79
	800	S10-3-8		915	8	3	6	8	65,000	17,240	485,327	53	4,300	86

Table C: Cont'd

Test Section (Year)	Strain Level	Beam ID	FEL (με) (NCHRP 09-38)	Modulus (ksi)			Thickness (in.)		Load (lbs)	[a]Beam Fatigue Life	Simulation Results			
				AC	GB	Soil	AC	GB			End Modulus (psi)	% Initial Modulus	β-Param	R^2
S11 (2009)	200	S11-3-1	84	743	10	5	6	10	7,260	1,764,680	389,330	52	10,100	81
	200	S11-3-6		702	10	5	6	10	6,850	4,786,300	359,068	51	8,945	76
	200	S11-3-7		887	10	5	6	10	8,750	4,641,580	457,046	52	11,285	85
	400	S11-3-4		598	8	3	6	8	13,260	114,370	281,406	47	4,185	89
	400	S11-3-8		539	8	3	6	8	11,860	185,490	301,227	56	3,500	58
	400	S11-3-9		786	8	3	6	8	17,870	298,530	385,871	49	5,000	69
	800	S11-3-2		513	8	3	6	8	33,660	9,160	267,741	52	2,075	89
	800	S11-3-5		554	8	3	6	8	36,660	15,130	295,522	53	2,100	89
	800	S11-3-10		703	8	3	6	8	48,020	7,220	371,368	53	2,900	84
S12 (2009)	200	S12-3-1	137	1,107	10	5	6	10	11,120	12,000,000	667,888	60	27,500	94
	200	S12-3-7		1,232	10	5	6	10	12,500	12,000,000	707,750	57	30,850	92
	200	S12-3-8		1,344	10	5	6	10	13,760	4,570,880	809,879	60	35,500	87
	400	S12-3-2		875	8	3	6	8	20,110	304,320	465,428	53	10,510	85
	400	S12-3-6		1,093	8	3	6	8	25,720	458,840	524,396	48	12,835	88
	400	S12-3-9		1,288	8	3	6	8	30,900	416,860	620,158	48	15,245	71
	800	S12-3-4		1,186	8	3	6	8	88,080	5,310	604,542	51	9,450	83
	800	S12-3-5		913	8	3	6	8	64,800	8,780	465,298	51	6,850	90
	800	S12-3-10		1,213	8	3	6	8	90,420	3,400	873,692	72	7,500	39
S5 Intermediate (2012)	200	S5-2-2	105	1,122	10	5	6	10	11,290	12,000,000	676,940	60	18,000	81
	200	S5-2-4		1,173	10	5	6	10	11,850	3,194,800	796,743	68	19,000	64
	200	S5-2-6		1,229	10	5	6	10	12,480	4,168,690	662,531	54	21,625	74
	400	S5-2-1		1,111	8	3	6	8	26,190	118,390	614,118	55	10,000	67
	400	S5-2-3		1,115	8	3	6	8	26,310	107,560	574,000	51	10,300	74
	400	S5-2-5		1,084	8	3	6	8	25,490	151,350	590,227	54	9,600	69

Table C: Cont'd

Test Section (Year)	Strain Level	Beam ID	FEL (με) (NCHRP 09-38)	Modulus (ksi)			Thickness (in.)		Load (lbs)	[a]Beam Fatigue Life	Simulation Results			
				AC	GB	Soil	AC	GB			End Modulus (psi)	% Initial Modulus	β-Param	R^2
S5 Intermediate (Repave) (2012)	200	S5-2 REP-5	161	1,212	10	5	6	10	12,280	12,000,000	794,850	66	40,500	43
	200	S5-2 REP-6		1,153	10	5	6	10	11,630	12,000,000	738,364	64	38,750	81
	200	S5-2 REP-7		1,146	10	5	6	10	11,540	12,000,000	722,834	63	38,575	94
	400	S5-2 REP-1		1,097	8	3	6	8	25,830	154,880	525,408	48	17,518	89
	400	S5-2 REP-3		1,098	8	3	6	8	25,850	74,890	541,416	49	18,650	90
	400	S5-2 REP-8		1,110	8	3	6	8	26,160	125,410	562,401	51	18,000	85
S6 Intermediate (2012)	200	S6-2-1	83	1,447	10	5	6	10	14,930	1,183,940	1,056,300	73	16,000	48
	200	S6-2-2		1,491	10	5	6	10	15,430	2,499,060	1,022,698	69	17,000	65
	200	S6-2-3		1,488	10	5	6	10	15,390	7,356,420	1,037,389	70	15,500	71
	400	S6-2-4		1,249	8	3	6	8	29,860	101,930	664,791	53	8,500	77
	400	S6-2-5		1,313	8	3	6	8	31,550	84,030	720,262	55	9,000	76
	400	S6-2-6		1,420	8	3	6	8	34,460	61,500	782,613	55	10,000	74
N5 (2012)	200	N5-3-3	105	1,340	10	5	6	10	13,720	3,311,310	975,141	73	20,000	47
	200	N5-3-5		1,412	10	5	6	10	14,520	5,964,240	867,619	61	23,500	81
	200	N5-3-6		1,475	10	5	6	10	15,250	3,940,530	922,762	63	25,000	80
	400	N5-3-7		1,402	8	3	6	8	33,960	52,210	935,675	67	12,000	60
	400	N5-3-8		1,365	8	3	6	8	32,960	63,580	869,083	64	12,000	65
	400	N5-3-9		1,367	8	3	6	8	33,020	86,870	839,904	61	12,750	63
	800	N5-3-11		1,349	8	2	6	7	83,670	3,320	757,931	56	7,550	72
	800	N5-3-12		1,299	8	2	6	7	80,190	2,890	780,720	60	7,100	63
	800	N5-3-13		1,349	8	2	6	7	83,700	1,120	792,557	59	8,500	57

Table C: Cont'd

Test Section (Year)	Strain Level	Beam ID	FEL (με) (NCHRP 09-38)	Modulus (ksi)			Thickness (in.)		Load (lbs)	[a]Beam Fatigue Life	Simulation Results			
				AC	GB	Soil	AC	GB			End Modulus (psi)	% Initial Modulus	β-Param	R^2
S5 Base (2012)	200	S5-3-5	211	1,188	10	5	6	10	12,010	12,000,000	Initial Critical Strain exceeds FEL			
	200	S5-3-9		1,242	10	5	6	10	12,610	12,000,000	Initial Critical Strain exceeds FEL			
	200	S5-3-10		1,323	10	5	6	10	13,520	12,000,000	Initial Critical Strain exceeds FEL			
	400	S5-3-3		1,161	8	3	6	8	27,500	336,250	590,170	51	25,600	94
	400	S5-3-7		1,101	8	3	6	8	25,930	582,100	572,347	52	23,250	89
	400	S5-3-8		1,272	8	3	6	8	30,450	260,010	645,908	51	28,625	86
	800	S5-3-2		1,035	8	3	6	8	75,040	3,160	554,312	54	15,000	79
	800	S5-3-4		1,078	8	3	6	8	78,680	2,710	643,869	60	15,000	72
	800	S5-3-6		980	8	3	6	8	70,400	1,190	596,531	61	15,000	61
S6 Base (2012)	200	S6-3-1	156	1,078	10	5	6	10	10,810	12,000,000	844,915	78	29,000	81
	200	S6-3-5		1,116	10	5	6	10	11,220	12,000,000	791,108	71	33,500	94
	200	S6-3-6		1,120	10	5	6	10	11,260	11,733,950	669,749	60	35,520	94
	400	S6-3-4		1,030	8	3	6	8	24,080	248,310	566,832	55	14,900	75
	400	S6-3-7		1,070	8	3	6	8	25,130	211,340	520,886	49	15,945	76
	400	S6-3-9		1,146	8	3	6	8	27,110	105,110	664,116	58	17,500	82
	800	S6-3-2		1,032	8	3	6	8	74,760	3,730	641,477	62	9,000	69
	800	S6-3-3		939	8	3	6	8	66,990	5,440	510,915	54	8,550	81
	800	S6-3-8		995	8	3	6	8	71,660	4,240	551,351	55	9,250	81

Note (a) Fatigue life was defined as 50% reduction in initial AC stiffness. Fatigue lives for beams with 12million load cycles were extrapolated

AC: Asphalt Concrete GB: Granular Base FEL: Fatigue Endurance Limit

APPENDIX D

Pavement Cross-Sections Simulated for Model Validation

Table D1: Pavement Cross-Sections Simulated for Model Validation

Test Section (Year)	Strain Level	Beam ID	FEL (με) (NCHRP 09-38)	Modulus (ksi)			Thickness (in.)		Load (lbs)	[a]Beam Fatigue Life	Model 1: Ln(BETA) = f (STR, E_0, FEL)					Expected β-Parameters				
				AC	GB	Soil	AC	GB			β-Param	R^2	End Modulus (psi)	% Initial Modulus	% of Beam Fatigue Life Simulated	β-Param	R^2	End Modulus (psi)	% Initial Modulus	% of Beam Fatigue Life Simulated
N10 (2006)	400	N10-3-5	146	834	8	3	6	8	19,055	562,660	10,935	65	342,048	41	61	10,400	89	446,469	54	100
	400	N10-3-6		1,039	8	3	6	8	24,300	497,170	13,953	83	443,189	43	50	13,200	91	515,929	50	100
	400	N10-3-7		894	8	3	6	8	20,569	1,191,490	11,741	75	421,525	47	28	10,655	94	442,473	50	100
	800	N10-3-1		764	8	3	6	8	52,810	11,410	4,919	0	516,010	68	100	6,100	94	376,439	49	100
	800	N10-3-2		753	8	3	6	8	51,950	21,400	4,856	0	480,020	64	100	5,700	93	352,943	47	100
	800	N10-3-3		743	8	3	6	8	51,162	15,420	4,798	0	487,980	66	100	5,750	92	365,605	49	100
N7 (2009)	400	N7-3-3	241	729	8	3	6	8	16,438	12,000,000	19,832	0	375,428	52	3	15,400	92	386,340	53	100
	400	N7-3-4		821	8	3	6	8	18,745	11,510,940	22,141	3	385,524	47	3	17,350	86	446,955	54	100
	400	N7-3-6		1,029	8	3	6	8	24,047	1,685,250	28,339	0	531,329	52	16	24,650	89	551,751	54	100
	400	N7-3-8		930	8	3	6	8	21,505	4,935,520	25,200	75	464,230	50	7	20,750	82	494,740	53	100
	600	N7-3-1		845	8	3	6	8	36,350	287,290	15,922	74	337,000	40	16	13,500	74	420,168	50	100
	600	N7-3-7		853	8	3	6	8	36,722	195,730	16,069	6	315,838	37	23	14,100	89	410,511	48	100
	600	N7-3-9		963	8	3	6	8	42,103	186,920	18,314	53	373,514	39	22	16,000	85	453,296	47	100
	800	N7-3-2		661	8	3	6	8	44,718	86,870	8,934	73	128,387	19	55	8,934	91	270,067	41	100
	800	N7-3-5		1,034	8	3	6	8	74,913	20,890	13,931	74	599,218	58	100	15,000	89	486,904	47	100
	800	N7-3-10		923	8	3	6	8	65,624	14,230	12,205	51	578,321	63	100	13,424	90	495,207	54	100
N11 (2009)	200	N11-3-4	134	1,254	10	5	6	10	12,739	12,000,000	23,544	5	984,612	79	100	30,250	93	710,724	57	100
	200	N11-3-6		1,396	10	5	6	10	14,337	12,000,000	27,873	35	1,060,027	76	100	33,700	92	778,653	56	100
	200	N11-3-7		1,404	10	5	6	10	14,429	4,501,250	28,144	43	1,100,565	78	100	36,000	92	805,667	57	100
	400	N11-3-2		1,249	8	3	6	8	29,837	100,000	16,360	78	529,654	42	85	16,100	83	619,725	50	100
	400	N11-3-5		1,197	8	3	6	8	28,448	149,050	15,374	64	359,300	30	71	14,432	80	686,481	57	100
	400	N11-3-8		1,199	8	3	6	8	28,513	124,920	15,419	65	490,565	41	84	14,469	80	710,308	59	100
	800	N11-3-1		1,104	8	3	6	8	80,872	2,530	6,726	3	804,460	73	100	8,909	67	625,295	57	100
	800	N11-3-3		970	8	3	6	8	69,522	3,060	5,736	0	708,825	73	100	7,500	72	565,304	58	100
	800	N11-3-9		1,125	8	3	6	8	82,700	2,110	6,898	0	827,169	74	100	9,800	75	565,796	50	100
S13 Intermediate (2012)	400	S13-2-7	184	970	8	3	6	8	22,536	162,180	17,160	66	622,523	64	100	18,610	92	486,346	50	100
	400	S13-2-10		1,098	8	3	6	8	25,859	78,020	19,982	70	734,145	67	100	22,250	86	593,006	54	100
	400	S13-2-12		1,113	8	3	6	8	26,232	128,820	20,323	62	700,161	63	100	21,750	89	553,987	50	100
S13 Base (2012)	400	S13-3-3	209	511	8	3	6	8	11,195	2,121,610	12,009	84	251,819	49	7	9,722	64	276,466	54	100
	400	S13-3-4		403	8	3	6	8	8,719	3,311,310	10,562	0	195,588	48	1	7,525	72	207,098	51	100
	400	S13-3-5		438	8	3	6	8	9,494	2,657,320	11,001	0	211,180	48	3	8,250	77	230,187	53	100
	600	S13-3-6		398	8	3	6	8	15,805	183,370	7,340	0	121,343	30	5	5,500	89	183,697	46	100
	600	S13-3-9		391	8	3	6	8	15,481	228,200	7,275	0	117,684	30	4	5,295	90	183,792	47	100
	600	S13-3-10		400	8	3	6	8	15,867	428,210	7,353	0	158,590	40	2	5,125	93	196,825	49	100
	800	S13-3-2		356	8	3	6	8	22,396	58,280	4,878	0	58,457	16	12	3,900	94	165,144	46	100
	800	S13-3-7		367	8	3	6	8	23,141	48,850	4,940	0	137,270	37	17	4,100	94	164,999	45	100
	800	S13-3-8		359	8	3	6	8	22,607	68,300	4,895	0	58,859	16	11	3,900	94	159,624	44	100

Note (a) Fatigue life was defined as 50% reduction in initial AC stiffness. Fatigue lives for beams with 12million load cycles were extrapolated

AC: Asphalt Concrete GB: Granular Base FEL: Fatigue Endurance Limit

Table D2: Pavement Cross-Sections Simulated for Model Validation

Test Section (Year)	Strain Level	Beam ID	FEL (με) (NCHRP 09-38)	Modulus (ksi)			Thickness (in.)		Load (lbs)	[a]Beam Fatigue Life	Model 2: Ln(BETA) = f (E_0, 1/STR, 1/ FEL)					Expected β-Parameters				
				AC	GB	Soil	AC	GB			β-Param	R^2	End Modulus (psi)	% Initial Modulus	% of Beam Fatigue Life Simulated	β-Param	R^2	End Modulus (psi)	% Initial Modulus	% of Beam Fatigue Life Simulated
N10 (2006)	400	N10-3-5	146	834	8	3	6	8	19,055	562,660	10,974	62	356,953	43	58	10,400	89	446,469	54	100
	400	N10-3-6		1,039	8	3	6	8	24,300	497,170	13,496	91	440,012	42	76	13,200	91	515,929	50	100
	400	N10-3-7		894	8	3	6	8	20,569	1,191,490	11,657	77	371,017	42	31	10,655	94	442,473	50	100
	800	N10-3-1		764	8	3	6	8	52,810	11,410	7,074	0	154,975	20	35	6,100	94	376,439	49	100
	800	N10-3-2		753	8	3	6	8	51,950	21,400	6,996	0	114,987	15	18	5,700	93	352,943	47	100
	800	N10-3-3		743	8	3	6	8	51,162	15,420	6,926	0	125,776	17	25	5,750	92	365,605	49	100
N7 (2009)	400	N7-3-3	241	729	8	3	6	8	16,438	12,000,000	15,479	93	379,123	52	93	15,400	92	386,340	53	100
	400	N7-3-4		821	8	3	6	8	18,745	11,510,940	16,996	76	491,850	60	100	17,350	86	446,955	54	100
	400	N7-3-6		1,029	8	3	6	8	24,047	1,685,250	20,956	62	742,899	72	100	24,650	89	551,751	54	100
	400	N7-3-8		930	8	3	6	8	21,505	4,935,520	18,969	42	626,995	67	100	20,750	82	494,740	53	100
	600	N7-3-1		845	8	3	6	8	36,350	287,290	13,614	79	332,181	39	97	13,500	74	420,168	50	100
	600	N7-3-7		853	8	3	6	8	36,722	195,730	13,720	86	470,275	55	100	14,100	89	410,511	48	100
	600	N7-3-9		963	8	3	6	8	42,103	186,920	15,331	74	550,454	57	100	16,000	85	453,296	47	100
	800	N7-3-2		661	8	3	6	8	44,718	86,870	9,989	0	136,284	21	18	8,934	91	270,067	41	100
	800	N7-3-5		1,034	8	3	6	8	74,913	20,890	14,564	89	545,719	53	100	15,000	89	486,904	47	100
	800	N7-3-10		923	8	3	6	8	65,624	14,230	13,018	84	528,118	57	100	13,424	90	495,207	54	100
N11 (2009)	200	N11-3-4	134	1,254	10	5	6	10	12,739	12,000,000	31,666	93	694,867	55	49	30,250	93	710,724	57	100
	200	N11-3-6		1,396	10	5	6	10	14,337	12,000,000	36,544	72	767,605	55	28	33,700	92	778,653	56	100
	200	N11-3-7		1,404	10	5	6	10	14,429	4,501,250	36,845	88	744,546	53	73	36,000	92	805,667	57	100
	400	N11-3-2		1,249	8	3	6	8	29,837	100,000	15,066	77	765,732	61	100	16,100	83	619,725	50	100
	400	N11-3-5		1,197	8	3	6	8	28,448	149,050	14,292	80	702,021	59	100	14,432	80	686,481	57	100
	400	N11-3-8		1,199	8	3	6	8	28,513	124,920	14,328	80	723,486	60	100	14,469	80	710,308	59	100
	800	N11-3-1		1,104	8	3	6	8	80,872	2,530	8,998	65	614,343	56	100	8,909	67	625,295	57	100
	800	N11-3-3		970	8	3	6	8	69,522	3,060	7,860	67	519,080	54	100	7,500	72	565,304	58	100
	800	N11-3-9		1,125	8	3	6	8	82,700	2,110	9,192	74	649,211	58	100	9,800	75	565,796	50	100
S13 Intermediate (2012)	400	S13-2-7	184	970	8	3	6	8	22,536	162,180	15,946	35	672,993	69	100	18,610	92	486,346	50	100
	400	S13-2-10		1,098	8	3	6	8	25,859	78,020	18,146	38	795,075	72	100	22,250	86	593,006	54	100
	400	S13-2-12		1,113	8	3	6	8	26,232	128,820	18,408	10	779,480	70	100	21,750	89	553,987	50	100
S13 Base (2012)	400	S13-3-3	209	511	8	3	6	8	11,195	2,121,610	11,176	92	249,392	49	16	9,722	64	276,466	54	100
	400	S13-3-4		403	8	3	6	8	8,719	3,311,310	10,022	31	206,476	51	2	7,525	72	207,098	51	100
	400	S13-3-5		438	8	3	6	8	9,494	2,657,320	10,374	56	215,158	49	5	8,250	77	230,187	53	100
	600	S13-3-6		398	8	3	6	8	15,805	183,370	7,798	0	156,121	39	3	5,500	89	183,697	46	100
	600	S13-3-9		391	8	3	6	8	15,481	228,200	7,739	0	141,233	36	2	5,295	90	183,792	47	100
	600	S13-3-10		400	8	3	6	8	15,867	428,210	7,810	0	116,107	29	1	5,125	93	196,825	49	100
	800	S13-3-2		356	8	3	6	8	22,396	58,280	6,605	0	37,818	11	1	3,900	94	165,144	46	100
	800	S13-3-7		367	8	3	6	8	23,141	48,850	6,677	0	30,056	8	2	4,100	94	164,999	45	100
	800	S13-3-8		359	8	3	6	8	22,607	68,300	6,626	0	37,829	11	1	3,900	94	159,624	44	100

Note (a) Fatigue life was defined as 50% reduction in initial AC stiffness. Fatigue lives for beams with 12million load cycles were extrapolated

AC: Asphalt Concrete GB: Granular Base FEL: Fatigue Endurance Limit

Table D3: Pavement Cross-Sections Simulated for Model Validation

Test Section (Year)	Strain Level	Beam ID	FEL (με) (NCHRP 09-38)	Modulus (ksi)			Thickness (in.)		Load (lbs)	[a]Beam Fatigue Life	Model 3: Ln(BETA) = f (LnE_0, 1/STR, 1/ FEL)					Expected β-Parameters				
				AC	GB	Soil	AC	GB			β-Param	R^2	End Modulus (psi)	% Initial Modulus	% of Beam Fatigue Life Simulated	β-Param	R^2	End Modulus (psi)	% Initial Modulus	% of Beam Fatigue Life Simulated
N10 (2006)	400	N10-3-5	146	834	8	3	6	8	19,055	562,660	11,330	28	354,011	42	39	10,400	89	446,469	54	100
	400	N10-3-6		1,039	8	3	6	8	24,300	497,170	14,110	79	411,940	40	44	13,200	91	515,929	50	100
	400	N10-3-7		894	8	3	6	8	20,569	1,191,490	12,141	55	442,464	50	18	10,655	94	442,473	50	100
	800	N10-3-1		764	8	3	6	8	52,810	11,410	7,224	0	297,086	39	29	6,100	94	376,439	49	100
	800	N10-3-2		753	8	3	6	8	51,950	21,400	7,121	0	121,317	16	16	5,700	93	352,943	47	100
	800	N10-3-3		743	8	3	6	8	51,162	15,420	7,027	0	134,714	18	22	5,750	92	365,605	49	100
N7 (2009)	400	N7-3-3	241	729	8	3	6	8	16,438	12,000,000	15,500	93	375,706	52	91	15,400	92	386,340	53	100
	400	N7-3-4		821	8	3	6	8	18,745	11,510,940	17,466	88	426,794	52	94	17,350	86	446,955	54	100
	400	N7-3-6		1,029	8	3	6	8	24,047	1,685,250	21,873	71	716,318	70	100	24,650	89	551,751	54	100
	400	N7-3-8		930	8	3	6	8	21,505	4,935,520	19,778	59	590,202	63	100	20,750	82	494,740	53	100
	600	N7-3-1		845	8	3	6	8	36,350	287,290	14,110	86	325,690	39	62	13,500	74	420,168	50	100
	600	N7-3-7		853	8	3	6	8	36,722	195,730	14,238	90	279,378	33	92	14,100	89	410,511	48	100
	600	N7-3-9		963	8	3	6	8	42,103	186,920	16,072	87	370,847	39	96	16,000	85	453,296	47	100
	800	N7-3-2		661	8	3	6	8	44,718	86,870	9,771	0	117,409	18	22	8,934	91	270,067	41	100
	800	N7-3-5		1,034	8	3	6	8	74,913	20,890	15,289	79	110,035	11	93	15,000	89	486,904	47	100
	800	N7-3-10		923	8	3	6	8	65,624	14,230	13,647	88	472,392	51	100	13,424	90	495,207	54	100
N11 (2009)	200	N11-3-4	134	1,254	10	5	6	10	12,739	12,000,000	31,789	93	686,195	55	46	30,250	93	710,724	57	100
	200	N11-3-6		1,396	10	5	6	10	14,337	12,000,000	35,383	88	779,857	56	46	33,700	92	778,653	56	100
	200	N11-3-7		1,404	10	5	6	10	14,429	4,501,250	35,589	90	857,692	61	100	36,000	92	805,667	57	100
	400	N11-3-2		1,249	8	3	6	8	29,837	100,000	15,323	80	743,342	60	100	16,100	83	619,725	50	100
	400	N11-3-5		1,197	8	3	6	8	28,448	149,050	14,682	80	651,805	54	100	14,432	80	686,481	57	100
	400	N11-3-8		1,199	8	3	6	8	28,513	124,920	14,713	80	683,931	57	100	14,469	80	710,308	59	100
	800	N11-3-1		1,104	8	3	6	8	80,872	2,530	9,421	50	549,331	50	100	8,909	67	625,295	57	100
	800	N11-3-3		970	8	3	6	8	69,522	3,060	8,279	36	425,717	44	100	7,500	72	565,304	58	100
	800	N11-3-9		1,125	8	3	6	8	82,700	2,110	9,602	78	597,796	53	100	9,800	75	565,796	50	100
S13 Intermediate (2012)	400	S13-2-7	184	970	8	3	6	8	22,536	162,180	16,670	54	644,863	66	100	18,610	92	486,346	50	100
	400	S13-2-10		1,098	8	3	6	8	25,859	78,020	18,866	52	773,253	70	100	22,250	86	593,006	54	100
	400	S13-2-12		1,113	8	3	6	8	26,232	128,820	19,110	30	754,208	68	100	21,750	89	553,987	50	100
S13 Base (2012)	400	S13-3-3	209	511	8	3	6	8	11,195	2,121,610	9,786	66	248,535	49	99.6	9,722	64	276,466	54	100
	400	S13-3-4		403	8	3	6	8	8,719	3,311,310	7,722	79	194,854	48	69	7,525	72	207,098	51	100
	400	S13-3-5		438	8	3	6	8	9,494	2,657,320	8,377	81	107,535	25	84	8,250	77	230,187	53	100
	600	S13-3-6		398	8	3	6	8	15,805	183,370	5,989	88	145,233	36	38	5,500	89	183,697	46	100
	600	S13-3-9		391	8	3	6	8	15,481	228,200	5,875	82	143,067	37	31	5,295	90	183,792	47	100
	600	S13-3-10		400	8	3	6	8	15,867	428,210	6,011	18	158,225	40	16	5,125	93	196,825	49	100
	800	S13-3-2		356	8	3	6	8	22,396	58,280	4,739	0	31,856	9	16	3,900	94	165,144	46	100
	800	S13-3-7		367	8	3	6	8	23,141	48,850	4,882	0	42,792	12	19	4,100	94	164,999	45	100
	800	S13-3-8		359	8	3	6	8	22,607	68,300	4,779	0	57,902	16	14	3,900	94	159,624	44	100

Note (a) Fatigue life was defined as 50% reduction in initial AC stiffness. Fatigue lives for beams with 12million load cycles were extrapolated

AC: Asphalt Concrete GB: Granular Base FEL: Fatigue Endurance Limit

Table D4: Pavement Cross-Sections Simulated for Model Validation

Test Section (Year)	Strain Level	Beam ID	FEL (με) (NCHRP 09-38)	Modulus (ksi)			Thickness (in.)		Load (lbs)	[a]Beam Fatigue Life	Model 4: Ln(BETA) = f (LnSTR, LnE_0, LnFEL)					Expected β-Parameters				
				AC	GB	Soil	AC	GB			β-Param	R^2	End Modulus (psi)	% Initial Modulus	% of Beam Fatigue Life Simulated	β-Param	R^2	End Modulus (psi)	% Initial Modulus	% of Beam Fatigue Life Simulated
N10 (2006)	400	N10-3-5	146	834	8	3	6	8	19,055	562,660	11,520	4	329,053	39	32	10,400	89	446,469	54	100
	400	N10-3-6		1,039	8	3	6	8	24,300	497,170	14,620	56	418,930	40	28	13,200	91	515,929	50	100
	400	N10-3-7		894	8	3	6	8	20,569	1,191,490	12,418	32	421,046	47	14	10,655	94	442,473	50	100
	800	N10-3-1		764	8	3	6	8	52,810	11,410	5,955	87	404,164	53	100	6,100	94	376,439	49	100
	800	N10-3-2		753	8	3	6	8	51,950	21,400	5,863	80	111,563	15	89	5,700	93	352,943	47	100
	800	N10-3-3		743	8	3	6	8	51,162	15,420	5,779	92	358,456	48	100	5,750	92	365,605	49	100
N7 (2009)	400	N7-3-3	241	729	8	3	6	8	16,438	12,000,000	18,581	61	378,259	52	6	15,400	92	386,340	53	100
	400	N7-3-4		821	8	3	6	8	18,745	11,510,940	21,154	48	425,026	52	6	17,350	86	446,955	54	100
	400	N7-3-6		1,029	8	3	6	8	24,047	1,685,250	27,008	38	517,094	50	29	24,650	89	551,751	54	100
	400	N7-3-8		930	8	3	6	8	21,505	4,935,520	24,210	87	472,266	51	11	20,750	82	494,740	53	100
	600	N7-3-1		845	8	3	6	8	36,350	287,290	15,677	81	318,364	38	19	13,500	74	420,168	50	100
	600	N7-3-7		853	8	3	6	8	36,722	195,730	15,832	29	261,492	31	27	14,100	89	410,511	48	100
	600	N7-3-9		963	8	3	6	8	42,103	186,920	18,058	65	361,100	38	25	16,000	85	453,296	47	100
	800	N7-3-2		661	8	3	6	8	44,718	86,870	9,487	1	115,857	18	29	8,934	91	270,067	41	100
	800	N7-3-5		1,034	8	3	6	8	74,913	20,890	15,427	72	192,791	19	85	15,000	89	486,904	47	100
	800	N7-3-10		923	8	3	6	8	65,624	14,230	13,636	88	473,644	51	100	13,424	90	495,207	54	100
N11 (2009)	200	N11-3-4	134	1,254	10	5	6	10	12,739	12,000,000	28,366	72	852,582	68	100	30,250	93	710,724	57	100
	200	N11-3-6		1,396	10	5	6	10	14,337	12,000,000	31,864	77	936,754	67	100	33,700	92	778,653	56	100
	200	N11-3-7		1,404	10	5	6	10	14,429	4,501,250	32,066	73	1,010,957	72	100	36,000	92	805,667	57	100
	400	N11-3-2		1,249	8	3	6	8	29,837	100,000	16,048	83	639,372	51	100	16,100	83	619,725	50	100
	400	N11-3-5		1,197	8	3	6	8	28,448	149,050	15,321	66	371,149	31	74	14,432	80	686,481	57	100
	400	N11-3-8		1,199	8	3	6	8	28,513	124,920	15,355	68	570,022	48	88	14,469	80	710,308	59	100
	800	N11-3-1		1,104	8	3	6	8	80,872	2,530	7,975	57	716,024	65	100	8,909	67	625,295	57	100
	800	N11-3-3		970	8	3	6	8	69,522	3,060	6,931	59	621,060	64	100	7,500	72	565,304	58	100
	800	N11-3-9		1,125	8	3	6	8	82,700	2,110	8,141	33	743,872	66	100	9,800	75	565,796	50	100
S13 Intermediate (2012)	400	S13-2-7	184	970	8	3	6	8	22,536	162,180	18,114	85	562,722	58	100	18,610	92	486,346	50	100
	400	S13-2-10		1,098	8	3	6	8	25,859	78,020	20,719	79	702,805	64	100	22,250	86	593,006	54	100
	400	S13-2-12		1,113	8	3	6	8	26,232	128,820	21,011	77	657,581	59	100	21,750	89	553,987	50	100
S13 Base (2012)	400	S13-3-3	209	511	8	3	6	8	11,195	2,121,610	10,589	85	228,359	45	33	9,722	64	276,466	54	100
	400	S13-3-4		403	8	3	6	8	8,719	3,311,310	8,187	88	196,171	49	30	7,525	72	207,098	51	100
	400	S13-3-5		438	8	3	6	8	9,494	2,657,320	8,944	92	214,349	49	33	8,250	77	230,187	53	100
	600	S13-3-6		398	8	3	6	8	15,805	183,370	5,804	92	154,523	39	54	5,500	89	183,697	46	100
	600	S13-3-9		391	8	3	6	8	15,481	228,200	5,685	92	148,917	38	44	5,295	90	183,792	47	100
	600	S13-3-10		400	8	3	6	8	15,867	428,210	5,827	55	152,717	38	23	5,125	93	196,825	49	100
	800	S13-3-2		356	8	3	6	8	22,396	58,280	4,060	88	56,713	16	74	3,900	94	165,144	46	100
	800	S13-3-7		367	8	3	6	8	23,141	48,850	4,193	89	59,375	16	86	4,100	94	164,999	45	100
	800	S13-3-8		359	8	3	6	8	22,607	68,300	4,098	83	53,457	15	63	3,900	94	159,624	44	100

Note (a) Fatigue life was defined as 50% reduction in initial AC stiffness. Fatigue lives for beams with 12million load cycles were extrapolated

AC: Asphalt Concrete GB: Granular Base FEL: Fatigue Endurance Limit

Table D5: Pavement Cross-Sections Simulated for Model Validation

Test Section (Year)	Strain Level	Beam ID	FEL (με) (NCHRP 09-38)	Modulus (ksi)			Thickness (in.)		Load (lbs)	[a]Beam Fatigue Life	Model 5: BETA = f (STR, E_0, FEL, STR*STR, STR*E_0, STR*FEL, E_0*FEL)					Expected β-Parameters				
				AC	GB	Soil	AC	GB			β-Param	R^2	End Modulus (psi)	% Initial Modulus	% of Beam Fatigue Life Simulated	β-Param	R^2	End Modulus (psi)	% Initial Modulus	% of Beam Fatigue Life Simulated
N10 (2006)	400	N10-3-5	146	834	8	3	6	8	19,055	562,660	11,429	16	313,189	38	35	10,400	89	446,469	54	100
	400	N10-3-6		1,039	8	3	6	8	24,300	497,170	14,985	32	404,794	39	21	13,200	91	515,929	50	100
	400	N10-3-7		894	8	3	6	8	20,569	1,191,490	12,467	29	408,146	46	13	10,655	94	442,473	50	100
	800	N10-3-1		764	8	3	6	8	52,810	11,410	6,491	47	139,187	18	74	6,100	94	376,439	49	100
	800	N10-3-2		753	8	3	6	8	51,950	21,400	6,376	0	148,782	20	40	5,700	93	352,943	47	100
	800	N10-3-3		743	8	3	6	8	51,162	15,420	6,271	0	131,694	18	58	5,750	92	365,605	49	100
N7 (2009)	400	N7-3-3	241	729	8	3	6	8	16,438	12,000,000	20,011	0	376,410	52	2	15,400	92	386,340	53	100
	400	N7-3-4		821	8	3	6	8	18,745	11,510,940	22,892	0	425,088	52	2	17,350	86	446,955	54	100
	400	N7-3-6		1,029	8	3	6	8	24,047	1,685,250	29,350	0	527,070	51	10	24,650	89	551,751	54	100
	400	N7-3-8		930	8	3	6	8	21,505	4,935,520	26,279	50	476,317	51	4	20,750	82	494,740	53	100
	600	N7-3-1		845	8	3	6	8	36,350	287,290	15,612	83	308,997	37	20	13,500	74	420,168	50	100
	600	N7-3-7		853	8	3	6	8	36,722	195,730	15,825	30	334,322	39	27	14,100	89	410,511	48	100
	600	N7-3-9		963	8	3	6	8	42,103	186,920	18,872	17	359,937	37	16	16,000	85	453,296	47	100
	800	N7-3-2		661	8	3	6	8	44,718	86,870	8,766	83	124,493	19	68	8,934	91	270,067	41	100
	800	N7-3-5		1,034	8	3	6	8	74,913	20,890	17,840	0	187,242	18	23	15,000	89	486,904	47	100
	800	N7-3-10		923	8	3	6	8	65,624	14,230	15,139	0	262,452	28	51	13,424	90	495,207	54	100
N11 (2009)	200	N11-3-4	134	1,254	10	5	6	10	12,739	12,000,000	28,148	69	861,257	69	100	30,250	93	710,724	57	100
	200	N11-3-6		1,396	10	5	6	10	14,337	12,000,000	30,848	67	976,487	70	100	33,700	92	778,653	56	100
	200	N11-3-7		1,404	10	5	6	10	14,429	4,501,250	31,003	65	1,038,967	74	100	36,000	92	805,667	57	100
	400	N11-3-2		1,249	8	3	6	8	29,837	100,000	16,416	77	502,426	40	82	16,100	83	619,725	50	100
	400	N11-3-5		1,197	8	3	6	8	28,448	149,050	15,600	51	503,132	42	60	14,432	80	686,481	57	100
	400	N11-3-8		1,199	8	3	6	8	28,513	124,920	15,639	51	357,040	30	72	14,469	80	710,308	59	100
	800	N11-3-1		1,104	8	3	6	8	80,872	2,530	8,869	67	630,023	57	100	8,909	67	625,295	57	100
	800	N11-3-3		970	8	3	6	8	69,522	3,060	7,692	71	542,278	56	100	7,500	72	565,304	58	100
	800	N11-3-9		1,125	8	3	6	8	82,700	2,110	9,055	71	663,805	59	100	9,800	75	565,796	50	100
S13 Intermediate (2012)	400	S13-2-7	184	970	8	3	6	8	22,536	162,180	19,293	90	244,798	25	66	18,610	92	486,346	50	100
	400	S13-2-10		1,098	8	3	6	8	25,859	78,020	22,219	86	597,404	54	100	22,250	86	593,006	54	100
	400	S13-2-12		1,113	8	3	6	8	26,232	128,820	22,544	94	471,055	42	66	21,750	89	553,987	50	100
S13 Base (2012)	400	S13-3-3	209	511	8	3	6	8	11,195	2,121,610	10,739	88	249,323	49	27	9,722	64	276,466	54	100
	400	S13-3-4		403	8	3	6	8	8,719	3,311,310	7,880	83	195,056	48	52	7,525	72	207,098	51	100
	400	S13-3-5		438	8	3	6	8	9,494	2,657,320	8,787	89	206,782	47	42	8,250	77	230,187	53	100
	600	S13-3-6		398	8	3	6	8	15,805	183,370	2,280	0	348,128	87	100	5,500	89	183,697	46	100
	600	S13-3-9		391	8	3	6	8	15,481	228,200	2,106	0	343,912	88	100	5,295	90	183,792	47	100
	600	S13-3-10		400	8	3	6	8	15,867	428,210	2,314	0	344,485	86	100	5,125	93	196,825	49	100
	800	S13-3-2		356	8	3	6	8	22,396	58,280	1,640	0	306,215	86	100	3,900	94	165,144	46	100
	800	S13-3-7		367	8	3	6	8	23,141	48,850	1,851	0	310,752	85	100	4,100	94	164,999	45	100
	800	S13-3-8		359	8	3	6	8	22,607	68,300	1,700	0	306,338	85	100	3,900	94	159,624	44	100

Note (a) Fatigue life was defined as 50% reduction in initial AC stiffness. Fatigue lives for beams with 12million load cycles were extrapolated

AC: Asphalt Concrete GB: Granular Base FEL: Fatigue Endurance Limit

APPENDIX E

Pearson Correlation Matrix for Regression Variables (Computed with SAS)

Pearson Correlation Coefficients, N = 114 Prob > |r| under H0: Rho=0											
	BETA	STR	E0	FEL	PGD	AC	RAP	NMAS	P4	P200	LOAD
BETA	1.00000	-0.63584 <.0001	0.47018 <.0001	0.29655 0.0014	0.32564 0.0004	-0.10934 0.2468	0.45130 <.0001	0.04851 0.6083	0.04546 0.6310	-0.03290 0.7282	-0.43111 <.0001
STR	-0.63584 <.0001	1.00000	-0.35236 0.0001	0.18125 0.0536	0.06758 0.4750	0.20531 0.0284	-0.18197 0.0527	-0.15413 0.1016	0.16019 0.0887	0.18801 0.0452	0.85153 <.0001
E0	0.47018 <.0001	-0.35236 0.0001	1.00000	-0.28338 0.0022	0.08763 0.3539	-0.54992 <.0001	0.72650 <.0001	0.18080 0.0542	-0.29033 0.0017	-0.11137 0.2381	0.09879 0.2957
FEL	0.29655 0.0014	0.18125 0.0536	-0.28338 0.0022	1.00000	0.39312 <.0001	0.67475 <.0001	-0.02049 0.8287	-0.28941 0.0018	0.73765 <.0001	0.39268 <.0001	0.04299 0.6497
PGD	0.32564 0.0004	0.06758 0.4750	0.08763 0.3539	0.39312 <.0001	1.00000	-0.06349 0.5022	0.01268 0.8935	0.27939 0.0026	0.17757 0.0588	-0.22373 0.0167	0.16350 0.0822
AC	-0.10934 0.2468	0.20531 0.0284	-0.54992 <.0001	0.67475 <.0001	-0.06349 0.5022	1.00000	-0.47659 <.0001	-0.48927 <.0001	0.52037 <.0001	0.53246 <.0001	-0.07843 0.4069
RAP	0.45130 <.0001	-0.18197 0.0527	0.72650 <.0001	-0.02049 0.8287	0.01268 0.8935	-0.47659 <.0001	1.00000	0.18222 0.0523	-0.09113 0.3349	-0.10169 0.2817	0.13122 0.1640
NMAS	0.04851 0.6083	-0.15413 0.1016	0.18080 0.0542	-0.28941 0.0018	0.27939 0.0026	-0.48927 <.0001	0.18222 0.0523	1.00000	0.01710 0.8567	-0.93567 <.0001	-0.05654 0.5502
P4	0.04546 0.6310	0.16019 0.0887	-0.29033 0.0017	0.73765 <.0001	0.17757 0.0588	0.52037 <.0001	-0.09113 0.3349	0.01710 0.8567	1.00000	0.21611 0.0209	0.00215 0.9818
P200	-0.03290 0.7282	0.18801 0.0452	-0.11137 0.2381	0.39268 <.0001	-0.22373 0.0167	0.53246 <.0001	-0.10169 0.2817	-0.93567 <.0001	0.21611 0.0209	1.00000	0.11151 0.2375
LOAD	-0.43111 <.0001	0.85153 <.0001	0.09879 0.2957	0.04299 0.6497	0.16350 0.0822	-0.07843 0.4069	0.13122 0.1640	-0.05654 0.5502	0.00215 0.9818	0.11151 0.2375	1.00000

Variable	Definition
BETA	Response variable
STR	Strain level in beam fatigue test (initial critical tensile strain at AC bottom), με
E_0	Initial AC modulus from beam fatigue testing, ksi
FEL	Fatigue endurance limit determined using NCHRP 09-38 Method, με
PGD	Difference between binder performance grades (e.g., for PG 70-22, PGD = 92)
RAP	Recycled asphalt pavement material content, %
NMAS	Nominal maximum aggregate size, mm
P4	Percent passing No. 4 sieve
P200	Percent passing No. 200 sieve
AC	Asphalt binder content, %
LOAD	Axle load used in structural analysis (WESLEA), kips

APPENDIX F

Notes on SAS-Generated Regression Diagnostic Plots

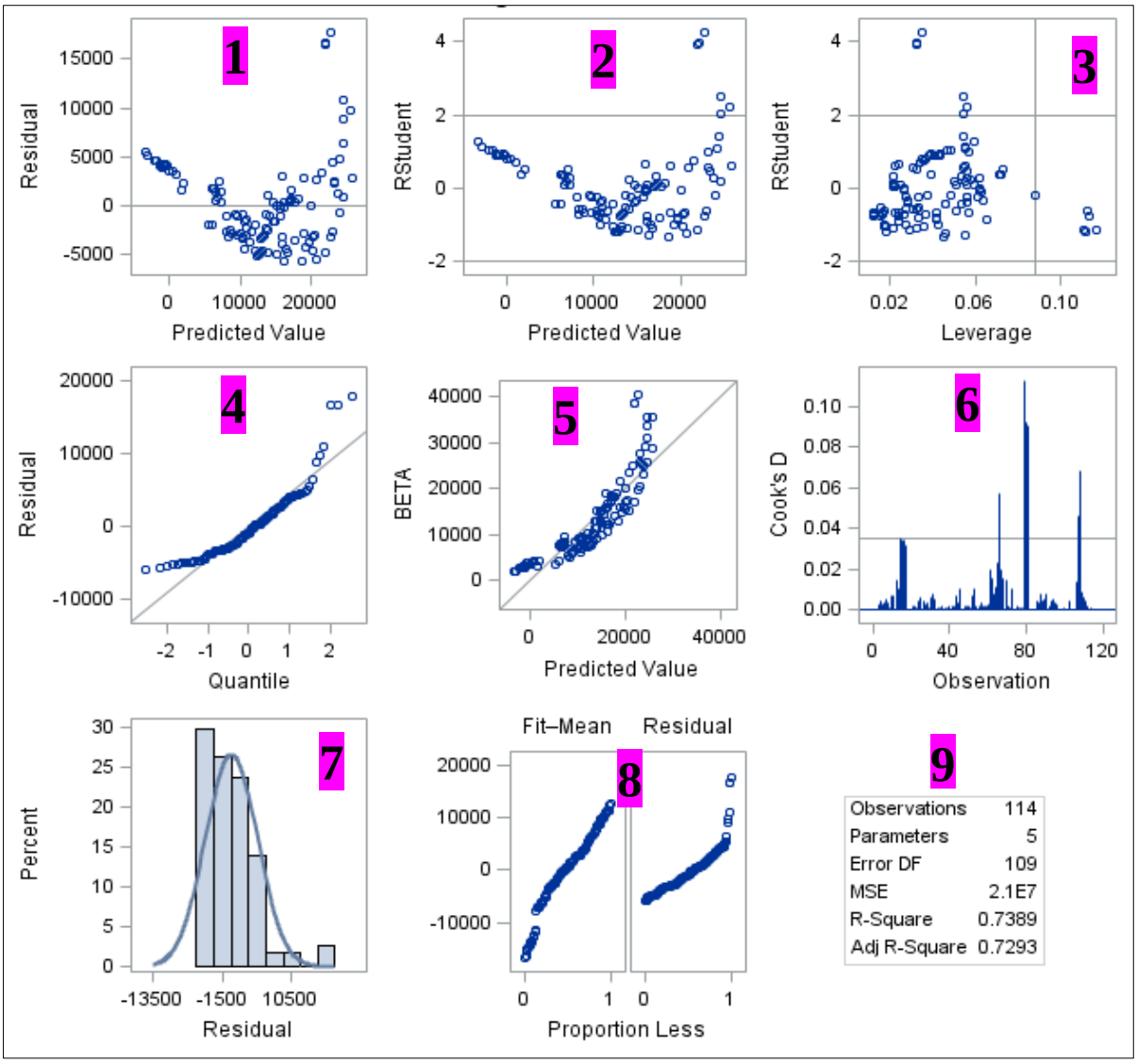

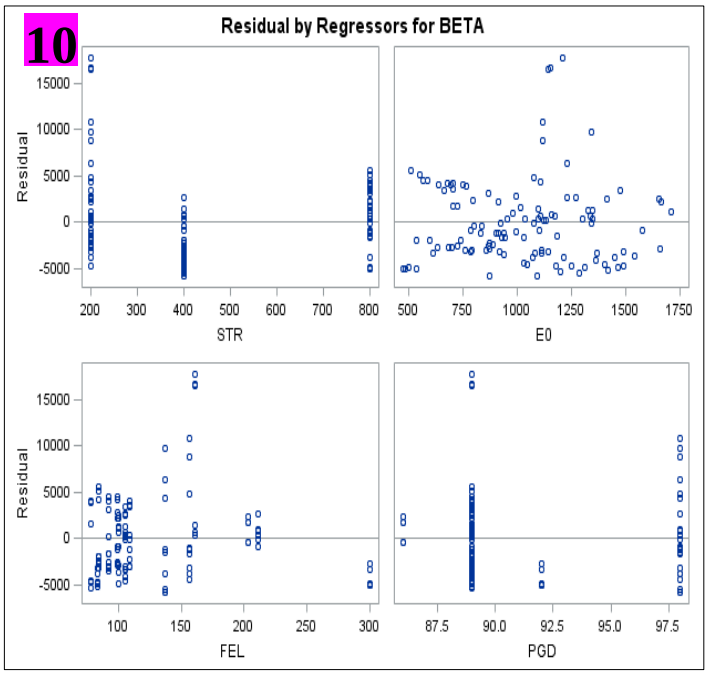

Figure F Sample SAS-Generated Regression Analysis Diagnostic Plots

Table F Notes on Sample SAS-Generated Regression Diagnostic Plots (based on Figure F)

Plot No.	Plot Description	Interpretation and Requirements
1	Residual (error) versus predicted response	Random distribution of residuals about the horizontal axis indicates the regression model is linear and its residuals have equal variance (linearity and equal error variance assumptions).
2	Studentized residual (residuals divided by their estimated standard error) versus predicted response	Apart from using to check the linearity and equal variance assumptions, this plot detects outliers in response variables. If response variable values have studentized residuals larger than 2 or 3 standard deviations away from zero, they are considered outliers (Chatterjee and Hadi, 2012).
3	Studentized residual versus leverage	Leverage detects outliers in predictor variables. For a large sample, leverage greater than 0.5 is high; those between 0.2 and 0.5 are moderate (Kutner et al., 2008). This plot simultaneously detects outliers in both the response and predictor variables.
4	Quantiles of the residuals versus quantiles of normal distribution	Points should fall on line of equality to indicate the regression errors are normally distributed (normality assumption).
5	Response (BETA) versus predicted response	Symmetrical distribution of points on the line of equality indicates validation of linearity assumption
6	Cook's distance versus observation (data points)	Cook's distance is used to determine if outlying data points are influential. Observations with Cook's distance greater than one are considered influential (Chatterjee and Hadi, 2012).
7	Histogram of residuals	Symmetric, bell-shaped distribution satisfies the normality assumption
8	Residual-fit spread plot	The spread of the centered fitted values (left side of the plot) is compared to the spread of the residuals (right side). If the left plot is taller than the right, the model explains majority of the variability in the response variable.

Table F cont'd

Plot No.	Plot Description	Interpretation and Requirements
9	This box summarizes the regression analysis results. • **Observations:** Data points (sample size) • **Parameters:** Number of regression coefficients • **Error DF:** Degree of freedom of regression errors (**Observations** minus **Parameters)** • **MSE:** Mean square of error (variance of regression errors) • **R-Square:** Coefficient of determination • **Adj R-Square:** Adjusted Coefficient of Determination	The smaller the MSE, the well-fitted the model is. Adjusted R-Square is preferred for evaluating regression models since it makes adjustment for the number of predictors. The ordinary R-Square will keep increasing as the number of predictor variables increase.
10	Residual versus each predictor variable	Random scatter of points about the horizontal line indicates satisfaction of the equal error variance and independence of errors assumptions.

APPENDIX G

Predicted Versus Expected β-Parameters

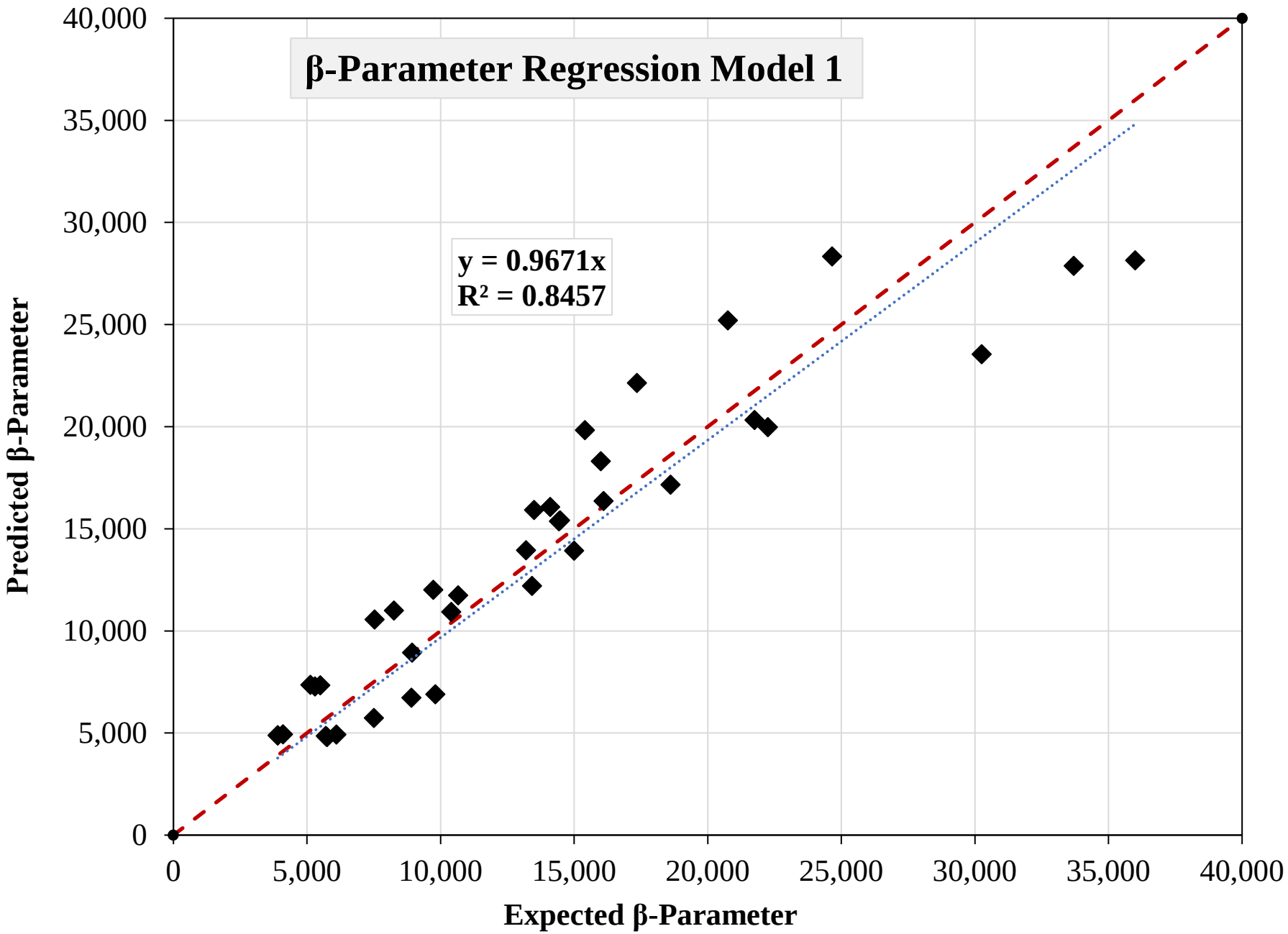
β-Parameter Regression Model 1
y = 0.9671x
R² = 0.8457
Predicted β-Parameter
Expected β-Parameter
0
5,000
10,000
15,000
20,000
25,000
30,000
35,000
40,000

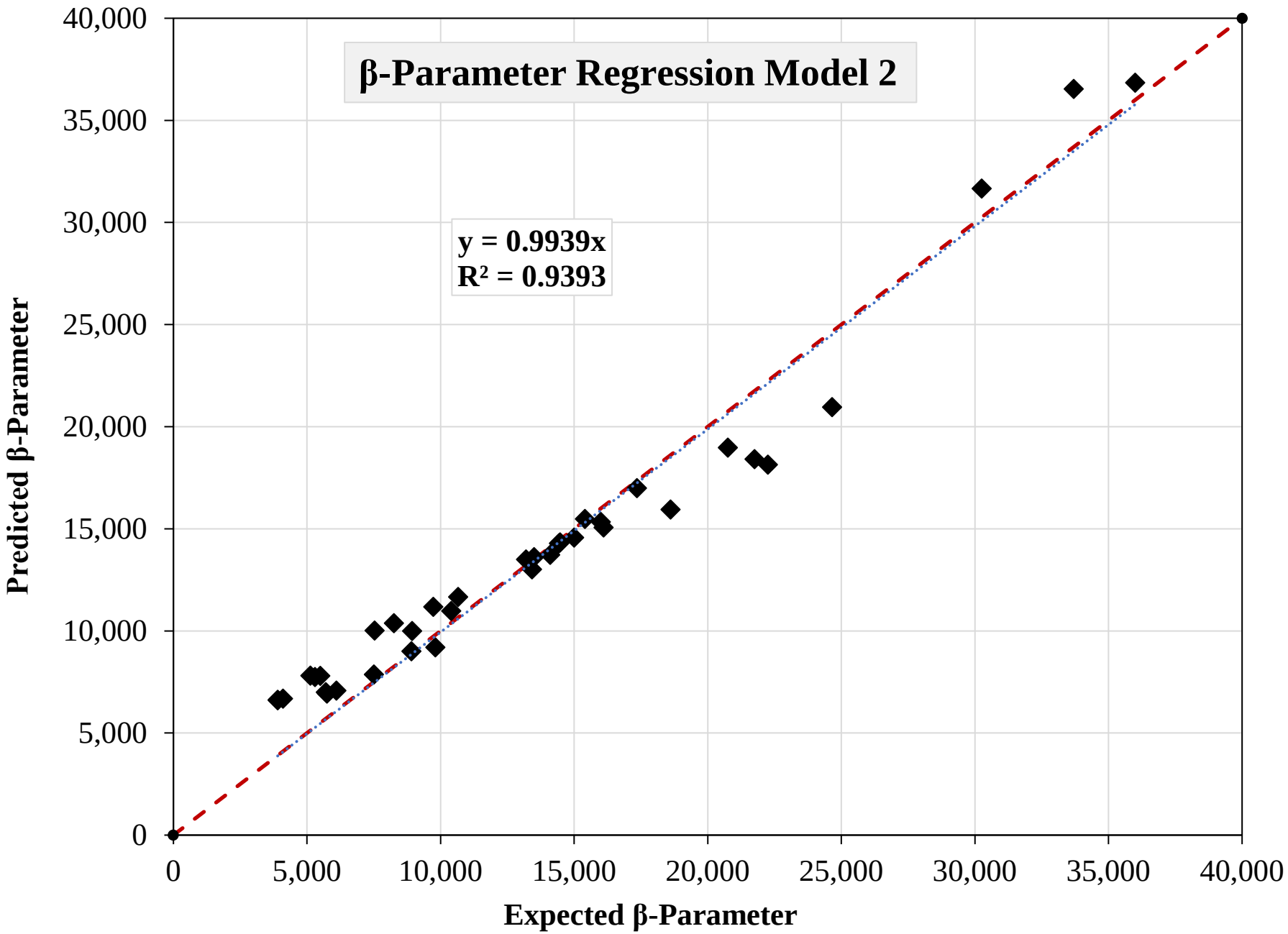
β-Parameter Regression Model 2
y = 0.9939x
R² = 0.9393
Predicted β-Parameter
Expected β-Parameter
0
5,000
10,000
15,000
20,000
25,000
30,000
35,000
40,000

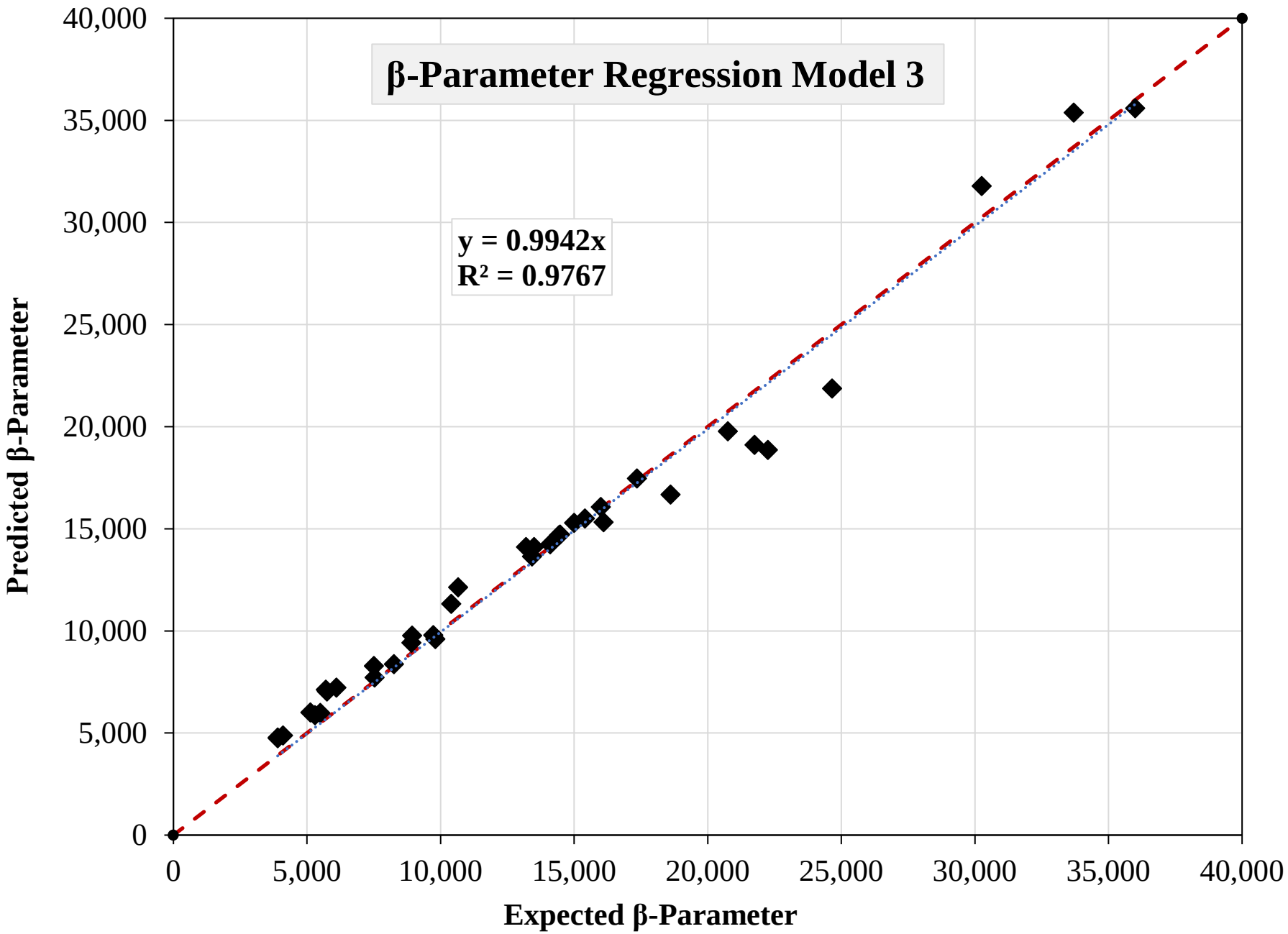
β-Parameter Regression Model 3
y = 0.9942x
R² = 0.9767
Predicted β-Parameter
Expected β-Parameter
0
5,000
10,000
15,000
20,000
25,000
30,000
35,000
40,000

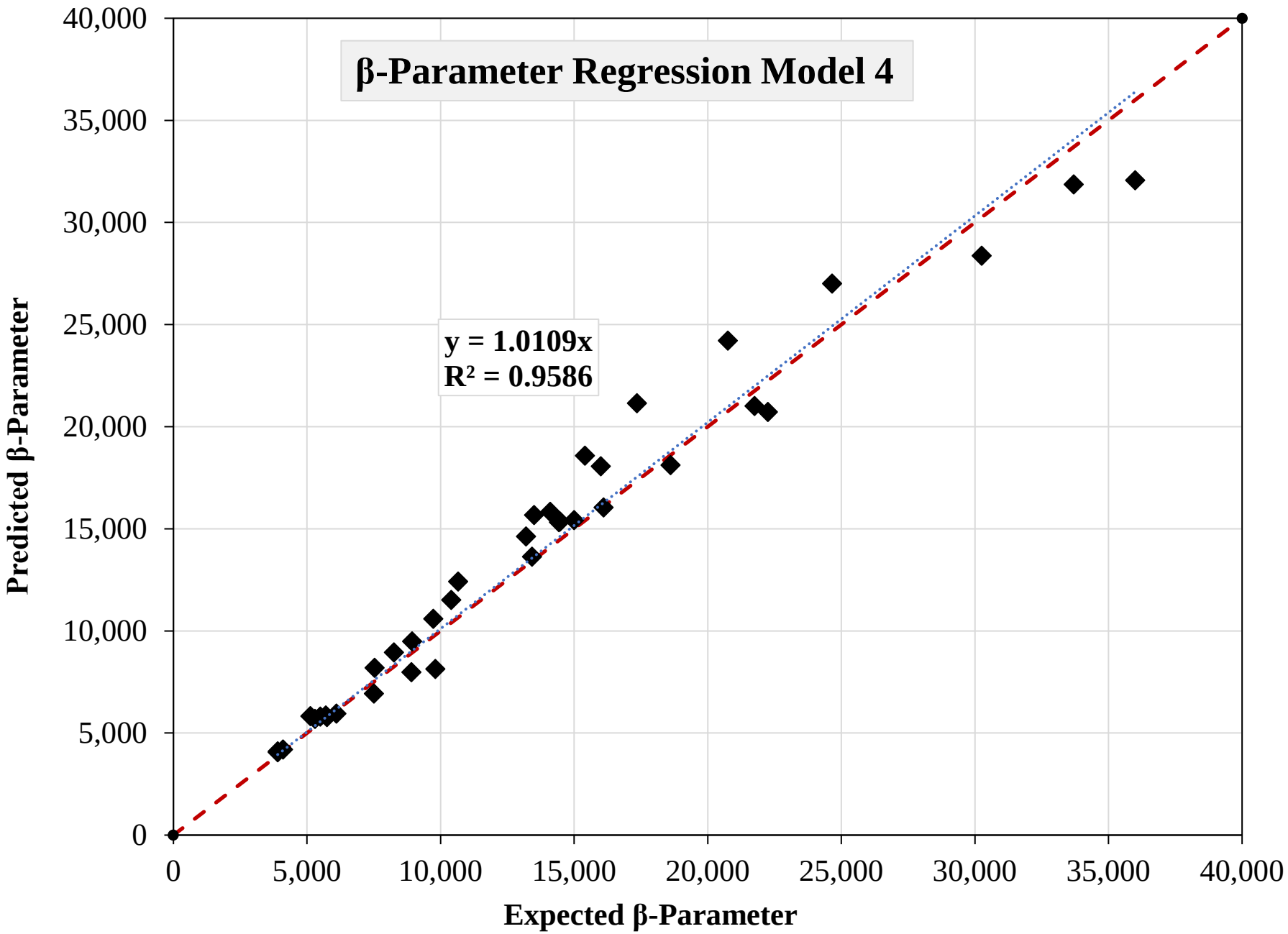
β-Parameter Regression Model 4
y = 1.0109x
R² = 0.9586
Predicted β-Parameter
Expected β-Parameter
0
5,000
10,000
15,000
20,000
25,000
30,000
35,000
40,000

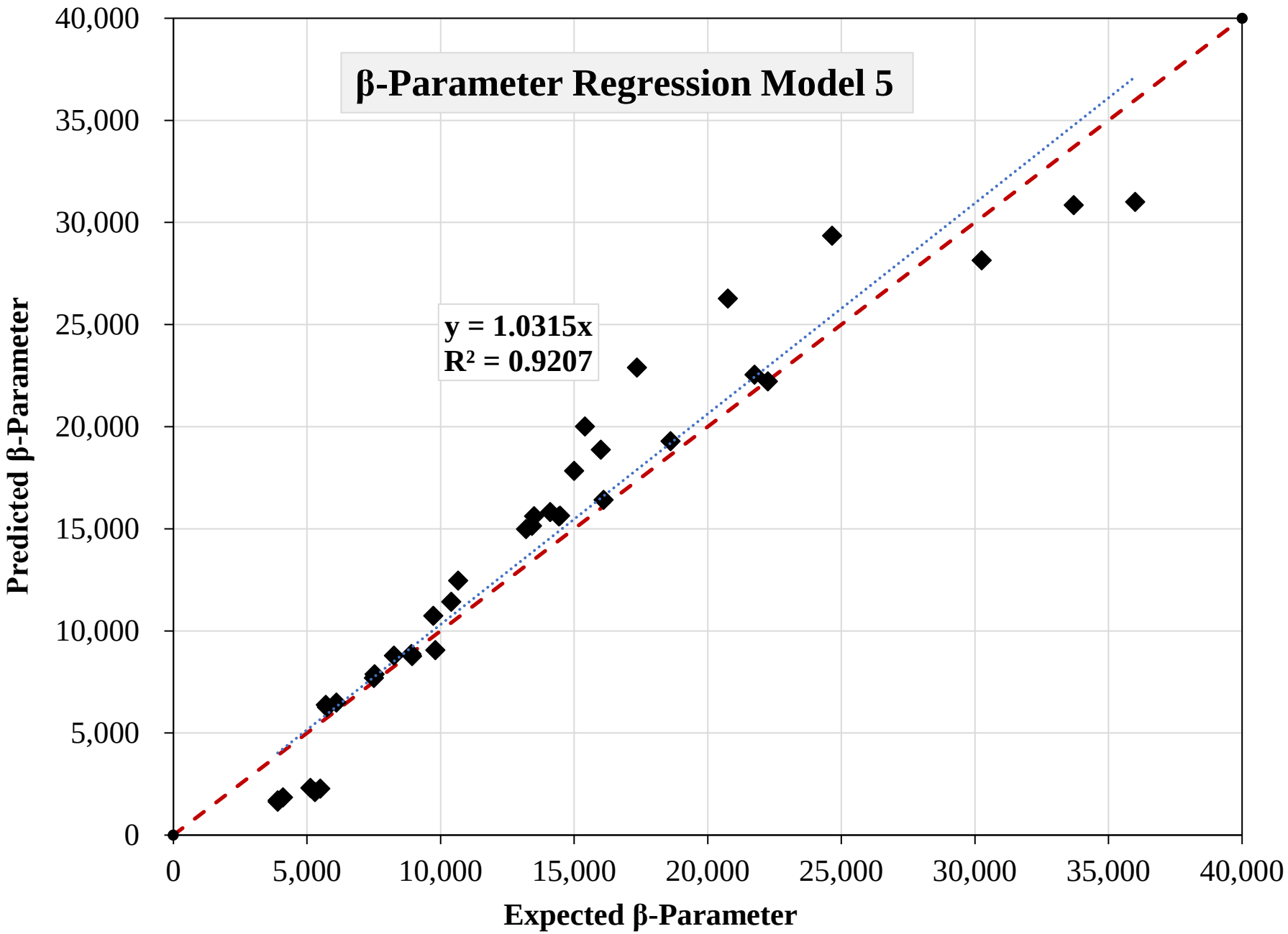
β-Parameter Regression Model 5
y = 1.0315x
R² = 0.9207
Predicted β-Parameter
Expected β-Parameter
0
5,000
10,000
15,000
20,000
25,000
30,000
35,000
40,000